Energy Storage for stability of microgrids

Jiravan Mongkoltanatas

UNIVERSITÉ DE GRENOBLE

THÈSE

Pour obtenir le grade de

DOCTEUR DE L'UNIVERSITÉ DE GRENOBLE

Spécialité : **Génie Électrique**

Arrêté ministériel : 7 août 2006

Présentée par

« Jiravan MONGKOLTANATAS »

Thèse dirigée par « **Mme., Delphine RIU »** et
codirigée par **« M., Xavier LE-PIVERT »**

préparée au sein du **Laboratoire de Génie Électrique de Grenoble (G2ELab) et**
dans **l'École Doctorale: Électronique, Électrotechnique, Automatique et Traitement du Signal (EEATS)**

Participation d'un Système de Stockage à la Stabilité des Réseaux Insulaires

Thèse soutenue publiquement le **3 Décembre 2014**,
devant le jury composé de :

M., Seddik BACHA
Professeur au G2ELab à Grenoble, Président
M., Serge PIERFEDERICI
Professeur au Green à Nancy, Rapporteur
M., Bruno FRANCOIS
Professeur au L2EP à Lille, Rapporteur
M., Hamid BEN AHMED
Maître de Conférences HDR au SATIE à Rennes, Examinateur
Mme., Delphine, RIU
Maître de Conférences au G2ELab à Grenoble, Directrice de thèse
M., Xavier LE-PIVERT
Ingénieur de Recherche au CEA, Co-encadrant

Acknowledgements

The research leading to these results has received funding from the CEA (Commissariat à l'énergie atomique et aux énergies alternatives) which is the French Alternative Energies and Atomic Energy Commission. I would like to thank you for financial support.

For three years and a half of working, my thesis cannot be accomplished without the patient and powerful people. I would like to express my sincere gratitude to all people who contributed this work. It is an unforgettable experience for me.

Especially, I want to express my deep thanks and appreciate to my supervisor, Mme. Delphine RIU, for her support for working at G2ELAB, and the correction of the thesis. This thesis cannot be possible without her guidance and her encouragement. I can overcome many difficulties and learned many things. Moreover, I am very grateful to my co-supervisor, M. Xavier Le-Pivert, for the insightful discussion, his guidance, and his support for working at INES. My thesis cannot be success without the help and patience from two important people; my supervisor and my co-supervisor. We have worked together since my master's thesis (January, 2011). I would like to thank for everything for this four years. Their confidence in me is one of powerful motivation to keep on working and make this thesis possible.

I would also like to thank members of the jury; M., Seddik BACHA, M., Serge PIERFEDERICI, M., Bruno FRANCOIS, and M., Hamid BEN AHMED, for their agreeing to serve as committees for my Ph.D. thesis defence. And I am very grateful for their valuable discussions, suggestions, and comments.

Many thanks also go to M. RUMEAU Axel for his help on the experimental in RTLAB at G2Elab. He instructed me everything about RTLAB and hardware. Without his support, the final part of this thesis cannot be accomplished which means that this thesis will not complete.

I would like to thank M. Quoc Tuan TRAN for his support and his guidance to do the experimental in RTLAB at INES. Equally, I am very thankful to M. Nicolas MATIN for his guidance about INSGRAF, his suggestions, his help, and his encouragement during my work.

I would like also to thank my friends, my colleagues, and various institutions at the National Solar Energy Institute (INES; Institut National de l'Energie Solaire) under the CEA, and at the Grenoble Electrical Engineering laboratory (G2Elab; Laboratoire de Génie Électrique de Grenoble) for their friendship, useful discussions, and encouraging supports. Although I cannot speak French fluently, they tried to communicate and help me everything. It makes such a good atmosphere of working.

Furthermore, I would like to take this chance to express my sincere thanks to Thai government for the best opportunity of higher education in France (Master's and Doctor's degree). I appreciate all financial support from full scholarship granted by the Thai Ministry of Sciences and Technology. I also would like to thanks the Office of Education Affairs, Royal Thai Embassy in France, for all support about official documents, and encouragement which relieve all difficulties for living in France.

I cannot finish without revealing my thankfulness and gratefulness to all my families and my friends for their support, understanding, and encouragement during seven years in France. My families (my parents, my sister, my grand-parents, and my aunts) are my best back up team. Their encouragement makes me overcome all difficulties. I want to express my gratitude and deepest appreciation to my father for the correction of my thesis, and my mother for her continuous support by sending food and books from Thailand. I also thank and appreciate my sister for her support, assistances, and taking care of our parents in place of me. I am very thankful to my boyfriend for his understanding, support, and encouraging. No matter what problems I meet, he is always by my side and reboots my energy to encounter and overcome all problems. Moreover, I would like to express my thanks to all my Thai friends (in France for their infinite friendship, and assistances in numerous ways during my seven years. They are my second family which relieves the loneliness of far away from home. My life in France could be hard without them. Thank you for everything. And I also thanks for my entire friends in Thailand for their support, encouragement, and all warm welcome when I came back.

Finally, I would like to sincerely thank everything which bring me here, in France. It is a valuable experience and the best memory in my life.

Jiravan MONGKOLTANATAS

09 October 2014

Contents

List of Figures

List of Tables

Notations

$H_i^{S_{ni}}$	Inertia of each rotating machine (generator or motor)	MWs/MVA
Ω_{0i}	Nominal rotation speed	rad/s
$\bar{X}$	Mean value	-
Δf_{std}, dFstd, dF_std	Acceptable frequency deviation	Hz
$\Delta P_{ch}(t)$	Independent power variation of load to frequency variation	per unit
$\Delta P_{ch\_d}(t)$	Dependent power variation of load to frequency variation	per unit
ΔP_{diff}	Total of power deviation	per unit
ΔP_m^*	Power deviation reference for diesel generator	per unit
ΔP_{max}, dPmax	Optimum power deviation of PV	W
$\Delta P_{pv}(\%)$	Percentage of power variation from rated power of PV	%
ΔP_{pv_limit}	Limitation of power variation of PV	per unit
Δt	Time difference or duration of power change	s
Δt_{limit}	Limitation of duration of power change of PV	s
D	Load damping coefficient	%
E_0	Voltage at full charge of battery	Volt
E_b	DC voltage source of battery model	V
E_{eq}	Kinetic energy of all rotating machines	MW.s
E_{st}	Participate of energy of energy storage	W.s
f, f_{res}	Frequency of power system	Hz
f_0	Nominal frequency	Hz
fc1	Cut-off frequency of low pass filter	Hz
fc2	Cut-off frequency of high pass filter	Hz
f_{cr}	Critical frequency	rad/s
H_{eq}	Equivalent inertia of power system	s
I	Current	A
I_{dc}	DC current	A
I_r	Current output of filter	A
I_s	Current outout of AC/DC before filter	A
I_{src}	DC current output of converter	A
I_{ES}	Current input of converter or current of energy storage device	A
J	Moment of inertia	$kg.m^2$
K	Primary energy reserved of diesel generator	Hz/W
k_{d1}	Derivative parameters of PD controller	-
K_i	Integral gain of PI controller	-
K_p	Proportional gain of PI controller	-
K_{ES}	Energy reserve of energy storage system	Hz/W
M_{eq}	Equivalent time characteristic of power system	s
P_{ES}, P_{ES_ref}	Power reference of energy storage system to regulate frequency	per unit
P_{ES_max}	Rated power of energy storage system	W
P_{ini}	Power initial of PV	W
P_{load}	Power of load	W
P_m	Current power output of diesel generator	W
P_{m0}	Scheduled power output of diesel generator	W
P_{max}	Nominal power of diesel generator	W
P_{pv}	Power of photovoltaic	W
P_{pv_rated}	Rated power of PV	W
Q	Actual capacity of battery	Ah

Q_0	Initial capacity of battery	Ah
s_d	Droop value of diesel generator	%
S_{diesel_rated}	Rated apparent power of diesel generator	VA
s_{es}	Droop value of energy storage system	%
S_{n_ES}	Apparent power of energy storage system	VA
S_{rated}	Rated apparent power of power system	VA
t	Times	s
T_1 and T_2	Times characteristic of diesel engine	s
t_a	Time average	s
T_a	Time response of actuator	s
T_c	Resistive torque of the generator	N.m
T_g	Combustion delay	s
T_{ge}	Mechanical torque of the turbine	N.m
t_{min}	Time of optimal frequency (in dynamic response)	s
t_r	Time response of controller	s
t_s	Time resolution	s
V	Voltage	V
V_{dc}	DC voltage output	V
V_{hj}	Voltage input of boost converter	V
V_r	RMS voltage phase to ground of power system	V
V_s	Voltage output of inverter (voltage before filter)	V
α_h	Switching function	-
β_1, β_2, β_3	Three phase switching functions	-
θ_{est}	Measured angle from PLL	rad
θ_r	Angle initial of AC voltage	rad
τ	Time delay of diesel engine	s
τ_1	Time constant of low pass filter	s
τ_2	Time constant of high pass filter	s
τ_m	Torque of coupling shaft	N.m
ω_r	Frequency of power system	rad/s

subscripts

A	Ampere
AC	Alternative component
AGC	Automatic Generation Control
Ah	Ampere-Hour
AVR	Automatic voltage regulator
C	Capacitor
CAES	Compressed Air Energy Storage
CH_4	Methane
CO_2	Carbon dioxide gas
DC	Direct component
DFT	Discrete Fourier transforms
DoD	Depth of discharge
EDLC	Electrochemical Double-layer Capacitors
EES	Electrical Energy storage
ES,es	Energy storage device

ESS	Energy storage system
FFT	Fast Fourier transforms
FHC	Fluctuation harmonic content
H_2	Hydrogen
Hz	Hertz
kW	Kilo Watt
L	Inductor
Li-ion	Lithium ion battery
Me-air	Metal air battery
MVA	Mega volt.amps
MW	Mega Watt
NSD	Normalized standard deviation
O_2	Oxygen
P	Active power
PEMFC	Polymer Exchange Membrane Fuel Cell
PHES or PHS	Pumped Hydro Energy Storage
PI	Proportional and Intregral controller
PLL	Phase Lock Loop
PSD	Power spectral density
pu	Per unit
PV	Photovoltaic
PWM	Pulse width modulation
Q	Reactive power
R	Resistor
rad/s	Radian per second
redox	Reduction-oxidation
S	Second
SC	Supercapacitors
SCC	Shout-circuit capacity
SD	Standard deviation
SMES	Superconductive magnetic energy storage
SNG	Synthetic natural gas
SoC	State of Charge
SOFC	Solid Oxide Fuel Cell
TES	Thermal energy storage
V	Volts
VAR	Variance
VSI	Voltage source inverter
μs	Micro second

Introduction

This project received the financial support from the Thai government and the CEA (Commissariat à l'énergie atomique et aux énergies alternatives) which is the French Alternative Energies and Atomic Energy Commission. All works were done at the LITEN laboratory (and in particular at the National Solar Energy Institute (INES)) and at the Grenoble Electrical Engineering laboratory (G2Elab).

Microgrids can be considered as one controllable load and one controllable generation unit for power grid defined by a much higher short-circuit power. They can operate with connecting to main grid, which guarantees the stability of microgrids. Nonetheless, the stability can be a critical situation for isolated microgrids. The stability of power systems is ensured if three parameters, i.e. internal angle of generator, frequency and voltage, come back over their initial values or in acceptable limits after any disturbance. In this thesis, only the frequency stability in isolated large microgrids (over 1MW) is considered.

Frequency variation is a function of the inverse of equivalent inertia, and depends also on the imbalance between load and supply active powers. The equivalent inertia of isolated microgrids is small because of the limited number of rotating machines. Therefore, frequency of such grids is highly sensitive to power variation of loads and productions. Many studies have considered the impact of active power variation of loads which change instantly. The impact of production side is particularly studied in this thesis, thanks to the massive integration of renewables, especially for islanding microgrids. Then, until now, thermal generator is the classical production unit in isolated microgrids. The active power of this generation unit can be controlled according to the active power variation of loads (or frequency variation); therefore, the frequency stability is guaranteed with the definition of droop characteristic for primary control of the frequency (i.e. during the first 15 minutes after deviation of frequency). However, the development of renewable energies, such as wind energy or photovoltaic, take a significant par between the other production systems and their installed capacity is increasing because of their zero emission greenhouse gas effects. Then, the rising of renewable energy presents high risks of frequency instability because of their intermittency.

To maintain the frequency stability of isolated microgrids, the first idea would be to increase the capacity of thermal generator; another way should be to design Energy Storage System (denoted ESS in following sessions) to provide of absorb or inject active power according to the frequency value of the grid. Increasing capacity of thermal generator is a very simple solution but it has impacts on the environment (e.g. with emissions of pollutants and greenhouse gas) and its operating cost can be high (with a higher price of fuels, oil and gas). Installation of energy storage could be an interesting solution for preventing frequency instability with more considerations for local environment. Furthermore, time response of energy storage is small thanks to the utilization of power electronics interfaces. Notwithstanding with the high investment cost of such a solution, this green energy has a significant role to play for energy generation, in the present and future. In this thesis, energy storage is selected to participate in frequency regulation in order to prevent the frequency instability linked to intermittency of solar production. Then, energy storage seems to be a relevant solution for primary frequency regulation thanks to its fast time response.

The installation of ESS leads of course to some questions:

- Therefore, which energy storage technology is suitable for frequency regulation in an isolated microgrid?

- How to design the interface, the installed power and capacity of such a system?
- How to design the architecture of control-command and select the appropriate control strategy?

Therefore, the objective of this thesis is to propose some solutions to this problematic and particularly, define a methodology to design the appropriate size and strategy of energy storage in isolated microgrids with a high penetration rate of photovoltaic. It would be also important to validate this approach with the help of an experimental bench.

This thesis is organized in seven chapters. In the first chapter, the three main key words of this thesis, i.e. frequency stability, isolated microgrids and ESS are presented. Frequency stability of isolated microgrids is the analyzed through the integration of renewable energy. Issues linked to energy storage devices and technologies are also described. Existed projects of development of ESS in microgrids and classical primary control strategies are finally summarized, before presenting the scientific issues of this work. In chapter 2 to 7, isolated large microgrid will be called isolated grid or islanding grid.

The second Chapter allows describing the different situations of photovoltaic power variations and the classical characterizations through statistic approach, probabilistic approach and spectral analysis. Some real signals of PV production are then studied using these methods to model disturbances of PV production. Each method will provide different levels of information on power fluctuation which will be used in the following sessions. This study enables to know the characteristics of power fluctuation which will be related to the frequency variation.

In the chapter 3, the impact of PV power fluctuation on the system frequency is studied both in frequency and time domains. The relationship between power fluctuation of PV and frequency variation is firstly studied in frequency domain by analyze the transfer function between the frequency and the photovoltaic power. Moreover, the impacts of power system parameters on this transfer function are studied. For time domain analysis, different situations of power variation (i.e. sine, step and ramp signals) are applied as disturbances to power system simulation. These studies enable to define critical impacts of power variation on frequency, which are presented by a limitation diagram of power fluctuations. Chapter 2 and 3 will be used for sizing and defining strategy for ESS in Chapter 5.

Energy storage system, which consists in a source of energy, a DC/DC converter, an inverter with its filter and its associated control loops, is presented in chapter 4. The power electronic converters (DC/DC, AC/DC) enable to control the active power of energy storage for frequency regulation. Three different energy storage systems are presented in this chapter, according a gradable complexity of the system.

In the chapter 5, different strategies of energy management for the ESS in order to participate to the primary frequency control are proposed taking into account of PV power variations. The link between the design of the storage device, its technology and the control strategies will be discussed. A comparison of the different strategies will be held according to their respective performances.

Chapter 6 presents an original strategy of control of the ESS based on robustness against parameter uncertainties of the system (on production, grid and ESS). Therefore, a H infinity controller has been designed according to dynamic specifications on frequency time response, and results have been compared to classical approach. Moreover, its robustness in stability and performances has been analyzed. Finally, in the last chapter, real time simulation have been done with hardware-in-the-loop (HIL) simulations, replacing some parts of the studied system by hardware and other models with numerical models. This experimental bench, depicter in this section, will conclude this report by validating all proposed strategies.

This report will be concluded by some perspectives of further works in order to complete the theoretical and experimental results of this thesis.

Chapter 1

Problematic of microgrids: the rule of storage devices

1.1 Introduction

Renewable energy has become fascinating source for electricity production according to green energy trends. Wind energy and solar energy or photovoltaic (PV) are widely in researches as well as in service. Because of its intermittent power, reliability and stability of power system is affected. Energy storage system is proposed as one of solutions to maintain the stability and improve power quality.

In this chapter, the general context is described in relation to three main key words: frequency stability, islanding micro power system or isolated micro grid, and energy storage. Firstly, general information of frequency stability and its control system is presented; followed by the elaboration of the general characteristics of micro power system which relate to the frequency variation problem. These two topics link to the main issue of this thesis concerning frequency variation according to renewable energy. Finally, descriptions and applications of energy storages are summarized.

1.2 Frequency stability

There are three types of stability in power system: angle, voltage, and frequency stability. The stability is the ability of power system to remain its value (angle, voltage, frequency) at a rated value or in acceptable limits during the normal operation or after any disturbance [1]. The angle stability is linked to the synchronous machine and its active power variation. Voltage variation is caused by imbalance of reactive power between production and load demand. In this thesis, only stability of frequency and its control are considered. Frequency stability is linked to the imbalance of active power between production and load demand. From the mechanical equation of (1.1), variation of angular velocity of turbine (ω_t) is expresses as a function of moment of inertia (J), mechanical torque of the turbine (T_{ge}) and resistive torque of the generator (T_c) [2]. T_g relates to power produced by the turbine and T_c relates to the power consumption in (see (1.2)). Consequently, from (1.1) and (1.2), the deviation of the square of angular velocity can be defined as a function of source and load active powers (equation (1.3)). When supply power is upper than the load, deviation of square of angular velocity is positive; means that velocity of the turbine rises up. Frequency of system increases from its nominal value. On the contrary, frequency decreases from its nominal value when load demand is over the source power. The deviation of the square of velocity is then negative; therefore, the velocity of turbine is slow down.

$$\mathbf{J}\frac{\mathbf{d}\boldsymbol{\omega_t}}{\mathbf{dt}} = \mathbf{T_{ge}} - \mathbf{T_c} \tag{1.1}$$

$$\boldsymbol{T_{ge}} = \frac{\boldsymbol{P_g}}{\boldsymbol{\omega_t}} \qquad \boldsymbol{T_c} = \frac{\boldsymbol{P_c}}{\boldsymbol{\omega_t}} \tag{1.2}$$

$$\frac{1}{2}\mathbf{J}\frac{\mathbf{d}\omega_t{}^2}{\mathbf{dt}} = \mathbf{T_{ge}}\omega_t - \mathbf{T_c}\omega_t = \boldsymbol{P_g} - \boldsymbol{P_c} \quad (1.3)$$

Generally, the frequency control is integrated in power plant with rotating generator, such as, gas turbine plant, diesel generator, and hydro power plant. Frequency control system is separated in three control levels: primary, secondary, and tertiary controls. The primary frequency control is highlighted in this thesis as it is the first action of control to limit frequency deviation after disturbance. After that, secondary control takes action to bring frequency back to nominal value (50Hz). Finally, the tertiary control is regulated manually by system operator (at least 15 minutes after disturbance) to complete secondary control; in case it cannot bring frequency back to nominal value. This control allows regulating the imbalance of active power between supply and demand in case of slow fluctuations [3]. Only primary and secondary frequency controls are elaborated in this section.

1.2.1 Primary frequency control

After imbalance of active power between generation and load, all generators, which participate to the primary frequency control, will limit the frequency deviation by changing their power supply. Each generator adjusts its power from the scheduled power (P_{m0}) to the current power output (P_m) by applying the droop control as shown in Figure 1.1a. The power variation (ΔP_m) is proportional to the frequency variation (Δf), the nominal frequency (f_0), the nominal power of generator (P_{max}), and the droop value (s_d) in (1.4). Frequency variation (Δf) corresponds to the difference between the current frequency (f) and the nominal one (f_0 or 50Hz). The droop value is the ratio between steady-state frequency deviation and active power variation in per unit in (see (1.5)). Therefore, the steady-state value of frequency during primary frequency control depends on droop value which is defined as the acceptable range of frequency variation in steady state (f_{max} and f_{min} in Figure 1.1a). For example, a droop of 4% of generators guarantee a frequency comprised between 49 and 51Hz (50Hz x 4% = 2Hz).

The ratio between frequency deviation to active power variation is equal to the primary energy reserved, denoted K (Hz/W) in (1.6) [1], [4]. This energy depends on the nominal frequency (f_0), the rated power of source (P_{max}), and the droop value (s_d). Power systems with small K (large droop value and/or small power generation) can meet higher frequency variation than systems with large K (small droop value and/or large power generation) for a same power deviation.

It is obvious that two important parameters in frequency control can then be mentioned: droop value and size of generation unit. Generally, droop value is defined by operator of system between 4 and 6%. Therefore, rated power of plants has to be overdesigned to guarantee frequency performance.

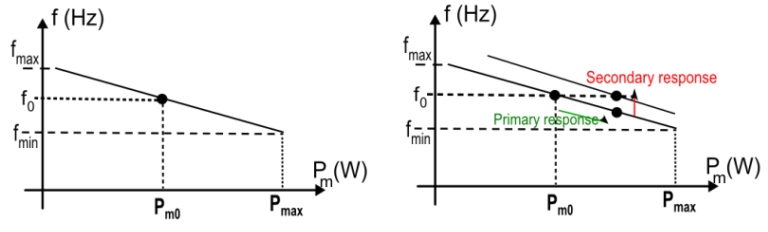

(a) (b)

Figure 1.1 (a) Droop characteristics of power source (b) secondary control description

$$\Delta\mathbf{P_m} = \mathbf{P_m} - \mathbf{P_{m0}} = -\frac{\mathbf{P_{max}}}{\mathbf{s_d}.\mathbf{f_0}}.\Delta\boldsymbol{f} \quad (1.4)$$

$$\boldsymbol{s_d}(\%) = \frac{\Delta f/f_0}{\Delta P_m/P_{max}}.\mathbf{100} \quad (1.5)$$

$$\mathbf{K} = \frac{\mathbf{1}}{\boldsymbol{s_d}}.\frac{\boldsymbol{P_{max}}}{\boldsymbol{f_0}} \quad (1.6)$$

1.2.2 Secondary frequency control

Several seconds after disturbance, frequency reaches a different stable value from the nominal one. Next, secondary control is turned on to bring the frequency back to 50 Hz. In France, this control will turn on within 30 seconds after the disturbance [5], [6]. This control changes the reference of power supply (see Figure 1.1b).

The primary and secondary controls are represented by PI controller in (1.7) [1], [7]. Proportional gain of PI controller (K_p) represents the primary frequency control and K_p is equal to the inverse of droop value ($K_p=1/s_d$). The integral gain (K_i) of the controller corresponds to the inverse of the time response of the secondary control.

$$\Delta \mathbf{P}_m(s) = -\left(K_i + \frac{K_p}{s}\right).\Delta f \tag{1.7}$$

Frequency response and participation of generation unit in primary and secondary frequency controls are presented in Figure 1.2. At time t0, the active power of generation unit is larger than load power so frequency drops from its nominal value of 50Hz. Then, frequency reaches its new value and remains stable with some steady state error until time t1. Active power of generation unit is increased (or decreased) from its reference power during primary frequency control (from t0 to t1 in several seconds). This active power deviation is called primary power. In a second time, secondary frequency control will turn on at time t1 and resume frequency back to its nominal value (50Hz). When secondary control is turned on, primary power decreases and secondary power increases.

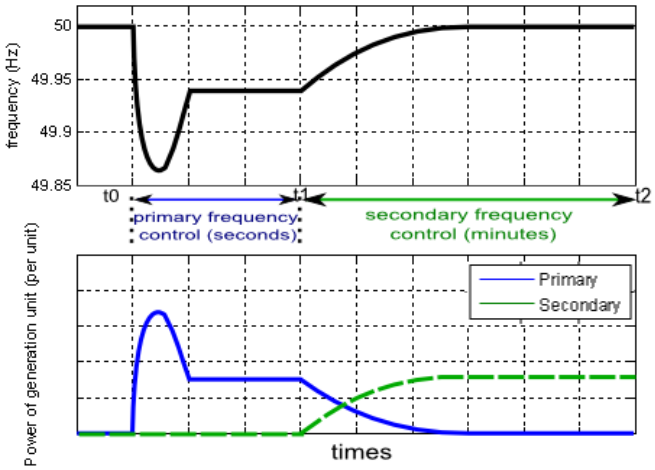

Figure 1.2 Frequency control (primary and secondary controls)

The secondary frequency control is not applied to all sources in a power system [8]. Some sources are merely controlled by primary and tertiary controls.

1.3 Micro power system (micro grid)

In modern life, electricity is one of the fundamental necessary needs of people. Everything around us needs to be powered and electricity happens to be the main source. Furthermore, electricity is a vital part to drive a business. The system which produces, transfers, and consumes energy is called electrical power system. “Electrical power systems are real-time energy delivery system” [9]. The customer has to consume energy at the same time as it is generated with equivalent amount which is the definition of real-time system. The power system is generally separated into three parts: generation, transmission, and distribution. Power plant (generation unit) produces energy which is delivered to different types of costumer or end use (distribution unit or load) by transmission line. Power systems are installed in every country around the world for supplying energy. Electrical power system in each country is in a very large scale and complex and has different characteristic and size. Loads, which are the end users of electricity around the country; are mostly far away from the power

plants which have been spreading allocated at selected appropriate places around the country to guarantee power quality and stability. Because of its complexity, generators and loads which locate within close geographic proximity of each others have then been grouped and represented to a main power system as a controllable load and a generator station [10]–[12]. This grouped power system is called micro power system or micro grid.

1.3.1 Characteristics of micro power system

Micro power system consists of micro sources, loads and transmission system. It can be classified into three groups: Isolated, Islandable, and Non-synchronous microgrids [13]. Isolated or islanding microgrids which do not connect to the utility grid and employ only in isolated mode like stand-alone system are installed in remote areas or islands [11]. Islandable microgrids are the micro power system which can operate in two different modes: islanding mode or connected to the utility grid [12], [14], [15]. Moreover, this system can participate in utility grid (consume and supply energy to utility grid). Non-synchronous microgrids will only consume energy from utility grid but they cannot inject energy back to it.

Stability of frequency of micro power systems in grid connected mode is guaranteed thanks to the high short-circuit power of the main grid. Micro power systems sometimes disconnect to main grid following a fault. Islanding micro power system can then be reconnected to main grid if voltage drop is below 3%, frequency variation below 0.1Hz, and phase-angle error below 10 degree for micro grid with distributed generation units in 1.5MW to 10MW plants [16]. The transition between grid connected mode and islanding mode is quite remarkable but it will not be considered here. Only isolated micro power systems are elaborated in this thesis thanks to their high frequency variations [15]. Two main characteristics of islanding micro power systems induce a high sensitivity to load and production variations [17]:

- A leak short-circuit power: short-circuit power or shout-circuit capacity (SCC) is the ratio between the square of voltage and the equivalent impedance of network (generator, load, transmission line, and transformer) [18]. Transmission voltage in islanding power system is very low. Furthermore, the number of generators connected in parallel is limited, so the equivalent impedance of network is high. According to these two characteristics, short-circuit capacity of islanding micro grid is very small.
- Small equivalent inertia of the grid: variation of frequency depends on unbalance power between generation and load and the inverse of equivalent inertia. This last parameter of power system is defined from the moment of inertia (J) of all rotating machine in power system. In islanding micro power system, the number of thermal generator is limited and its inertia is small. Consequently; the equivalent inertia of such a power system is relatively small.

The equivalent inertia has a great influence on frequency variation in micro grids. Inertia of each rotating machine (generator or motor) ($H_i^{S_{ni}}$) in MWs/MVA is calculated from moment of inertia (J_i), nominal rotation speed (Ω_{0i}), and nominal power of the machine (S_{ni}) in (1.8), where i denotes the index of each rotating machine [19]. Kinetic energy of all rotating machines (E_{eq}) (n for generator and m for motor) in MW.s is defined from inertia and nominal power of all rotation machines in (1.9). Finally, equivalent time characteristic (M_{eq}) and equivalent inertia (H_{eq}) of power system are calculated in (1.10), where M_{eq} equals to twice of H_{eq} [1], [19].

$$\boldsymbol{H_i^{S_{ni}} = \frac{\frac{1}{2}J_i\Omega_{0i}^2}{S_{ni}}} \tag{1.8}$$

$$\boldsymbol{E_{eq} = \sum_{i=1}^{n}(H_i^{S_{ni}}.S_{ni}) + \sum_{i=1}^{m}(H_i^{S_{mi}}.S_{mi})} \tag{1.9}$$

$$\boldsymbol{M_{eq} = \frac{2.E_{eq}}{VA_{base}}} \quad \text{or} \quad \boldsymbol{H_{eq} = \frac{E_{eq}}{VA_{base}}} \tag{1.10}$$

Microgrids is an attractive system to be used in rural remote areas and islands. Microgrids have many advantages. For instance, they require small capital investment; especially can offset the need for new conventional generation. Furthermore, it can coordinate in the reduction of transmission system congestion, support the local voltage, and improve power quality resulting in the enhancement of local power reliability [20]. Fuel consumption will also be reduced because renewable energy can be appropriately integrated with it. As grouped loads are quite known; it enables to design an appropriate renewable energy generating system to cope with the demand. Besides, the improvement in power quality is improved because transmission loss is small (loads and generation unit are not far away). The micro power system is also claimed to have a high reliability in operation as it is able to maintain the operation during or after accidental problems or disaster occurred to the main grid [11].

There are many microgrids around the world which have different sizes as presented in Figure 1.3. It can be seen from the illustration that about 32% of the total are small and very small systems. Microgrids of these sizes, which are easy to design, implement, and operate; usually have been installed in small remote areas with least problems. Notwithstanding with this fact; the majority of micro power systems are in large and very large scale (34% and 19% respectively) which are more difficult and complicated in design and operation. However, they have profound impacts on the future of energy utilization of the world. This thesis has therefore been designed to undertake study for the development of these majority systems.

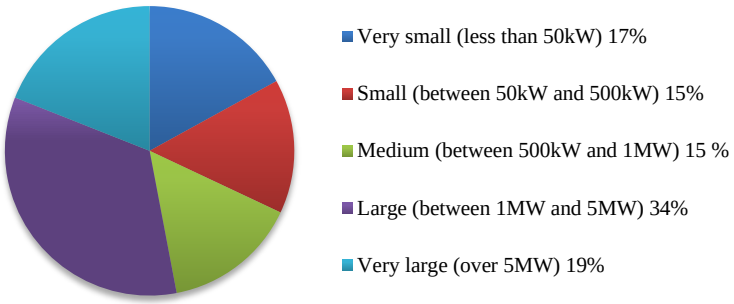

Figure 1.3 Sizes of micro grid around the world [11]

1.3.2 The energy mix in micro power system

The power generations of micro power system is the mixture of different energy. At least one of multiple power sources of micro grid is a renewable energy that is zero-emission generation sources [11]. Renewable energy refers to infinite natural resources which can be naturally replenished; such as, solar, wind, falling water, plant materials (biomass), and heat (geothermal), etc. Although renewable energy cannot run out, it is not available all the time and everywhere. It depends on the weather and geographic. Therefore, renewable energy can be called intermittent energy.

Number of mixed energy of various renewable energy types (Fuel cells, wind energy, photovoltaic) and non-renewable energy types around the world is presented in Figure 1.4. More than 50% are renewable energy which has been installed around the world. Very small, small, and medium micro power system generation plants can be relied on this energy up to 100%. Wind energy is the most popular renewable energy which is accounted at 30%. Moreover, penetration rate of renewable energy can be high in some micro power systems because of the connection with wider power system. For isolated micro power system, penetration rate of renewable energy reduces because of the instability problem when size of micro grid increases. For example, power is produced by wind and solar for 100% in 100kW micro power system in Chengde and Zhangbei in China against 6%-14% in 4MW-12MW Cape Verde wind-diesel systems in Cape verde Islands, Republic of Cape verde [11]; and wind penetration is just at 18% in 13.6MW King island micro grid in Tasmania, Australia. However, in small micro power system with 100% sustainable energy, energy storage is necessary, for

example, 180kWh and 400kWh lithium battery are installed in Chengde and Zhangbei micro grid respectively.

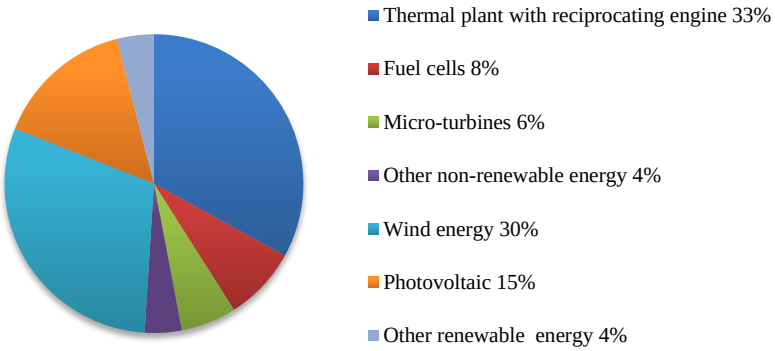

Figure 1.4 Composition of microgrid installation around the world (focus on renewable energy) [11]

The mixed energy of large and very large micro power system in different French overseas departments and territories (Corse, Guadeloup, Guyane, and Martinique) are shown in Figure 1.5. All power systems except in Corse are isolated. Power generation plant in Corse (an island in the Mediterranean Sea) bases on the interconnection of 32.9%. Main energy source is oil and gaz (thermal) in Corse, Guadeloup, and Martinique which have been estimated at about 50% but hydroelectric power generation is the dominant source in Guyane. This two energy sources have to be connected to synchronous machine which normally has some inertia which is able to absorb some load variation. It therefore is advisable that the main power generation of micro power system should be energy source coordinated with rotating machine. Although hydroelectric is one of renewable energy and does not produce greenhouse effect gas as the same as thermal plat do, its installation requires an enormous area for construction of a huge dam. It undoubtedly creates some severe effects on the present worldwide environmental situation such as the destruction of limited forest areas, animals and human's habitat around the plant area.

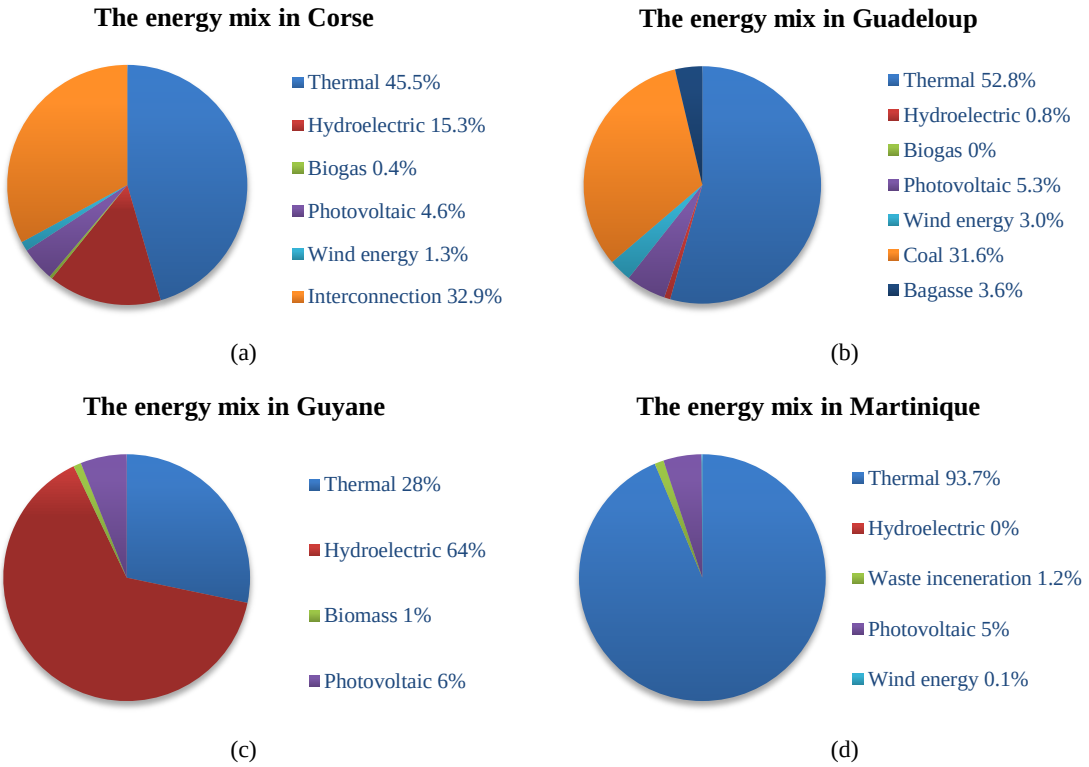

Figure 1.5 Mixed energy in different power system (a) Corse (b) Guadeloupe (c) Guyane (d) Martinique in 2012 [21]–[23]

In spite of the possibility to use others renewable energy sources such as solar and wind energy to produce electricity to micro power system, their penetration rates are very low (less than 10%) because of reliability and stability problem. Moreover, these sources are quite promising for the replacement of thermal energy (gas and oil) which occurred to be a limited source. For example, penetration rate of photovoltaic power plant should be developed to be able to replace the thermal generating source (93.7%) in micro power system of Martinique. However, the increasing of solar energy tends to induce frequency instability problem which will be elaborated in the following topic.

1.3.3 Microgrids in Thailand

Electrical power generation and transmission in Thailand are operated by the Electricity Generating Authority of Thailand (EGAT) under the Ministry of Energy. About 45% of installed generating capacities are power plants of EGAT which compose by 3 thermal power plants, 6 combined cycle power plants, 22 hydropower plants, 8 renewable energy plants, and a diesel power plant. EGAT purchases other 55% of electricity generation from Independent Power Producers.

Electricity generation in Thailand is profoundly relied on thermal energy at around 90% of energy; with mixed composite of: 70% natural gas, 10% coal, and about 2% oil [24], [25]. Renewable energy takes part only 8% in energy mixed and mostly is hydroelectric energy (about 5%). In 2011, renewable energy (excluded hydroelectric) reached 3.7% from 0% in 2001 [26]. Attractive renewable energy is biofuels and co-generation from biomass and biogas which are mostly in operation by private sector. According to energy mixed, Thailand energy system is not quite sustainable and reliable because natural gas is imported form Myanmar. To make independent energy system, renewable energy happens to be a sound promising source. Furthermore, it is obviously that generation capacity of sustainable sources have to be increased because of the continual rising of power demand and green energy extension target according to the Power Development Plan (PDP) lunched in 2010 [24], [27], [28]. National Renewable Energies Development Plan 2008-2022 (REDP) has been ongoing implemented to bring renewable energy application up to 25% of energy mixed in 2022 for all sectors (electricity production, transports, and heat) [29]. And it will be 7.3% of electric generation in 2030 [26]. To increase renewable energy, smart grids and microgrids are the attractive power systems for the integration of this energy. Moreover, isolated microgrids with renewable energy are quite appropriate for most remote areas in Thailand where have not yet had electricity. Present microgrids implemented in Thailand is mostly small system (about 10-100kW) with PV-diesel based hybrid system [25]. However, many large microgrids are ongoing developed in the universities under the government sponsorship with little in private sector [30] and has not been yet in service [11].

1.3.4 Frequency variation issue according to intermittency

Islanding micro power systems are weak in frequency stability because of its own characteristics. Frequency is very sensible to variations of active power of productions or loads. As a matter of fact, power from renewable energy (wind, solar, etc) is quite instable but it is increasingly installed as one production of micro power system. Undoubtedly, power quality (frequency and voltage) is affected [11], [31]–[33]. When intermittent energy production is increased or installed in isolated micro grids, other production sources have to increase their production or new generation plants have to be installed. For example, for every 10% wind penetration, other generation sources about 2%-4% of the installed wind capacity is needed for a stable power system operation [32].

Renewable energy can be installed with limitation penetration rate to assure power quality (such as voltage and frequency performance). Frequency deviation should be in a range of ±0.5Hz for system with wind energy [34], [35] or 1% of nominal frequency [33]. Penetration rate of wind turbine is classically limited at 20% according to economic and technology constraints [17]. In current French islanded micro grid (presented in previous topic), the penetration rate of renewable is limited at 30% [36]. Renewable energy induces an extra cost for the reserved sources to guarantee stability of

power system. For example, thermal plant has to be overdesigned to guarantee frequency performance. Installation of intermittent energy with penetration rate of 10 and 30% will cause additional costs of 225-600 M€/year and 300-750 M€/year respectively [2].

Many studies analyzed frequency variation corresponds to the consequence of power variation of load or loss of production supply which is a step variation [37]–[39]. However, active power of renewable energy fluctuates quite slowly; for example, power variation of wind energy can be about 100kW for 10 seconds [2], which causes different impacts on system frequency. Active power of wind energy is characterized in [40]. Frequency of fluctuation can be separated into three regions: low (below 0.01 Hz), medium (0.01-1Hz), and high (over 1 Hz) frequency. Most of power fluctuation of wind energy fluctuates at low and medium frequency. Frequency variation has large affected from medium frequency fluctuation [41]. Nevertheless, the inertia of turbine generator will absorb the high fluctuation of active power [40].

1.4 Energy storage in micro power system

"Electrical Energy storage (EES) (or energy storage) refers to a process of converting electrical energy from a power network into a form that can be stored for converting back to electrical energy when needed" [32], [42], [43]. According to green energy trend, energy storage has become an attractive source for transportation and utility applications. Plug-in electric hybrid car and electrical car have been developed for decades and already in service in order to reduce CO_2 emission and fossil oil consumption. Batteries are quite suitable in transportation domain because of their modularity and portability even though their life cycle is quite short [32]. For utility service, energy storage technologies play an important role in addition of renewable energy to power system and development of smart-grids, smart-micro grids, and smart houses [44]–[46]. Grid connected energy storage will rapidly increase and will reach 6GW in 2017 and will be over 40GW in 2020; according to HIS report [47]. Increasing trend projection of energy storages installation in microgrids as illustrated in Figure 1.6 based on the growth of renewable energy in this grid.

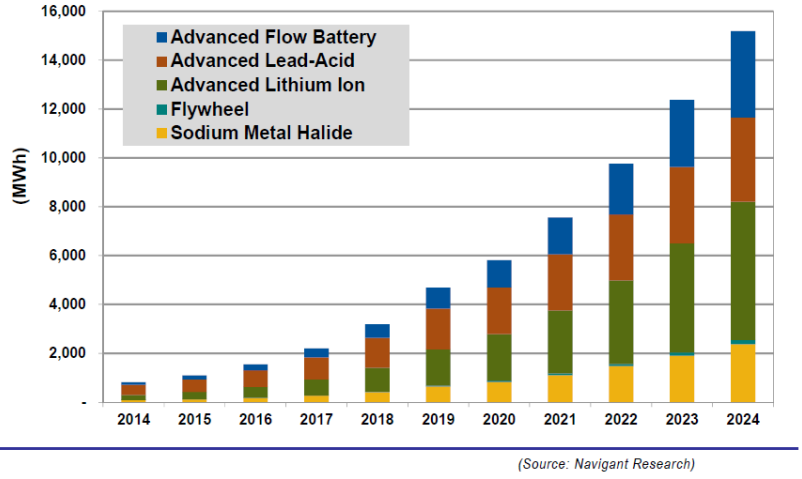

Figure 1.6 Trend of energy capacity of installed ES in Microgrids by technology in world markets 2014-2024 [48]

Various technologies of energy storage are firstly presented and followed by their different applications in micro grids. Finally, different control strategies for frequency control of energy storage will be summarized.

1.4.1 Energy storage technologies

Energy storage system can be categorized by storing form of energy into five groups: mechanical, electrochemical, chemical, electrical, and thermal storage [44]. However, electrochemical and chemical energy storage can be grouped into one group of chemical energy storage system [43]. Different energy storage transforms different forms of energy to electricity and vice versa. There are

two function modes of energy storage. It is in "charge" mode when electrical energy from power system is converted in other forms and stored in energy storage. On the contrary, when energy is transformed to electrical energy in order to inject to the system, it then is in "discharge" mode.

1.4.1.1 Mechanical energy storage

Electrical energy is stored and converted back in potential or kinetic energy by rotating part of the generator or motor (turbine) for mechanical storages such as Pumped Hydro Energy Storage (PHES or PHS), Compressed Air Energy Storage (CAES), and Flywheel. Energy from rotating part is stored in different media. Pumped hydro energy storage of which capacity is accounted around 99% of global energy storage installation [44], stored energy in form of water in upper level and flow down to lower reservoir while passing through the micro turbine to release energy. Water is then pumped back to upper reservoir to store in form of potential energy. This energy storage technology has been developed for high power applications (a few less than one-tenth of GWh or 100 of MW) [49]. There are number advantages of PHES such as high efficiency (70-85%), very long life time, long storage period, practically unlimited cycle stability of the installation, and relatively low capital cost per unit of energy generated [43], [44], [49]. However, it need wide space area and a high cost for construction as well as risk of environmental deterioration issues.

For Compressed air energy storage, turbine of generator operates reversely as motor to compress and stock air in reservoir for later use [32]. And compressed air is then be used in combustion process to produce energy back to the system. The advantages and disadvantages of this energy storage are similar to PHES with high efficiency around 70-89% [43]. However, this technology is dependent on fossil fuel. It has to be connected to gas turbine plant and cannot use with other power plants [43]. This happened to be its prime draw back.

For the last technology, flywheel stores electrical energy in form of kinetic energy in rotating mass. The stored energy in flywheel depends on the constancy of speed as well as its mass and configuration [43], [50]. Rotating part is accelerated by motor to store energy. On the contrary, it will be slowed down by the same motor which will act as a generator to pull out its stored energy. Notwithstanding with its very high efficiency of around 90-95% [43], flywheel has a quite high self-discharge loss. It therefore has been considered to be an unreliable energy storage type.

1.4.1.2 Electrochemical energy storage

Electrochemical energy storage or battery converts electrical energy to chemical energy by electrochemical reactions and vice versa [49]. It can be classified into two groups: secondary and flow batteries [44]. Rechargeable secondary batteries consist of negative and positive electrodes (anode and cathode) and electrolytes. When battery is in discharge mode (supply energy to external circuit) and connects to load, oxidation reaction between ions of electrolyte and cathode is occurred at anode (negative electrode), and electrons are then released. While the cathode substance, ions and free electrons are combined at cathode side (positive electrode) which is called reduction reaction at the same time. Therefore, electricity flows through load from cathode to anode which is the reverse direction of electrons. On the contrary, oxidation reaction (release electrons to external) and reduction reaction (consume electrons from external are occurred at cathode and anode, respectively, during charging. Various technologies of secondary battery are Lead acid battery (Pb-acid), Nickel cadmium battery (NiCd), Nickel metal battery (NiMH), Lithium ion battery (Li-ion), Sodium sulphur battery (NaS), Metal air battery (Me-air), and Sodium nickel chloride battery (NaNiCl). The difference of technologies is classified by different materials of cathode and anode and electrolytes. The characteristics of all secondary batteries are compared in [32], [43], [44]. For this batteries type, electrodes are the active elements which cause the transformation of energy for charge and discharge modes. In case of flow battery types, "chemical energy is stored in one or more electro-active species which are dissolved in liquid electrolytes" [44].

Flow battery consists of two electrolytes which have been stored in different tanks, and a cell of two electrodes (positive and negative) and a micro-porous membrane between the two electrolytes. The membrane will screen ions from electrochemical reaction which can pass through it in order to create an electrical current [32], [44], [49]. Electrolytes are pumped and pass through the cell in order to create reduction-oxidation reaction and back to its particular tanks again. This battery type can be classified into two groups: redox (reduction-oxidation) flow batteries and hybrid flow batteries. Developed electrolytes are zinc (ZnBr), sodium (NaBr), vanadium (VRB) and, more recently, sodium polysulfide [49]. Hybrid flow battery is the combination of secondary and redox flow batteries but does not consist of two different tanks of electrolyte. There is only one external tank filled with liquid electrolyte for storing only one active mass, whereas the others is stored in the electrochemical cell (electrodes and membrane module) [44].

The advantages of battery are fast time response and high energy efficiency of about 60-95% [43]. Notwithstanding with its advantages, there are numbers of inferior characteristics; such as, low energy density, small power capacity, high maintenance costs, short life cycle (about 100 to 1000 cycles), limited discharge capability, and contain toxic materials [43], [49].

1.4.1.3 Chemical energy storage

Chemical energy storage is composed with two different functions: production of fuels (hydrogen or methane) or storing energy which is equivalent to the charge mode of battery, and electricity production or discharge mode [32]. Its main working principle can described as follows: chemical A (fuels) is consumed in order to produce electricity and chemical B, and then electricity and chemical B is consumed to produce chemical A in reverse reaction [43]. It consists of an electrolyzer, a storage tank, and fuel cell or electrochemical cell (which consists of two electrodes and electrolytes). External supplies of fuel (refer to chemical A) and oxidant are passed through two electrodes (anode and cathode) in the cell. Electricity and product of reaction (chemical B) is then produced by electrochemical reaction. The reverse reaction is occurred in electrolyzer by consuming external electrical energy in order to produce fuel and store in a storage tank for future use. This energy storage can also be called fuel cells.

The structure of cell is similar to battery. However, the electrodes of fuel cells do not react and change as the electrodes of battery. They are catalytic and relatively stable [43]. Furthermore, all reactions of batteries are occurred in one closed system and there is no product of reaction flowing out while fuel cells consume reactant (fuel and oxidant) and there is reaction product flowing out. This energy storage can produce electricity as long as fuel and oxidant are supplied to the cell but capacity of batteries is limited (low energy density and power capacity) in a short life cycle.

There are many combinations of fuel and oxidant. Fuels or energy carriers of this energy storage can be Hydrogen (H_2) (so it is called hydrogen storage in some studies) or synthetic natural gas (SNG) (methane – CH_4) ,which is a secondary energy source and the oxidant is oxygen. In the electrolyzer, water is decomposed into hydrogen (H_2) and oxygen (O_2) with consumption of electricity which is called electrolysis of water for hydrogen fuel cells. Hydrogen is stocked in a storage tank as a fuel for future use. Oxygen is not stored but is injected back to the atmosphere. As it is a powerful oxidizer which requires expensive and high security storing in order to avoid flam and explosive. Hydrogen (from reserve tank) and oxygen (from air) are passes through the fuel cell to create an electrochemical reaction, which is the reverse reaction of splitting water, in order to produce water and electricity [44], [49], [50]. There are various technologies of flue cells such as Polymer Exchange Membrane Fuel Cell (PEMFC), Solid Oxide Fuel Cell (SOFC), etc. which are different in the electrolyte uses, operating temperature, design and applications [49].

The electrolysis of water and its reverse reaction can be replaced by methanation reaction to produce methane and oxygen from hydrogen and carbon dioxide (CO_2) and vice versa to produce electricity for synthetic natural gas fuel cells [44]. Furthermore, hydrogen or methane can be used as

fuel in combustion process by replacing fuel cells with gas motors, gas turbines and combined cycles of gas or steam turbines [44], [50].

Fuel cells are able to be stored in large amount of energy (up to the terawatt-hour (TWh) range). However, their energy efficiency is low (less than 50%) comparing to other energy storage types [44].

1.4.1.4 Electrical storage system

Capacitor is the simplest way in storing electrical energy. The structure of conventional capacitor is consisted of two metal plates (electrical conductors) and a dielectric (a non-conducting layer) which is quite similar to structure of battery (two electrodes and one electrolyte). When capacitor is connected to a direct-current source, energy is charged to capacitor while one plate is induced to be a positive electrode and the other plat is induced to be a negative electrode. After charging, capacitor performs as a direct-current source which can supply energy to direct-current load. Its capacity to store energy has been defined as "Capacitance" which depends on the area of two plates, the permittivity of dielectric, inverse of the distance between two plates.

The conventional capacitor has limitation in application due to its low energy density [43]. Electrochemical Double-layer Capacitors (EDLC) and supercapacitors (SC), which work similar to conventional capacitor, have been developed to enhance its energy density by using very high electrodes surface area and high-permittivity dielectric [43], [32], [49], [50]. EDLC and supercapacitors consist of two electrodes partitioned by a very thin porous separator; immersed in an electrolyte. However, there is no chemical reaction, ionic or electronic is therefore not transferred in the cell. Their terminal voltage is proportional to the State of charge (SoC). Another technology of this energy storage type is Superconductive magnetic energy storage (SMES) which store energy in the magnetic field produced by a direct current flowing through a superconducting coil [32], [44], [50].

The principle advantage of electrical energy storage systems is the very fast time response; in the range of milliseconds (both in charge and discharge modes) [44], [49]. Furthermore, they have a long cycle life (very durable: 8-10 years or up to one million cycles [44], [49]) because electrode is not degraded during normal operation as battery [32], [49], enhanced by their high efficiency (90-95% for EDLCs or supercapacitors and 85-90% for SMES [36]). Besides the prime advantages; they have wide range of operation, and high power density (SMES is the highest). Notwithstanding with all cited advantages, as electrons are not confined by chemical reactions, energy density of this storage is therefore very low, and they can be completely discharged (high self-discharge loss; 5% per day [49]) which will cause very large terminal voltage variation [32], [43], [44], [49].

1.4.1.5 Thermal energy storage

Thermal energy storage (TES) stores energy in a form of heat by different methods in an insulated repository [44]. TES can be classified by operating temperature of the energy storage medium (with comparing to the room temperature) into two groups: low and high-temperature TES [43]. Energy or heat is stored by changing temperature of the storage medium which can be a liquid (such as water or thermo-oil) or a solid (such as concrete or the ground). Electricity is consumed to cool or heat medium storage for future use. The capacity of this energy storage system is defined by the specific heat capacity and the mass of the medium used. Various technologies of this energy storage are storage of sensible heat, storage of latent heat, and, thermo-chemical and absorption storage. The most well-known thermal energy storage is storage of sensible heat.

Thermal energy storage is friendly to environment but its overall efficiency is very low (30-60%) [43]. This energy storage is widely spectrum of applications such as heating and cooling system in aerospace, industrial application, and electricity production integrated with renewable energy. For example, a synthetic oil or molten salt is used to store energy from solar thermal power plants to smooth down the power production and extend the production period (1-10 hours after sunset) [32].

Besides, thermal energy storage has also been used in residential and industrial in order to reduce electricity consumption during peak demand.

1.4.1.6 Comparing different technologies of energy storage

Different energy storage systems can be compared in technical or economic approach. The cost investment of various technologies was studied in [19], [43], [50], [51], which will not be taken into this study. The technical characteristics of energy storage: energy density or specific energy, power density or specific power, energy efficiency, life cycle (life time), and self-discharge are elaborated as follows.

- Specific energy (Wh/kg) and power (W/kg) are the energy to weight ratio and the power to weight ratio respectively. Power density refers to the ability of energy storage to provide instantaneous power [31]. While energy density specifies the ability to provide continuous energy over a period of time. Energy storage with higher power density can discharge large amounts of power on demand. And high energy density indicates that energy storage technologies can discharge energy for a long period.
- Energy efficiency (%) is the ratio of released energy to stored energy [49] or the output and input electricity without concerning of self-discharge [43].
- Life cycle or durability (cycles) is the number of times which energy storage can release the designed energy level after each recharge. One cycle means one charge and one discharge [49].
- Self-discharge is the ratio of initial stored energy to dissipated energy over a non-use time [49].

The characteristics of various technologies of energy storage are summarized in Table 1.1. The energy storages which have the highest energy efficiency are flywheel and EDLC. On the contrary, CAES has very low efficiency and NiMH is the lowest efficiency in battery technology. As having mention previously, mechanical energy storage technologies (PHES, CAES, and flywheel) are very durable. Battery technology has short life cycle while lead acid battery (Pb-acid) is the shortest in this group. Although flywheel has long life time, its self-discharge is very high. EDLC also has very self-discharge notwithstanding with its very high efficiency. Self-discharge can be neglected for PHES and VRB (vanadium redox battery).

Table 1.1: Characteristics of energy storage systems [32]

Type	Energy Efficiency (%)	Energy Density (Wh/kg)	Power Density (W/kg)	Cycle Life (cycles)	Self-Discharge
Pumped hydro (PHES)	65-80	0.3	-	>20 years	Negligible
CAES	40-50	10-30	-	> 20 years	-
Flywheel (steel)	95	5-30	1000	> 20000	Very High
Flywheel (composite)	95	>50	5000	> 20000	Very high
Pb-acid	70-80	20-35	25	200-2000	Low
Ni-Cd	60-90	40-60	140-180	500-2000	Low
Ni-MH	50-80	60-80	220	< 3000	High
Li-ion	70-85	100-200	360	500-2000	Med
Li-polymer	70	200	250-1000	> 1200	Med
NaS	70	120	120	2000	-
VRB	80	25	80-150	> 16000	Negligible
EDLC	95	<50	4000	> 50000	Very High

Furthermore, power and energy density of all energy storage technologies can be plotted in logarithm chart which is called Ragone chart as shown in Figure 1.7(a) [52], [53]. The diagonal axis represents discharge time which signifies the duration of energy storage discharging at rated power. Energy and power density in ratio to volume is plotted in Figure 1.7(b). Mostly energy storage

technologies have either high energy density or high power density, but lithium ion battery (Li-ion) has quite high both energy density and power density. This characteristic makes lithium ion battery the mostly uses in mobility application because it needs small weight and volume for high energy and power (see Figure 1.7(a) and (b)).

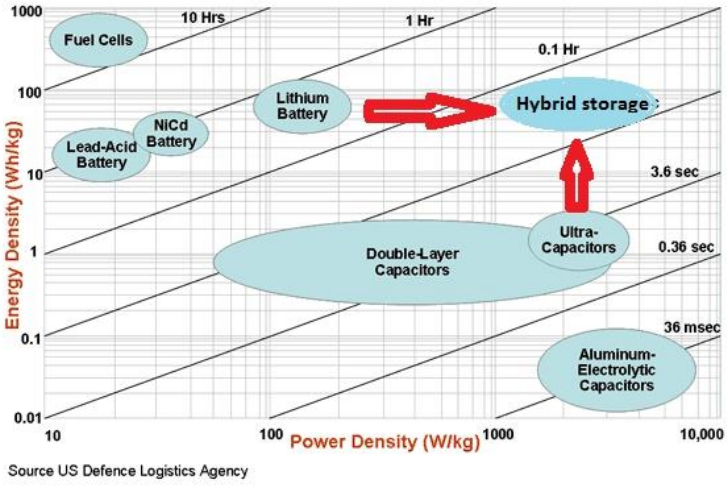

(a)

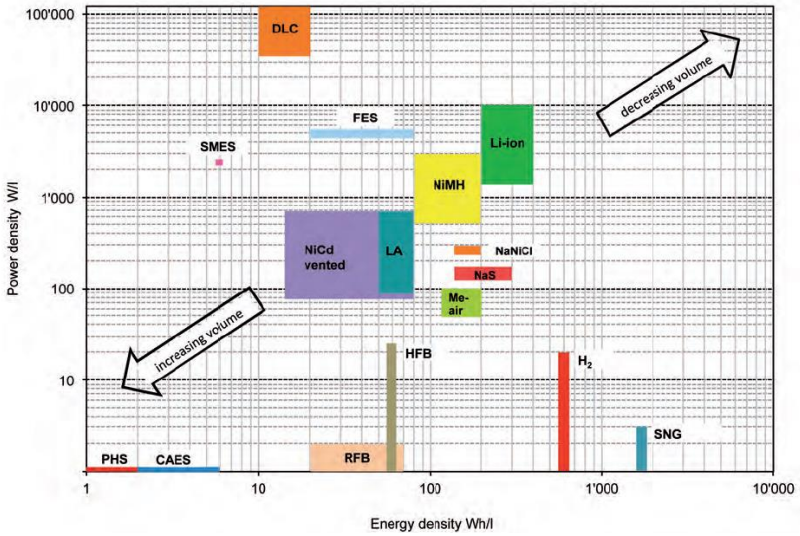

(b)

Figure 1.7 (a) Ragone chart of different energy storage technologies [52] (b) Chart of power density and energy density in ratio to volume for various energy storage technologies [44]

Technologies of energy storage can be separated into two groups: high energy density and low power density, and, low energy density and high power density. Energy storage with high energy density and low power density like batteries is suitable for a long period service (about an hour) but its time response is large. Energy storage with low energy density and high power density such as supercapacitor and flywheel provides fast time response but it cannot be in service for a long period (in several seconds to minutes). Choosing technology of energy storage depends on desired service.

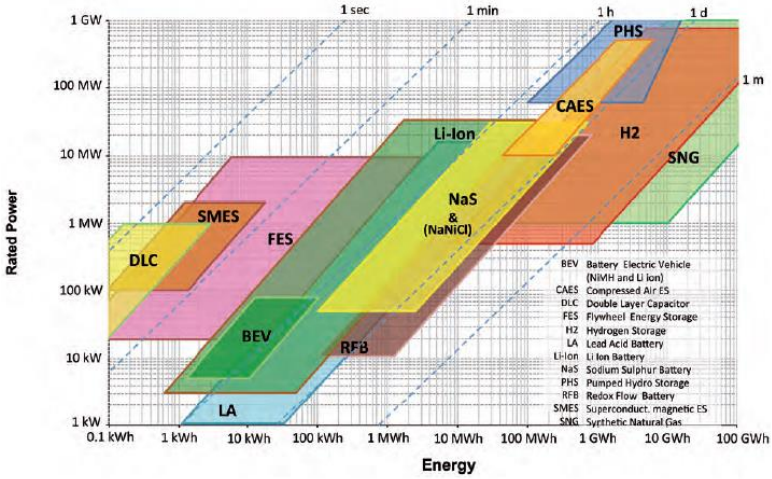

Figure 1.8 Comparison of rated power, energy content and discharge time of different energy storage technologies (Fraunhofer ISE) [44]

For better understanding, rated power and energy content of energy storage system for present and future applications are plotted in logarithm diagram presented in Figure 1.8. Discharge time is also presented in the diagonal axis. This chart will be used in the following study to select energy storage technologies related to the desired applications. Discharge time response divides energy storage into three groups: short discharge time (seconds to minute; such as, electrical storage system and flywheel), medium discharge time (minutes to an hour; such as, flywheel, Li-ion battery, etc.), and long discharge time (hours to months; such as, PHES, CAES, chemical energy storage, etc.) [44]. Energy storage technologies can be compared with other criteria; such as, technical maturity [43], [44], reliability [49], and environmental impact [43], [49].

Furthermore, energy storages have some limitations. They cannot absorb or supply energy if they are already full of or empty respectively. Therefore, either energy stored or energy used of energy storage has to be elaborated. State of Charge (SoC) and Depth of discharge (DoD) are introduced. State of Charge signifies level of energy which remains in storage comparing to the total capacity of energy storage in percentage. Depth of Discharge is the contary of SoC. It defines how much energy is used or discharges in percentage to the total capacity. In control system, SoC is one important parameter which has profound impacts on the control strategy of energy storage. For example, if energy storage cannot supply energy because SoC is very low, control strategy has to recharge storage as soon as possible and other sources have to be spared to supply compensating energy.

1.4.2 Applications of energy storage in micro grids

Energy storage technologies have been classified by their characteristics in the previous topic. However, they can be grouped by their applications. Energy storage applications can be divided into two group: transportation and utility service [32]. In this thesis, only utility application is highlighted.

1.4.2.1 General applications for utility services

Many studies classified utility applications of energy storage by its connection point which is at generation-side (or electricity utility industry application), and demand-side (or grid connected end user application) applications [19], [31], [44], [46], [54]. For end user, application of energy storage can be as back-up power, time-shift (storing, consuming and selling during off-peak and on-peak periods), peak shaving (reducing peak load), power quality (protecting loads from voltage and frequency variation, harmonics, etc.), and demand response (turning off part of load from order of the grid operator while using ES to take over the supply of this load). It also can be in service of primary reserved power (to maintain grid frequency), secondary reserve power, reserved capacity (in case the normal electricity supply resources become unavailable), Grid stability & performance/ Ancillary services to support transmission, time-shift (storing and selling during off-peak and on-peak period),

and peak-shaving, for generation side [46]. From the technical point of view, the function of utility application or period of energy storage in service can be one of the criteria to classify energy storage system, which are: power quality (to ensure the quality of power; for a few seconds), bridging power (or buffer and emergency storage; to ensure service continuity; for seconds to minutes), and energy management (to decouple synchronization between power generation and consumption) [43], [49].

As a matter of fact, one of the general applications of energy storage is time-shift. When energy storage is applied for end user application, it is called load levelling [32]. During low demand or off-peak period, energy storage is charged and then is discharged to cope up with the peak demand during on-peak period (high price of electricity). This application of energy storage is called energy arbitrage when energy storage is connected at generation side. Energy is charged during cheap electricity price and exploited at a higher price. Furthermore, energy storage can be used in primary frequency control as an ancillary service because of its fast time response [32], [51].

Hybrid energy storage system has also been proposed in some studies. As energy storage is needed to guarantee the stability of power system; it therefore should be characterized by both high energy and power densities. However, there are none mature technologies of energy storage having both two characteristics. Such hybrid energy storage system, with combination of battery and supercapacitors or flywheels, mostly used for transportation have been studied for micro grids [15]. Adding of the other energy storage will coordinate in regulating imbalance of power, increases its life cycle as well as reduces power losses but undoubtedly induces higher economic cost. Hybrid energy storage system with VRB battery is used in power system from wind energy. Depth of discharge (DoD) of VRB is decreased and power losses of energy storage system are then reduced [15]. Hybrid energy storage (Fuel cell plus battery plus supercapacitor) is proposed for residential demand to compensate PV [55] in order to reduce the size of reversible fuel cell and battery.

1.4.2.2 Applications for micro power systems

Many studies have proposed various different strategies for energy storage in micro power system. Two principal applications of energy storage in micro grids are power quality for system with renewable energy and in service with it. For system without renewable energy impact, energy storage maintains the stability in both frequency and voltage after transition from connected mode to islanding mode [12], [56]. It can support the thermal plant in frequency regulation during islanding micro grid. It has been proofed that energy storage is a relevant source for replacing or reducing some production of diesel generators in order to reduce the emission of CO_2. Past studies and current projects of energy storage in frequency regulation in micro grid (in both grid connected mode and islanding mode) are summarized in [19]. As having mentioned earlier that energy storage technologies used in micro power system are: battery, flywheel, supercapacitors, and fuel cells. The selection relies on application criteria and their characteristics accomplished with the feasibility. For instance, fuel cell is not widely used because of its expensive investment cost [11]. Flywheel has been used in micro grid for primary and secondary frequency controls in order to avoid load shedding because of its fast response [57].

For micro grid with renewable energy, energy storages has been considered as a mean to increase the ratio of renewable energy integration while maintaining a high quality of reliability by keeping the balance between power production and demand [11], [31], [32], [46], [58], [59]. Energy storage coordinates to smooth power of renewable energy and make it as a constant power source. For instance, a battery of 50kW-150kW is installed in a small micro grid which consists of diesel generator of 70kW, photovoltaic, and load to compensate imbalance of active power [34].

In case of fragile isolated micro power system, energy storage is a very promising production source in remote isolated areas, for regulating and increasing the quality of the current (constant and continuous voltage), for renewable applications [49]. Mostly energy storages is installed in rural area with small micro grids (100-800kW) to guarantee the stability according to variation of renewable energy power [60]. All examples of islanding microgrids presented in Table 1.2 have renewable

energy but energy storage is needed only in some projects. As having mentioned earlier, thermal plant can guarantee power quality and stability for some penetration rate of renewable energy. To increase the capacity of renewable energy and/or decrease thermal energy production for environmental reasons, energy storage is an appropriate source.

Table 1.2: Current isolated microgrids with renewable energy [11], [22], [23], [61], [62]

Microgrids project	**Site**	**Energy mix**				
		thermal	**Wind**	**Solar**	**Other production**	**Energy storage**
Verve Energy's Bremer Bay wind diesel system	Australia	1.3MW	660kW	-	-	-
Cape Verde wind-diesel systems	Cape Verde Island	4-12MW	600-900kW	-	-	-
Lan Island Project	Thailand	500kVA	200kW	60kW	-	-
Power Corp Flores Island microgrid	Portugal	600kW	600kW	-	Hydroelectric 1.48MW	-
Gauloupe microgrid	France	382MW	27.4MW	52MW	Hydroelectric 837MW Other renewable energy 15MW	-
Gayane microgrid	France	131MW	-	1.5MW	Hydroelectric 114MW Biomass 2MW	-
Kythnos Microgrids	Greece	5kW	-	12kW	-	5kW
King island Microgrid	Australia	-	2.45MW	110kW	-	1MWh
Miyako project	Japan	300kW	-	750kW	-	3.058kWh

Generally, in isolated microgrids with energy storage, renewable energy is the dominant production source. In Kythnos microgrid, droop frequency control is applied to battery and SoC limitation is also applied. Whenever the SoC is too low, some loads have to be disconnected from the grid or diesel generator has to be in operation. The production of PV is limited if SoC of energy storage is very high or it is already fully charged. For Miyako project, energy storage is a dominate source of power balance or frequency regulation which will be explained in the following topic.

1.4.2.3 Sizing of energy storage

Another important question of installation energy storage in micro power system is its sizing. Installed power and energy of energy storage is designed based on different proposes. If energy storage is installed in load levelling application, energy storage has to be dimensioned by the peak load power and power production maximal. However, sizing of energy storage is done project by project and normally overdesigned. Sometimes economic approach is taken into account in sizing of energy storage [50], [51].

Furthermore, sizing of energy storage can be determined according to penetration rate of renewable, in case that energy storage is in service of ensuring stability and energy quality of system with renewable energy. For example, energy storage is dimensioned according to penetration rate of wind energy [63]. If the total power of conventional generator is much over installed power of wind turbine, wind turbine becomes passive generator of which energy storage is not needed. If 50% of

production is wind energy, sizing of energy storage relates to power rated of wind turbine. Finally, if wind power plant is the main production source, energy storage has to be designed according to the capacity of the micro grid. In [64], power rated of energy storage is defined from power maximal of photovoltaic. Moreover, sizing of energy storage and photovoltaic is designed according to frequency deviation and environmental constrain (emission of CO2) [34]. Overloading characteristic has been used in [65] to minimize power installed of energy storage (low investment cost) in islanding microgrids for primary frequency control (SoC is taken into account).

1.4.3 Energy storage system for primary frequency control in isolated micro grid

Control strategies of micro-sources and energy storage system has then an important role to play on the stability of micro grid [20]. Energy storage cannot be directly connected to the grid; an inverter is necessary for interfacing. Power electronic instruments are used to control the participation of sources in maintaining the stability of micro grid. Energy storage device coordinated with the power electronics devise is called Energy storage system (ESS). The participation of ESS or power reference is calculated from different strategies of frequency control. There are many strategies proposed for ESS. Some studies have not taken renewable energy into account but ESS is installed to coordinate in frequency regulation of diesel generator and improve frequency response [19]. As the time response of diesel generator is large [12] which profoundly affected the variation of the system frequency. Impact of renewable energy on system frequency has been analyzed and proofed to be reduced by ESS in some studies [66], [67].

1.4.3.1 ESS is the main source of frequency regulation

This strategy confides the diesel generator to operate at constant power or not supply energy, and the renewable energy is acts as the main production. ESS plays an important role in frequency regulation by balancing power production and demand. For instance, a hybrid Photovoltaic-Diesel power generation system has been operated since 1994 at Miyako Island, Japan [68], [69].

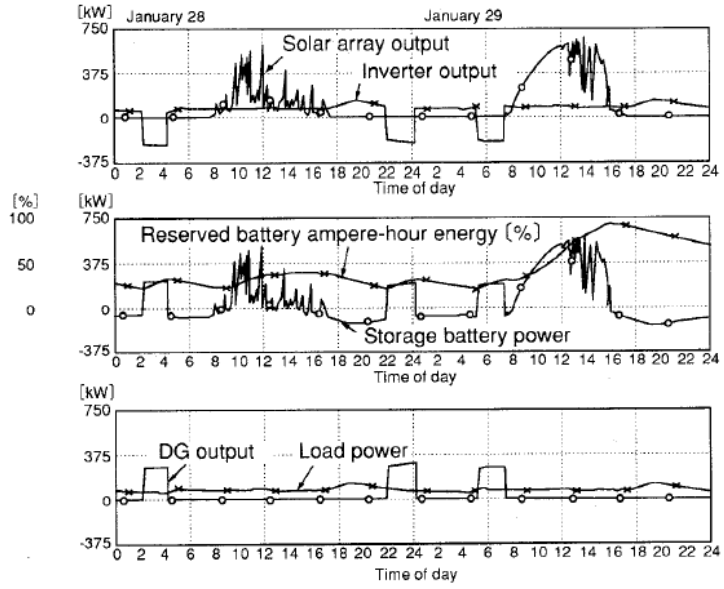

Figure 1.9 Production powers and loads during two days of Miyako Island project

The mixed energy of this system is: photovoltaic (PV) 750kW, Diesel 300kW, and Battery 3.058 kWh. The average power of load is 90kW and peak load is 200kW. The photovoltaic production is twice of diesel generator. Therefore, PV is the main source of production and battery is in service to maintain constant power production. Diesel generator is an auxiliary source which operates during critical situation. In normal operation, summation of power of PV and battery equals to power of loads. During the day (see Figure 1.9), the energy storage system absorbs energy if the power of PV more than the power of loads. Whenever there is no solar energy (during night), energy storage system

will supply energy until its SoC is below the limit. Diesel generator will then be turned on to supply power to loads and also for charging energy storage. Battery will be charged when the SoC of battery is below 20 % until its SoC is over 30 %. The diesel will merely operate at night if it is sunny during the day. It seems that diesel generator may consume much more fuel as it has to operate at high power. However, this study claimed that the fuel consumption of diesel generator (l/day) for both load supply and battery charging is smaller than in case that diesel supply only load power (battery will be charged by PV) because the diesel generates power for both load supply and battery charging less frequently.

1.4.3.2 Classical primary frequency control (droop characteristics)

Droop characteristic in topic 1.2 is applied to energy storage system in order to coordinate with diesel generator in limiting frequency variation [37]–[39]. The rated power of energy storage system is designed from the power rated of diesel generator, and droop value of diesel generator and of energy storage system [38]. Participated power of energy storage system in frequency regulation depends on the maximum power variation of load, droop value and its rated power. Therefore, energy storage system capacity has to be large enough in order to reduce the frequency variation.

1.4.3.3 ESS as impulse source

Another sizing of energy storage system method has been proposed [19]. Frequency variation is limited by injecting entire power of energy storage during several times after disturbance as shown in Figure 1.10. Energy storage system acts as an impulse energy source. Dynamic frequency equation in function with parameters of diesel generators (droop value, time responses) and parameters of power system (inertia equivalent, and load damping constant) has been proposed and are used to calculate the maximum frequency variation after imbalance between production and demand. Load power variation is the critical situation which is used in design. Energy storage system is dimensioned to reduce this maximum frequency variation to a specific value.

The participation of energy storage system which depends on frequency variation which can be divided into three zones: below 0.05Hz, between 0.05Hz and 0.2Hz, and over 0.2Hz [70]. Energy storage system will not participate in frequency regulation for frequency variation below 0.05Hz. Power of energy storage system is defined from droop characteristic for frequency variation between 0.05Hz and 0.2Hz. Finally, energy storages will supply or absorb at the full device rated power for frequency variation over 0.2Hz. Consequently, the optimal size of energy storage is calculated in accordance to this strategy and SoC limitation [70].

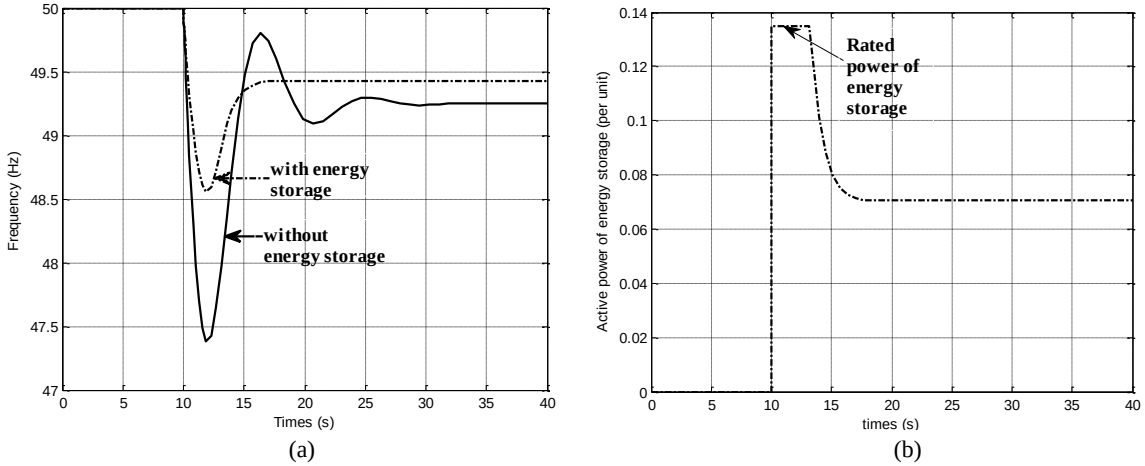

(a) (b)

Figure 1.10 (a) Frequency response (b) Active power of energy storage for energy storage as impulse source in [19]

1.4.3.4 Robust control for frequency regulation by ESS (H infinity controller)

To limit frequency deviation, the time response of frequency should be as small as possible. From the classical droop frequency control, derivative part of frequency should be taken into

frequency control consideration in order to improve the time response. Proportional and Derivative controller (PD) is applied; however, gains of this controller are quite difficult to find with the achievement all desired performance. When derivative gain is increased for better good transient response, some oscillation occurs in the response and system is more sensitive against the measurement noise. H infinity controller is then applied to ESS and/or diesel generator for fast frequency response and low frequency variation as illustrated in Figure 1.11(a) [71], [72]. H infinity controller is a robust controller and is calculated by compromising all the desired performances (such as good reference tracking, robust to measurement noise, reject disturbance, etc.). Desired performances (specifications of frequency) are fixed by the weighting function in controller design. The limitation of energy storage which is State of Charge (SoC) can also be considered in the robust controller design. H infinity controller has been proofed to be robust against measurement noise of the measured frequency. In this study, system frequency is faster and has smaller deviation than the classical droop and PD controller (with various derivative parameters (k_{d1})) as illustrated in Figure 1.11(b). In conclusion, energy storage control system has to be robust to measurement noise.

1.4.3.5 Filter strategy

According to characteristics of power fluctuation of wind energy and characteristics of system frequency in [40], [41], [66], participated power of ESS can be defined by output of high pass filter of wind power. Cut-off frequency is defined from power system characteristics. Power of wind is smooth, so frequency variation is small as illustrated in Figure 1.12. Capacity of ESS is defined from the rated power of wind energy and the maximum variation of wind power [66].

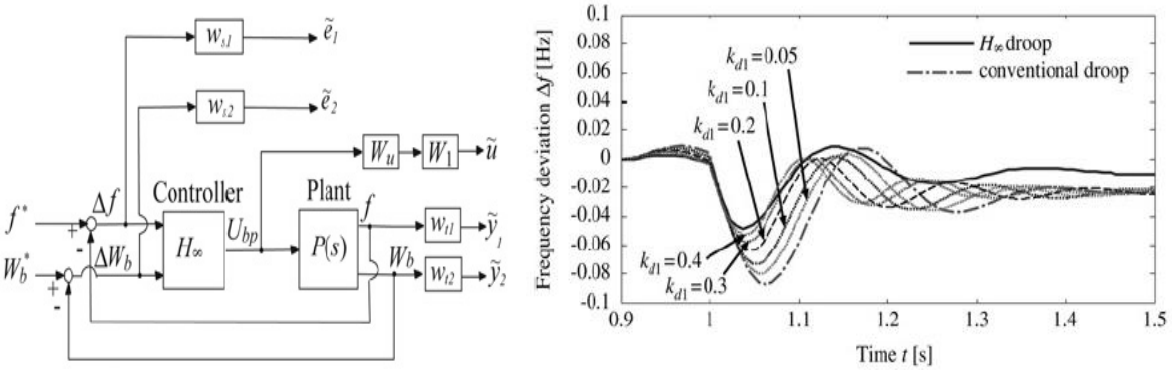

(a) (b)

Figure 1.11 H infinity controller for ESS

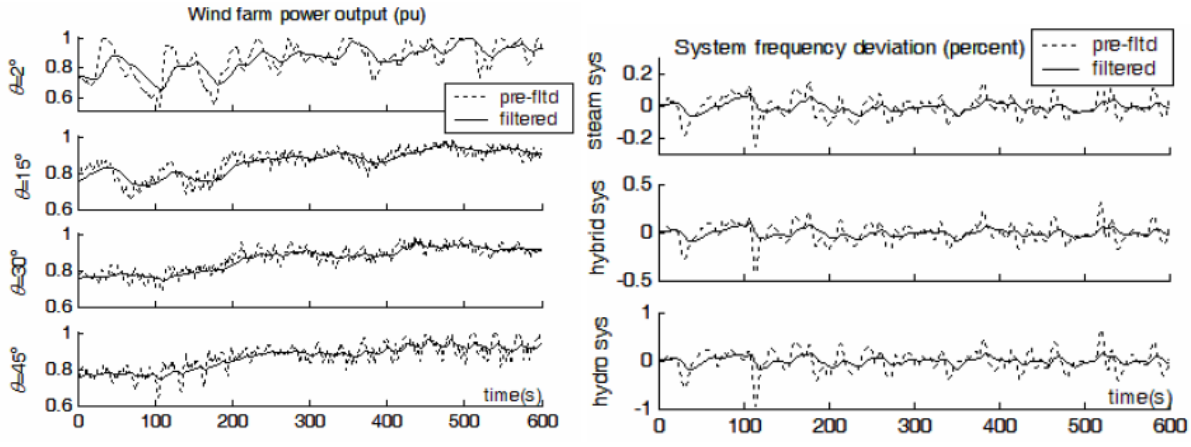

(a) (b)

Figure 1.12 (a) Pre- and Post-filtered (with ESS) powers of wind farm at different wind directions (b) System frequency response of system without (pre-filtered) and with ESS (filtered) according to wind power variations for steam unit, hybrid, and hydro units power system [40]

1.5 Conclusion

Micro grids are a fascinating power system which is increasingly installed especially in rural and remote area or island. Renewable sources play an important role in these grids. The stability and reliability of isolated microgrids are significant issues. In current grids, penetration rate of renewable energy has already reached its limitation. Many studies and projects try to increase the renewable energy capacity (goal is reaching 50% of penetration rated). Generally, thermal generators like gas turbine plant or diesel generator which are the main sources for frequency regulation have to increase their capacity and production level in order to maintain the frequency stability of isolated micro power system. While the greenhouse effects from power plants exhausted fume emission has become an international concerning issue. Other production source like energy storages is a very relevant source to maintain frequency stability because of its characteristics and no CO_2 emission.

There are many strategies of frequency regulation proposed for energy storage system as having mentioned earlier. Mostly control strategies are based on power variation of load or loss of generation, which is the step power variation, and some control strategies have been defined from analysis of wind power fluctuation. However, there are very few studies on the impacts of power PV variation on system frequency. Only characteristics of intermittent signals (irradiance and power) have been analysed [73]–[79]. Therefore, in the following study, power signals of photovoltaic are studied and linked to system frequency variation. Control strategy and sizing of energy storage system will be defined according to the power variation of PV in order to limit frequency variation as well as maintain frequency stability.

Chapter 2

Characteristics of photovoltaic power variation

2.1 Introduction

The utility system operators and planners need to understand the effect of fluctuating power on system regulation and stability. Without high-frequency power data and realistic power plant models to analyze the problem, utilities often rely on conservative assumptions and worst-case scenarios to make engineering decisions [80]. The data of intermittent sources like power, irradiance, and wind speed are studied in time and frequency domains in order to know their characteristics of fluctuation which are helpful to save cost and avoid problems from power fluctuations. Objective of this study is to find an appropriate method to study the photovoltaic production power that can be related to the issue of frequency variation. Knowing characteristic of power fluctuation could then be useful to maintain frequency stability. Furthermore, this study would be useful to design the size and the control strategy of energy storage devices later. Various methods to analyze power of photovoltaic in both time and frequency domains are applied to real power PV signal. Firstly, all data analysis methods are summarized. Then, power data in function with time is studied with a statistical approach to calculate average value, variance, and standard deviation. A second method will study power data using a probabilistic approach to find out the possibility of occurrence of each situation. Then, signal is analyzed into the frequency domain by Fourier transform for spectral analysis. Finally, each method is compared and linked to frequency variation problems.

2.2 State of art

Data analysis is important and useful in many fields such as, social science, psychology, science, etc. Data analysis permits to study what happen in the past and also forecast for the future. Raw data contains much information but it is difficult to understand without interpretation. Interpretation or analysis data is needed to present or summary raw data in a meaningful way. Six steps of data analysis enable us to understand the nature of the problems, deciding what and how to measure them, collect data, allow data summarization and preliminary analysis, formal data analysis and interpretation of results [81].

In renewable energy study, data of intermittent sources such as: power, irradiance and wind speed are studied in time and frequency domains in order to analysis its characteristics which could help to find model of their intermittency, and to protect our power system according to its variation. There are many methods for intermittency study but each method will be appropriate for a particular objective.

The statistical approach is used by the National Renewable Energy Laboratory (NREL) to study high-resolution (1-hertz [Hz]) wind power output data from large wind power plants in various regions. The objective of this project is to systematically collect actual wind power data from large commercial wind power plants so that wind power fluctuations, their frequency distributions, the effects of spatial diversity, and then the ancillary services requirements can be analyzed [80]. This

project analyses the power deviation by calculation with step changes and with ramping rates. The histograms of power deviation with different calculation are then analyzed. The power deviation with step change gives information of power deviation with fixed time scale. The power deviation with ramping rate is the calculation between optimum points. Besides, the rate of change of power deviation by ramping rates is calculated by (2.1) where P (j+1) is the optimum actual power, P (j) is the previous optimal power, t (j+1) is the actual time at which P (j+1) appears, and t (j) is time at which P (j) appears.

$$\text{Rate of change of power deviation (j)} = [P(j+1)-P(j)] / [t(j+1)-t(j)] \quad (2.1)$$

The rate of change of power deviation by ramping rate is also proposed by [82] for analysis of irradiance data of solar energy. The histograms of irradiance data and ramps of irradiance (or clearness index) over a period of time are analyzed. Furthermore, the auto covariance and autocorrelations in the time series of clearness index and of ramps of clearness index are calculated.

The change in irradiance level (ΔR (j)) of duration $\Delta t(j)$ is calculated by (2.2), (2.3) where R(j) is the optimum irradiance value at time t(j). Sequences $\{(\Delta R(j),\Delta t(j))_i\}$ are obtained and then, the bivariate histogram of $\{(\Delta R(j),\Delta t(j))_i\}$ is plotted. The x-axis is the change in irradiance level ΔR (j), the y-axis is the duration $\Delta t(j)$ and the z-axis, number of occurrences.

$$\Delta R(j) = R(j+1)-R(j) \quad (2.2)$$

$$\Delta t(j) = t(j+1)-t(j) \quad (2.3)$$

The statistical approach is also used to study the irradiance of solar energy in [83]. Ramp rates of 1 minute are defined as the absolute value of the difference between the instantaneous power of PV at the beginning and at the end of a period of 1 minute. Different time scales of ramp rates are also used such as one second ramp rates, ten seconds ramp rates, one minute ramp rates and ten minutes ramp rates. The ramp rates or rates of change of power in this study are not calculated by power deviation between optimum points. This approach shows the power deviation of different time scales. The ramp rate values are highly dependent on the time range used to determine the scalar ramp rate. The annual ramp rates are compared with the annual ramp rates of power system equipped with energy storage. The statistic values are calculated from data of clear day and variable day. The calculation of the ramp rates based on the moving average is also taken into account. This study proposes to limit the output power of PV at 50% of its rated value. The results show the significant reduction in larger ramp rates due to this limitation of power. Furthermore, the power fluctuation with limiting power at 50% is applied to power system to study the frequency fluctuation. The frequency response is in the acceptable range by applying limit power to photovoltaic. Irradiance signal is analyzed to estimate the impact of meteorologically induced irradiance fluctuation on distribution networks with PV power generation and to evaluate the smoothing effect by statistical and probability approach [84], [85]. Standard deviation of power data is computed in [85] to be related to the largest power fluctuation.

Other methods for characterizing the intermittency of renewable, for instance analysis in frequency domain, are also proposed. The Fourier transform or the wavelet transform are then applied to the recorded data [86], in order to evaluate the smoothing effect. These two methods are applied to classify the fluctuation characteristics of one individual site and nine average sites for different weather, such as: a clear weather day, a cloudy after fine weather day, a slightly cloudy sky day, and a rainy weather day. Irradiance data are measured every 1 min. Moreover, [87] used wavelet transform for estimating the impact of meteorologically induced irradiance fluctuation on distribution networks with PV power generation. The power spectrum is used to calculate the average spectrum in order to identify each signal. Wavelet transform is also applied to irradiance to study smoothing effect [77].

Wind power is also analyzed in frequency domain by power spectrum [88]. The wind power is measured at every one second for several months. The power spectrum of wind can then be separated

in 4 regions: upper limit, linear (exponential in frequency), low pass filter and noise floor. The linear region is then identified to a variation law according to f^{α} (in [88], α has been identified to -5/3).

Power of large PV plants (4.59MWp) is analyzed using a statistic approach and in frequency domain [89]. Power data are collected for 2 years with a sampling of 1 min and for 2 months with a sampling time of 10s. The power spectral density (PSD) is used to analyze the fluctuation of large PV and compared to small PV and wind turbine. The power spectrum of power PV has linear region for frequency more than $2x10^{-3}$ Hz. The power spectrum of PV is flatter than wind turbine. It can be implied that the magnitude of fluctuation in 10 min and up to several hours of PV is larger than wind.

The irradiance and power of PV are analyzed in frequency domain to find a correlation [74]. In this reference, data are acquired during 1 year with a sampling time of 1 s. The power is equivalent to the irradiance signal passing through a low pass filter. The cut-off frequency of this filter depends on the peak power and area of PV. The larger the maximal power of PV or area is, the smaller the cut-off frequency is. So the fluctuation of large PV is mostly in the low frequency region. Intermittent signal is analyzed in frequency domain by power spectrum [86], [88], [89]. The power spectrum of PV is flatter than wind turbine [89]. The magnitude of fluctuation in 10 min to several hours of PV is larger than wind energy. The compensation of variation of PV is taken into account in this frequency region for large PV.

Not only intermittent signals are characterized in the literature, their impacts on system frequency are also studied. Impact of power variation of wind energy on the system frequency is analyzed in the frequency domain in [41], and [66]. The spectral analysis is applied to power signal for periods of 10 min and sampling time of 1 s. The variation of signal is then characterized by the Fluctuation Harmonic Content (FHC). FHC specifies the intensity of the power fluctuations over particular frequency regions [66]. Frequency regions of fluctuations can be separated into 3 zones: low frequency (below 0.01 Hz), medium frequency (0.01-1Hz), and high frequency (above 1Hz). The frequency of fluctuation in low and medium frequency has an impact on the system frequency. The high frequency of fluctuation is filtered by the equivalent inertia of the power system. Statistic approach is also applied to analyze insolation in [90]; then, the estimation of power fluctuation of high penetration PV and for analyze the impact of power fluctuation on load frequency control.

In conclusion, there are various methods to treat and analysis some data. Each different method is appropriate for a particular objective. According to our objective, three methods (statistical analysis, probability approach, and spectral analysis) are selected. Power signals of PV are analyzed in time domain for two information; amplitude and time duration of fluctuation, and in frequency domain for characterizing frequency characteristic of power variation.

2.3 Studied PV data

Analysis methods presented in previous section are applied to real power PV signal. The sampling time of intermittent data recorded is quite important, some studies using large sampling time (i.e. low sampling frequency) between 1 to 10 min in [66], [86], [89]. Some studies used high sampling frequency or several seconds (1-10 seconds) in [66], [74], [80], [88], [89]. Low sampling frequency is normally useful for study of several months or several years data in order to characterize global information of intermittent source. On the contrary, high sampling frequency is quite proper to distinguish different signals. In our study, high sampling frequency is needed to study impact of power variation on system frequency.

The power data of solar energy have been recorded on PV plants in three different location in France: north of Orange in the Vaucluse department (called later as the PV plant #1), north of Poitiers in the Vienne department (called later as the PV plant #2), and west of Arles in the Bouches du Rhône department (called later as the PV plant #3). PV plant #1 is located in Orange city which is on south-east of France. Poitiers (location of PV plant #2) locates at central of France. Finally, Arles (location

of PV plant #3) is a city in the south of France.

These three PV plants have different rated power. The power data of PV plant #1 have been recorded on a PV plant of 250kW during 24/08/2011 to 30/11/2011 with a sampling time of 5 seconds. A rated power of PV plant #2 is 10kW. And the data during one year of this plant have been recorded from 11/2010 to 09/2011. Finally, photovoltaic productions of PV plant #3 have been recorded on a PV plant of 190kW during 11/2010 to 09/2011.

2.4 Analysis methods

In our study, three different approaches have been studied on real PV data: statistical analysis, probability approach, and spectral analysis are chosen. Actually, statistical analysis and probability analysis can be grouped together. In this study, statistical approach is a method to process raw data directly. But for probabilistic approach, power deviation for various step times is computed from raw data. The frequency distribution and the maximum value of these power fluctuations are then investigated.

Global information of each analysis is presented and analyzed towards their impact on grid frequency variation. Methodology of each strategy is described. Each analysis is based on several indicator linked to fluctuation. Then, the indicators linked to the statistical analysis and the probability approaches are the standard deviation and the frequency distribution of power variation respectively. Fluctuation Harmonic Content (FHC) and the average spectrum are indicators of fluctuation for spectral analysis. Firstly, all data of full period and monthly period are analyzed. This allows us to study global characteristics of the studied photovoltaic plant. Then, power data for daily period is studied. Finally, we will try to distinguish different fluctuation signals and link them to frequency variation issue.

2.4.1 Statistical analysis

Statistic tool is simple and well known to analyze large time domain data in many domains such as environmental sciences, social science, business, etc. This tool is used to summarize or interpret large data into simple and few values. Representing large data into one value can cause loss of some information; however, it depends on application or data interpretation. Basic statistical values are the mean, the median, the standard deviation and the variance. Mean and median values are parameters to measure a central tendency [91]. Mean value ($\bar{X}$) is the arithmetic average of a distribution of data or the ratio between the sum of all data and the total number of data in (2.4) where X_i is data, n is series number of data (1 to N) and N is the total number of data. Mean value is commonly used to represent data because it is simple but it is a too rough summary of them. It does not give information of how spread out of data (variance) or if this mean is high or low value, etc. [91].

$$\bar{X} = \frac{\sum_{i=1}^{N} X_i}{N} \tag{2.4}$$

$$VAR = \frac{\sum_{n=1}^{N} (X_i - \bar{X})^2}{N} \tag{2.5}$$

Therefore, measurement of variability is also examined to complete the data analysis. Three mostly used indicators to determine dispersion of data are the range, the variance and the standard deviation. Range is the difference between a maximum and a minimum value of data, but it will not be used in this study. Variance signifies dispersion or variability of distribution [91], [92]. If the variance is equal to zero, it means that all data are identical. The square of difference between each data (Xi) and its average is divided by the number of total data defines the variance (denoted VAR in (2.5)). Generally, this parameter is not used as a stand-alone indicator for dispersion but it is used as a step in the calculation of other statistics [91]. The square root of variance corresponds to the standard deviation (SD in (2.6)), that is a famous indicator to determine variability of data because it signifies how far away data evaluate from their average value with the same unit as studied signal. For example

if a power signal in kW is analyzed, the SD of signal is expressed in kW too. Besides, SD can be normalized by the average value (SD/$\bar{X}$) to compare variation of signal whose average is different. The reliable data depends on accuracy of raw data and number of data.

$$SD = \sqrt{\frac{\sum_{n=1}^{N}(X_i - \bar{X})^2}{N}} \quad (2.6)$$

2.4.1.1 Statistical analysis methodology

Firstly, power data in time domain for three months duration are analyzed. Then, monthly and daily power data are analyzed. Power average (P_{av}) and standard deviation (SD) for each time length are calculated in (2.7) and (2.8) where P(n) corresponds to the collected data for the n-sampling data and N is the total number of data (for three months period, for each month, for each day). Power data of PV for a one day period is illustrated in black line in Figure 2.1. The average power (P_{av}) is in red line to represent the global power production and standard deviation of power data in blue line signifies the variation of power from its average.

$$\mathbf{P_{av}} = \frac{\sum_{n=1}^{N} \mathbf{P(n)}}{\mathbf{N}} \quad (2.7)$$

$$\mathbf{SD} = \sqrt{\frac{\sum_{n=1}^{N}(\mathbf{P(n)} - \mathbf{P_{av}})^2}{\mathbf{N}}} \quad (2.8)$$

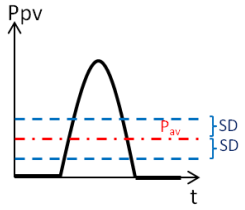

Figure 2.1 Power distribution of PV for one day with its average value and standard deviation

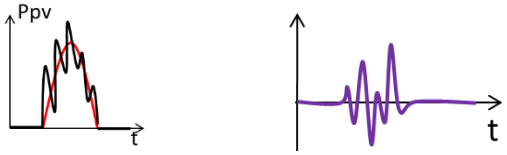

(a) (b)

Figure 2.2 Power deviation from reference signal (a) Power of PV signals (b) Power deviation from reference signal

$$\Delta P_{pv} = P_{pv} - P_{pv\_ref} \quad (2.9)$$

$$SD_{\Delta} = \sqrt{\Delta P_{pv}{}^2 / N} \quad (2.10)$$

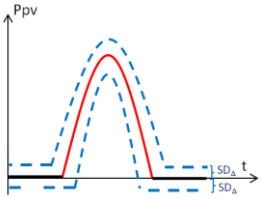

Figure 2.3 Standard deviation from reference signal

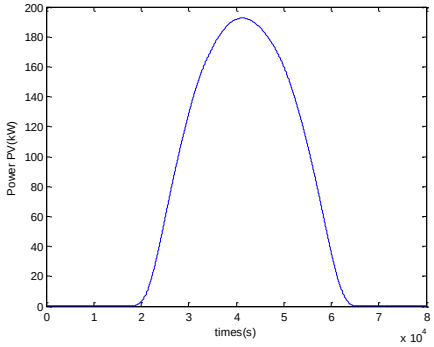

Figure 2.4 Perfect power PV distribution on 18/09/2011

These two simple statistic values can help to interpret data but they may not be suitable for our dynamical study. The power fluctuation that relates to the system frequency variation can be defined from the power reference, desired or estimated using predictability tools. As an instance, PV Power ($P_{pv,}$ black line in Figure 2.2(a)) is compared to perfect power PV signal (P_{pv_ref} , red line in Figure 2.2(a)) and power difference (denoted ΔP_{pv}) in (2.9) is computed and illustrated in Figure 2.2(b). Standard deviation of difference signal, denoted SD_{Δ}, is calculated by (2.10) ; so now this standard deviation (blue line in Figure 2.3) signifies how far the PV power fluctuates from the reference. The calculations will be done even for one-month collected data. The number of data which are out of SD or SD_{Δ} limit (not in zone between blue lines in Figure 2.1 and Figure 2.3) are computed to analyze the number of large variation. The perfect power PV distribution (power reference) is chosen for power data on 18/09/2011 and it is illustrated in Figure 2.4.

2.4.1.2 Results

a.) Monthly analysis

From PV signal during 24/08/2011 to 30/11/2011, the average power is equal to 54.13 kW and the standard deviation to 65.037kW (besides a maximal power maximal of 271.8kW and a minimal power of 0kW have been recorded). The average value is quite low compare to the maximal value because there are numerous of null power (especially during nights!). Then, the power data of each month are analyzed and the results are summarized in table 2.1. The percentage of data which are out of SD limit (not in the zone between blue lines in Figure 2.1) is also shown in table 2.1.

Table 2.1: Power signal analysis in time domain

Period	Pav(kW)	SD(kW)	% Power more than SD
24-30/08/2011	81.83	74. 6	49.52%
sept-11	70.07	70.11	42.95%
oct-11	52.05	64.74	32.21%
nov-11	32.964	48.28	25.00%
24/08/2011-30/11/2011	54.13	65.07	34.07%

The average power of November is the smallest because there is less solar energy during winter as illustrated in Figure 2.5 (b). Furthermore, SD of PV power in November is also the smallest. This is linked to the least fluctuation. Power of PV in November is grouped mostly within SD so fluctuations are small.

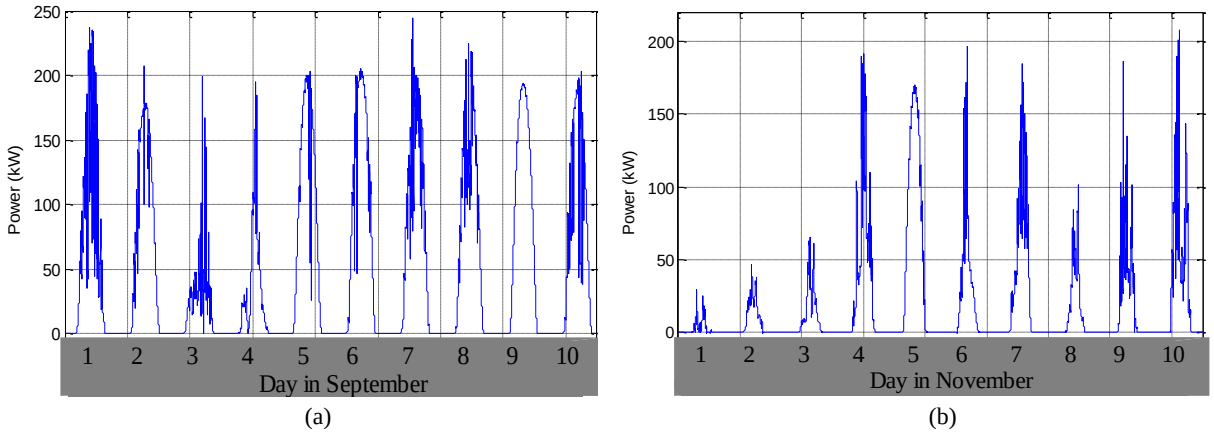

(a) (b)

Figure 2.5 PV production of PV plant #1 in (a) September and (b) November

Power data are then compared to ideal PV power time-distribution. All results are shown in table 2.2. The percentage of PV power upper than SD_{Δ} (i.e. out of limit) is also computed to signify the variation of signal. The results in table 2.2 show that the SD_{Δ} for November is the highest value but the percentage of power upper than SD_{Δ} of October is biggest. The signal in November has many large variations but they are mostly within SD_{Δ}. Whereas, variations of October are also quite large but

almost half of data are out of within SD_Δ. This signifies that PV power in October is highly fluctuated compared to the reference.

Table 2.2: Results of power signal analysis in time domain (differences from reference signal)

Period	ΔPav(kW)	SD_Δ (kW)	% Power more than SD_Δ
24-30/08/2011	-3.95	26.87	15.14%
sept-11	-12.76	34. 4	3.43%
oct-11	-26. 29	51.46	42.73%
nov-11	-40.6	66.54	18.54%
24/08/2011-30/11/2011	-24.73	50.87	37.64%

b.) Daily analysis

The SD_Δ is also calculated for each day during 4 months signal. The SD_Δ of each month is plotted in Figure 2.6, Figure 2.7, Figure 2.8, and Figure 2.9 for each month. Variations of PV power from the reference are maximal at around 100kW on 31/10/2011, 01/11/2011, 19/11/2011. Powers produced in August and September is less fluctuated than in October and November. In Figure 2.9, power deviations are quite large for almost every day in November, which is in good agreement with the value of SD_Δ in Table 2.2. On the other hand, variations in October in Figure 2.8 are quite important but there are some small variations which mean a smaller SD_Δ for October than those of November in Table 2.2.

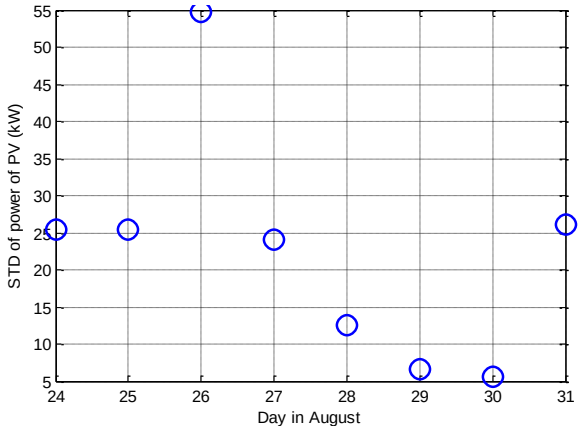

Figure 2.6 Daily standard deviation from reference signal in August

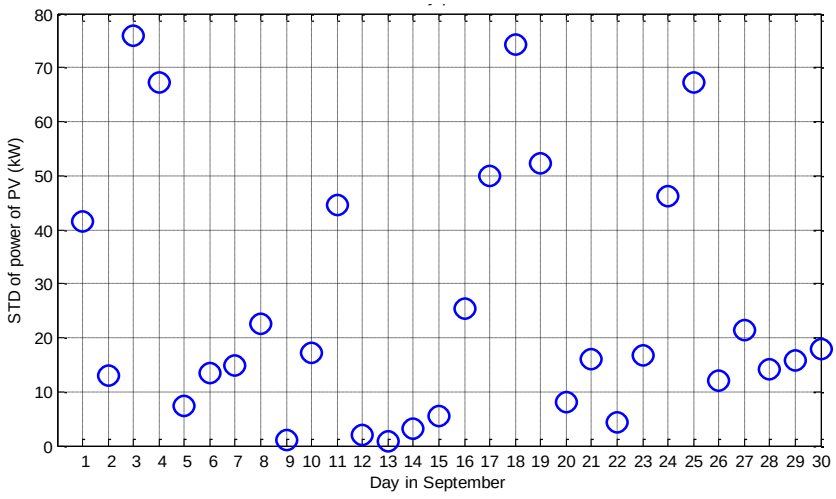

Figure 2.7 Daily standard deviation from reference signal in September

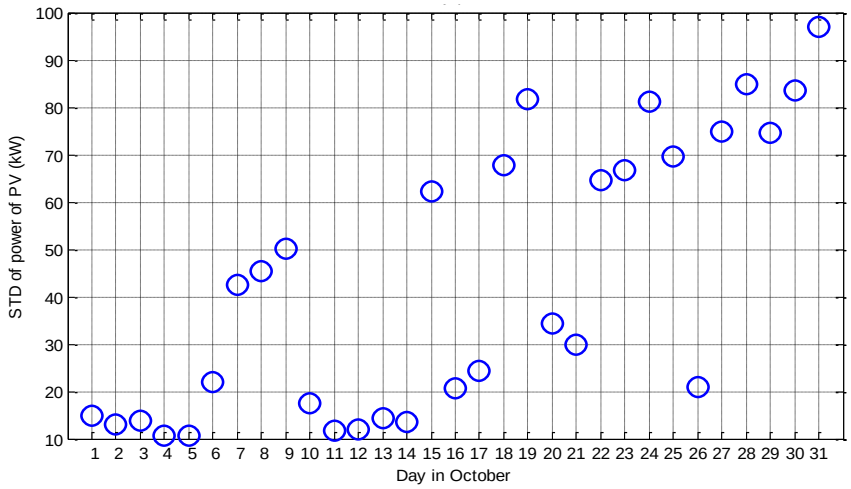

Figure 2.8 Daily standard deviation from reference signal in October

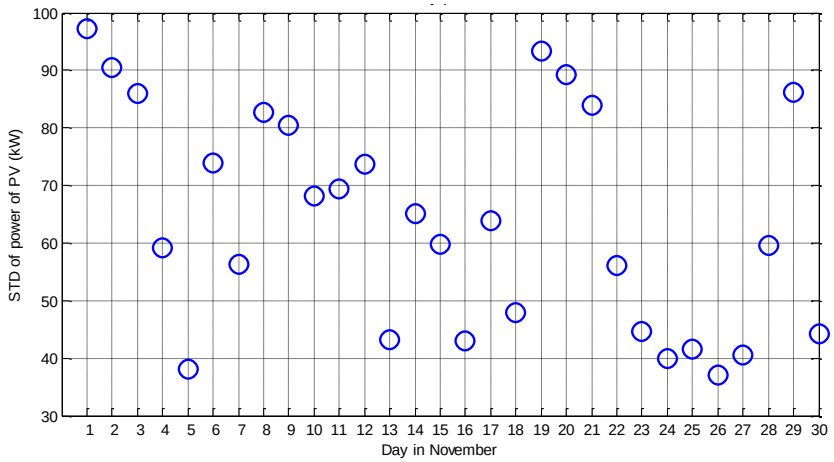

Figure 2.9 Daily standard deviation from reference signal in November

2.4.1.3 Conclusion of statistical approach

Statistic values can be used to represent signal for extraction of global information. Standard deviation, that defines variation of PV power from both average and reference signal; will be used as a representation of signal in the next chapter. This information will help us to classify signals and link them to frequency problem. In the next section, other methods are analyzed to more precisely characterize PV power fluctuations.

2.4.2 Probability approach

In the previous section, simple statistic values (mean and standard deviation) summarize the fluctuation of power data in one value. However, only amplitude of power deviation is obtained but frequency variation which also depends on time change of each variation is not considered. In this topic, power data situation is analyzed to quantify the occurrence and the periodicity of PV power fluctuation.

"Probability is used to quantify the likelihood, or chance, that an outcome of a random experiment will occur" [92]. Data can be separated into many categories. If data are distinguished by a number of data set, they can be classified into mono variable data (single data set), bivariate data set (with two variables), and multivariate data set (for two or more variable) [81]. Moreover, data can be categorical, or qualitative, or nominal if data are in a verbal or narrative format [81], [93]. This data type can be grouped and can be ordered (from least to most). Furthermore, data set can be numerical or quantitative or metric if data is a number where numerical operations such as addition or multiplication can be performed.

Large categorical data or discrete quantitative data can be grouped and presented in frequency distribution table which presents possible coincided groups with the associated frequencies and/or relative frequencies. **Frequency** is the number of times that each grouped data are presented in the data set. And the **relative frequency** is the proportion of number of occurrences to the total number of data set [81]; this value is then less than one. Moreover, relative frequency can be defined as probability of each occurrence or data grouped. Frequency distribution can be presented by table but it is quite difficult to understand for large amount of data groups. So it can be presented in bar charts or histograms. Histogram are commonly used as the best graphical diagram to represent frequency or probability data in statistic approach [94]. The horizontal axis of this diagram is the groups of data and the vertical axis is the frequency or probability of each data group.

Moreover, the cumulative distribution is one useful parameter to interpret data. Cumulative distribution function (denoted F(x)) is the possibility that data (X or x_i) is less than data range (x). It is then equals to the summation of all frequency of data ($f(x_i)$) below data range (x) in (2.11) [92].

$$F(x) = P(X \leq x) = \sum_{x_i \leq x} f(x_i) \tag{2.11}$$

2.4.2.1 Statistical analysis in probability methodology

The deviation of photovoltaic power is calculated for different periods of time such as 10 seconds, 30 seconds, 1 minutes, etc. The different time periods are used to distinguish different situations of PV variation because the same magnitude of power deviation can cause different frequency variation depending on duration of variation. For example, a power change of 100 kW during 10 seconds or 20 seconds will cause different occurrence of frequency variation. The different situations depicted in Figure 2.10 needs to be classified. If a time period of power change is less than the time duration specified, this peak cannot be seen. If the power deviation changes when the time duration rises, the power fluctuation is slow as is illustrated in Figure 2.10(a). On the other hand, if the value of power deviation is not changed when the time duration rises, it means that PV power decreases or increases rapidly and after it remains constant, even at a low value (see Figure 2.10(b)).

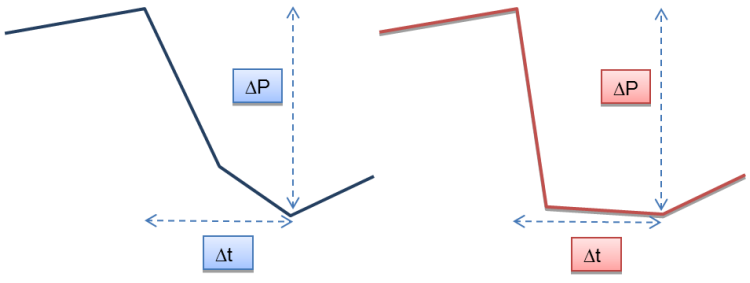

(a) (b)

Figure 2.10 Different situation of power fluctuation

Moreover, moving average and normal average are applied to power data to filter small variations of PV power which are not interesting. Firstly, the data in one day is analyzed because it is practical to analyze precisely. We choose to study power data for 16th September, 2011. After that, data of three months in 2011 (September, October, and November) are studied. Finally, the other power plants are analyzed. Step by step of this study are:

1st step: Treatment of data and calculation of power deviation (simulations 1 to 3 below). The power deviation (denoted ΔP(t)) is calculated by (2.12) for various step time (denoted Δt) of 10s, 30s, 1 min, 2min, 5min, 10min, and 15 min. This power deviation corresponds to the power difference between actual power and power measured at the last sampling time in Figure 2.11.

$$\Delta P(t) = P(t) - P(t - \Delta t) \tag{2.12}$$

$$\Delta P_{max}(n) = \begin{cases} max[\Delta P(t_1), \Delta P(t_2)]; & \Delta P(i) > 0 \\ min[\Delta P(t_1), \Delta P(t_2)]; & \Delta P(i) < 0 \end{cases} \tag{2.13}$$

− *Simulation 1*: Power deviation of photovoltaic is calculated from data recorded with various time durations (Δt). This is our reference analysis that gives all occurrences of fluctuations.

− *Simulation 2*: The moving average (equation (2.14) and (2.15)) with different average time of average (t_a) is applied to our initial data and the deviation in power is calculated with various time durations (Δt) from this average data. The moving average is like a filter. Some information will then be loosed from the first simulation.

− *Simulation 3*: The average (equation (2.14) and (2.16)) with different average time (t_a) is applied to our initial data and the power deviation is calculated with various time durations (Δt) from this average data. This is the same approach as the moving average but data are filtered with a different matter.

$$\overline{P}(n) = \frac{1}{N}\sum_{i=0}^{N-1} P_{n-i} \tag{2.14}$$

n=N, N+1, N+2,… for moving average (2.15)

n=N, 2N, 3N,… for classical average (2.16)

2nd step: Finding of the maximal power deviation (ΔP_{max}) with conserving the sign. The maximal point of power deviation for positive and negative values is searched. The negative values are linked to power reduction, while positive values mean increasing power. To find maximal power deviations in Figure 2.11, points for which power deviation (ΔP(t)) changes its sign (positive to negative or negative to positive) are firstly searched and denoted as $\Delta P(t_1)$ and $\Delta P(t_2)$, where t_1 is the first time for which power signal change and t_2 is the last time the time before a next signal change. Next, maximal and minimal points are searched between $\Delta P(t_1)$ and $\Delta P(t_2)$ in (2.13). For example, let's consider the power change variation from negative to positive at t=200s in Figure 2.11; in this case, $\Delta P(t_1)$ equals to ΔP(t=200). The next change signal is observed when t=330s, so $\Delta P(t_2)$ is equal to ΔP(t=330). The maximal variation between $\Delta P(t_1)$ and $\Delta P(t_2)$ is then founded to 180kW (ΔP(t=250)).

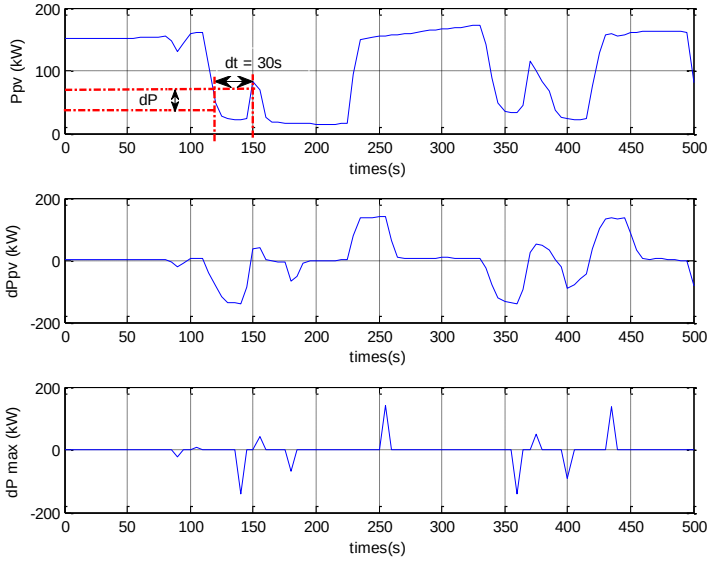

Figure 2.11 Detection of maximal power deviation

3rd step: Plot distribution histogram of ΔP_{max}. This histogram illustrates the frequency of occurrence of ΔP_{max} for each different time. Moreover, the cumulative distribution of maximal or minimal power deviations is plotted. The distribution histogram and the cumulative distribution of optimal power deviation are then analyzed, particularly according to parameters as data treatment method, time duration (Δt), and time for

average calculation (t_a). Besides, maximal values of ΔP_{max} for each day (and for different time duration Δt) are also analyzed for complementary information.

Finally, the methodology can be represented on the Figure 2.12.

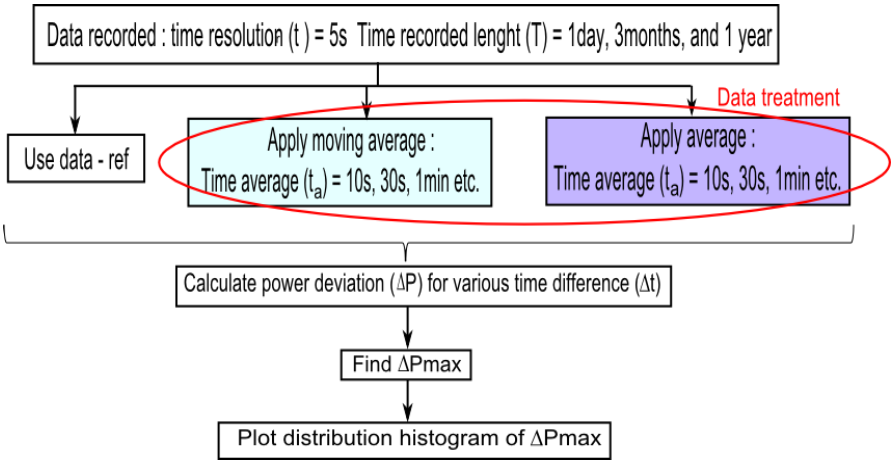

Figure 2.12 Chart of our methodology

For example, the power deviation is calculated and represented (in brown) in Figure 2.13(a) with a 2 minutes time duration from power data recorded (P, with a sampling time of 5s) in blue, which is zoomed in for one hour. After that, the optimal power deviation is determined in Figure 2.13(b). Finally, the distribution histogram of optimal power deviation with time duration of 2 minutes for one day is plotted in Figure 2.13(c).

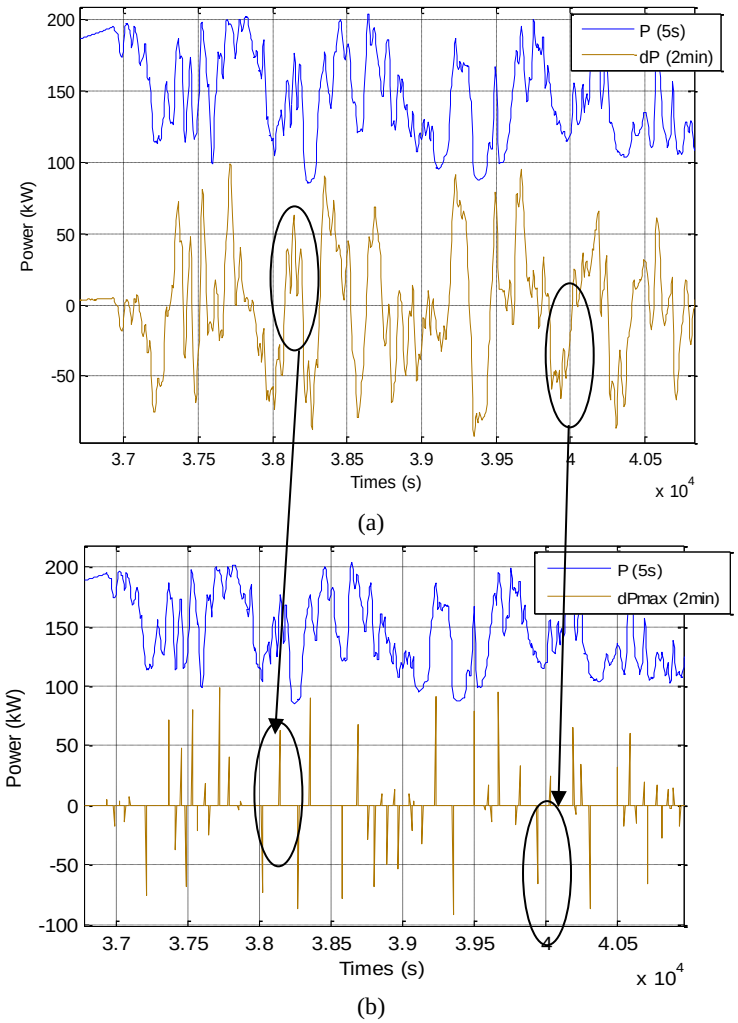

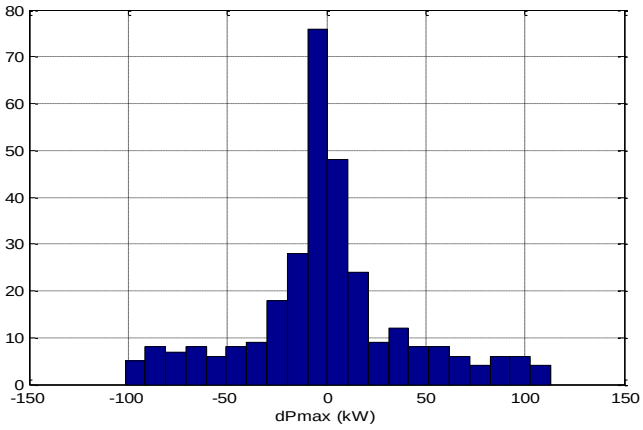

(c)

Figure 2.13 Application of the statistical methodology (a) PV power and power deviation (with a time duration of 2 min) (b) Maximal power deviation (c) Histogram of maximal power deviation

2.4.2.2 Results of probability approach

a.) Daily analysis

The power of solar energy is recorded in one day on 16th September, 2011, as illustrated in Figure 2.14. Firstly, this raw data is analyzed directly without any treatment. The occurrences of fluctuation are separated in 3 types: the fast fluctuation, the slow one, and the loss of production (for long period). The impact of various time durations on different situation is analyzed.

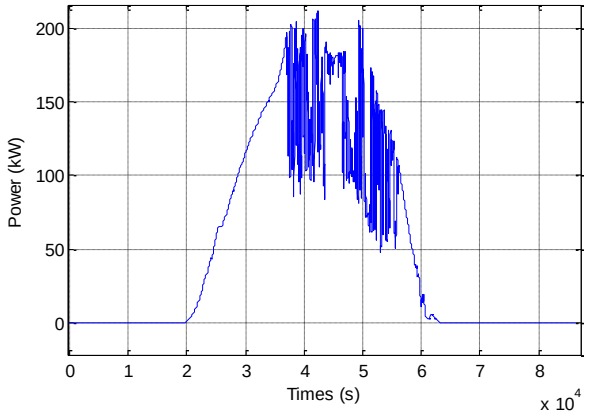

Figure 2.14 Power production on 16th September, 2011

The time duration of 10 seconds is too small to present power variation of PV because it cannot distinguish different situations in Figure 2.15(a). The occurrence of fast fluctuation is well illustrated for time of 30 seconds and 1 minute as shown in Figure 2.15(a), but some errors can be observed for power deviation with a 30 seconds time duration. Furthermore, duration of fast fluctuations is supposed to do not exceed 1 minute. However, these two time durations give information on small variations during the decreasing or increasing of power (see Figure 2.16(a)). Nevertheless this should be neglected. Therefore, the large power deviation (loss of power) is not shown for these two time durations. If the time duration period increases to 2 minutes or even 5 minutes, some occurrence is cancelled in Figure 2.15(b). For example, the power deviation 75 kW cannot be seen by time duration 5 minutes. However, the occurrence of power loss or slow fluctuation is shown well by these two time durations in Figure 2.15(b), because the small peaks are filtered. The time durations of 10 and 15 minutes are too long to calculate the power deviation during fast fluctuation (see Figure 2.15(c)). Power peaks during fast fluctuation are brought together to be one peak, so a lot of information are lost. For slow fluctuations, the small peaks can be also vanished as the time durations of 2 and 5 minutes in Figure 2.16(c).

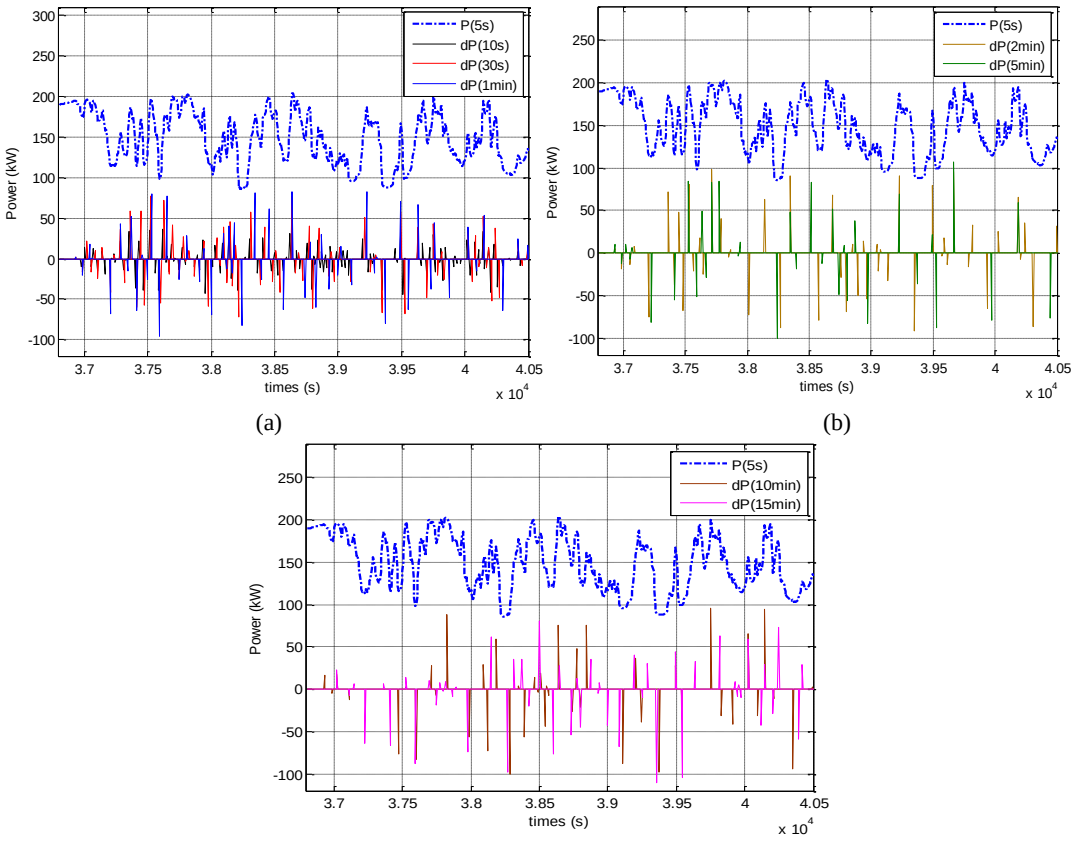

Figure 2.15 Zoom in the optimum power deviation for the fast fluctuation situation (during 3.68e4 to 4.05e4 seconds) with various time durations (a) 10 seconds, 30 seconds, and 1minute (b) 2 and 5 minutes (c) 10 and 15 minutes

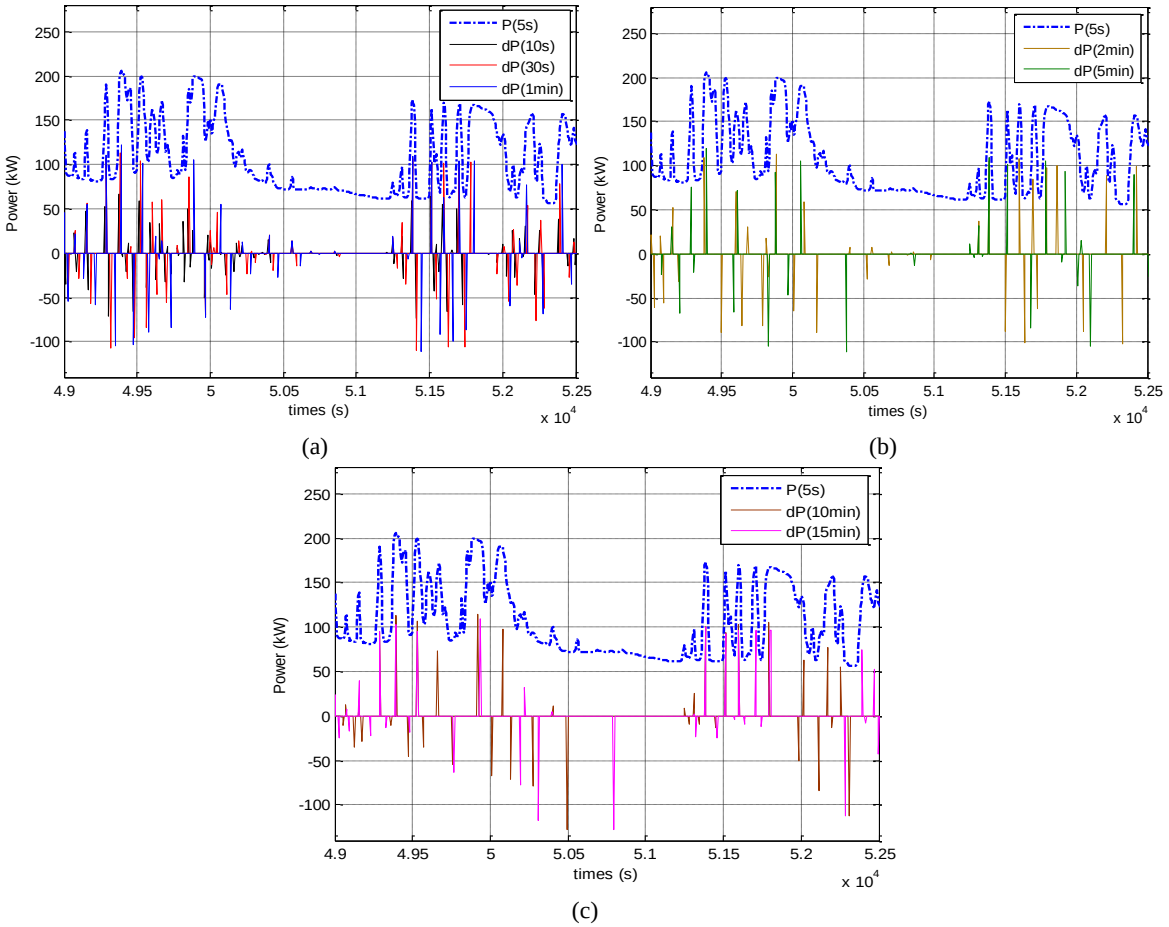

Figure 2.16 Zoom in the optimum power deviation for the loss of power situation (during 4.9e4 to 5.25e4 seconds) with various time durations (a) 10 seconds, 30 seconds, and 1minute (b) 2 and 5 minutes (c) 10 and 15 minutes

The frequency of maximal or minimal power deviations is summarized by histogram in Figure 2.17. The increase of time duration causes the reduction of number of occurrence of small peaks (for power deviation between +/-15kW). Moreover, a time duration of 10 seconds is too small as described before because the large power deviation of 100 kW does not appear in Figure 2.17(a).

The frequencies of maximal power between 85kW and 115 kW for each time duration are presented in table 2.3. The power between 85kW and 115 kW for time durations of 30 seconds, 1, and 2 minutes in table 2.3 are the power deviation during fast fluctuation. The average period of fast fluctuation is comprised between 30 seconds and 1 minute. A lost of production of 100kW (for a long period) can be seen by time duration above 2 minutes. Some information of power deviation between 85kW and 115 kW with time duration of 5 minutes during fast fluctuations is lost. Power reduction upper than 115 kW is represented by time duration of 10 and 15 minutes because the power deviation are calculated for more long time.

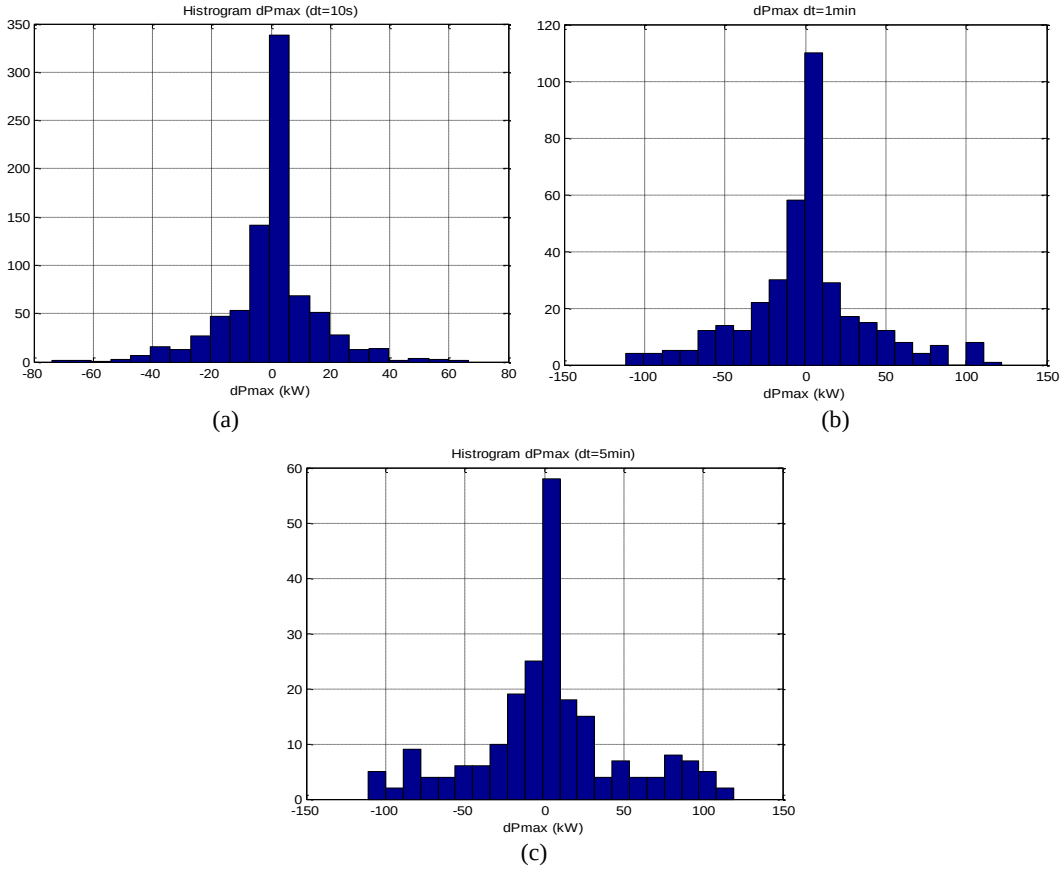

Figure 2.17 Distribution histogram of optimum power deviation with various time durations (a) 10 seconds (b) 1 minute (c) 5 minutes

Table 2.3 : Frequency distribution of maximal power deviation between 85 kW and 115 kW (different Δt)

	dP max between -115kW and -85 kW						
Δt	10s	30s	1min	2min	5min	10min	15min
number	0	7	10	11	8	10(+2 <-115kW)	10(+1 <-115kW)

	dP max between 85kW and 115 kW						
Δt	10s	30s	1min	2min	5min	10min	15min
number	0	9	8(+1 >115kW)	15	14(+1 >115kW)	16	13

From Figure 2.17, frequency data in histrograms for different time duration are presented. To collect all frequency data for different time durations into one figure, cummulative distribution is plotted in Figure 2.18. Time duration of 5 and 10 seconds induce loss of some information (see Figure 2.18). The cumulative distribution function of large rising power (more than 100 kW) is quite identical

for time duration of 30 seconds to 15 minutes. The number of high power reductions (less than 100 kW) can be well observed for time durations higher than 2 minutes. The time duration chosen to study power fluctuation is based on which situation is relevant and which occurrence should be neglected. Indeed, we can conclude that fast fluctuations of PV power is observed for durations around 30 seconds to 1 minute and loss of PV is observed for at least 2 minutes durations.

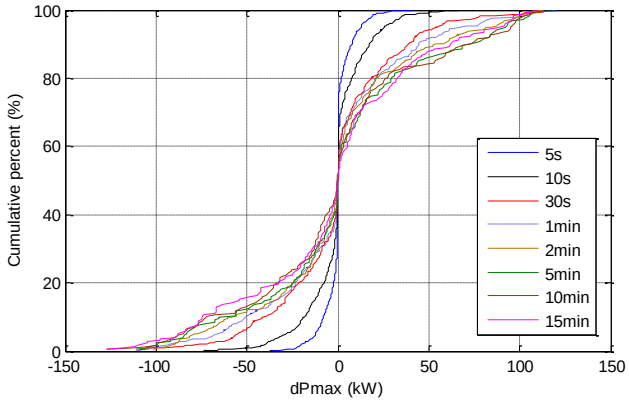

Figure 2.18 Cumulative distribution of maximal power deviation for various time durations

The moving average with different average times of 10, 20, 30 seconds or 1, 2, 5, and 10 minutes are applied to data recorded. The power data after data treatment with different average time are plotted in Figure 2.19. Average times of 10, 20, and 30 seconds can only reduce amplitude of power but they cannot filter power signal. The power data can be filtered by average time of 1, 2, 5, and 10 minutes but they cancel some large peaks during fast fluctuations. The peaks during fast fluctuations are brought together in Figure 2.19(a) and the small peaks during slow fluctuation or loss of production are filtered in Figure 2.19(b). Therefore, if loss of production or slow fluctuation is observed, a moving average with average time over 1 minute should be applied to raw power data.

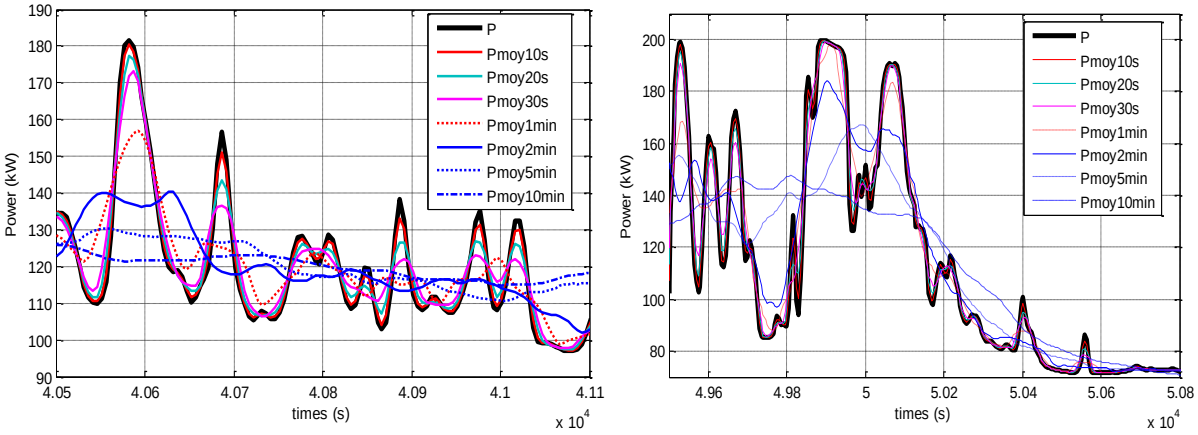

(a) (b)

Figure 2.19 Power signal moving average for various average times during (a) 4.05e4 to 4.11e4 seconds (b) 4.95e4 to 5.08e4 seconds

The data with moving average is translated to power deviation for various time durations. The time duration is never lower than the average time; for example, if the average time is equal to 1 minute, the time duration can be given by 1, 2, 5 or 10 minutes. There is no difference in power deviation values between the recorded data and the data with moving average times of 10 and 20 seconds whatever time duration is. The distribution histogram shows that there are less small variations for data with moving average of 10 and 20 seconds.

As the power deviation is studied for fixed time duration (Δt) with different average time (t_a), fluctuations are lessen by the increase of average time. Average time of 1 minute filters power signal while time duration of 2 minutes is used to calculate the power deviation (and does not filter the signal again). But time duration of 5 minutes filters the power signal with moving average of 1 minute again.

Although, the moving average for small average time cannot filter the power signal, the time duration of 5 minutes can alleviate some small peaks during slow fluctuations. The time duration of 5 minutes is quite a large period so it can filter small peaks of initial signal. Therefore, this long time duration is not suitable to calculate the power deviation for data with moving average because it has filtered the signal again. Some information will be lost. For example, 3 peaks are turned to 2 peaks by the moving average of 1 minute to 2 minute and, after calculations, the power deviation with 5 minutes induces another loss of 1 peak.

In Figure 2.20, the cumulative distribution of maximal power deviation is plotted. It can be seen that the increase of average average timelessens the number of large power deviations because the large average time has decreased the power deviation value. Figure 2.20(d) shows that average times of 5 and 10 minutes cause an error in power deviation calculation (as large power deviations are lost). So, the average average timeshould not be more than 2 minutes. Moreover, the large power deviations can not be seen when the average average timeis equal to the time duration. Therefore, the average average timeshould be less than time duration.

Finally, data is averaged with fix window for various average times such as: 10, 20, 30 seconds or 1, 2, 5, and 10 minutes. The moving average and classical average with the same average time are applied to the same initial signals to study the impact of data treatment method. The power signals after treatment with the two studied methods for average time of 30 seconds are mostly identical except that the amplitude of power fluctuation is different as shown in Figure 2.21(a) (during 3.82e4 to 3.97e4 seconds). For average time of 1 minute in Figure 2.21(b), one can observe several differences during fast fluctuations. Then, the moving average conserves some small peaks during fast fluctuations, even though these small peaks disappear with the classical average.

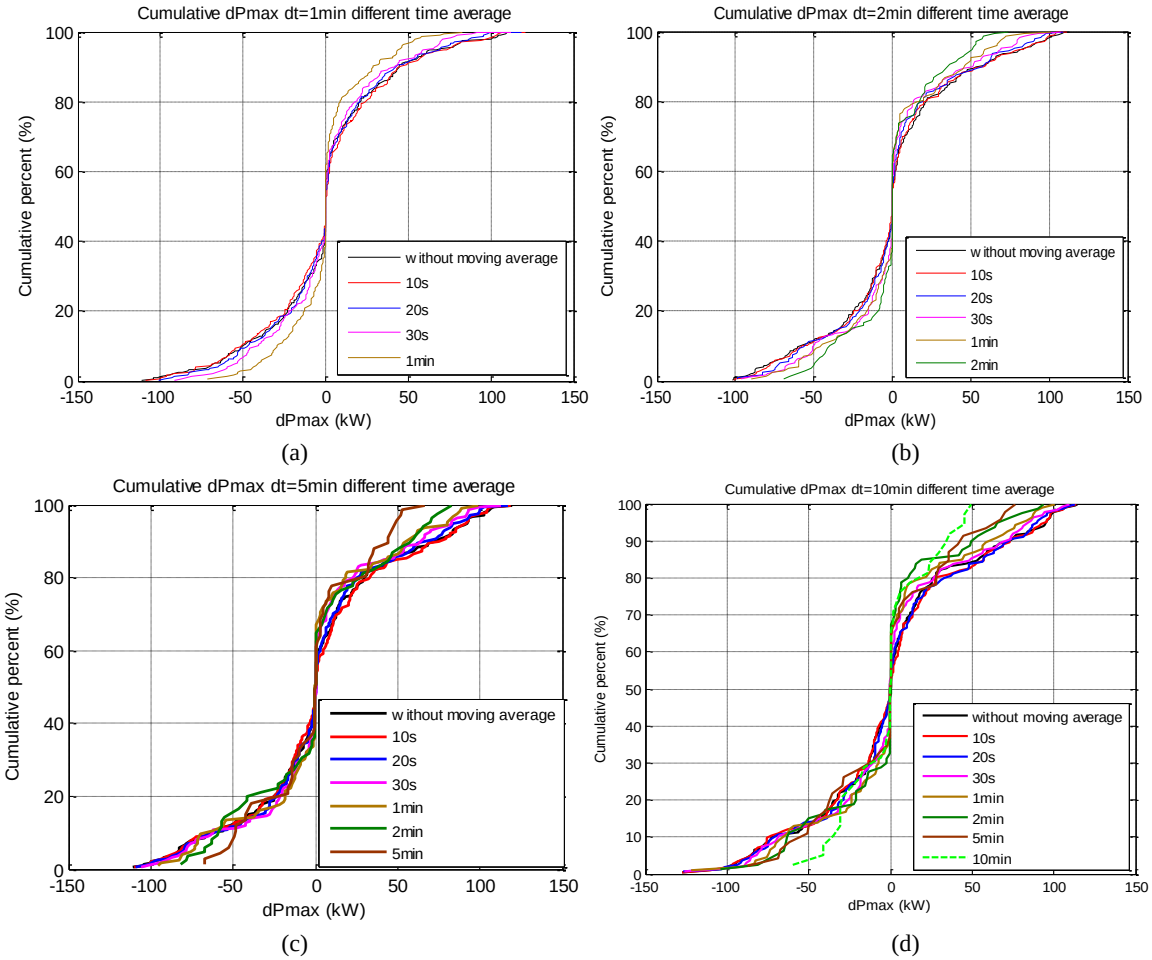

Figure 2.20 Cumulative distribution of optimum power deviation for various average times with time duration (a) 1 minutes (b) 2 minutes (c) 5 minutes (d) 10 minutes

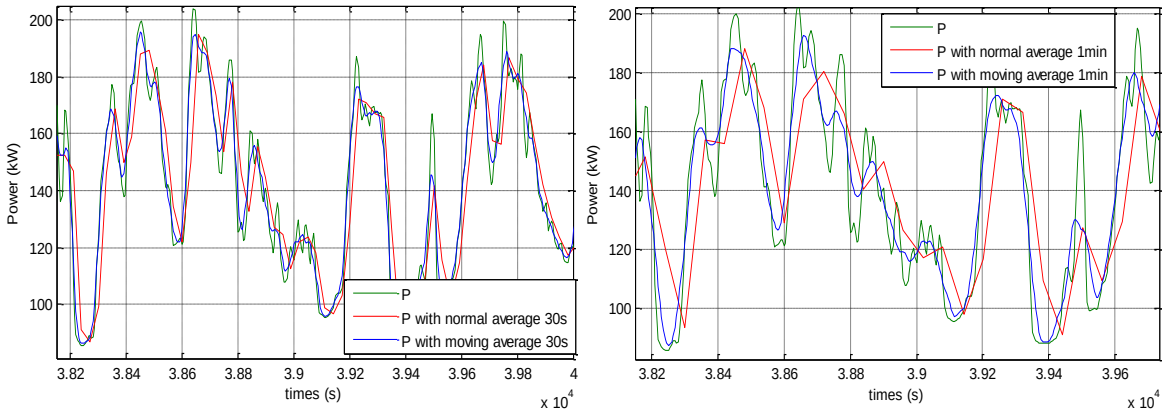

(a) (b)

Figure 2.21 Compare signal initial with signal applied moving average and normal average for average time (a) 30 seconds (b) 1 minute

An average time of 10, 20 or and 30 seconds can only reduce amplitude of power variations, but these durations do not filter the power signal as well as the moving average. The power data can be filtered by average time of 1, 2, 5, and 10 minutes but they alleviate some large peaks during fast fluctuations**.** Moreover, the small peaks during slow fluctuations or loss of production are filtered. The power deviation calculated with the classical average has almost the same characteristics as with moving average.

b.) <u>Three-months data study</u>

The power data are recorded for 3 months in September, October, and November 2011. Firstly, power data of each month is studied. Next, the whole three months data are analyzed, with or without any moving average.

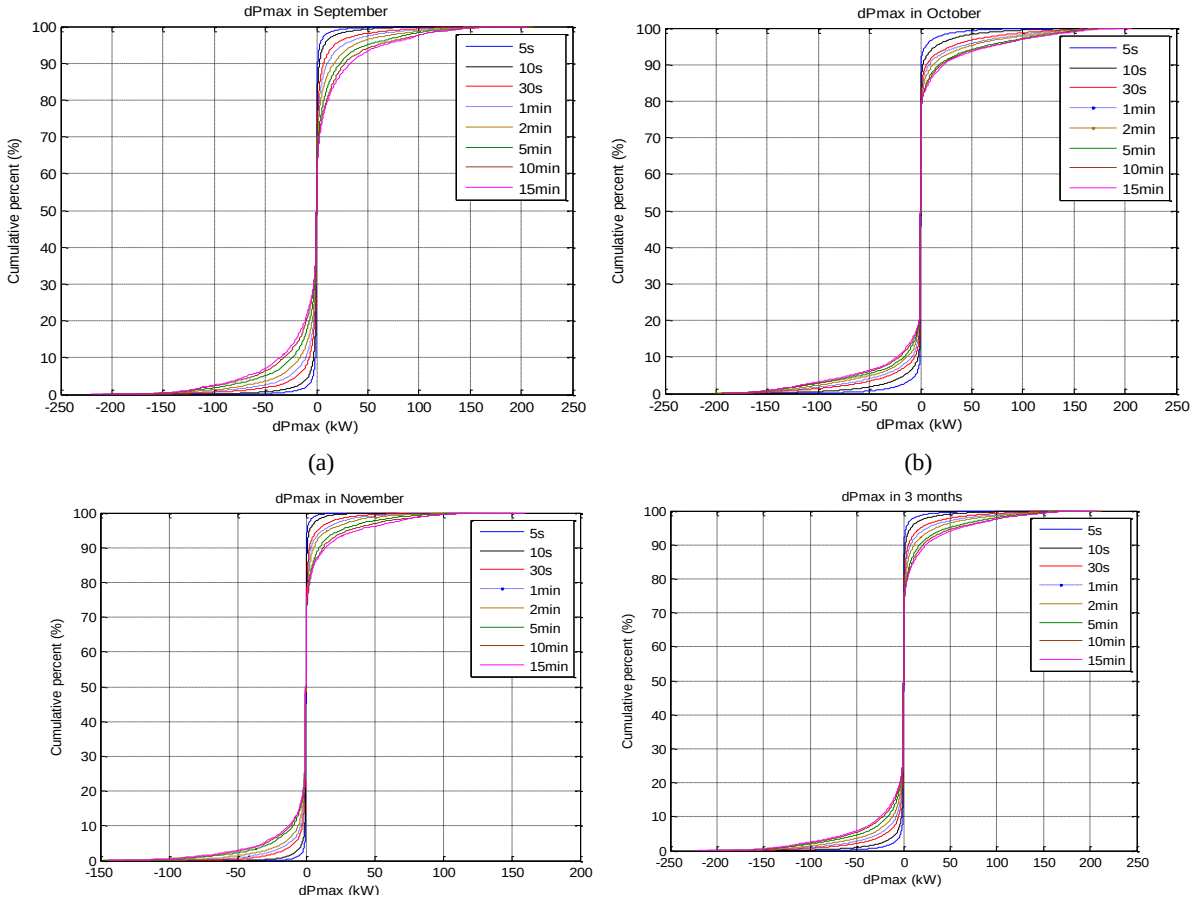

(a) (b)

(c) (d)

Figure 2.22 Cumulative distributions of optimum power deviation in (a) September (b) October (c) November (d) 3 months

The cumulative distributions of maximal power deviation for each month and during a three months period are plotted in Figure 2.22. The power of solar energy in November is less fluctuated than the power data in September and October. The power data of 3 consecutive months in Figure 2.22(d) show all occurrences of power variations. The time duration of 10 seconds is always too small to characterize such different situations of power fluctuations as it has been explained earlier. Other time durations can characterize the occurrences of fluctuation. The time duration depends on which occurrence is studied (fast fluctuation, slow fluctuation, and production lost). The maximal power deviation in three months data is +180 kW, which occurs in September and October.

c.) Maximum of power deviation for each time duration for every day in 3 months

In this section, the maximum of power deviation for each time duration is searched regardless to the signals in order to know the most critical power variation in each day. This maximum power will be compared to the limitation of power variation for each time duration for defining frequency problem. If the maximal power deviation is over the limitation power, frequency variation will be out of limit. In the first study, the number of occurrences of each power deviation is computed to characterize the different situations of power fluctuation. Therefore, power data for one day is translated to the maximal power deviation (see Figure 2.23, Figure 2.24 and Figure 2.25 for September, October and November respectively). Maximal power deviation of short time duration is smaller than of large time duration. Maximum of power variation in November is the smallest in three months. And the maximal power deviation of 200kW at time duration 1 minute is on 19 September 2011.

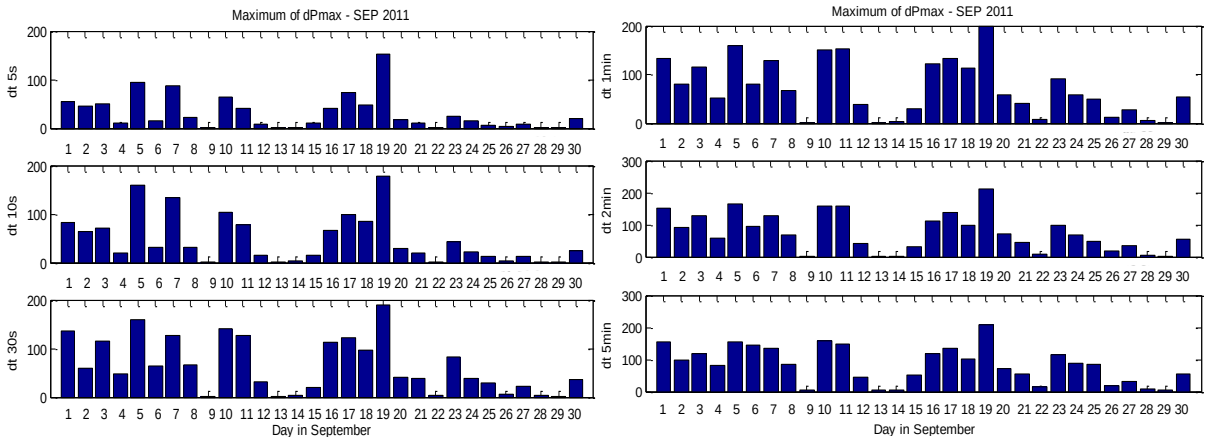

(a) (b)

Figure 2.23 Maximum of maximum power deviation in September with time duration (a) 5, 10, and 30 seconds (b) 1, 2, and 5 minutes

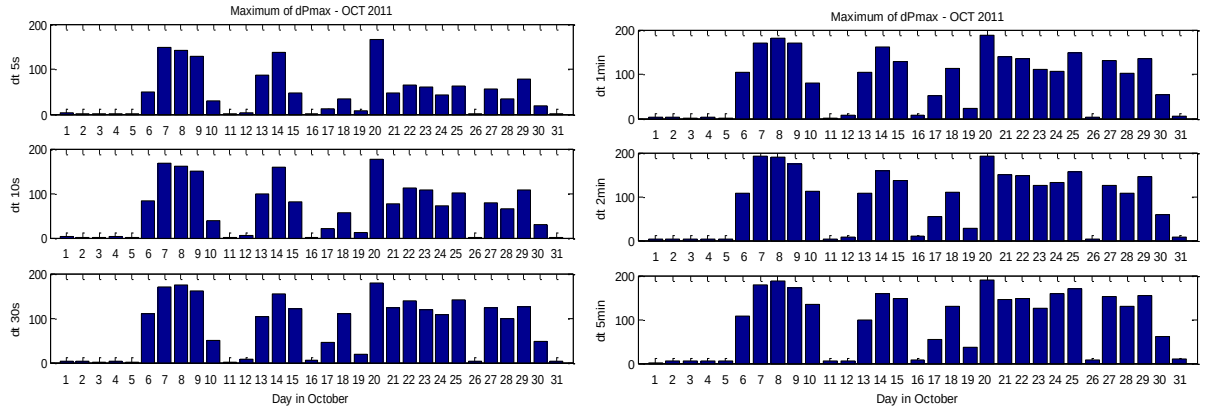

(a) (b)

Figure 2.24 Maximum of maximum power deviation in October with time duration (a) 5, 10, and 30 seconds (b) 1, 2, and 5 minutes

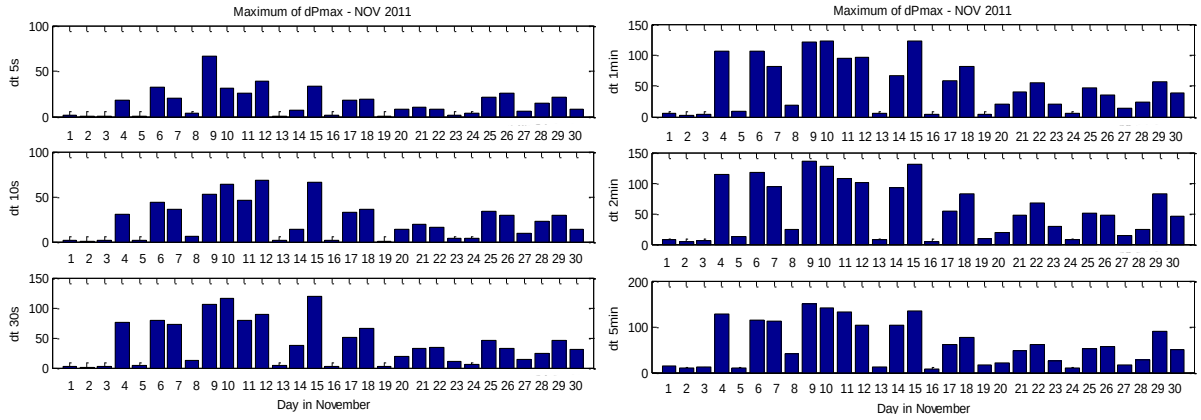

(a) (b)

Figure 2.25 Maximum of maximum power deviation maximum in November with time duration (a) 5, 10, and 30 seconds (b) 1, 2, and 5 minutes

d.) Influence of PV rated power

The influence of the PV plant on the preceding analysis is studied in this section, according to the rated power of solar energy. The power data in one year are then recorded from different photovoltaic plants:

- PV plant #2, with a rated power of 10kW and data recorded from 11/2010 to 09/2011,
- PV plant #3, with a rated power of 190kW and a recording from 11/2010 to 09/2011.

The maximal power changes (ΔP_{max}) for various time durations (Δt) are calculated for each plant. In this study, relative power fluctuation (ratio between the maximum power difference and the rated power ($\Delta P_{max}/P_{rated}$)) is used to compare several PV plants with different rated power. The summary results of number of occurrences for each maximum power variation of each plant are presented in Appendix I. We can see that the number of occurrence of power deviation increases when the rated power decreases.

Cumulative plot of all plants for time duration of 10 minutes is illustrated in Figure 2.26. It shows that the number of occurrence of large power variations for small rated plant (e.g. PV plant #2) is upper than that for large rated power plant (e.g. PV plant #3).

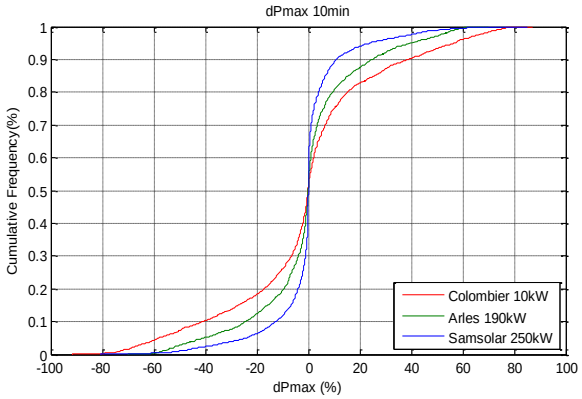

Figure 2.26 Cumulative distribution of PV plant #1, 2, and 3 for time duration 10 minutes

2.4.2.3 Conclusion of probability approach

To characterize different situation of fluctuations, time duration of 10 seconds seems to be too small. However, selection of time duration depends on which occurrence (fast fluctuation, slow fluctuation, and production lost) are relevant to the counting of occurrences of each situation. Time duration of 30 seconds is suitable for studying fast fluctuations. Time durations of 1 minute and 2 minutes seem to be the most adaptive time for the study of almost all occurrences. And time durations of 5, 10 and 15 minutes can be used to analyze slow fluctuations and losses of production. However, time duration above or equal to 2 minutes can filter small peaks.

Sliding and classical average calculations work as filters for data signals. The calculation of power deviations from the recorded data and data treated with average (with or without sliding) for time durations of 5, 10 and 15 minutes, are identical for slow fluctuations. Large time duration can be assumed as filter. The average time should not be upper than 2 minutes and less than time duration.

Finally, this section shows how to characterize any occurrence on PV power. But some questions have not been answered yet. For example: which situation of power fluctuation affects grid frequency? The following section is focused on this point.

2.4.3 Frequency analysis of PV signals

In the two preceding sections, signals of PV power were analyzed using a statistical approach. In this section, the power of PV signal is analyzed in the frequency domain in order to classify the characteristics of different signals. Spectrum of signal in frequency domain is obtained using the Fourier transform.

The frequency domain representation describes the signal in terms of its frequency content [95]. A spectrum of signal consists of a DC component (spectrum at zero frequency), and a component at each frequency. The DC component is equivalent to the average value in time domain. For example, signal in Figure 2.27(a) is transformed into frequency domain as presented in Figure 2.27(b). Spectrum in Figure 2.27(b) consists of DC component, a fundamental frequency component (w_0), a fifth harmonic component ($5w_0$), and a ninth harmonic component ($9w_0$) [96]. The signal is presented in frequency and time domain in Figure 2.28.

Fourier transforms (FT) is used to transform signal in time domain to frequency domain. As PV signal is discrete so it can be transformed to be in frequency domain by Discrete Fourier transform (DFT) in equation (2.17) where x(nT) is the discrete signal in time domain, N is number of sampled data, F is spacing of frequency domain samples, and T is the sampling period in time domain [95].

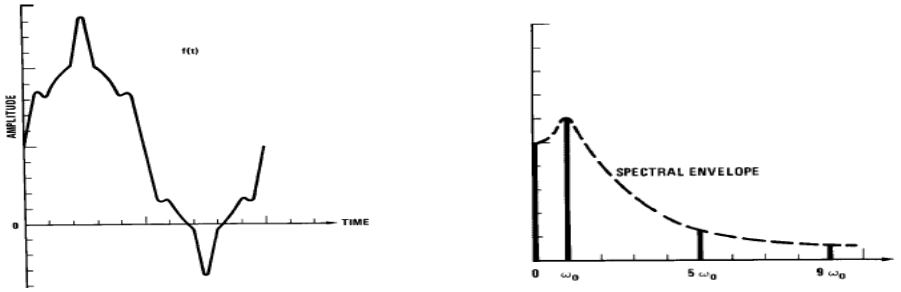

(a) (b)

Figure 2.27 (a) Signal in time domain (b) Spectral of signal (a)

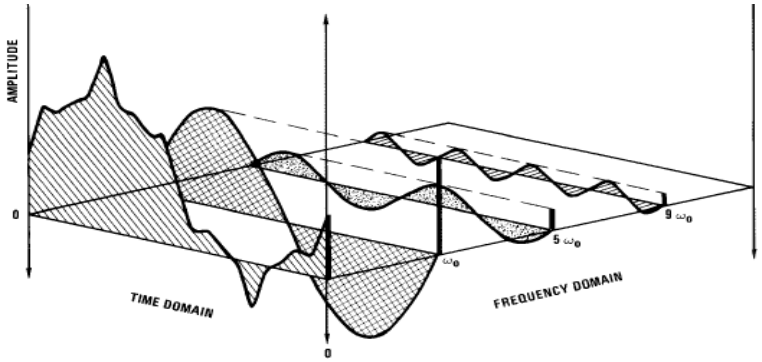

Figure 2.28 Signal presented in time domain and frequency domain

$$\boldsymbol{X(kF) = \sum_{n=0}^{N-1} x(nT) e^{-j2\pi(kF)(nT)/N}} \quad (2.17)$$

In our analysis, function of Fast Fourier transform (FFT) in MATLAB is used for calculating a DFT. FFT is a very fast and efficient algorithm for implementing a DFT [95]. DFT needs N^2 number of computations but FFT requires only $N\log_2 N$ operations.

DFT has some limitations. It is valid only in certain frequency and depends on sampling time and number of data. Moreover, the DFT assumes that signal is periodic. This causes a phenomenon known as "leakage" [95]. When signal is replicated, the discontinuity can occur. Spectral line spreads out over the wide frequency range. The solution is to force signal to zero at the end of the time record. Signal in time domain has to be multiplied to window function such as Hanning, Hamming, exponential, Blackman, etc. Window has to be well chosen to match our signal. In our analysis, the window method is not applied which is the same as [88] (analyze wind power in frequency domain by power spectrum). The spectrums of data with and without window methods are quite equivalent because, replicating our signal, no overlapping can be observed. Therefore, PV power is equal to zero at the end of measurement for each day.

From literature review in the first section, the power spectrum is used for frequency analysis [1]–[3]. The power spectrum corresponds to the square of the coefficients of Fourier transform. Furthermore, the "average spectrum", which means the intensity of the distribution of fluctuations during the entire day, is calculated [97]. The power spectrum is useful because the square of many electric component (like current (I), Voltage (V)) is homogeneous to power [96]. The power spectral density (PSD) corresponds to the normalized power spectrum by frequency.

Furthermore, the Fluctuation Harmonic Content (FHC) in equation (2.18) is computed to define fluctuations for each frequency, where P(f) is the spectrum at each frequency and P_0 is the average power [66]. If F is a whole range of frequency, FHC is equivalent to normalized standard deviation (NSD) in time domain. Large FHC means large fluctuations.

$$\mathbf{FHC(F)} = \frac{\sqrt{\sum_{\mathbf{f}\in\{\mathbf{F}\}}\left(\mathbf{P(f)}/\sqrt{\mathbf{2}}\right)^{\mathbf{2}}}}{\mathbf{P_0}} \tag{2.18}$$

Firstly, studies about signal analysis of intermittent energy in frequency domain are summarized. Next, the Fourier transform, data and indicators are defined for our case study. Finally, results and conclusions are presented

2.4.3.1 Frequency analysis methodology

Power data in time domain are transformed to frequency domain by DFT. To increase the resolution in frequency domain, the number of data for DFT will be increased to be 8 times of initial data (adding zero to initial data by MATLAB). DC value is analyzed as it is equal to the average value of power signal in time domain (P_{av}). Then, power spectrum and average spectrum are computed. Average spectrum gives some indications on the fluctuations of signal. In our analysis, the average spectrum for frequency upper than 0.01 Hz is computed. If the average spectrum has a large bandwidth, the signal is highly fluctuating. On the other hand, tight average spectrum means low fluctuations. Finally, FHC_Δ is calculated. Our FHC_Δ is calculated by (2.19) without any normalization by average power or DC value. Only one PV production plant is analyzed. If various PV plants are compared their characteristics, it should be normalized by average power or rated power. FHC_Δ is equivalent to standard deviation (SD) in time domain.

$$\mathbf{FHC_\Delta(F)} = \sqrt{\sum_{\mathbf{f}\in\{\mathbf{F}\}}\left(\mathbf{P(f)}/\sqrt{\mathbf{2}}\right)^{\mathbf{2}}} \tag{2.19}$$

Our frequency range for FHC_Δ is separated into 2 regions for low frequencies (below 0.01 Hz) and "high" frequency region (above 0.01 Hz). The separating frequency is approximated thanks to the cut-off frequency of secondary control of diesel (around 0.02Hz for our system). Frequency of power

fluctuations below this value is then filtered by secondary control of diesel. In our analysis, the maximal frequency of spectral is equal to 0.1 Hz for data with a sampling time of 5 seconds.

2.4.3.2 Frequency analysis results

The data recorded during one month are first analyzed, before studying fluctuations during one day.

a.) Monthly analysis

Spectrum in Figure 2.29 presents different peaks reported in Table 2.4. Peak at 1.25e-5 Hz signifies the period of signal for one day of 8e4 seconds. Other peaks are two to six times the base frequency of 1.25e-5 Hz. Average spectrums (for frequencies upper than 0.01 Hz) of 08/2011 to 11/2011 are equal to 1.572, 0.52, 1.332, and 0.083 respectively. So power in November presents always fewer fluctuations than for other months.

Table 2.4: Frequency at pics of spectrum

Period	Pic at frequency (x10-5 Hz)
24-30/08/2011	1,25//2,48//3,78//5
sept-11	1,25//2,5//4,99//7,51
oct-11	1,25//2,5//5
nov-11	1,25//2,48//3,78//8
24/08/2011-30/11/2011	1,25//2,5//3,75

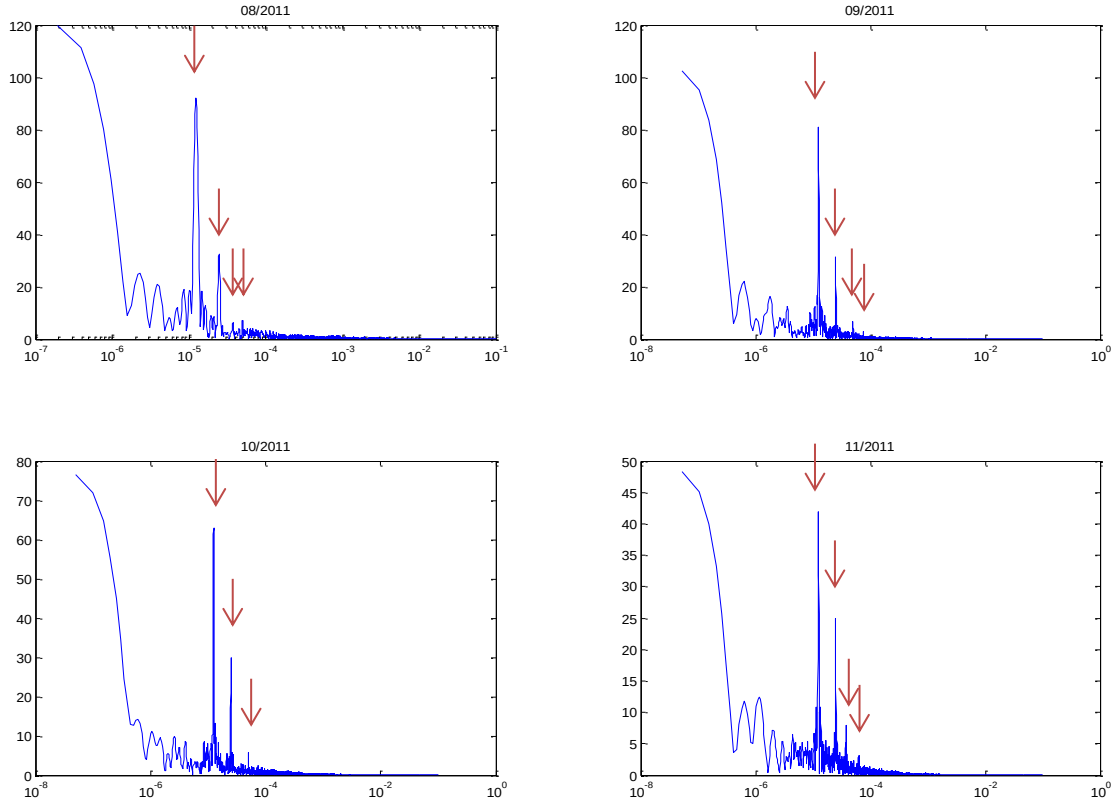

Figure 2.29 Spectral of power data in each month

b.) Daily analysis

The data for each day are analyzed. Signal in time domain of August 2011 that is illustrated in Figure 2.30 is transformed to frequency domain by FFT as presented in Figure 2.31. FHC for high frequencies and average spectrum of each day are also presented in Figure 2.32 (a) and (b) respectively.

Spectrums in Figure 2.31 have the same cut-off frequency. The FHC on 26/08 and 27/08 are much larger than other signals in August (Figure 2.32(a)). Signals on 29/08 and 30/08 have fewer variations. The average spectrum has the same trends in Figure 2.32(b). It is always largest on 26/08

and 27/08. So we may use FHC or average spectrum to classify situations related to frequency problems.

The FHC and average spectrum are computed for all signals in September, October, and November. The FHC in high frequency region (>0.01 Hz) of each month is illustrated in Figure 2.33, Figure 2.34, and Figure 2.35. The FHC in high frequency of November in Figure 2.35 is minimal and is maximal in October as shown in Figure 2.34.

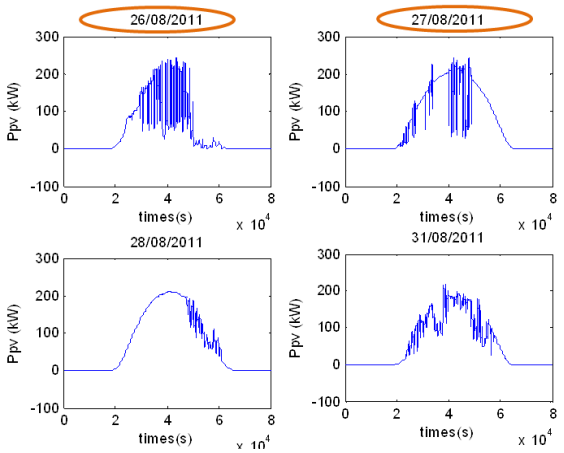

Figure 2.30 Power PV signals of four days in August

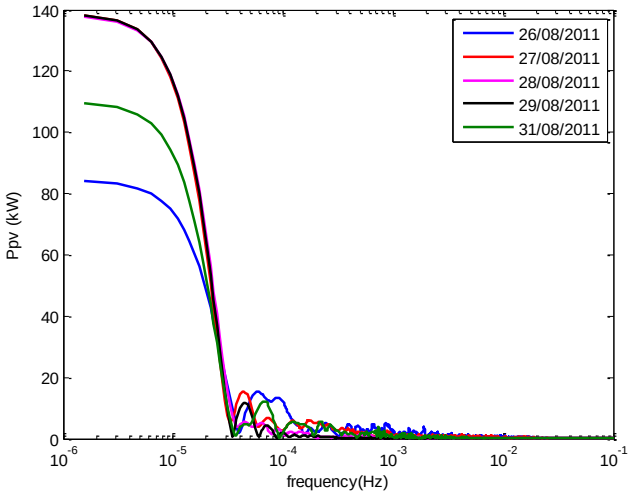

Figure 2.31 Spectral of five days in August

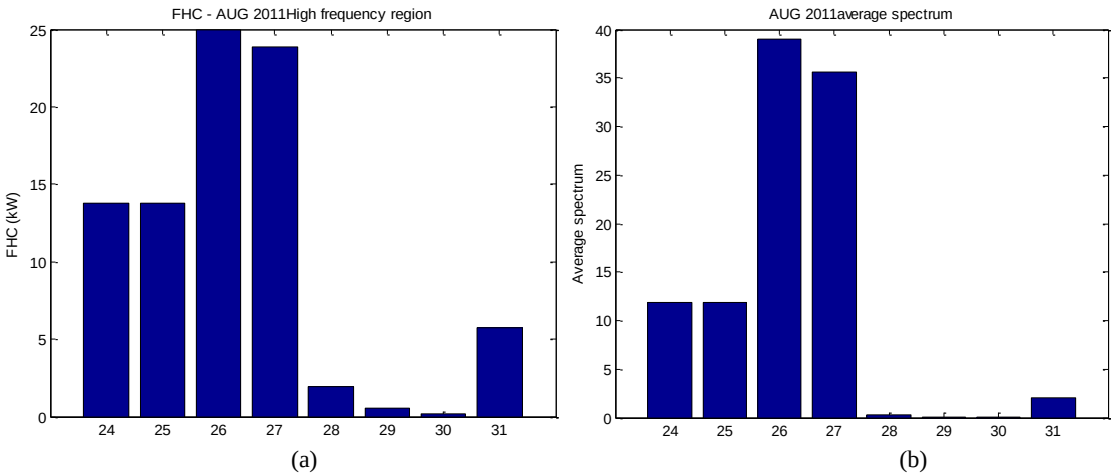

(a) (b)

Figure 2.32 (a) FHC in high frequency of each day in August (b) Average spectrum of each day in August

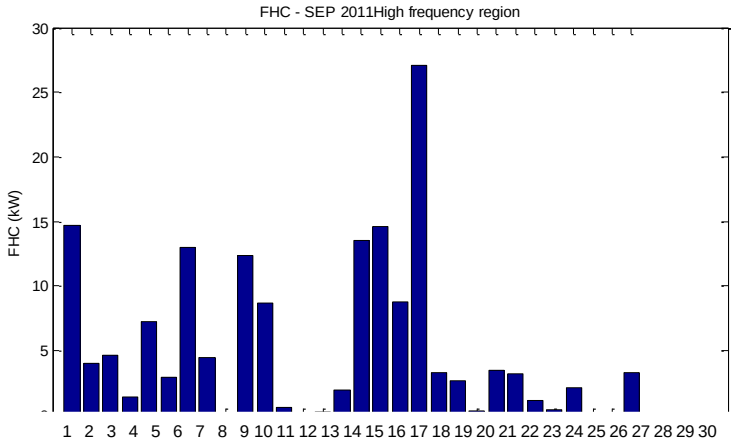

Figure 2.33 FHC in high frequency of each day in September

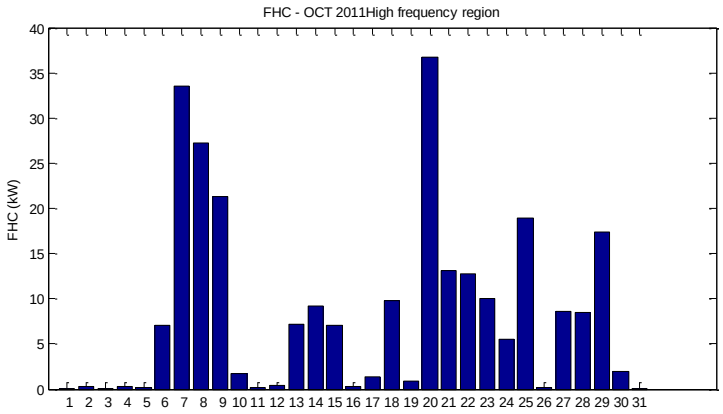

Figure 2.34 FHC in high frequency of each day in October

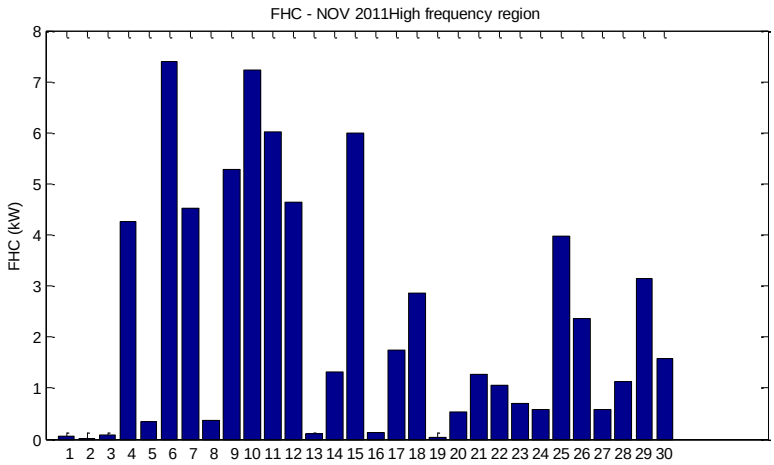

Figure 2.35 FHC in high frequency of each day in November

2.4.3.3 Conclusion of frequency analysis

Frequency analysis allows us to focus on frequency of fluctuations. There are many parameters to study any frequency spectrum. Average spectrum and FHC are quite suitable parameters to define variations of signal. High and low frequency regions are separated to be linked to frequency problems in the following section.

2.5 Comparison and link to frequency problem

Three different analysis methods have been applied to power data in the previous sections for both daily and monthly analysis. In this topic, methods are compared and linked to frequency issue. Firstly, the frequency variation according to PV variation is studied.

Real power data of the PV plant #1 (PV plant of 250kW) with a 5 seconds sampling time are used as a disturbance source of isolated micro power system. Islanding micro power system that consists of diesel generator of 2MW and global load of 1MW (corresponding to "Les Saintes" microgrid) is modeled in MATLAB Simulink. Active power of load is first assumed to be constant. The equivalent inertia is equal to 1 second. Frequency regulation of diesel generator is designed for primary and secondary frequency controls (with a droop value of 8%). The frequency response for any PV variation is then analyzed. Acceptable frequency range is 49.8-50.2Hz. If the frequency deviation from 50 Hz is always less than 0.2 Hz, it means no frequency problem. Frequency problems could be different if parameters of power system such as power rated of diesel, droop value of primary frequency control of diesel, inertia equivalent of system, etc. Then, acceptable frequency range is modified.

The PV signals inducing frequency issues are:

- for August => 2 signals : 26/08/2011 and 27/08/2011
- for September => 1 signal : 19/09/2011
- for October => 5 signals : 07/10/2011, 08/10/2011, 09/10/2011, 14/10/2011, 20/10/2011
- for November => 0 signal

So variations of PV power in November do not cause any problem to grid frequency. The most critical month is October. The analysis of signal fluctuation in the following topic is linked to this result in order to find the relationship between signal fluctuation and grid frequency problem.

2.5.1 Monthly analysis

From Table 2.1, the standard deviation of November, that is the minimal value, coincides with the absence of frequency problem. Many fluctuations in November may be presented in low frequency region. So this fluctuation study has to be combined with the signal analysis in frequency domain to know how much variations are presented in each frequency region.

The most critical month on grid frequency is October, but the SD and the percentage of powers out of limit for this month are less than for August or September. Therefore, SD signifies only that weather frequency is out of limit but it cannot identify impacts on frequency problem. Then, parameters in Table 2.2 are analyzed. Percentage over SD_{Δ} is in good accordance with frequency situations for October and November, excepted in September which presents a less percentage over SD_{Δ} than November. This may be caused by fast and large amplitude of variations in September but in few times, so these fluctuations have less impact on SD_{Δ}. The average power (P_{av}) and SD (variation from average value) can represent signal but SD_{Δ}, which means the variation from the reference signal, is much related to frequency problem, as power deviation which induces frequency variation is defined from the reference power point for which the frequency is equal to 50 Hz. So among five chosen signals analysis, only SD_{Δ} will be used as an indicator of fluctuation.

It has been indicated that parameters of signal analysis in time domain cannot be linked to fluctuation occurrences. It merely indicates that there is a risk to have a frequency problem. Standard deviation from both mean value and reference signal presents the global variation of signal but large frequency variations can happen at one time of large and fast fluctuations, which are neglected in SD and SD_{Δ} calculations. So maximal power deviation from reference signal of each month and all three months are searched.

The cumulative plots of each month data in Figure 2.21(a), (b) and (c) are analyzed. The power of solar energy in November is less fluctuate than the power data in September and October that coincides with result of normal statistical analysis and frequency problem. The cumulative distribution of maximal power deviation in three months period for various time durations is illustrated in Figure 2.21(d). The power deviation for 5 and 10 seconds are smaller than others. These two time durations give information of fast fluctuation. When time duration increases, the calculated power deviation also rises up. The maximum power deviation of this photovoltaic plant is 120kW and 180 kW with time

duration lower and over 30 seconds, respectively. This analysis with three months period is a global description and it could give useful information for sizing energy storage later.

The power data recorded during three months in time domain are transformed to frequency domain. Average spectrums (for frequency more than 0.01 Hz) of 08/2011 to 11/2011 are 1.572, 0.52, 1.332, and 0.083 respectively. High average spectrum signifies high fluctuations. So PV power in November presents fewer fluctuations than the other months, which is in good accordance with the two previous studies. Moreover, FHC for high frequencies of November (Figure 2.35) is less than one for the other months in Figure 2.32, Figure 2.33, and Figure 2.34. Calculations of maximal power deviation by probabilistic approach and average spectrum by frequency analysis can be classified from small to large values for November, September, and October respectively, which are in agreement with frequency problem.

To precise this first analysis, daily variations are analyzed in the next section.

2.5.2 Daily analysis

From all data, five different signals which illustrated in Figure 2.36 are studied. Signal A on 13/09/2011 is the reference case with a PV power presenting few fluctuations). Signals B and C which present some fluctuations are on 06/09/2011 and 14/10/2011, respectively. The last two signals (denoted signal D and E) recorded on 20/10/2011 and 25/10/2011 are very high fluctuated signals. Power signals A, B, and E do not cause any frequency problem. Besides, frequency response of power signals C and D is out of limit. The most critical frequency issue is caused by power signal D.

The SD_{Δ} of these different signals are presented in Figure 2.37. SD_{Δ} of power signals B and C, which are less fluctuated and quite similar to reference signal or signal A, are smaller than SD_{Δ} of signal D and E. However, the most fluctuated signal is signal E. Then, statistical analysis cannot always coincide with frequency problem. This is the same results as monthly analysis. The most fluctuation signal by this study is signal E but this signal does not cause any frequency problem.

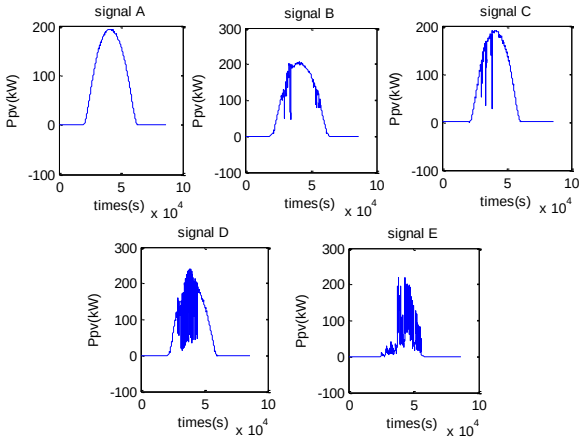

Figure 2.36 Studied power signal

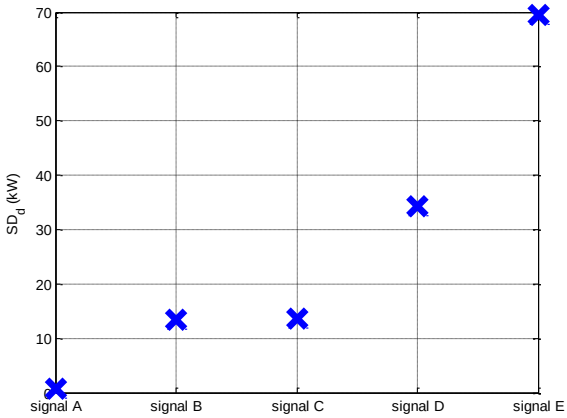

Figure 2.37 SD_{Δ} of six studied signals

The distribution histograms of maximal power deviation of signal A, B, and D with various time durations are shown in Figure 2.38(a), (b), and (c) respectively. The increase of time duration induces reduction of number of occurrences of small peaks (i.e. for power deviations between +/-15kW). Furthermore, maximal power deviation of reference signal (A) in Figure 2.38(a) is much smaller than signal D in Figure 2.38(b). Large power deviations of signals B and C (which have less fast fluctuations) appear for time duration over 30 seconds (that corresponds to slow fluctuations). Large power deviations of signal D and E appear for time duration of 10 seconds because it corresponds to fast fluctuations. The chosen time duration depends on which occurrence (fast or slow fluctuation) is relevant and which occurrence should disappear. Small time duration is adapted for fast fluctuation analysis and vice versa for slow fluctuation analysis.

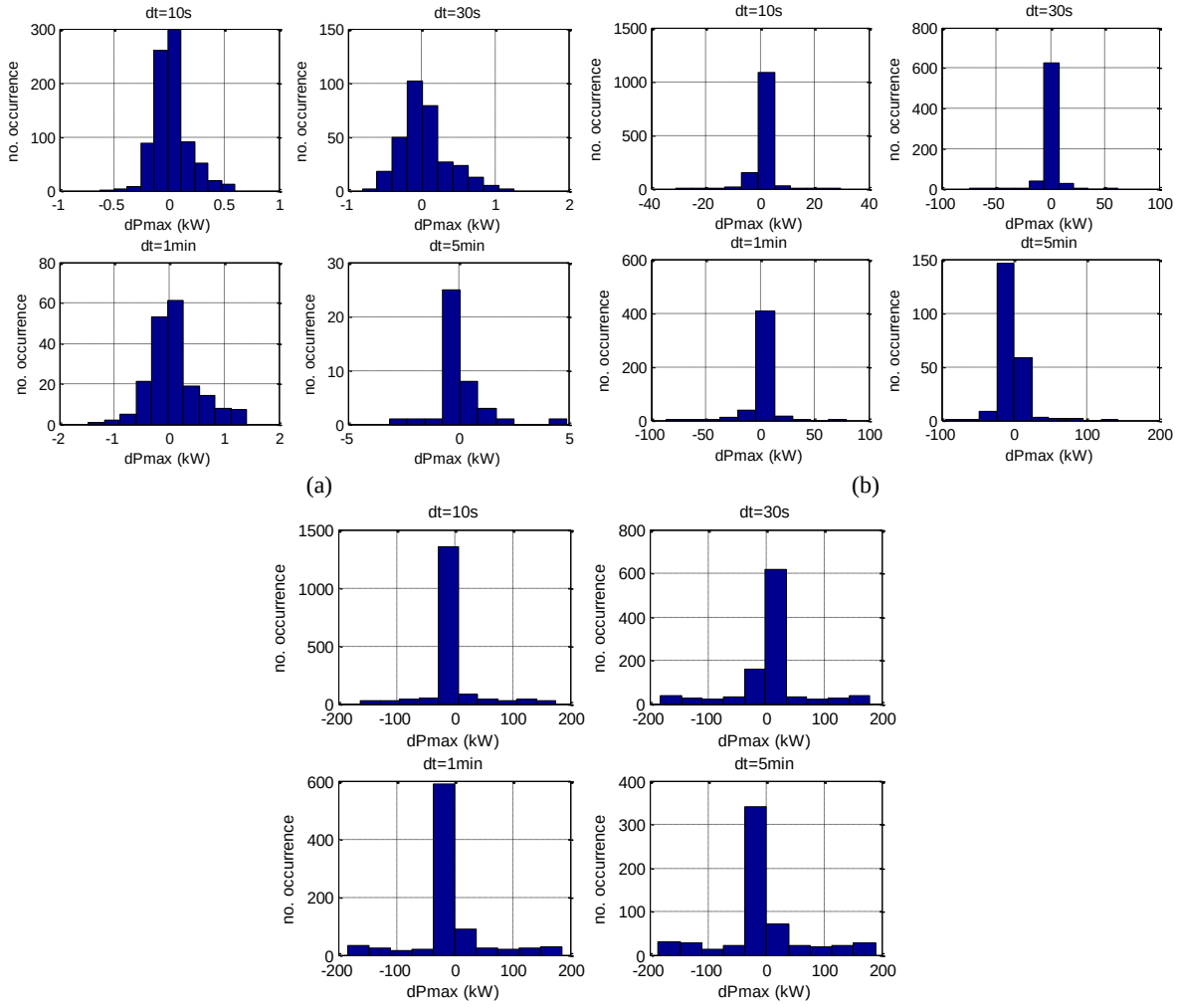

Figure 2.38 (a) Histogram of dPmax signal A (b) Histogram of dPmax signal B (c) Histogram of dPmax signal D

Moreover, cumulative plot of signal A, B, D, and E are illustrated in Figure 2.39. Large maximal power deviation of signal A is very different for each step time because power deviation is cumulated. Power deviation of signals B, D, and E for time duration over 30 seconds are quite similar as shown in Figure 2.39.

Figure 2.40 presents the maximum value of maximal power deviation (dPmax) of signal A to E. Signal D has the highest maximum power deviation for all time durations. Although signal C has less variation than signal E, the maximum of dPmax of signal C with time duration below 1 minute is larger than signal E. By this analysis, the largest fluctuation signal in signal D is different from previous study.

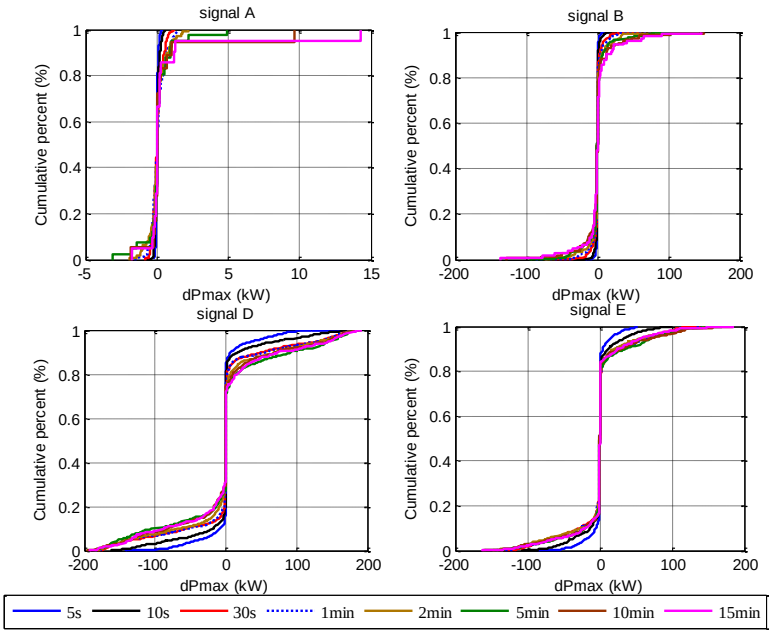

Figure 2.39 Cumulative plot of different studied signals

Data for each day are analyzed in the frequency domain. Spectrum of each signal is then illustrated in Figure 2.41 and the FHC_{Δ} in low and high frequency regions are shown in Figure 2.42 for each situation. We can then observe that:

- DC value of signal E is smaller than others.
- Cut-off frequencies of spectrum of signals A, B, and C in Figure 2.41 are quite identical.
- FHC_{Δ} calculated for signal A in high frequency region is closed to zero, which means that no fast fluctuations occurred. This coincides with signal represented in time domain in Figure 2.36.

In Figure 2.42, FHC_{Δ} of signal E in low frequency region is smaller than the others and FHC_{Δ} of signal D is larger than other signals in high frequency region. For future study on system frequency problem, the high frequency region is quite relevant. Therefore, the most fluctuated signal by this analysis is signal D, which is in good agreement with the probabilistic analysis.

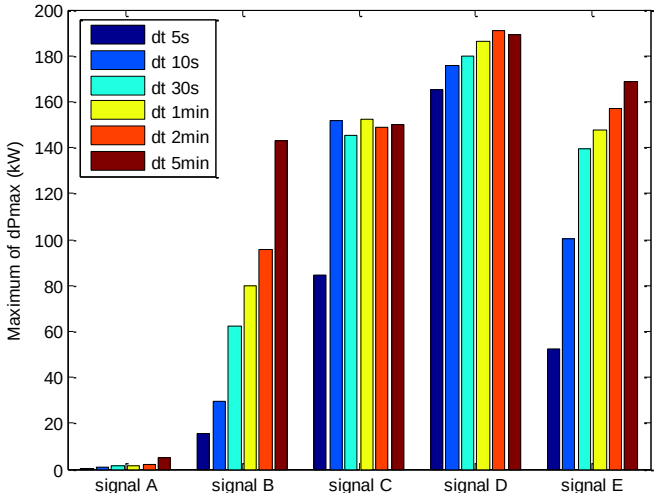

Figure 2.40 Maximum of dPmax

Maximum power deviations of C and D are larger than the others as shown in Figure 2.40. Moreover, FHC_{Δ} of high frequency region in Figure 2.42 of signal C and D are larger than the others. These two results coincide with frequency problem. These two power signal C and D cause frequency variation larger than limit.

The signal E in Figure 2.36 seems to be more fluctuated and may be the most critical situation of frequency problem but frequency response according to signal E respects frequency limitations. However, signal C which is less fluctuated than signal E also cause frequency problem. Frequency problem of signal C and E cannot be explained by FHC in high frequency alone because FHC in high frequency of signal C is smaller than signal E. It needs complementary information from maximum power deviation in Figure 2.40. Maximum of the maximum power deviation of signal C is larger than signal E for time duration from 5 seconds to 1 minute. Therefore, signal E is much fluctuated but amplitudes of variations are small. On the other hand, signal C is less fluctuated but there are fast fluctuations with large amplitude. The few times of large power deviation are not presented in FHC or in the average spectrum.

From these five chosen signals, we can conclude that if the FHC in high frequency is upper than 15 kW, frequency deviation will be higher than 0.2 Hz (signal D). If the FHC in high frequency is between 5 and 15 kW, the frequency has a risk to be out of limitations (it is the case of signals C and E). In this range of FHC values, the maximal power deviation for different time duration has to be analyzed. If the maximum power deviation at time duration of 10 seconds is more than 100kW, frequency problem will occur (signal C). On the contrary, frequency remains in acceptable limit if the maximum power deviation is small (signal E). Finally, a very small FHC in high frequencies (less than 5kW) signifies an absence of frequency problem (signals A and B).

These results should in future studies be strengthened and maybe generalized with another data from several PV plants.

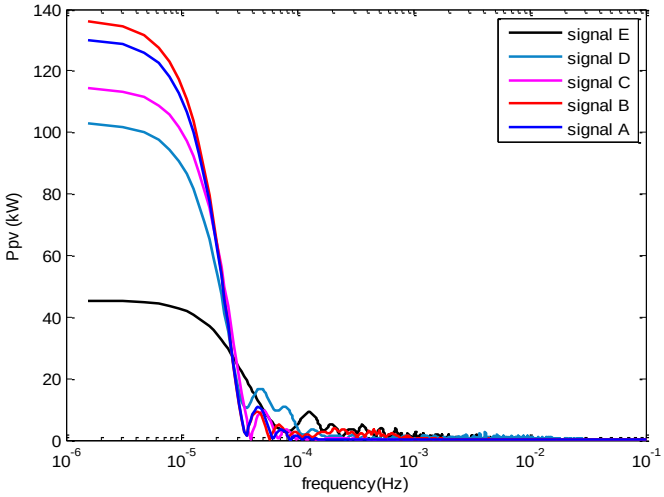

Figure 2.41 Spectrum of studied signals

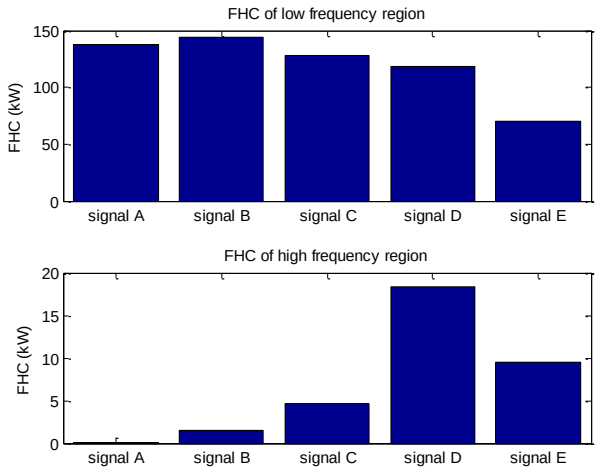

Figure 2.42 FHC_{Δ} in low and high frequency region of studied signals

2.6 Conclusion

This study investigates the relationship between power fluctuation and system frequency variation. The standard deviation which is an indicator of fluctuation in statistical approach does not coincide with system frequency variation. This indicator can only notice a risk of frequency problem. The standard deviation presents only global information about fluctuations. But one large frequency problem can be caused from only one large power variation, and this phenomenon cannot be taken into account in the standard deviation calculation.

Probability analysis and frequency domain analysis are applicable for the investigation of power fluctuation impact on system frequency. However, frequency distribution of power deviation from probability approach could be useful for design or sizing energy storage which will be elaborated in chapter 3.

Separation FHC value is approximated from the observation in three months data. If there are more analyzed data, this range will change. The value to separate region of FHC depends on the maximum frequency deviation (acceptable range of frequency), rated power of PV, and of diesel. Power deviation range will be studied another time in chapter 3 to evaluate the impact of PV power variation on grid frequency, in order to specify the relation of this range to the parameter of islanding micro power system.

For further study, frequency problem can be predicted in associate with weather forecast. Power variation of PV can be specified from predicted irradiance of meteorological study. Furthermore, Generic indicator based on PV production should be established in order to identify the risk of maintaining frequency, and the interest in hybridizing the main source with an energy storage system. Besides, Kernel methods may be quite relevant for advance statistical analysis in order to classify different signals.

Chapter 3

Impact of photovoltaic power variations on system frequency

3.1 Introduction

Grid frequency is usually regulated by interconnecter synchronous generators. However, if the electrical grid integrates many renwable energy, the frequency regulation by synchronous generator can not be sufficient ever. Thus, an energy storage system (ESS) can be an interesting alternative for the system to garuantee the frequency stability. The question is: for which situation of fluctuation an energy storage would be really needed? In the previous chapter, power signals of photovoltaic production have been studied and several characteristics of fluctuations have been identified thanks to indicators and analyses in frequency and time domains. This chapter will then focus on the impact of various fluctuations on the system frequency. The objectives of this study are to search for different critical situations of power fluctuation on grid frequency.

Firstly, the studied power grid of "les Saintes" is modeled. Then, the transfer function between the grid frequency and the photovoltaic power is studied taking into account of variation of power system parameters. The different situations of PV power variation according to different wave forms (as sine, step and ramp signals) are analyzed. Finally, the design of the energy storage device is discussed with a closed link to the characteristics of power fluctuation.

3.2 Grid modelling and simulated system

The studied islanding grid in Figure 3.1 consists in a direct connection of a unique diesel generator, a plant of solar energy production and an agregated load. Each element is modeled using dynamical models, in order to study frequency stability. The global control architecture is summarized in Figure 3.2. In this study, the generator is modeled only by its equivalent time response which depends on its rated power. The load power is constant. The small or large power fluctuations of photovoltaic are modelled as disturbances which cause frequency variations.

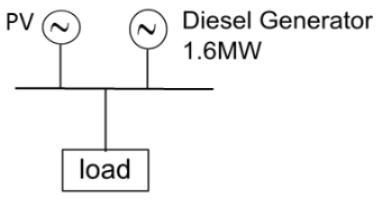

Figure 3.1 Simulated system representation

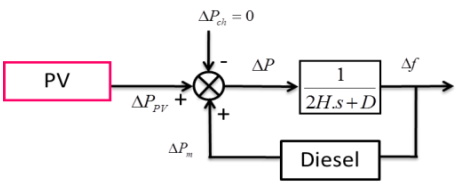

Figure 3.2 Simulated system control architecture

3.2.1 Diesel generator

Diesel generator system is constituted with a governor, fuel injection and engine, coupling shaft, automatic voltage regulator (AVR), and synchronous generator as illustrated in Figure 3.3(a). Only frequency control of synchronous generator (governor, fuel injection and engine, and coupling shaft) is considered. Controlling synchronous speed of generator (ω_{en}) enables us to control power of diesel generator via controlling torque of coupling shaft (τ_m). From Figure 3.3(a), governor is turned to frequency control; fuel injection, engine, and coupling shaft are grouped into diesel system in Figure 3.3(b).

Model of diesel generator in Figure 3.3(b) is separated into two parts: the frequency control and the dynamic behavior of engine. Frequency control will generate power deviation reference for diesel generator (ΔP_m^*) in relation with frequency variation (Δf). Power deviation of diesel that participate to frequency regulation (ΔP_m) is a function of power reference (ΔP_m^*) from frequency control and dynamic properties of diesel engine.

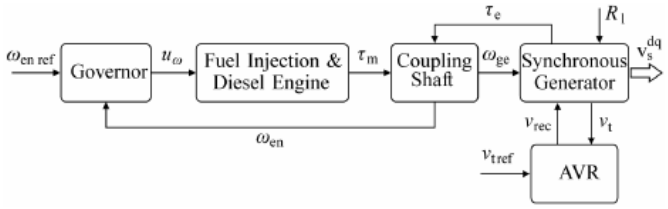

(a) [98]

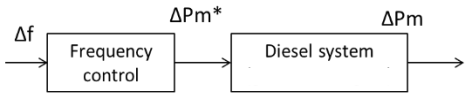

(b)

Figure 3.3 Modelling of diesel generator

3.2.1.1 Frequency control of synchronous machine

As it has been already seen in chapter 1, there are three levels of frequency control: primary, secondary, and tertiary controls. The role of energy storage device will be only associated to primary frequency control in this thesis.

Firstly, frequency control of diesel generator in this chapter is modeled with primary frequency control (equation (1.1)) in (3.1) where P_{m0} denotes the scheduled power, P_m the actual output power, ΔP_m^* the reference of power deviation, Δf the frequency variation, and s_d, the droop value. Frequency variation (Δf) is the difference between actual frequency (f) and nominal frequency (f_0 or 50Hz) in per unit. Besides, frequency control in equation (1.4) that presents primary and secondary control by PI controller is represented in (3.2) Proportional term of this controller is equivalent to primary frequency control, with a proportional gain K_p equals to the inverse of droop value (s_d). Integral part corresponds to the secondary frequency control, where integral gain K_i is linked to the inverse of time response of secondary control. Power and frequency in (3.1) and (3.2) are expressed in per unit.

$$\Delta \mathbf{P_m}^*(\mathbf{s}) = \mathbf{P_m} - \mathbf{P_{m0}} = -\frac{\mathbf{1}}{\mathbf{s_d}}.\Delta \mathbf{f}(\mathbf{s}) \tag{3.1}$$

$$\Delta \mathbf{P_m^*}(\mathbf{s}) = -\left(\mathbf{K_i} + \frac{\mathbf{K_p}}{\mathbf{s}}\right).\Delta \mathbf{f}(\mathbf{s}) \tag{3.2}$$

3.2.1.2 Modeling of synchronous machine

Dynamic part of thermal generator consists of actuator, governor and turbine. The reheat stream turbine, non-reheat steam turbine, and hydraulic unit are studied in [1], [40]. For diesel generator, turbine is replaced by engine. Dynamic of diesel engine can be modelled using different ways and degrees of complexity. In many studies (for instance in [7], [60],and [99]), actuator is simply modeled as a first order transfer function and diesel engine is modelled as a time delay in (3.3), where T_a is the time response of actuator, and τ, the time delay of diesel engine. Moreover, dynamic part (governor

and engine) can be modelled as a transfer function with one pole and one zero in (3.4), where T_1 and T_2 are linked to characteristics of diesel engine [19]. To simplify the model, a first order transfer function in (3.5), where T_g denotes the combustion delay as presented in [61], [67], [100], is also used. This last model is considered to be sufficient to simulate micro turbine for grid frequency problem [67]. Time response of diesel generator of 500kW varies classically between 0.8 and 1 second [100].

$$\Delta \mathbf{P_m}(\mathbf{s}) = \frac{\mathbf{1}}{\mathbf{T_a}.\mathbf{s}+\mathbf{1}}.\boldsymbol{e}^{-\boldsymbol{\tau s}}.\Delta \mathbf{P_m^*}(\boldsymbol{s}) \tag{3.3}$$

$$\Delta \mathbf{P_m}(\mathbf{s}) = \frac{\mathbf{T_1}\mathbf{s}+\mathbf{1}}{\mathbf{T_2}.\mathbf{s}+\mathbf{1}}.\Delta \mathbf{P_m^*}(\mathbf{s}) \tag{3.4}$$

$$\Delta \mathbf{P_m}(\mathbf{s}) = \frac{\mathbf{1}}{\mathbf{T_g}.\mathbf{s}+\mathbf{1}}.\Delta \mathbf{P_m^*}(\boldsymbol{s}) \tag{3.5}$$

3.2.2 Photovoltaic production

Power variation of photovoltaic corresponds to a disturbance on system frequency. Power of photovoltaic is first modeled in time domain using different signals. Then, the power of photovoltaic will evaluate from an initial value (P_{PV0}) to a final one (P_{PVn}) either rapidly (as a step signal) or continuously (as a ramp signal). Finally, the power fluctuations around the initial power (P_{PV0}) will be considered with different frequencies in a sine signal. It will be modeled in the following section. Only simulated signals are analyzed in this chapter. Real power PV presented in Chapter 2 will be used later in Chapter 5 in order to validate control strategy which is defined from results of studies in Chapter 2 and 3.

3.2.3 Load modelling

Active power variation of load ($\Delta P_{load}(t)$) can be separated into two parts, according to its independence ($\Delta P_{ch}(t)$) and dependence ($\Delta P_{ch\_d}(t)$) on frequency variation as shown in (3.6) [19]. The active load power independent to frequency variation is constant and equals to the summation of initial power of generator (P_{m0}) and initial power of photovoltaic (P_{PV0}). Initial means "conditions of frequency equilibrium". Therefore, load power deviation $\Delta P_{ch}(t)$ is equal to zero. Active power of load that depends on frequency variation is defined in (3.7), where D denotes the load damping coefficient.

$$\Delta \mathbf{P_{load}}(\mathbf{t}) = \Delta \mathbf{P_{\boldsymbol{ch}}}(\mathbf{t}) + \Delta \mathbf{P_{\boldsymbol{ch\_d}}}(\mathbf{t}) \tag{3.6}$$

$$\Delta \mathbf{P_{\boldsymbol{ch\_d}}}(\mathbf{t}) = \mathbf{D}.\Delta \mathbf{f}(\mathbf{t}) \tag{3.7}$$

In [1], load damping constant is defined as the percentage of load power variation for 1% of change in frequency. For example, a load damping constant equal to 2 means that 1% change in frequency would be related to a load variation of 2%. This parameter D is classically defined by experience [101], [102]. However, as information about load characteristic is quite limited, define an appropriate value of load damping constant is actually a little bit hard. In spite of this difficulty, it can be defined by frequency response of real system [8]. In [10] and [11], load frequency dependency can be separated into two types: impedance and motor loads. Relation between power and frequency depends on the power factor of impedance load. For motor load type, coefficient of load dependency with frequency is linked to the inverse of the motor slip. If frequency decreases, power of motor load will then decrease. Finally, the load damping constant (D) is the summation of coefficient of power and frequency dependency of all loads.

Classically, damping load constant has value ranged between 0.5 to 1 [19]. In many studies of frequency stability, load damping constant is even assumed to be equal to zero because this is the most critical situation. Large load damping coefficient means that active power of load can reduce frequency variations. This is relevant for the reduction of imbalance between load and generation, so frequency undergoes smaller variations.

3.2.4 Modelling of power system

From equations (1.1), (1.2) and (1.8) to (1.10), the deviation of angular velocity in per unit (ω_{pu}) can be defined as a function of source powers (diesel generator and photovoltaic power supplies, denoted P_m and P_{pv} respectively), load power (P_{load}) and equivalent inertia (H) in (3.8). Linear equation around an equivalent point of frequency deviation is presented in (3.9), using the Laplace transform. Frequency deviation (Δf) is then defined as a function of equivalent inertia and the difference between power variation of diesel generator (ΔP_m), photovoltaic (ΔP_{PV}) and load (ΔP_{load}).

$$\frac{d\omega_{pu}(t)}{dt} = \frac{1}{2.H.\omega_{pu}(t)}(P_m(t) + P_{pv}(t) - P_{load}(t)) \quad (3.8)$$

$$\Delta f(s) = \frac{1}{2.H.s}(\Delta P_m(s) + \Delta P_{pv}(s) - \Delta P_{load}(s)) \quad (3.9)$$

From equations (3.6), (3.7), and (3.9), the characteristic of system frequency can then be defined by the power unbalance between load and production (ΔP), the equivalent equivalent inertia of the system (H) and the load-damping constant (D) in (3.10). From equations (3.2) and (3.5), transfer function between frequency deviation and power deviation of photovoltaic is defined in (3.11), where power variation of load independent from frequency part is equal to zero (ΔP_{ch}=0). Besides, if diesel generator participate only to primary frequency control (Ki=0), transfer function between frequency deviation and power variation of PV is given in (3.12).

$$\Delta f(s) = \frac{1}{2.H.s+D}\Delta P(s) = \frac{1}{2.H.s+D}(\Delta P_m(s) + \Delta P_{pv}(s) - \Delta P_{ch}(s)) \quad (3.10)$$

$$\frac{\Delta f(s)}{\Delta P_{pv}(s)} = \frac{(1+T_g s).s}{(2.H.T_g).s^3+(2.H+T_g.D).s^2+(D+K_p).s+K_i} \quad (3.11)$$

$$\frac{\Delta f(s)}{\Delta P_{pv}(s)} = \frac{(1+T_g s).s_d}{(2.H.T_g.s_d).s^2+(2.H+T_g.D).s_d.s+(s_d.D+1)} \quad (3.12)$$

From equations (3.11) and (3.12), frequency variation then depends on parameters of: generator, power system, and characteristics of power fluctuation of photovoltaic. Parameters of the studied system in Figure 3.1 are presented in the Table 3.1 [19].

Table 3.1 : Parameter of islanding micro power system

Diesel generator		
Rated power	1.6MW, 2MVA	
Initial power	1MW	(0.5pu)
Droop	8%	
Ki	2	
T_g	0.8 seconds	
Power min. - Max.	0.2pu-0.8pu	
Load		
Power	1.2MW	(0.6pu)
Photovoltaic (at PV plant #1)		
Rated power	0.25MW	(0.125pu)
Initial power	0.2MW	(0.1pu)
Power system		
Equivalent inertia (H)	1seconds	
Load damping constant (D)	0.12	

3.3 Isolated grid analysis according to parameter variation

The impact of power fluctuation due to wind energy on system frequency has been already studied in [40],and [41]. The dynamic response of system frequency for a step change is then analyzed

in [40]. The frequency deviation linked to wind power is different because of the different types of turbine-governor. The reheat stream turbine, non-reheat steam turbine, and hydraulic unit are studied. All turbine types have a large impact in the medium frequency region. The hydro unit has a much larger transient frequency deviation than steam units because of its unique characteristics due to water inertia [1]. The impact of Automatic Generation Control (AGC) is also studied. However, it is slow and barely affects the transient peak value of the frequency deviation.

Power fluctuations with various frequency have been studied with sine signal in [40]. A frequency of fluctuation of 0.1 Hz was the dominant frequency that caused large impact on system frequency. The transfer function between the frequency deviation and the power perturbation is analyzed. The high frequency power fluctuations are absorbed by generator inertia and the low frequency ones are damped by AGC. Without AGC, at low frequency of fluctuations, the gain of this transfer function is flat and equals to the droop [40].

In this study, the different fluctuations of PV production are analyzed as they cause different effects on frequency response. So, various power fluctuations of solar energy (i.e. step, ramp, and sine signals) are applied to the system.

3.3.1 Frequency analysis of isolated grid transfer function

Transfer function between frequency deviation and power variation of PV is analyzed in frequency domain using Bode diagram. Only the magnitude between frequency deviation and power deviation is plotted in the following section. The most critical situation of frequency variation is first studied; then, a suitable region around the critical frequency will be defined for storage participation. Finally, an analysis of sensitivity of grid is proposed to analyze frequency variations.

3.3.1.1 Critical frequency

A zero and poles of system no secondary control in (3.12) with parameters in the Table 3.1 are -1.25, and -0.66 + 2.73i and -0.66 – 2.73i respectively. And zeroes of system with secondary control in (3.11) with parameters in the Table 3.1 are 0 and -1.25. And poles are -0.16, -0.57 + 2.72i and -0.57 – 2.72i. Therefore, frequency system initial (without ESS) is stable because all real parts of poles are negative. Transfer function from (3.11) and (3.12) is analyzed in frequency domain with Bode diagram in Figure 3.4. The system with only primary frequency control can be assumed as a low pass filter. Fluctuations in high frequency are then absorbed by equivalent inertia of power system. Magnitude of transfer function in low frequency domain is constant at -21.85 dB or 0.08. This value is equal to the droop value of synchronous generator. It is well-known that frequency in steady-state does not return to 50 Hz with primary control. The low frequency variation is damped by secondary control or AGC. It corresponds to slow response and barely affects the transient peak value of the frequency deviation [1].

We can mention a particular frequency called the critical frequency (f_{cr}), i.e. the frequency of power fluctuation that causes the dominant impact on system frequency. This critical frequency can be defined from amplitude of poles of system (3.11) or (3.12). Amplitudes of poles of system with and without secondary control are 2.78 and 2.81, respectively. It has been assumed that critical frequencies of these two different systems are identical. So, system with primary control in (3.12) is used to define critical frequency because of low order equation. To calculate poles of this system, the parameter A_F in (3.13) is defined to separate real pole (for A_F in positive value) and imaginary pole (for A_F in negative value). Finally, critical frequency in rad/s is calculated in (3.14). This frequency depends on characteristics of synchronous generator (T_g), equivalent inertia (H), load damping constant (D) and droop coefficient of generator (s_d). Impact of parameters on critical frequency will be discussed later.

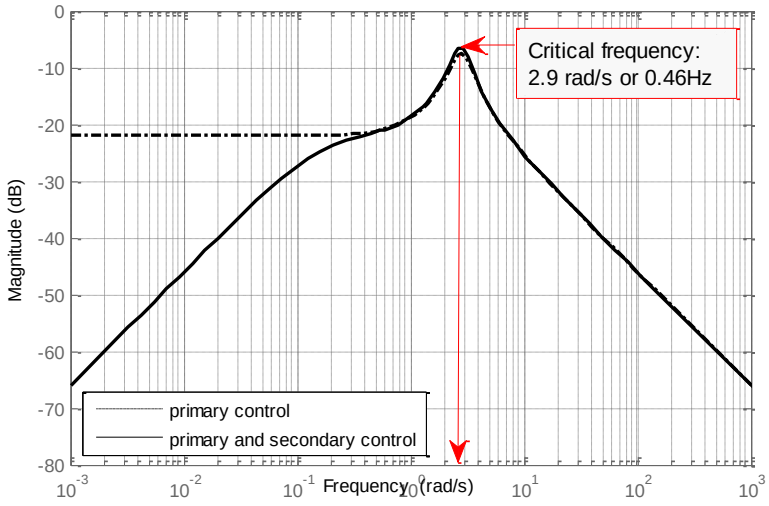

Figure 3.4 Bode diagram of different frequency control of diesel

$$A_F = \left(2.\mathrm{H}.s_d + s_d.\mathrm{T_g}.D\right)^2 - \left(8.\mathrm{H}.\mathrm{T_g}.s_d(D.s_d + 1)\right) \tag{3.13}$$

$$f_{cr} = \begin{cases} \frac{1}{4.s_d.H.T_g}\left|-(2.H.s_d + s_d.T_g.D) \pm \sqrt{(2.H.s_d + s_d.T_g.D)^2 - (8.\mathrm{H}.\mathrm{T_g}.s_d(D.s_d+1)}\right| & ;A_F \geq 0 \\ \sqrt{\frac{(D.s_d+1)}{2.H.s_d.T_g}} & ;A_F < 0 \end{cases} \tag{3.14}$$

The definition of critical frequency is used to classify worst case situation of power photovoltaic variation. Frequency of power fluctuation much higher than this critical frequency is filtered, resulting small frequency variations. On the contrary, frequency of power variation around critical frequency can cause very large frequency variations. Therefore, this situation is interesting for energy storage to limit grid frequency variations.

From spectral analysis of PV power in topic 2.4.3, there is some power variation over 0.01Hz (from results of FHC in high frequency region). However, analyzed frequency of fluctuation in topic 2.4.3 is limited at 0.1 Hz according to 5 seconds – data sampling time. Firstly, we will assume that there is no power variation of PV at critical frequency. However, this PV power fluctuation occurs in primary frequency zone which can be specified by cut-off frequency in the following topic. In order to study characteristic of PV power around critical frequency for further study, data sampling time should be lessen.

3.3.1.2 Analysis of Bode diagram

In this section, frequency of fluctuation is classified in several zones according to the regulation of system frequency. As it has been discussed in chapter 2, frequency of power fluctuation can be separated in three zones according to low (<0.01Hz), medium (0.01-1Hz), and high frequencies (>1Hz) [40]. Each frequency region corresponds to the band-width of secondary control, primary control and equivalent inertia of power system respectively. Secondary control of diesel generator filters low frequencies of power variation like a high pass filter. The equivalent inertia works as low pass filter. Define cut-off frequencies to separate frequency zones would be useful to define the interesting band-width of participation for an energy storage system. To calculate these cut-off frequencies, the dynamic part of diesel generator is firstly neglected in order to simplify the expression of the transfer function (T_g=0) in (3.15). Magnitude of transfer function in (3.12) and (3.15) are then illustrated in Figure 3.5. Dynamic part affects the medium frequency region which is the region of primary frequency control and it hardly affects the cut-off frequency. Therefore from (3.15), two cut-off frequencies denoted $w_{c1,2}$ can be calculated in (3.16). These frequencies depend on parameters of power system and frequency control system of diesel generator.

$$\frac{\Delta f(s)}{\Delta Ppv(s)} = \frac{s/_{2.H}}{s^2+\frac{D+Kp}{2.H}s+\frac{Ki}{2.H}} \tag{3.15}$$

$$w_c = \pm\frac{D+Kp}{4.H} + \frac{1}{2}\sqrt{\left(\frac{D+Kp}{2.H}\right)^2 + \frac{4.Ki}{2.H}} \tag{3.16}$$

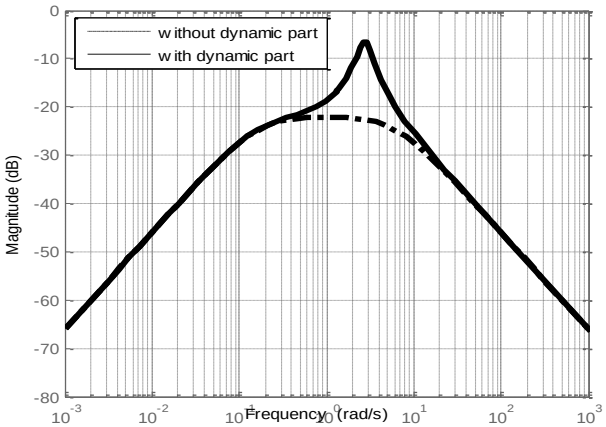

Figure 3.5 Bode diagram of system with secondary control (with and without dynamic part of diesel)

From equation (3.16), low and high cut off frequencies are 0.025Hz and 1Hz. Therefore, for the studied islanding grid, the secondary frequency control limits frequency deviation for PV fluctuations below 0.025Hz. Power fluctuations above 1Hz are filtered by the equivalent inertia of the grid. Finally, the most critical frequency variation is situated between 0.025 Hz and 1 Hz, which is likely to be a suitable zone for the participation of an energy storage device.

3.3.1.3 Sensitivity analysis of grid parameters

Poles evolution of system with secondary control in Figure 3.6 is firstly analysis. The increasing of droop value (s_d) does not affect to real part of poles two complex poles but it make a real pole increase which is risky to be in instable zone (positive real part). Inertia equivalent (H) and load damping constant cause the reduction of a real pole. But real part of two complex pole increase when inertia equivalent increases. Furthermore, time response of diesel generator does not cause any effect to a real pole but it cause the same effect to two complex poles as inertia equivalent. The results of two complex poles also validate for system without secondary control (there is no real pole).

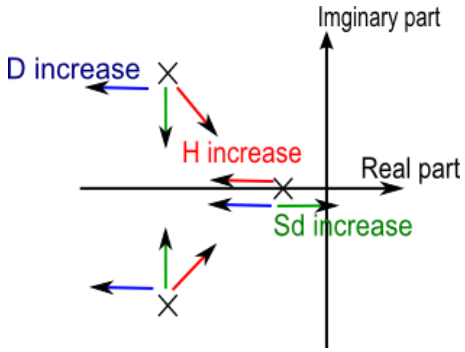

Figure 3.6 Poles evolution of system according to parameters variation

Sensitivity of parameters of the transfer function between frequency deviation and power variation is then analyzed by Bode diagram. System without secondary control is firstly studied in order to study the impact of parameters on steady-state frequency (low frequency region). The equivalent inertia (H) has a great impact on the magnitude of transfer function only in high frequency region as illustrated in Figure 3.7. It can also be observed from Figure 3.7(b) and (c) that the droop value and the load damping constant have impacts on the magnitude of transfer function especially in low and medium frequency regions. In the low frequency region, the magnitude of transfer function is

constant and equals to the droop value (for D=0 only). Magnitude of transfer function decreases when load damping constant increases.

System with secondary control is then studied. The equivalent inertia (H) has an effect on the critical frequency and high cut-off frequency in Figure 3.8. The constant inertia does not affect the low frequency region. In high frequency region, all responses have the same slop. Therefore, we verify that a power system with a high equivalent equivalent inertiapresents less frequency variations than system with low equivalent inertiafor an identical PV power variation. Next, the damping load constant and droop of diesel are varied. The damping load constant barely impacts the cut-off frequency in Figure 3.8(b). And it impacts only the magnitude of transfer function in medium frequency region.

Droop value or primary frequency control parameter has the same effect on the transfer function as load damping constant. It impacts only on medium frequency in Figure 3.9; but the integral gain (K_i) has large impact on low frequency and low cut-off frequency as shown in Figure 3.9. A large Ki term (i.e. a small time response of AGC) increases low cut-off frequency, so bandwidth for primary control is smaller (secondary control takes part in some medium fluctuations).

Impact of time response of diesel generator is also studied as illustrated in Figure 3.10. Time response of diesel generator barely affects to the cut-off frequencies. It casues much impact on medium frequency region. Increasing time response of the diesel generator will cause decreasing in critical frequency but magnitude of transfer function will rise up. Consequently, a large frequency variation of system with a large time response of diesel generator can occur.

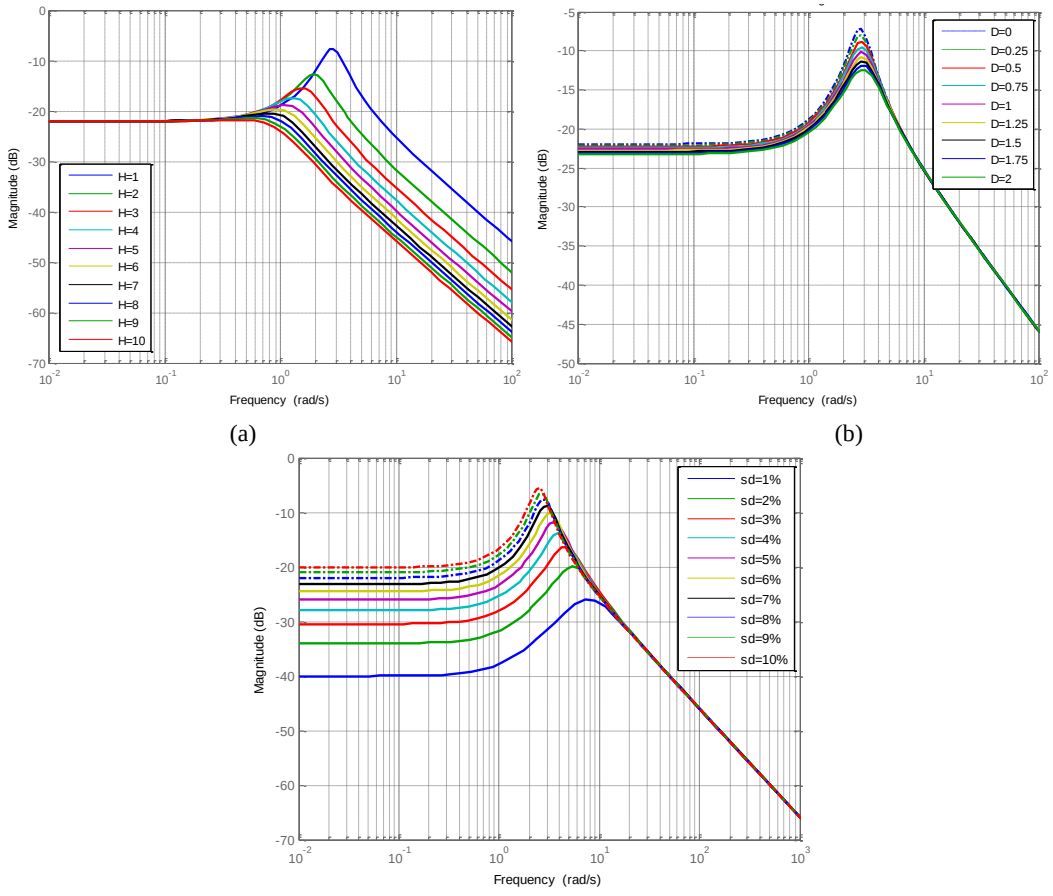

Figure 3.7 Bode diagram of system (with only primary frequency control of diesel generator) with (a) different equivalent inertia (b) different load damping constant (c) different droops of diesel generator

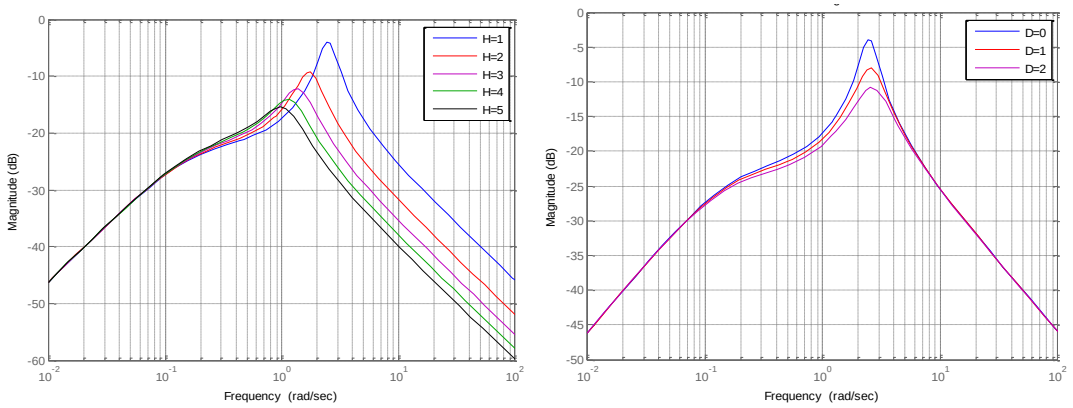

(a) (b)

Figure 3.8 Bode diagram of system (with primary and secondary control of diesel generator) with (a) different equivalent inertia (b) different load damping constant

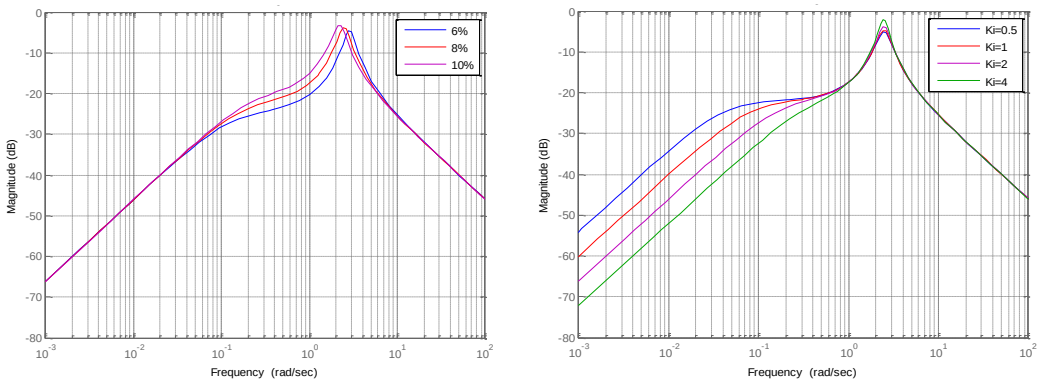

(a) (b)

Figure 3.9 Bode diagram of system (with primary and secondary control of diesel generator) with (a) different droop value of diesel (b) different integral gain

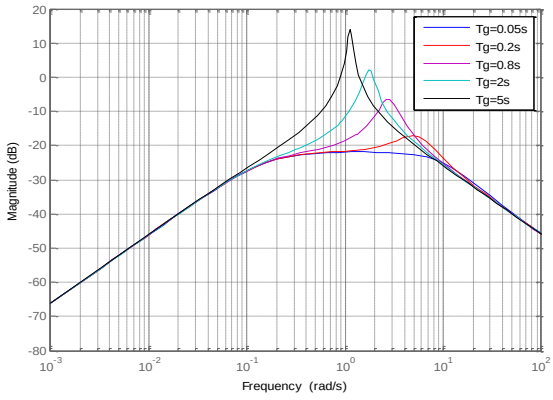

Figure 3.10 Bode diagram of system (with primary and secondary control of diesel generator) with different time response of diesel generator

3.3.2 Time domain analysis according to PV time variations

In order to analyze the impact of PV power variations on grid frequency, the system response is studied in this section without secondary control, because energy storage will assist diesel generator to limit frequency deviation in transient regime. Thus, different models of time variations are studied with step, ramp and sine signal inputs of our system.

3.3.2.1 Impacts of tep and ramp signals on grid frequency

PV power variation modelled with ramp signal in Figure 3.11 can be presented in function with time in (3.17), where $\Delta P_{pv}(t)$ denotes the power deviation of PV in function with time, ΔP_0 is amplitude of power deviation (or P_{pv1}-P_{pv0}), and Δt is the duration of power change from P_{pv0} to P_{pv1}.

Power deviation ΔP_0 is negative if power fall down in Figure 3.11(a) and positive for increasing power in Figure 3.11(b).

$$\Delta P_{pv}(t) = \begin{cases} \frac{\Delta P_0}{\Delta t}.t \ ; & 0 < t \leq \Delta t \\ \Delta P_0 \quad ; & \Delta t < t \end{cases} \tag{3.17}$$

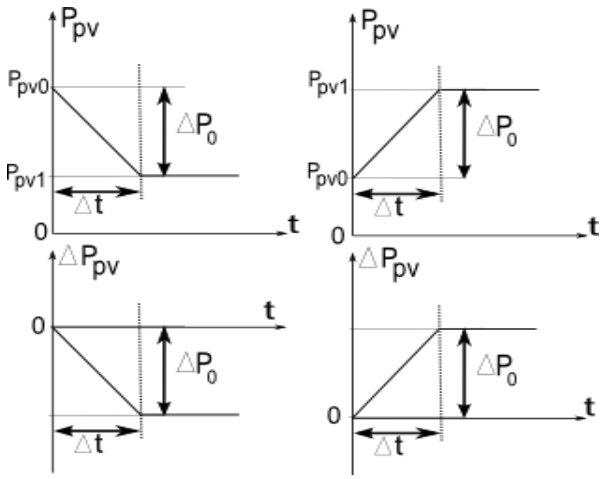

(a) (b)

Figure 3.11 Power and power deviation of PV in time domain (a) decreasing case (b) increasing case

The power of solar energy decreases from P_{pv0}=200kW to P_{pv1}=100kW (or 0.1 per unit to 0.05 per unit according to rated power 2MVA) with different durations (Δt) such as 0s (step), 5s, 10s, 15s,…, 60s as shown in Figure 3.12(a). The frequency response is presented in Figure 3.12(b).

The characteristics of frequency response with different durations (Δt) are presented in Table 3.2. The rise time is duration for which the frequency response rises from 10% to 90% of steady-state value. The settling time is the time for which the frequency response is in the window +/-2% of the steady-state value.

The duration of power change impacts the transient response of the frequency variation but the steady-state value of frequency is identical. The frequency value at steady state is 49.8 Hz. The minimum value of the frequency increases (i.e. frequency deviation decreases) when the changing duration increases. For 0s to 5s, the minimum frequency rises rapidly but after 5 to 60 seconds it barely increases. Study is also undertaken on the different amplitude of power change. The amplitude of power fluctuation impacts only the steady-state response. More power fluctuations are presented, more frequency variations in steady state are observed

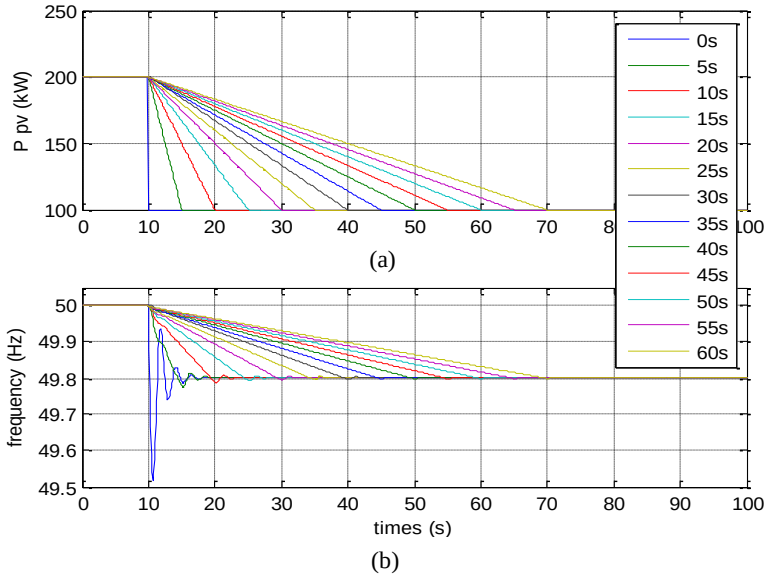

Figure 3.12 (a) Power variations of solar energy (b) Frequency responses

Table 3.2 : Summary results of frequency response for different time of power change

Δt (s)	f minimum (Hz)	time at f minimum (seconds)	rise time (seconds)	settling time (seconds)
0	49.520	0.65	0.13	6.77
5	49.770	5.2	3.45	9.00
10	49.790	10.2	7.86	11.90
15	49.790	15.2	12.20	16.90
20	49.790	20.2	16.50	21.60
25	49.800	25.2	20.15	26.20
30	49.800	30.2	23.80	31.50

The power fluctuation is changed with different durations. The minimum frequency (in transient response) is plotted versus the duration for various power fluctuations in Figure 3.13(a). It can be observed that the minimum frequency changes rapidly for the small duration (0 to 10 seconds), but it changes slowly for durations more than 10 seconds for all power fluctuations. The most critical situation of power fluctuations for frequency variations corresponds to PV step change with large magnitude of power change. Finally, the amplitude of frequency deviation in steady state is also plotted versus different durations of change in Figure 3.13(b).

It can also be seen in Figure 3.14 that the maximal absolute frequency deviation evaluates as a linear function with the absolute power change for all durations. The equations represented relation between frequency variation, maximal power variation, and time duration will be specified in the following topic.

The maximal frequency deviation according to PV power with ramp signal is smaller than step signal for the same amplitude of power variation. For the long durations (above 10 seconds), the slope of frequency deviation with power change is quite identical. For long duration of change, the power deviation should be high enough to have the same frequency deviation as the step power fluctuation. For example, frequency deviation 0.3 Hz is occurred by the step power variation 0.03 per unit. But power in ramp signal with durations above 10 seconds should be about 0.07 per unit for the same frequency deviation.

Parameters of system such as droop value, equivalent inertia and load damping constant are also changed. The results of frequency response for variations of these different parameters are summarized in Annex II. When the droop value increases, the minimum frequency will fall down (the frequency deviation from nominal frequency (50Hz) increases) but the frequency deviation at steady-state rises up. However, the frequency response takes more time to recover to its steady state when the droop goes up.

The frequency deviation in transient response decreases when the equivalent inertia (H) increases. This parameter does not cause any impacts on the frequency at steady-state value but the frequency response takes more time to return back to its steady state for high equivalent inertia.

The frequency deviation decreases both in transient and steady state when the load damping constant goes up but the frequency response takes less time to come back to its steady state value for high damping load constants. These results are much closed to physical interpretations of these parameters.

Finally, sensitivity of these parameters is also studied for different durations of power change of (from 0 to 60 seconds). The minimum frequency is plotted versus the duration of change for each variation of parameters as illustrated in Figure 3.15(a), (b), and (c). The equivalent inertia (H) does not cause any effects on the system frequency for a duration upper than 20 seconds. The frequency deviation increases when the droop value increases or when the load damping constant decreases. Therefore, a power system with a large droop value and a load damping constant closed to 0 present high risks on frequency variations for PV fluctuations with long duration of change.

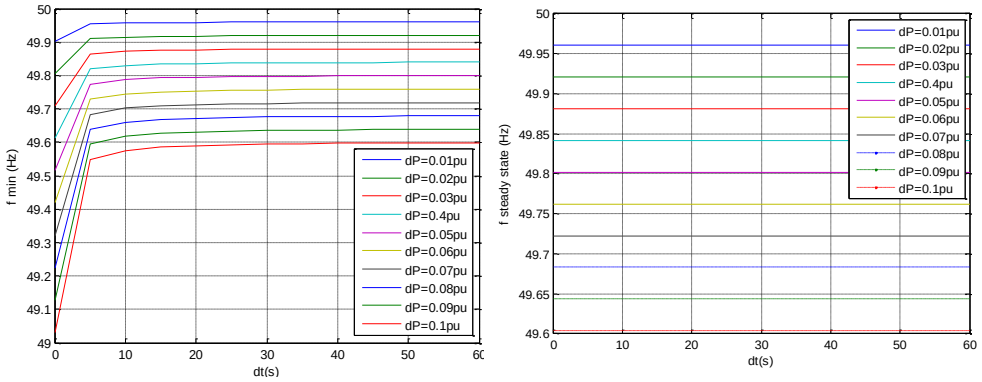

(a) (b)

Figure 3.13 (a) minimal value of grid frequency (b) frequency deviation in steady state versus different duration of change for various amplitude of power deviation

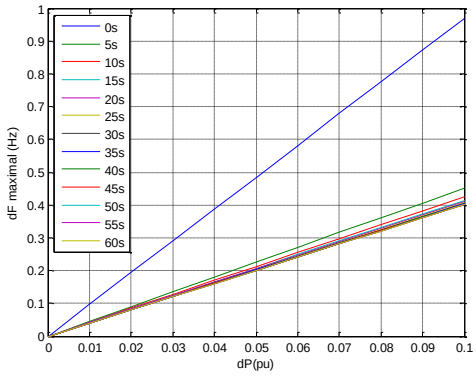

Figure 3.14 The maximum frequency deviation versus amplitude of power deviation for various durations of change

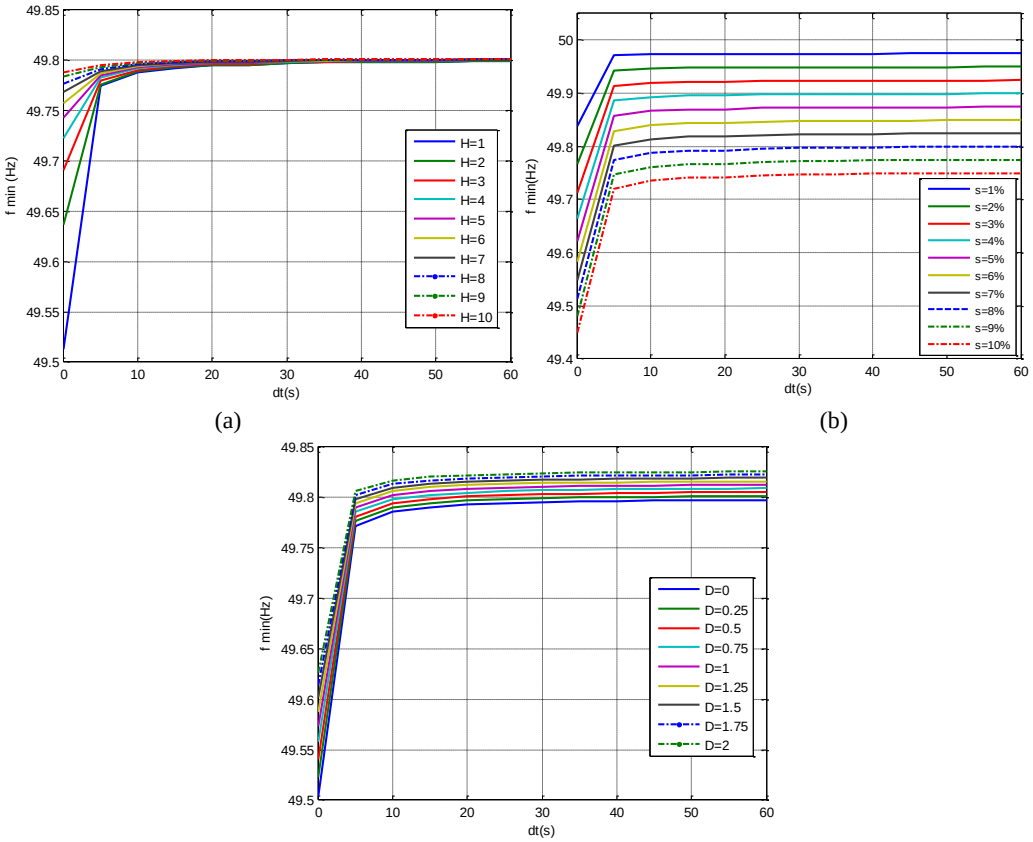

(a) (b)

(c)

Figure 3.15 Minimum frequency versus the duration of change for variation of (a) equivalent inertia(b) droop value of diesel generator (c) load damping constant

3.3.2.2 Impacts of sine signal on grid frequency

Power of photovoltaic is assumed to be modelled as a sine signal in (3.18) where P_{v0} denotes the initial power of photovoltaic, dP is the maximum power deviation, f_{PV} is the frequency of power signal. In this study, the solar plant is supposed to produce 0.05 p.u. (100kW) (P_{v0}=0.05 p.u.) and the maximum power deviation is firstly equal to 0.05 per unit (dP=0.05 per unit). The example of power signal is presented in Figure 3.16. The frequency of power fluctuation (f_{PV}) varies from 0.05 Hz to 1 Hz, around the critical frequency.

$$Ppv(t) = P_{v0} + (dP*\sin(2*pi*f_{PV}*t)) \quad (3.18)$$

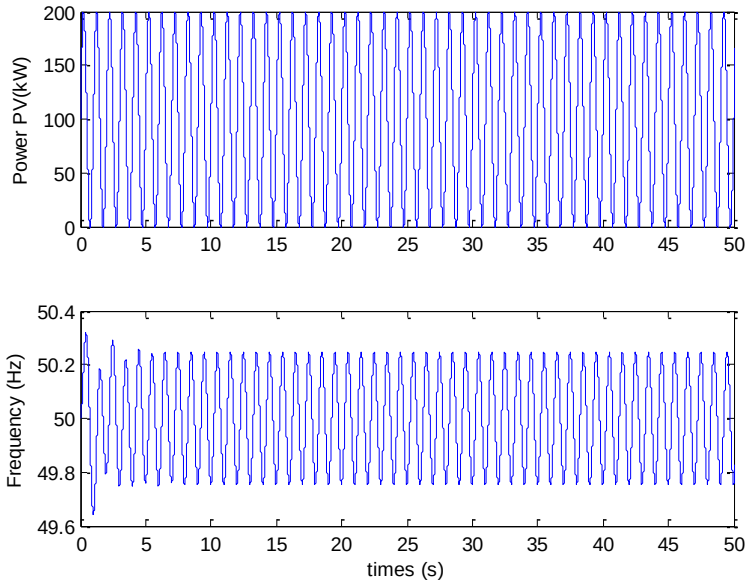

Figure 3.16 Power fluctuation of solar energy in sine signal f_{PV}=1Hz and its frequency response

The frequency response evaluates in sine signal as the power signal in Figure 3.16. The frequency can be defined as shown in (3.19) where df is the system frequency deviation from nominal frequency (1 per unit or 50 Hz), f_frequency response is the frequency of system frequency response, and phase shift is the angle shifting of frequency response from the power signal. The characteristic of frequency response which is presented in the following table is analyzed where f_{PV} is the frequency of power variation and f_frequency calculated is the frequency of frequency response.

$$System\ frequency(t) = 1+df*\sin(2*pi*f\_frequency\ response\ *t + phase\ shift) \quad (3.19)$$

Table 3.3 : Summary result of frequency response for various fluctuation frequencies

f_{PV} (Hz)	frequency (Hz)		df	f_frequency calculated (Hz)	Phase shift calculated	
	max	min	Hz		rad	degree
0.05	50.210	49.79	0.210	0.050	-0.22	-12.33
0.08	50.22	49.78	0.220	0.075	-0.17	-9.68
0.10	50.23	49.77	0.230	0.100	-0.36	-20.52
0.20	50.34	49.66	0.340	0.200	-0.51	-29.23
0.30	50.57	49.43	0.57	0.300	-0.31	-17.71
0.40	50.96	49.04	0.96	0.400	0.05	2.7
0.50	50.9	49.09	0.900	0.500	1.23	70.74
0.75	50.39	49.61	0.390	0.750	1.45	83.16
1.00	50.25	49.75	0.250	1.000	1.51	86.40

From the data reported in Table 3.3, it can be obviously seen that the frequency of grid frequency response is identical to the frequency of power fluctuation signal. The system frequency deviation (df) increases when the frequency of power fluctuation (f_{PV}) rises up until the frequency of power signal is 0.4-0.5Hz. While the frequency of power signal is continuously increased, the system

frequency deviation decreases as shown in Figure 3.17. Frequency of power PV that causes maximal frequency deviation is called critical frequency, studied previously with Bode diagram.

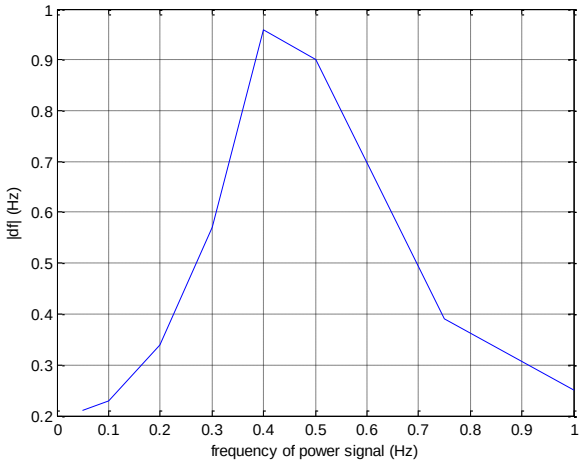

Figure 3.17 Amplitude of grid frequency response for different frequencies of PV fluctuation

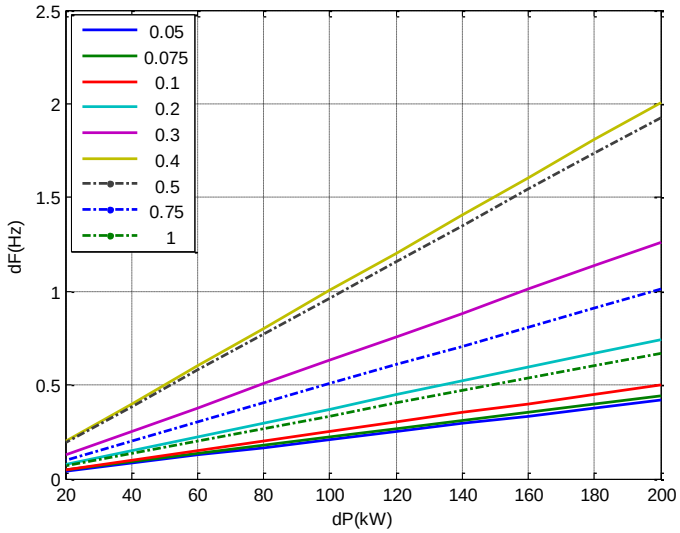

Figure 3.18 Maximal frequency deviations versus power deviations for various frequencies of fluctuation

The maximal power deviation (dP) varies for different frequencies of power fluctuation (f_{PV}) where other parameters are kept constant. The frequency of grid frequency response and its phase shift are not affected by the variation of the maximal power deviation. However, the different maximal power deviations cause difference in amplitude of system frequency deviation which can be seen in Figure 3.18. Slope of frequency deviation goes up when the frequency of power signal increased until 0.4Hz; after that, the slope falls down if the frequency of power fluctuation continues to decrease. These results are quit identical as those presented in for wind farms [41].

The impact of parameters such as inertia constant (H), load dumping constant (D) and droop value are studied. All parameters vary for each frequency of fluctuation with amplitude of power fluctuation equal to 100kW. The first studied parameter is the droop value of generator, from 1 to 10%. The maximal frequency deviation is plotted for different droop values and frequencies of fluctuations as shown in Figure 3.19. The frequency deviation is directly linked to the variation of droop value for frequencies of fluctuation below 0.4Hz. Frequency deviation increases when the droop value of diesel rises up for frequencies of power fluctuation below 0.4Hz. Frequency deviation is maximal for droop values of 6%, 3%, and 2% for frequency of power fluctuation of 0.5Hz, 0.75Hz, and 1Hz respectively. Nevertheless, a droop value upper than 6 % has less impact on system frequency at frequency of fluctuation of 0.75Hz and 1Hz.

Droop value of diesel generator has impacts on the critical frequency of power fluctuation. In Figure 3.19, the frequency of power fluctuation which causes maximum frequency variation is different for each droop value. For instant, droop values of 1-2% are found when the critical frequency is above 1Hz. While the droop value of 2%-4% are at the frequency of fluctuation 0.75Hz where the largest frequency deviation occurred. Critical frequency is around 0.5Hz and 0.4 Hz for a droop between 4-7.5% and 7.5%-10.0% respectively.

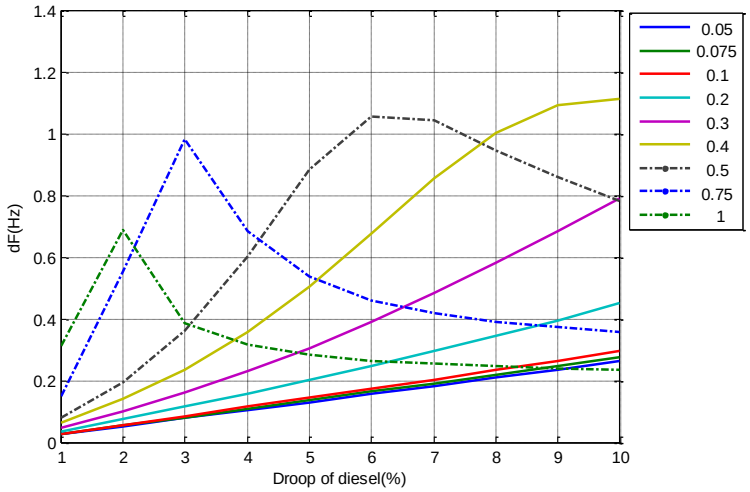

Figure 3.19 Maximal frequency deviations versus droop values for various frequencies of PV fluctuation

The impact of equivalent inertia (H) is varied from 1 to 10. The frequency deviation maximum is plotted for difference equivalent inertia values and frequency of fluctuation in Figure 3.20. The frequencies of fluctuation above 0.4 Hz cause the same tendency of frequency deviation for various equivalent inertias. It causes a large impact on frequency for small inertia (below 3 seconds). The frequency deviation is decreased by the increasing of the equivalent inertia value. But it has less impact on frequency for equivalent inertia more than 3 seconds. Frequency variation is identical for different equivalent inertia for frequency of power fluctuation 0.05Hz, 0.075Hz and 0.1 Hz. For frequency of power fluctuation 0.2Hz and 0.3Hz, frequency deviation is maximal at equivalent inertia of 2-3 seconds, and 2 seconds respectively. Low frequency of power fluctuation has more effect on the frequency variation than fast power fluctuation in large equivalent inertia (more than 7 seconds).

Various load damping constants are studied according to their impact on system frequency for different fluctuation frequencies. In this simulation, the load damping constant varies from 0 to 2. The zero load damping constant means that there is no load sensitive to frequency deviation. Higher the load damping constant value is, higher the load power decreases for the same frequency deviation.

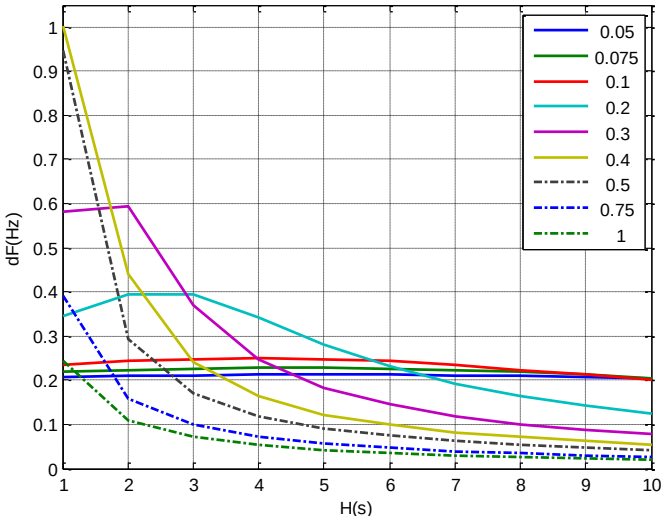

Figure 3.20 Maximal frequency deviations versus equivalent inertias for various frequencies of fluctuation

The maximal frequency deviation is plotted for different load damping constant values and frequencies of fluctuation for droop value of 4%, and 8% in Figure 3.21. Figure 3.21 illustrates that the dumping load constant has no effect on the system frequency when the frequency of power fluctuation is far away from critical frequency (0.4-0.5Hz for a droop value of 8% and 0.75Hz for 4%). For frequency of fluctuation around the critical frequency, the frequency deviation decreases when the load damping value increases.

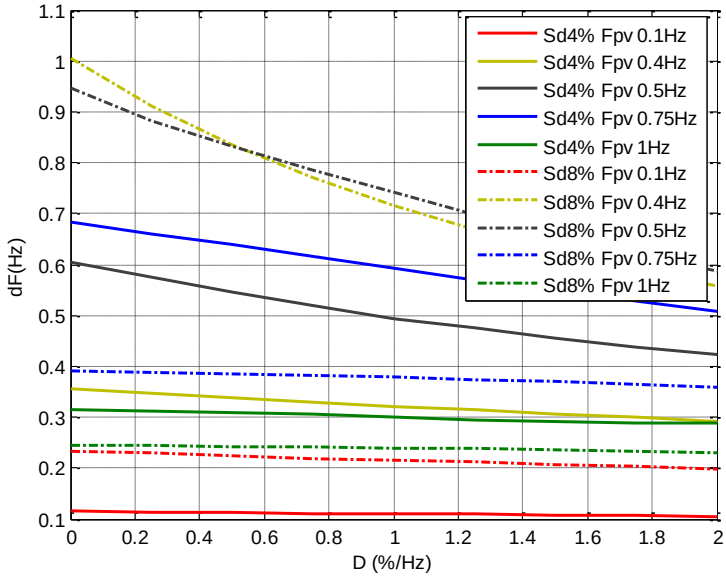

Figure 3.21 Maximal frequency deviations versus load dumping constant for various frequencies of fluctuation (droop value of 4% in solid line and 8% in dash-dot line)

All above results of this topic can also be founded by transfer function analysis with diagram de Bode.

3.4 Analysis relation between frequency and power deviations

From Figure 3.13 and Figure 3.17, relation between amplitude of frequency deviation and amplitude of power deviation is linear. In this section, efforts have been put to define this linear function for different signals of power fluctuations. The parameters of these equations depend on the parameters of power system (droop value, equivalent inertia and load damping value) and the characteristics of fluctuation signals such as, the duration of change and the frequency of PV fluctuations.

3.4.1 Analysis for step signal

Step signal expressed in Laplace domain in (3.20) is applied to transfer function in (3.12) and frequency response is obtained in (3.21). Parameters of (3.21) are redefined by A, B_1, and B_2 in (3.22) to simplify equation, so equation (3.21) turns to (3.23).

$$\Delta \boldsymbol{P_{pv}}(\boldsymbol{s}) = \frac{\Delta \boldsymbol{P_0}}{\boldsymbol{s}} \tag{3.20}$$

$$\Delta f(s) = \frac{(1+T_g s).s_d}{(2.H.T_g.s_d).s^2+(2.H+T_g.D).s_d.s+(s_d.D+1)} . \frac{\Delta P_0}{s} \tag{3.21}$$

$$A = \frac{1}{D+K_p}, B_1 = \frac{2.H.T_g}{D+K_p}, B_2 = \frac{2.H+T_g.D}{D+K_p} \tag{3.22}$$

$$\Delta f(s) = \frac{A.(1+T_g s)}{B_1.s^2+B_2.s+1} . \frac{\Delta P_0}{s} \tag{3.23}$$

Inverse Laplace transform is applied to (3.23) to find the grid frequency response in time domain; then time instant (denoted t_{min}) of maximal frequency is found. Finally, the amplitude of

maximal frequency deviation is found and expressed as a linear function of the amplitude of power variation, according to a slope denoted by parameter K in (3.24). This parameter depends on parameters of isolated grids and diesel generator in (3.25) or (3.26).

$$|\Delta \boldsymbol{f_{max}}| = \boldsymbol{K}.|\Delta \boldsymbol{P_0}| \tag{3.24}$$

If $\boldsymbol{B_2^2 - 4.B_1 \geq 0}$

$$\mathbf{K} = \frac{\mathbf{1}}{\mathbf{2.H.T_g}}\left[\frac{\mathbf{T_g}}{\boldsymbol{a-b}}\left(\boldsymbol{e^{-bt_{min}} - e^{-at_{min}}}\right) + \frac{\mathbf{1}}{\boldsymbol{ab}}\left(\mathbf{1} + \frac{\mathbf{1}}{\boldsymbol{a-b}}\left(\boldsymbol{be^{-at_{min}} - ae^{-bt_{min}}}\right)\right)\right] \tag{3.25}$$

; where $t_{min} = \frac{1}{a-b}\ln\left(\frac{T_g a-1}{T_g b-1}\right)$, $a = \frac{B_2+\sqrt{B_2^2-4.B_1}}{2.B_1}$, $b = \frac{B_2-\sqrt{B_2^2-4.B_1}}{2.B_1}$

If $B_2^2 - 4.B_1 < 0$

$$\mathrm{K} = \mathrm{A}.\left[1 + \frac{e^{-\varepsilon\omega_n t_{min}}}{\sqrt{1-\varepsilon^2}}\left(T_g\omega_n \sin\left(\sqrt{1-\varepsilon^2}\omega_n t_{min}\right) - \sin\left(\sqrt{1-\varepsilon^2}\omega_n t_{min} + \theta\right)\right)\right] \tag{3.26}$$

; where $t_{min} = \frac{\frac{\pi}{2}+\delta}{\omega_n\sqrt{1-\varepsilon^2}}$, $\tan\delta = \frac{1-T_g\omega_n\cos\theta}{T_g\omega_n\sin\theta}$, $\tan\theta = \frac{\sqrt{1-\varepsilon^2}}{\varepsilon}$, $\omega_n = \frac{1}{\sqrt{B_1}}$, $\varepsilon = \frac{B_2}{2.\sqrt{B_1}}$

3.4.2 Analysis for ramp signal

The maximal frequency deviation can also be expressed as a linear function with power variation. To find this relation between maximal frequency deviation and power deviation of ramp signal, Laplace transform is also applied to (3.17) and power deviation in (3.27) is obtained. This PV power signal is an input of system in (3.12). Amplitude of frequency deviation maximum is then calculated in function with parameter K(Δt) and amplitude of power deviation in (3.28), assuming that frequency response is minimum or maximum at time equal to Δt (t_{min} =Δt).

$$\Delta P_{pv}(s) = -\frac{\Delta P_0}{s}e^{-s.\Delta t} - \frac{\Delta P_0}{\Delta t.s^2}e^{-s.\Delta t} + \frac{\Delta P_0}{\Delta t.s^2} \tag{3.27}$$

$$|\Delta f_{max}| = K(\Delta t).|\Delta P_0| \tag{3.28}$$

Parameter K(Δt) is a function of parameters like frequency control of diesel (s_d), time response of diesel generator (tg), equivalent inertia of power system (H), damping load constant (D) and duration of change (Δt) in (3.29) or (3.30).

If $B_2^2 - 4.B_1 > 0$

$$\mathrm{K}(\Delta t) = \frac{1}{2.H.T_g.\Delta t}\left[-\frac{T_g+\Delta t}{ab} + \frac{3(a+b)}{(ab)^2} + \frac{T_g}{ab(a-b)}\left(a.e^{-b\Delta t} - b.e^{-a\Delta t}\right) + \frac{1}{(ab)^2(a-b)}\left(b^2e^{-a\Delta t} - a^2e^{-b\Delta t}\right)\right] \tag{3.29}$$

; where $a = \frac{B_2+\sqrt{B_2^2-4.B_1}}{2.B_1}$, $b = \frac{B_2-\sqrt{B_2^2-4.B_1}}{2.B_1}$

If $B_2^2 - 4.B_1 < 0$

$$\mathrm{K}(\Delta t) = \frac{\mathrm{A}}{\Delta t}.\left[-\Delta t - T_g + \frac{T_g e^{-\varepsilon\omega_n\Delta t}}{\sqrt{1-\varepsilon^2}}\sin\left(\sqrt{1-\varepsilon^2}\omega_n\Delta t + \theta\right) - \frac{e^{-\varepsilon\omega_n\Delta t}}{\omega_n\sqrt{1-\varepsilon^2}}\sin\left(\sqrt{1-\varepsilon^2}\omega_n\Delta t + 2.\theta\right)\right] \tag{3.30}$$

; where $\tan\delta = \frac{1-T_g\omega_n\cos\theta}{T_g\omega_n\sin\theta}$, $\tan\theta = \frac{\sqrt{1-\varepsilon^2}}{\varepsilon}$, $\omega_n = \frac{1}{\sqrt{B_1}}$, $\varepsilon = \frac{B_2}{2.\sqrt{B_1}}$

3.4.3 Analysis for sine signal

The maximum frequency deviation can be defined in linear function with power deviation of PV in (3.31) where K_{sine} is slope in Figure 3.17. Parameter K_{sine} can be defined from amplitude of transfer function between frequency deviation and power deviation with the replacement of s by $j\omega_{PV}$ in (3.32) where ω_{PV} corresponds to the PV fluctuation frequency. Parameter K_{sine} in (3.33) depends on parameters of power system, diesel generator and frequency of power variation (ω_{PV} in rad/s).

$$|\Delta \boldsymbol{f_{max}}| = \boldsymbol{K_{sine}}.|\Delta \boldsymbol{P_0}| \tag{3.31}$$

$$\frac{\Delta f(j\omega)}{\Delta P_{pv}(j\omega)} = \frac{(1+T_g(j\omega)).s_d}{(2.H.T_g.s_d).(j\omega)^2+(2.H+T_g.D).s_d.(j\omega)+(s_d.D+1)} \quad (3.32)$$

$$K_{sine} = \frac{s_d}{1+s_d D}\cdot\frac{1}{D_{1eq}{}^2\omega^4+(D_{2eq}{}^2+2D_{1eq})\omega^2+1}\sqrt{(T_g D_{1eq})^2\omega^6+(T_g{}^2 D_{2eq}{}^2+D_{1eq}{}^2-2T_g{}^2 D_{1eq})\omega^4+(T_g{}^2+D_{2eq}{}^2-2.D_{1eq})\omega^2+1} \quad (3.33)$$

3.5 Limitation of power deviation diagram

In the next chapter on control strategy for energy storage device, the power deviation of PV is assumed to be described only with step ($\Delta t = 0$) and ramp signals. If the maximal frequency deviation (Δf_{max}) is chosen and fixed, (3.24) and (3.28) can be turned into (3.34), which defines an analytical relation between power variation (ΔP_{pv}) and duration of power change (Δt) for a fixed maximal frequency deviation. Power deviation of (3.34) is then plotted as a function of fluctuation duration in Figure 3.22 ; the curve indicates the limitation of power variation to respect limitation on frequency variation. This limitation line, which depends on parameters of diesel generator and isolated grid, thus defines the acceptable zone for power deviation of photovoltaic. The area below the limitation line is defined as the acceptable zone (frequency variation is in the limits). On the other hand, the area above this line corresponds to an inacceptable zone (with frequency deviations out of limits).

$$|\Delta P_{pv}| = fn(\Delta f_{max}, K, \Delta t) \quad (3.34)$$

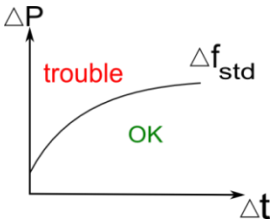

Figure 3.22 Limitation on PV power deviations according to maximal frequency deviation

For example, if the maximal acceptable frequency deviation is fixed at 0.2Hz, power deviation at this frequency deviation can be plotted versus different durations of power change as illustrated in Figure 3.23.

This limitation diagram in Figure 3.22 will be used in order to define a new control strategy for energy storage device in order to calculate the reference power of energy storage which will participate to primary control. This will be the main object of the chapter 5.

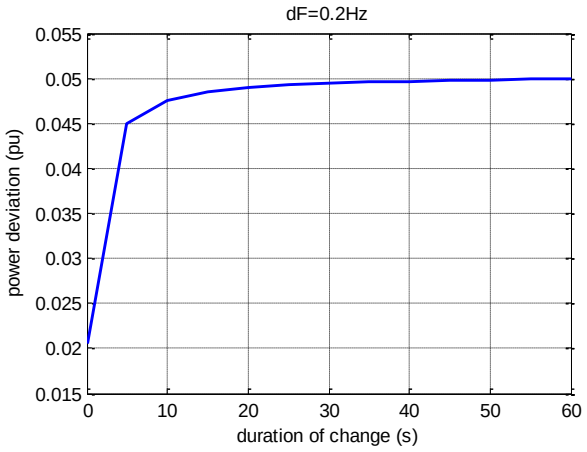

Figure 3.23 Power deviation PV limit for (Δf_{max}=0.2Hz)

3.6 Methodology to analyze power system with renewable energy

One of the main questions to be answered is whether an expensive energy storage system should be installed in isolated grids with intermittent energy to participate to frequency regulation (to guarantee frequency stability and/or decrease frequency deviation).

Equations between the maximal frequency deviation (Δf_{max} (pu)) and the amplitude of power fluctuation (ΔP_{pv}) in (3.24), (3.28), (3.31) have brought some answers to this question. Amplitude of power fluctuation (ΔP_{pv}) in per unit can be defined as a fraction of percentage of power variation (ΔP_{pv} (%)) from rated power of PV (P_{pv_rated}) and of diesel generator (S_{diesel_rated}) in equation (3.35). The proportion between these two rated powers ($P_{pv\_rated}/S_{diesel\_rated}$) corresponds to the penetration rate of photovoltaics. The maximal frequency variation according to variation of PV power (Δf_{max}) should be smaller than defined acceptable frequency deviation (Δf_{std}) in (3.36). Therefore, from (3.24), (3.28), (3.31), (3.35), and (3.36), limitations of power deviation can be defined by (3.37). If PV power variations are assumed as step signals, K_{eq} is equivalent to K calculated by (3.25) or (3.26). On the other hand, K_{eq} equals to K(Δt) ((3.29) or (3.30)) or K_{sine} ((3.33)), if power of PV is defined as ramp signal and sine signal, respectively. Furthermore, the maximal of power penetration can be found by (3.38) with a fixed percentage of power fluctuation (ΔP_{pv}(%)).

$$|\Delta \boldsymbol{P_{PV}}| = \Delta \boldsymbol{P_{PV}}(\%).\frac{\boldsymbol{P_{PV\_rated}}}{\boldsymbol{S_{diesel\_rated}}} \tag{3.35}$$

$$|\Delta \boldsymbol{f_{max}}| \leq |\Delta \boldsymbol{f_{std}}| \tag{3.36}$$

$$\Delta \boldsymbol{P_{PV}}(\%).\frac{\boldsymbol{P_{PV\_rated}}}{\boldsymbol{S_{diesel\_rated}}} \leq \frac{|\Delta \boldsymbol{f_{std}}|}{\boldsymbol{K_{eq}}} \tag{3.37}$$

$$\boldsymbol{max}(\frac{\boldsymbol{P_{PV\_rated}}}{\boldsymbol{S_{diesel\_rated}}}) = \boldsymbol{max}(\boldsymbol{P_{PV\_pene}}\%) = \frac{|\Delta \boldsymbol{f_{std}}|}{\Delta \boldsymbol{P_{PV}}(\%).\boldsymbol{K_{eq}}} \tag{3.38}$$

First analysis concerns the requirement of energy storage system. Methodology of analyze is proposed by separating situations into two different cases if fluctuations evaluate as sine or step signals (step signal causes larger frequency deviation than ramp signal). The specifications of system such as, the droop value, the equivalent inertia, the load damping, the initial power penetration of photovoltaic and the acceptable frequency deviation, are then defined. The maximal penetration rate of photovoltaic in equation (3.38) is then calculated where ΔPpv(%) equals to a given value according to previsions or observations. If the specified power penetration rate is less than the maximal power penetration one (from (3.38)), then an energy storage should be needless for power system.

In this study, PV power is assumed to be a step signal (the worst case of power fluctuation). The maximal penetration rate of PV in (3.38) is plotted versus percentage of power fluctuation (ΔPpv(%)) for various acceptable frequency deviations (Δf_{std}) in Figure 3.24 which the coefficient K_{eq} of step signal equals to 0.1947 from (3.29) and parameters of system presented in Table 3.1).

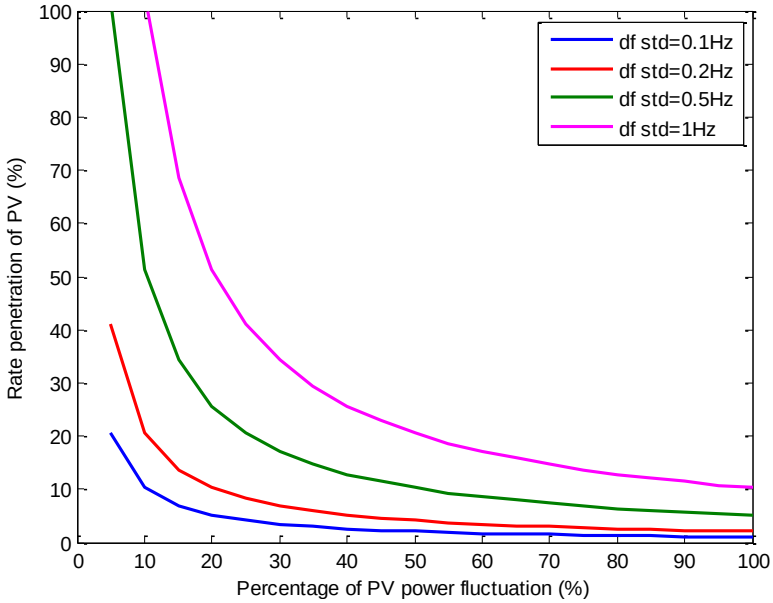

Figure 3.24 Maximal penetration rate of photovoltaic versus percentage of power fluctuation from equation (3.28) for various acceptable frequency deviations (PV power in step signal and K_{eq} = 0.1947)

For example, the acceptable frequency deviation (Δf_{std} (pu)) is equal to 1/50 per unit (1 Hz) and the amplitude of power fluctuation (ΔP_{pv} (%)) is taken equal to 80%. The maximal power penetration calculated by (3.38) is then equal to 12.84%. If the initial power penetration of photovoltaic is more than 12.84%, the energy storage is needed but if it is less than 12.84%, the energy storage should not be installed to guarantee frequency stability.

3.7 Conclusion

Frequency variation according to intermittent energy depends on frequency of power PV fluctuation (or duration of change), amplitude of power variation of photovoltaic and parameters of power system. Then, the power system works as a low-pass filter. High fluctuations of photovoltaic power cause less effects on the system frequency because of the equivalent inertia of the system (sum of inertia of all rotating machines). On the other side, low frequencies of power fluctuations are filtered by secondary control of diesel generator. Therefore the secondary control of the diesel generator acts as a high pass filter. Primary frequency control takes action in medium frequency of power variation.

A complete analysis of parameter sensitivity on grid frequency has been proposed. Then, transfer function between the system frequency and the power fluctuation variations permit to define a critical frequency and cut-off frequencies which impact grid frequency time response. The critical frequency corresponds to the fluctuation which causes the largest grid frequency variation. In this study, it is about 0.45 Hz. This frequency depends on the parameters of system, such as the equivalent inertia and the generator droop value. A load damping constant has less affect to this frequency. Cut-off frequencies separate low, medium and high frequencies of fluctuations and depend also on all parameters. From Bode diagram analysis, the low cut-off frequency mainly depends on integral gain of frequency control of diesel (K_i) but the high cut-off frequency mainly depends on equivalent inertia (H). If the frequency of fluctuation is upper than high cut-off frequency, the power variation causes less impact on system frequency. Equivalent inertia has large effect on this high frequency region. On the other hand, the less frequency of fluctuation is the less of frequency deviation when the frequency of fluctuation is less than low cut-off frequency. In low frequency of fluctuation region, secondary control brings frequency back to the nominal value. For system without secondary control, this low frequency region is affected by droop value (primary frequency control) and load damping constant which defines the steady-state frequency value. Consequently, the medium frequency of the power fluctuation which is taken by primary frequency control causes the largest frequency deviation. Critical frequency is also included in this frequency region. Load damping constant, equivalent inertia, droop value, and time response of diesel generator cause large impacts on frequency deviation.

Study on different time response of PV power fluctuations reveals that power variation in step and sine signals with critical frequency cause large effects on frequency variations. When the duration rises up, the frequency deviation falls down. Linear equation between frequency variation and amplitude of power deviation has been illustrated and analytically defined for each power signal. Besides, if the frequency deviation is fixed for PV power described by step and ramp signals, the maximal acceptable power variation can be specified for different durations of change.

Measured or estimated PV power variation that is over this power limitation can define participation of energy storage to frequency primary control. Furthermore, an analytical relation has been established defining the maximal PV penetration rate of an isolated grid from maximal frequency deviation, according to grid parameters.

These results and analytical calculations will be used in Chapter 5 to define new strategies for energy management of storage devices dedicated to frequency control.

Chapter 4

Energy storage system modelling and control

4.1 Introduction

According to the analysis of PV power fluctuations in Chapter 2 and the study of their impact on grid frequency in Chapter 3, energy storage devices seem to be a challenging source to guarantee or improve frequency performance of an isolated grid with a high penetration rate of intermittency. In the case of electrochemical or electrostatic storages, the active power of energy storage which participates in frequency regulation must be controlled via switching functions of an inverter (AC/DC conversion), with or without a DC/DC converter (of buck-boost type).

Before defining any energy management strategy of energy storage, defining a power reference for energy storage in the following chapter, the complete system associated to an energy storage device as batteries or supercapacitors, consisting in a source of energy, a DC/DC reversible converter, an AC/DC inverter, a AC filter and associated control loops are described and validated with simulations in this chapter.

4.2 Energy storage system (ESS)

To control the participation of ESS in order to balance the power generation and consumption in isolated micro power system, it has to be connected to converter and/or inverter. PQ inverter control and voltage source inverter (VSI) control have been proposed for ESS in islanding mode [14]. Many possible control strategies have been proposed for ESS, for example, PQ control which fixes active and reactive power for connected mode, droop control for which power of ESS change according to frequency variation and droop value, and frequency/voltage control which fixes frequency and voltage at initial value [20]. The droop and frequency/voltage control seem to be quite compatible with islanding mode.

Renewable energy source is connected to power system via voltage source converter [103]. Frequency of islanding micro power system is controlled via active power. Current output of inverter in d-axis is used to control the active power of intermittent source. And current output of inverter in q-axis is used to control the reactive power which allows us to control voltage output.

The energy storage system can be separated in 3 parts: power source, transmission, and control part. The energy storage device can be connected to power system via only inverter (AC/DC) as illustrated in Figure 4.1, in the case where DC voltage is assumed to be constant. The energy storage can also be connected to power system via converter (DC/DC) and inverter (AC/DC) as presented in Figure 4.2. The converter and inverter are controlled by their switching function which depends on the control strategy. Therefore, the proposed energy storage system consists of:

i. Energy storage device
ii. Interfacing energy storage device to power system (Converter, Inverter, and filter)
iii. Frequency control – controller for ESS

One must paid attention to another component, particularly in the case of frequency regulation: the PLL (for Phase Lock Loop) which aims to estimate frequency and phase angle of grid voltage, used for modelling and control of the inverter.

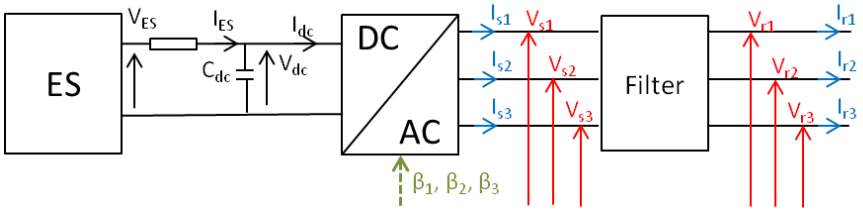

Figure 4.1 Energy storage device connected to system via inverter, and AC filter

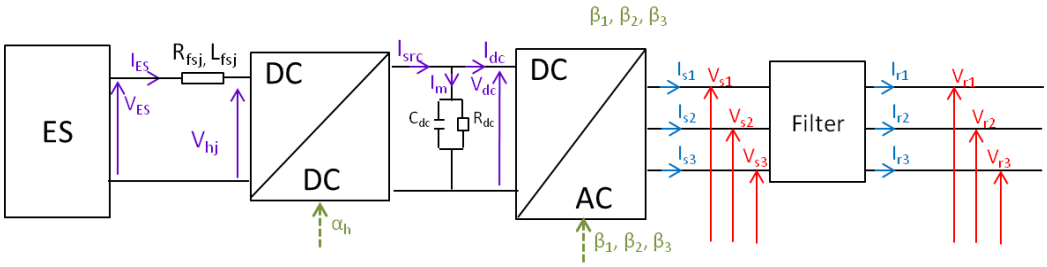

Figure 4.2 Energy storage device connected to system via DC/DC converter, inverter, and AC filter

AC or DC currents and grid power have to be specified. In our study, when energy storage is in discharge mode (i.e. injection of active power to the grid), the active power, the output current in d-axis and the storage current are positive. On the other hand, all values are negative when energy storage is in charging mode.

4.2.1 Energy storage device

There are many kinds of energy storage technologies such as lead-acid or lithium-ion batteries, supercapacitors, flywheels, etc. Each type has different characteristics such as specific energy, specific power, time response, etc. Flywheel and supercapacitor have less time response so they are adapted to deliver faster power than battery technologies. However, their specific energy is small, so they cannot supply power for a long period. Selection of energy storage technologies depend on the application and power variations.

Energy storage device is modeled as a DC voltage source in [14] by assuming that its output voltage remains constant whatever its state of charge or grid solicitations. However, DC voltage of energy storage is not constant: it varies along time and depends on output current of energy storage or State of Charge (SoC). Therefore, two energy storage technologies are studied and modelled in this thesis: electrochemical batteries with high power density (Li-ion for instance) and supercapacitors.

Taking into account of frequency band-width for which an ESS should be interesting for primary control, a quasi-static model of battery has been used. This model, presented as an equivalent electrical circuit in Figure 4.3, consists in a DC voltage source (E_b) and its internal resistance (R_i). This model is valid for all batteries technologies with different parameters. DC voltage (E_b) corresponds to the open-circuit voltage that depends on accumulated energy or State of Charge (SoC). Internal resistance (R_i) combines all ohmic and faradic losses and depends on SoC, current of charge or discharge and also, temperature. To simplify the model, the internal resistance (R_i) is assumed to be constant [104]. DC voltage E_b is calculated by (4.1) where E_0 denotes the voltage at full charge in Volt (V), Q the capacity of battery in Amps.Hour (Ah), K the polarization voltage in Volt (V), and i_t the integral of energy storage current (i_{bat}) in (4.2). Each parameter is determined from discharging characteristics at nominal current.

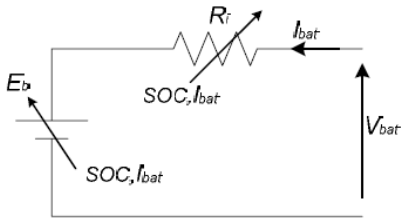

Figure 4.3 Equivalent model of Battery

$$E_b = E_0 - K_b.Q.\frac{1}{Q-i_t} + A.e^{-B.i_t} \quad (4.1)$$

$$i_t = \int_{t_0}^{t} i_{bat}(t).dt \quad (4.2)$$

The supercapacitor is modelled by internal capacitor (C_0), resistance (R_s), series of capacitor and resistance in parallel (C_1//R_1 and C_2//R_2) in Figure 4.4 [105]. Voltage output of super capacitor in (4.3) depends on output current of super capacitor (i_{sc}) and elements of equivalent model. In this study, supercapacitor modelled by internal capacitor (C_0), and resistance (R_s) is sufficient for our simulation in order to simplified model equation. For defining voltage output of super capacitor in (4.3), only first and second components remain.

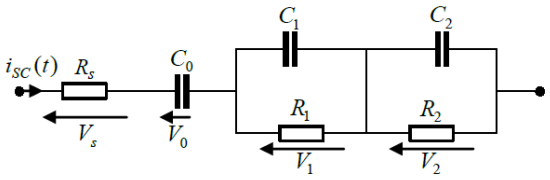

Figure 4.4 Model of Super Capacitor

$$V_{SC}(s) = i_{SC}(s)R_S + \frac{i_{SC}(s)}{C_0 s} + \frac{i_{SC}(s)R_1}{R_1C_1s+1} + \frac{i_{SC}(s)R_2}{R_2C_2s+1} \quad (4.3)$$

An energy storage device is quite a compatible power source because of its fast time response and more considerations for local environment. However, its energy can be quite limited. The state of charge (SOC) of energy storage has to be calculated and managed in control system to check the availability of its energy.

For batteries, the state of charge is approximated by the quantity of energy which is stored into the energy storage and depends on its initial capacity (Q_0) in Amp-hour as presented in (4.4). The stored energy is then the integral of the energy storage current (i_{bat}).

$$SOC(t) = \frac{\int_{t_0}^{t} i_{bat}(t).dt}{Q_0}.100 \quad (4.4)$$

For supercapacitors, the State-of-Charge is also calculated from an approximation of stored energy, but in this case, the energy depends on the square of internal voltage.

4.2.2 Interfacing energy storage to power system

A power electronic interface is mandatory to connect the energy storage to electrical grid. This is the transmission part. In some study [65], [106]–[108], energy storage has been connected to DC/AC inverter directly by assuming that the direct voltage of energy storage is quite constant. The inverter is used to control the active and reactive powers for grid. This interface may include also a DC/DC converter to control the current of energy storage and an inverter to control the DC voltage and reactive power [19]. After AC/DC inverter, signals will be filtered at AC side in order to limit harmonic distortion, particularly in the case of high penetration of renewable energy. Currents are finally filtered in order to limit high harmonic distortion, particularly in the case of high penetration of renewable energy.

In this study, energy storage is first directly connected to power system via AC/DC inverter because this system is simple. Then, focus is put on the association of DC/DC and DC/AC converters because it can be used to control the DC bus voltage and can be applied to any kind of energy storage. Moreover, this structure is interesting if PV source and different technologies of energy storage are connected together on the DC bus.

Finally, inverter has to be connected to filter in order to reduce oscillation and harmonic in voltage and current output of inverter. There are many types of filter such as L, LC, and LCL. Filter with L or LCL structures are used when output current is controlled. In the case where the system is a voltage source, a filter LC is appropriate [109].

4.2.2.1 DC/DC interfacing

Equivalent diagram of the buck-boost converter is presented in Figure 4.5. Two IGBT with anti-parallel diodes are controlled by switching function whose value is between 0 and 1. Voltage input of boost converter (V_{hj}) can be calculated by output DC voltage (V_{dc}) and switching function (α_h). The output DC current of converter (I_{src}) depends on storage current input (I_{ES}) and also switching function (α_h).

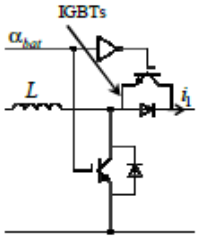

Figure 4.5 Model of DC/DC converter [105]

4.2.2.2 DC/AC interfacing

In Figure 4.6, equivalent electric circuit of inverter AC/DC is illustrated. Switches are also controlled by switching functions (U_1, U_2 and U_3) [110]. AC output voltages of inverter (V_{s1}, V_{s2}, V_{s3}) is defined by three switching functions (β_1, β_2, β_3). DC current (I_{dc}) is a function with AC current output (I_{s1}, I_{s2}, and I_{s3}), and three switching function (β_1, β_2, β_3). Furthermore, three phase switching function, AC voltage, and AC current are transformed into Park representation to be compatible with controller design in the following topic which control the current output of inverter in d and q axis. Voltage output in d and q axis (V_{sd},V_{sq} respectively) are defined by switching functions in d and q axis (β_d, β_q). And DC current is a function with switching function in d and q axis (β_d, β_q) and current in d and q axis (I_{sd}, I_{sq}).

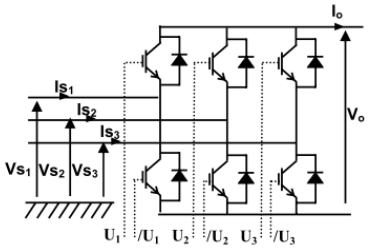

Figure 4.6 Model of AC/DC inverter [110]

All dynamic models of converter and inverter are presented in the following chapter in order to form state-space representation of ESS.

4.2.2.3 Design of interfacing of ESS

The energy storage system described in Figure 4.2 is designed. This design is assumed to be also applicable to energy storage system with AC/DC converter only as shown in Figure 4.1. The converter is connected to energy storage via a resistance (R_{fsj}) and an inductance (L_{fsj}). The inverter is connected to DC/DC converter via a capacitor (C_{dc}) and a resistance (R_{dc}). The AC bus of inverter is

connected to power system via filters RL, LC, or LCL to eliminate high frequencies harmonics. A filter with only an inductance is not suitable because it needs a PWM frequency of PWM upper than 20 kHz [19]. All parameters are designed base on frequency of PWM 7 kHz in Appendix III. Besides, frequency of PWM 5 kHz and 10 kHz are also be used to design parameters of AC bus in Appendix III.

4.2.3 Control loops of energy storage system

Control architecture consists in three levels of control. The first one corresponds to a high-level control, which defines the active power reference to limit grid frequency variation. Generally, the droop frequency control is used to calculate the power reference for energy storage by the variation of system frequency; which is measured by Phase Lock Loop (PLL).

The secondary level of control consists in regulation of inverter currents in d and q axes to achieve references. Using the transformation in Park reference frame, the aim of this control loops is classically to synthesis PI controllers. The last level of control generates the switching functions to control state of switches using PWM or Hysteresis.

The DC voltage and the reactive power can also be controlled depends on interfacing between energy storage and power system. If the energy storage is connected directly to the AC/DC inverter (called later as the ESS control #1), active power is controlled by switching function in d-axis (β_d) and reactive power is controlled by switching function in q-axis (β_q). As having mention earlier, DC voltage is assumed to be constant.

Energy storage can also be connected to grid via a DC/DC and a AC/DC converters to control also the DC voltage. In this case, this voltage can be controlled by switching function of DC/DC converter (called ESS control #2) or by switching function in d-axis (β_d) of inverter (or ESS control #3). The active power is controlled either by switching function in d-axis (β_d) of inverter AC/DC or switching function of DC/DC converter respectively. The reactive power is always controlled by switching function in q-axis (β_q).

4.2.4 PLL description

The Phase Lock Loop is an electronic system which is used to measure grid frequency. This element is very important for our study on frequency stability. Moreover, the angle of system that is used in Park's transformation for inverter modelling and control is obtained also with this element. There are a lot of types of PLL. The classical three-phase PLL or SRF-PLL in Figure 4.7(a) consists of a PD block that is constituted by a Park-transformation, a low pass filter (denoted LF) which is often a PI regulator and a VCO which can be approximated to an integrator for small variations of frequency [19], [111].

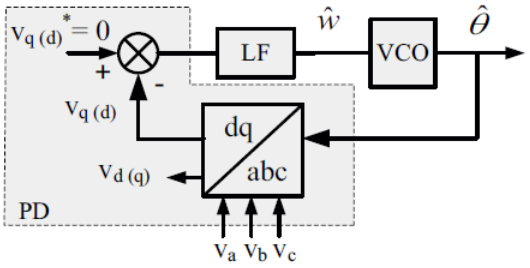

Figure 4.7 General diagram of classical Phase Lock Loop

4.3 Control system architecture of energy storage system

Control architecture is separated into two parts according to the different interfaces of Energy Storage (denoted ES) with power electronics converters (DC/DC and AC/DC). In this chapter, control objectives are to achieve references of active power, AC currents and DC voltage. Three types of systems have been presented earlier according to the structure of the ESS and the controlled variables

(ESS control loops #1, 2 or 3). However, these three control systems have two identical parts which are the droop frequency control and the Phase Lock Loop which are firstly described.

4.3.1 Droop frequency control

If the frequency deviation is negative (e.g. frequency falls under the nominal frequency (50Hz)), the energy storage supplies active power in a discharging mode. On the contrary, energy is stored when the frequency deviation is positive (the ESS absorbs thus active power). The droop control of storage device is presented Figure 4.8.

The active power variation of energy storage is obviously limited to the maximum charging and discharging powers of the storage device. These powers are commonly related to the rated power of energy storage, and are assumed to be equal to $\pm P_{st\_max}$. Currently, the droop characteristic is then symmetrical according to the rated frequency. However, some asymmetrical curves are also studied in order to optimize operating costs of ESS.

The normal active power of energy storage is of course equal to zero. The energy storage takes part in the frequency control only when the frequency is different from the rated value (f_0). Consequently, the reference of storage power (P_{st}) is defined in (4.5), where K_{st} denotes its own energy reserve. This energy is linked to the storage droop (s_{st}) and the maximal power denoted P_{st_max}.

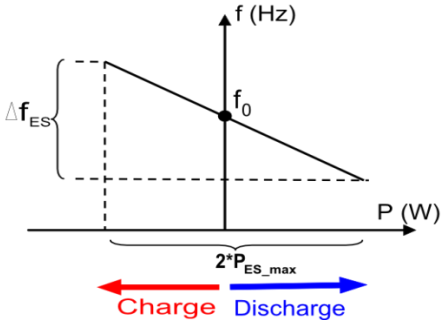

Figure 4.8 Droop characteristic for energy storage

$$P_{ES}(f) = -K_{ES}(f - f_0) \tag{4.5}$$

$$K_{ES} = \frac{1}{s_{es}} . \frac{2*P_{ES\_max}}{f_0} \tag{4.6}$$

This part can be called the active power reference calculation for energy storage. As the load power is supposed to be constant, the active power of energy storage is then calculated according to the variation of PV power.

4.3.2 Energy storage control #1: ES+AC/DC (no control of Vdc)

From Figure 4.9, the Phase Lock Loop (PLL) calculates frequency from measured voltage. Then, power reference of energy storage is defined by droop frequency control and reference current in d-axis is calculated by (4.13) without any control of reactive power. Finally, current controller will define the reference voltage for Pulse Width Modulation (PWM) which generates switching function to AC/DC inverter.

$$I_{rd\_ref} = \frac{2}{3.V_{rd}} P_{ES\_ref} \tag{4.7}$$

Measured line currents of inverter are transformed with Park representation in d and q axes; these transformed currents are then compared to their reference value. Then, a PI controller calculates reference voltage in d (V_{sd_ref}) from current error in (4.8) where K_{pi} and K_{ii} are the proportional gain and the integral gain of the controller respectively.

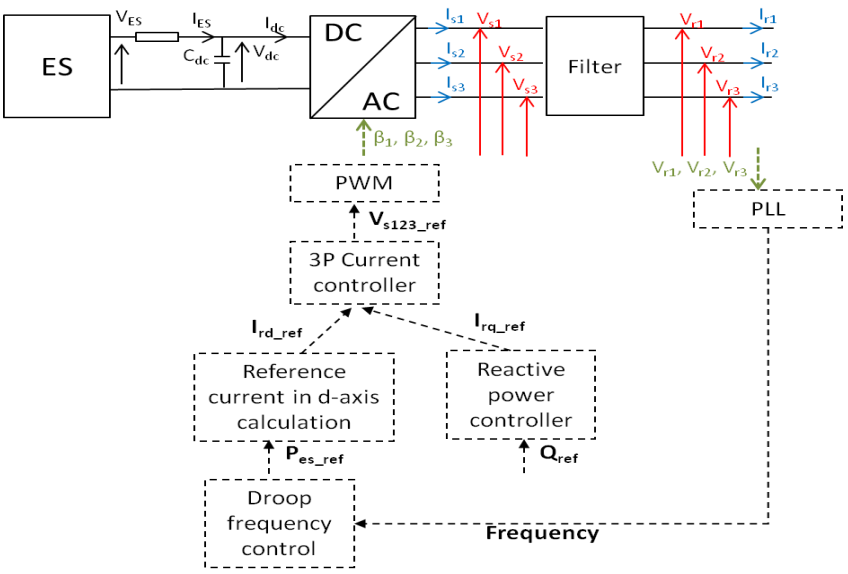

Figure 4.9 Control diagram of energy storage control # 1

$$V_{sd\_ref} = \left(K_{pi} + \frac{K_{ii}}{s} \right).\left(I_{rd\_ref} - I_{rd} \right) \tag{4.8}$$

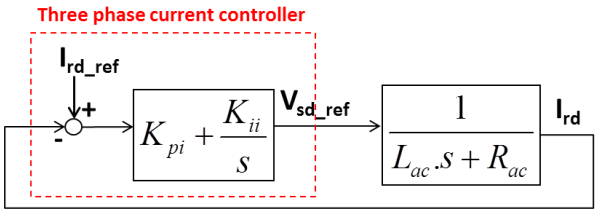

Figure 4.10 Closed loop of three phase current control

$$\frac{I_{rd}}{I_{rd\_ref}} = \frac{s.\left(s + R_{ac} / L_{ac} \right)}{s^2 + \frac{R_{ac} + K_{pi}}{L_{ac}}.s + \frac{K_{ii}}{L_{ac}}} \tag{4.9}$$

It has been supposed that the filter in Figure 4.9 is a RL filter. Therefore, the current in d-axis can be calculated from output voltage in d-axis of inverter by inductance of filter (L_{ac}) and resistance of filter (R_{ac}) [109]. Closed loop diagram of current in d-axis is illustrated in Figure 4.10. To define parameter of PI controller, the closed loop transfer function between current (I_{rd}) and reference current (I_{rd_ref}) is defined in (4.9). Then, the denominator of closed-loop transfer function (4.9) is compared to the canonical form of (4.10) when ξ is the damping constant and ω_n signifies time response of this controller (t_r with $\omega_n=5/t_r$). Consequently, parameters of PI controller are defined in (4.11). In this study, ξ is equal to 0.7 and time response of controller of 7ms.

$$s^2 + 2\xi\omega_n s + \omega_n^2 \tag{4.10}$$

$$K_{pi} = 2\xi\omega_n L_{ac} - R_{ac}, \quad K_{ii} = L_{ac}\omega_n^2 \tag{4.11}$$

According to the selected parameters of three phase current controller, Figure 4.10 represents the response of d-axis current with a reference change from 10A to 15A at 1 second. Time response of current in d-axis in Figure 4.11 presents an overshoot of 16.07A and a settling time of 7ms, which is identical to the time response of the selected controller.

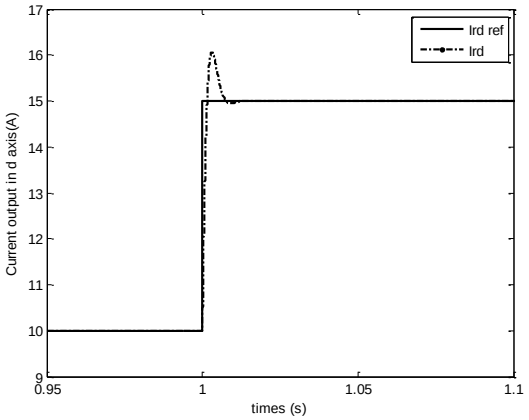

Figure 4.11 Time domain response of current of energy storage with step change in reference (P controller)

Design of this energy storage control system is not too complicated because there is only one controller. Time response of this controller should be selected according to the PWM frequency of 7kHz.

4.3.3 Energy storage control #2: Control V_{dc} by DC/DC and control i_d by AC/DC

This type of energy storage is connected to AC bus via DC/DC converter and AC/DC inverter. The control architecture of energy storage system becomes more complicated. Indeed, only one controller as the previous case is insufficient. At least, two controllers are needed: one for the DC/DC converter and another for the inverter. In this case, the power of energy storage is controlled with the inverter, as the previous case.

In Figure 4.12, DC voltage is controlled by switching function of DC/DC converter. The DC voltage control consists in the DC voltage controller, the controller of the energy storage current (I_{sst}) and the local control of switches (PWM). Control of AC/DC inverter or power active control is equivalent to the energy storage system #1 which has already been designed earlier. Therefore, only DC voltage control is presented in this section.

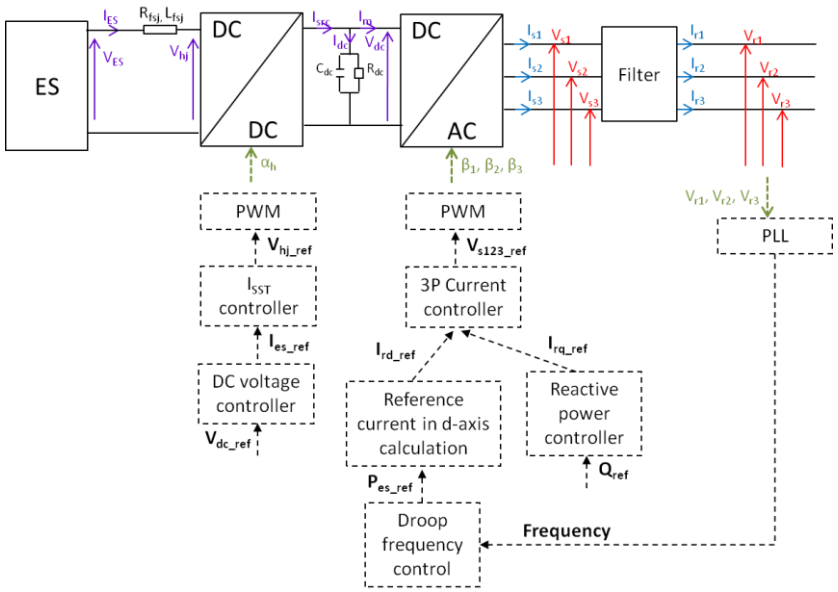

Figure 4.12 Control diagram of energy storage control # 2

4.4.1.1 Internal control loop of storage current

This controller defines voltage reference signal to PWM which generates switching function to converter. A proportional controller (P controller type) is selected to obtain short time response [109]. Closed loop control of current of energy storage is illustrated in Figure 4.13.

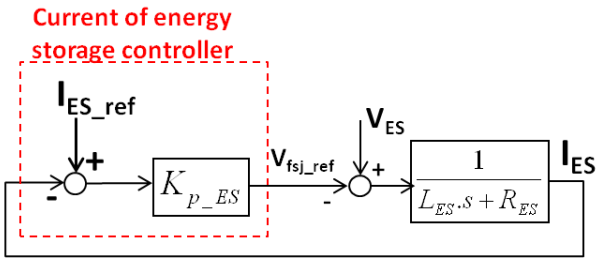

Figure 4.13 Closed loop system of current of energy storage control

The current of energy storage is calculated from the input voltage of DC/DC, and parameters of smoothing inductance (L_{ES}) and the total resistance modelling converter losses (R_{ES}). Transfer function of energy storage current and its reference is reported in (4.12) with K_{p_es} is the gain of proportional controller. From (4.12), we have designed K_{p_es} from a determined band-width of frequencies (BP_ES) of controller in equation (4.13). We have chosen a pass band frequency of 1000 rad/s. Energy storage current control with P controller is validated with MATLAB. The initial reference current is equal to 5A and it changes to 10A at 1 second. Energy storage current in Figure 4.14 reaches the reference value with good performances. There is no steady-state error and its settling time is around 5ms.

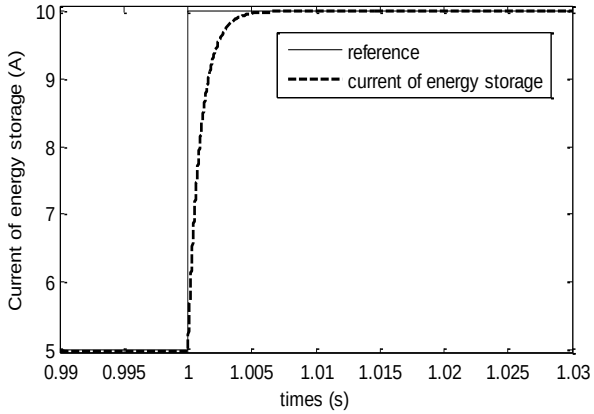

Figure 4.14 Time domain response of current of energy storage with step change in reference (P controller)

$$\frac{I_{ES}}{I_{ES\_ref}} = \frac{K_{p\_es}.}{L_{ES}.s + R_{ES} + K_{p\_es}.} \tag{4.12}$$

$$BP\_ES = \frac{K_{p\_es}. + R_{ES}}{L_{ES}.} \tag{4.13}$$

4.4.1.2 DC voltage controller

DC voltage is controlled by a PI controller which is used to calculate the current reference of energy storage by the difference of square of DC voltage from square of reference value. This control uses square value of DC voltage because current of energy storage is in linear function with square of DC voltage in (4.14). Therefore, from Figure 4.15 and (4.14), the closed loop transfer function between square of DC voltage and its reference is presented in (4.15). Parameters of this PI controller are defined in (4.16) where K_{pv} is proportional gain and K_{iv} is integral gain of controller.

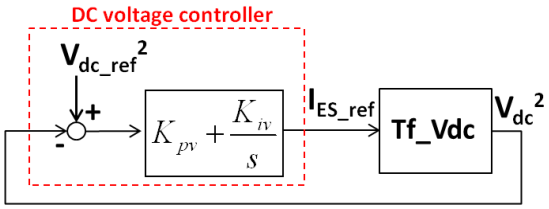

Figure 4.15 Closed loop system of DC voltage control

$$\frac{{V_{dc}}^2}{I_{ES\_ref}} = \frac{V_{ES}.R_{dc}}{\frac{C_{dc}.R_{dc}}{2}.s+1} \tag{4.14}$$

$$\frac{{V_{dc}}^2}{{V_{dc\_ref}}^2} = \frac{V_{ES}.R_{dc}.\left(K_{pv}s+K_{iv}\right)}{s^2+\frac{2.\left(1+K_{pv}V_{ES}.R_{dc}\right)}{C_{dc}R_{dc}}.s+\frac{2.K_iV_{ES}}{C_{dc}}} \tag{4.15}$$

$$K_{pv}=\frac{1}{V_{ES}}\left(\xi.\omega_{nv}.C_{dc}-\frac{1}{R_{dc}}\right), \quad K_{iv}=\frac{C_{dc}\omega_{nv}^2}{2.V_{ES}} \tag{4.16}$$

Time response of this controller ($t_{rv}=5/\omega_{nv}$) has to be also well selected in relation to the frequency of PWM of converter (f_{conv}). If frequency of PWM of converter is equal to 7 kHz, time response of DC voltage controller is selected as 500 times of time response of PWM ($500/f_{conv}$), so it is about 70ms. The selected DC voltage controller with parameters K_{pv} and K_{iv} is validated in MATLAB with a voltage reference at 800 V and 805 V at 5 seconds. In Figure 4.16, DC voltage follows the reference value but there is an overshoot at 805.7 V. There is no steady-state error and the settling time is around 0.07s (for ±1% of ΔV (5V)). Moreover, output of this controller (I_{ES_ref}) is used as an input or reference of energy storage current controller in Figure 4.13 (with P controller). Current of energy storage in Figure 4.17 has a large overshoot at 1 second with the DC voltage variation.

For inverter control, frequency of PWM of inverter (f_{inv}) is selected at 7 kHz. Time response (t_r) of three phases current controller is then selected at 50 times of time response of PWM ($50/f_{inv}$) so it is 7ms. Parameters of PI controller K_{pi} and K_{ii} in (4.11) are defined.

This energy storage system control is more complicated than energy storage system control #1 but DC voltage is now controlled. Results of simulation are reported in the following section to compare the energy storage system controls.

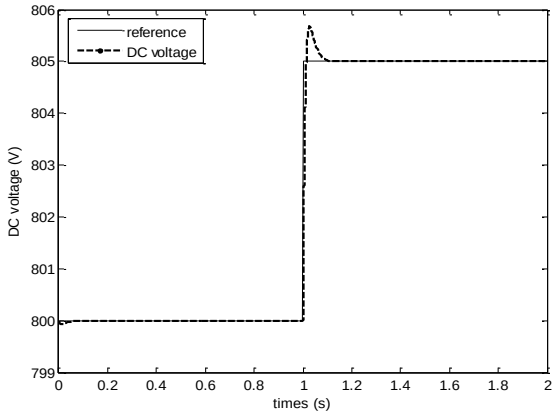

Figure 4.16 DC voltage response with DC voltage reference change at 1 second

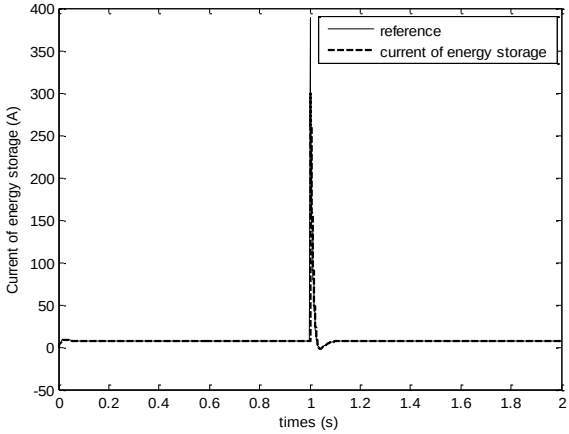

Figure 4.17 Current of energy storage response with DC voltage reference change at 1 second

4.3.4 Energy storage control #3: Control I_{ES} by DC/DC and V_{dc} by AC/DC

In this case, energy storage is connected to AC bus via two power electronics converters (DC/DC and AC/DC) as illustrated in Figure 4.18, which is the same as the energy storage control #2, excepted that the active power of energy storage which participates to frequency regulation is controlled by switching function of DC/DC converter. Meanwhile, the DC voltage is controlled by switching function in d-axis of AC/DC inverter.

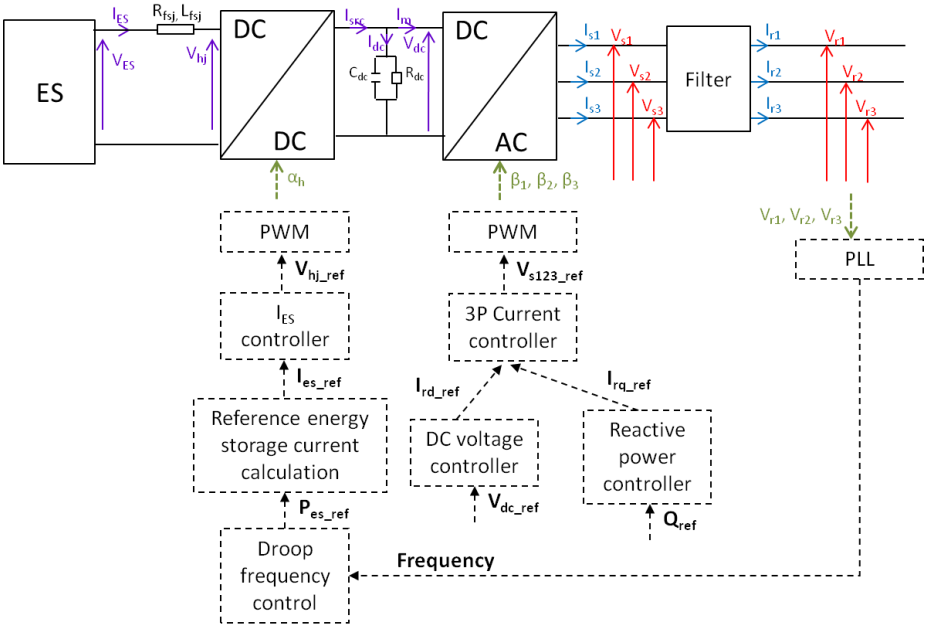

Figure 4.18 Control diagram of energy storage control # 3

In Figure 4.18, for a specified power reference (P_{es_ref}), the current reference of energy storage (I_{es_ref}) is calculated by (4.17), where V_{ES0} is the voltage of energy storage which is assumed to be fixed at its rated value. Then, the energy storage current controller has for output the voltage reference signal of DC/DC converter.

According to the defined DC voltage reference, the current reference in d-axis is calculated by the DC voltage controller. Then, the current in q-axis reference is defined by the reactive power controller as the reactive power reference. Currents in d-axis and q-axis are sent to three phase current controller to generate the output voltage reference of inverter. Consequently, the PWM generates the switching function for inverter.

$$I_{ES\_ref} = \frac{P_{ES\_ref}}{V_{ES0}} \tag{4.17}$$

4.4.1.3 Current of energy storage controller

This controller is equivalent to that of energy storage current, designed in the previous section in Figure 4.13 (with energy storage system control #2). The current of energy storage is then controlled to follow the reference of (4.17). Parameters of P controller are also defined by (4.13).

4.4.1.4 Three phases current controller

The controller of AC currents is equivalent to controller defined in section 4.3.2. Voltage output reference in d-axis and q-axis are calculated from the difference between measured value and actual value of current output in d-axis and q-axis, respectively, as shown in Figure 4.10. Parameters of PI controller of three phase current controller is defined in (4.11) where ξ (damping constant) is chosen at 0.7 and t_r (time response of controller ($\omega_n=5/t_r$)) is also fixed at 7ms.

4.4.1.5 DC voltage controller

DC voltage controller consists in PI controller and transformation of DC current to output current reference in d-axis of inverter (see red box of Figure 4.19). Current output reference in d-axis of inverter will be used in three phase current controller in the following section. PI controller will generate DC current reference which is DC current at C_{dc} and R_{dc} bus. Then, the DC current input to inverter is calculated as the difference between DC current output of converter DC/DC (i_{src}) and DC current (i_{dc_ref}). Finally, current output reference in d-axis of inverter is calculated by (4.18) where V_{dc_mes} is measured DC voltage and V_r is rms AC voltage phase to ground. To define parameters of PI controller (K_{p_vdc} and K_{i_vdc}), closed loop system of DC voltage in Figure 4.19 is defined in (4.19). The proportional gain of DC voltage controller (K_{p_vdc}) and the integral gain of DC voltage controller (K_{i_vdc}) are defined in (4.20) while comparing (4.19) to (4.10).

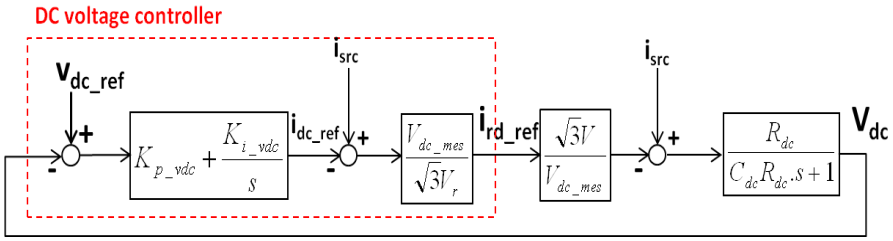

Figure 4.19 Closed loop system of DC voltage control

$$i_{rd\_ref} = \frac{V_{dc\_mes}}{\sqrt{3}V_r}.(i_{src} - i_{dc\_ref}) \tag{4.18}$$

$$\frac{V_{dc}}{V_{dc\_ref}} = \frac{R_{dc}.\left(K_{p\_vdc}s + K_{i\_vdc}\right)}{s^2 + \frac{\left(1 + K_{p\_vdc}R_{dc}\right)}{C_{dc}R_{dc}}.s + \frac{K_{i\_vdc}}{C_{dc}}} \tag{4.19}$$

$$K_{p\_vdc} = 2.\xi.\omega_{n\_vdc}.C_{dc} - \frac{1}{R_{dc}},\ K_{i\_vdc} = C_{dc}\omega_{n\_vdc}^2 \tag{4.20}$$

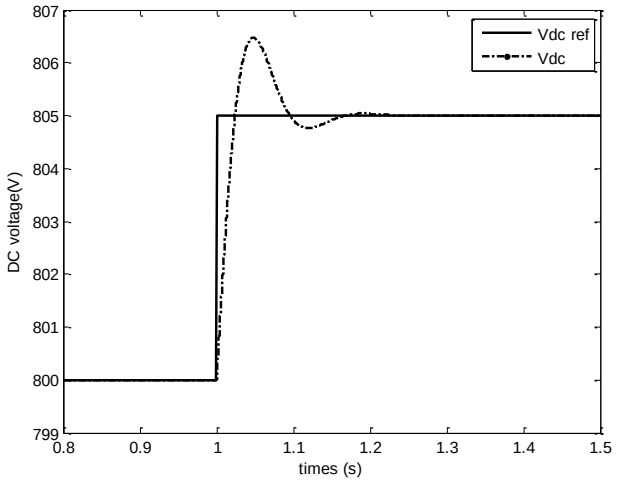

Figure 4.20 DC voltage response according to DC voltage reference change at 1 second

Time response of this DC voltage controller (t_{r_vdc}) has to be well selected in relation to time response of three phase current controller. We have finally chosen 10 times of time response of three phase current controller. DC voltage controller with the selected parameters K_{p_vdc} and K_{i_vdc} with t_{r_vdc} 70ms and ξ 0.7 is validated in MATLAB with a voltage reference change from 800 V to 805 V at 1 second. The DC voltage reaches its reference and has no steady-state error in Figure 4.21. However, an overshoot of 806.5V is resulted which is larger than DC voltage response of energy storage control # 2. Settling time of DC voltage response is equal to 0.157 second which is larger than time response of controller (0.07s). Output of this controller (I_{rd_ref}) is used as an input or reference of three phase

current controller in Figure 4.10. The current of inverter in d-axis in Figure 4.22 has large overshoot at 1 second when DC voltage varies.

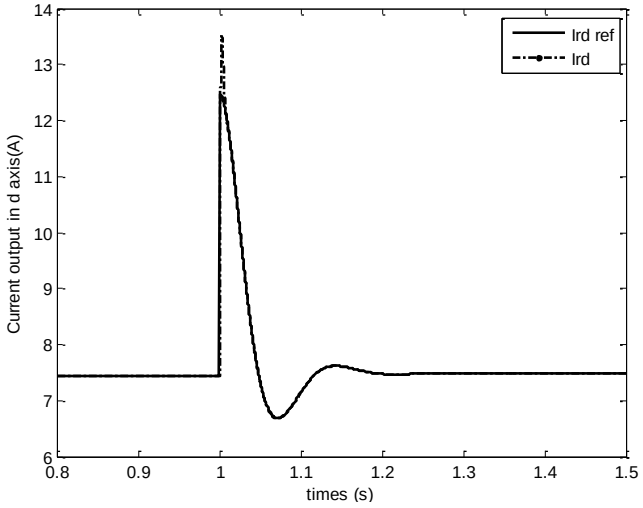

Figure 4.21 Current output of inverter in d-axis response according to DC voltage reference change at 1 second

Energy storage controls #2 and #3 have three controllers which are validated by reference signal. All control signals (current and voltage) well follow their reference.

4.3.5 Phase Lock Loop (PLL)

To define the power reference of ESS needed for droop characteristics, the grid frequency has to be well-known. The Phase Lock Loop (PLL) permits to measure frequency of power system. According to Phase Lock Loop in Figure 4.7, low pass filter is replaced by controller PI where K_{P_PLL} is a proportional gain and K_{I_PLL} is an integral gain in Figure 4.22. Furthermore, low pass filter can also be replaced by IP controller [19].

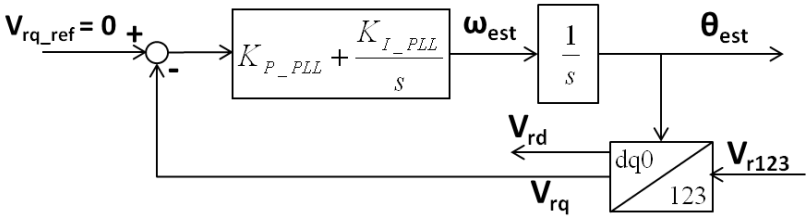

Figure 4.22 Phase lock loop with PI controller

Voltage output in d-axis and q-axis can be presented as function of the RMS voltage phase to ground (V_r), the initial angle of AC voltage (θ_r), and the measured angle (θ_{est}). The angle variation has been around $\theta_{est} - \theta_r$ which is equal to $-\pi/2$, thus the voltage in d-axis is equal to $\sqrt{3}V_r$ and voltage in q-axis is zero, followed with the assumption of $\cos(\Delta\theta)$ in (4.22). Consequently, closed loop transfer function between voltage in q-axis and its reference in Figure 4.22 can be written in (4.23) and the parameter of PLL can be defined by (4.24).

$$\begin{bmatrix} V_{rd} \\ V_{rq} \end{bmatrix} = \begin{bmatrix} \sqrt{3}V_r.sin(\theta_{est} - \theta_r) \\ -\sqrt{3}V_r.cos(\theta_{est} - \theta_r) \end{bmatrix} \quad (4.21)$$

$$\cos(\Delta\theta) \approx \Delta\theta \quad (4.22)$$

$$\frac{V_{rq}}{V_{rq\_ref}} = \frac{-\sqrt{3}V_r(K_{P\_PLL}s + K_{I\_PLL})}{s^2 - (\sqrt{3}V_r K_{P_{PLL}}).s - \sqrt{3}V_r K_{I\_PLL}} \quad (4.23)$$

$$K_{P\_PLL} = \frac{2.\xi_{PLL}.\omega_{n\_PLL}}{-\sqrt{3}V_r}, \; K_{I\_PLL} = \frac{{\omega_{n\_PLL}}^2}{-\sqrt{3}V_r} \quad (4.24)$$

However, measured frequency by PLL has some errors in dynamic response. Frequency response of PLL has fast variations. A low pass filter is proposed to eliminate this fast dynamics of measured frequency (time constant of low pass filter is chosen to 10ms, which corresponds to a cut-off frequency of 16Hz) [19].

The studied isolated grid is simulated in MATLAB with load variation from 0.5MW to 1MW at 3 seconds. Frequency response from PLL with varying ω_{n_PLL} and frequency from diesel generator (angle velocity of synchronous machine) are illustrated in Figure 4.23. Fast dynamic are presented in frequency response. Large bandwidth of PLL (fast time response) causes large fast dynamic response in Figure 4.23. However, small bandwidth of PLL (for slow time response) can cause oscillations on response and instable system. The low pass filter designed with a time constant of 10ms cannot eliminate all fast dynamic responses. To improve frequency response of PLL, the time constant of low pass filter has to be increased but it will cause some delay to frequency response as it is illustrated in Figure 4.24.

It is too difficult to select parameters of PI controller or filter to satisfy the fast tracking and good filtering characteristics. Therefore, a bandwidth frequency of PLL (ω_{n_PLL}) equal to 50rad/s is selected with a cut-off frequency of low pass filter of 20 ms by trade-off between a fast tracking and good filtering characteristics.

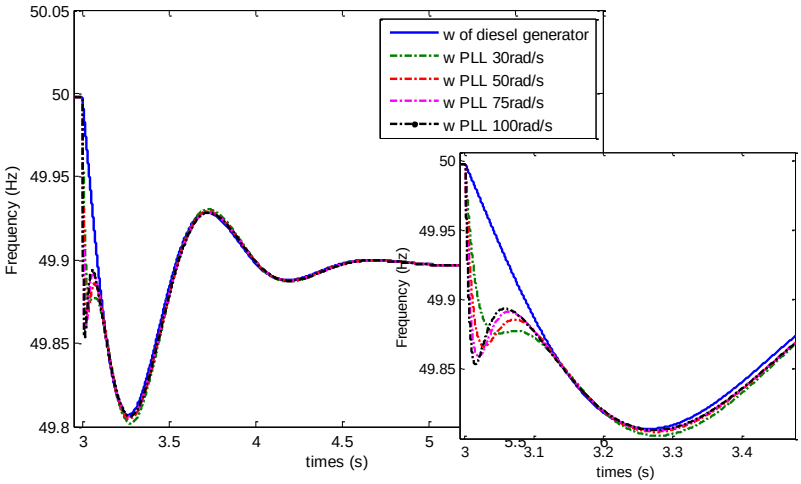

Figure 4.23 Measured frequency from PLL for various ω_{n_PLL}

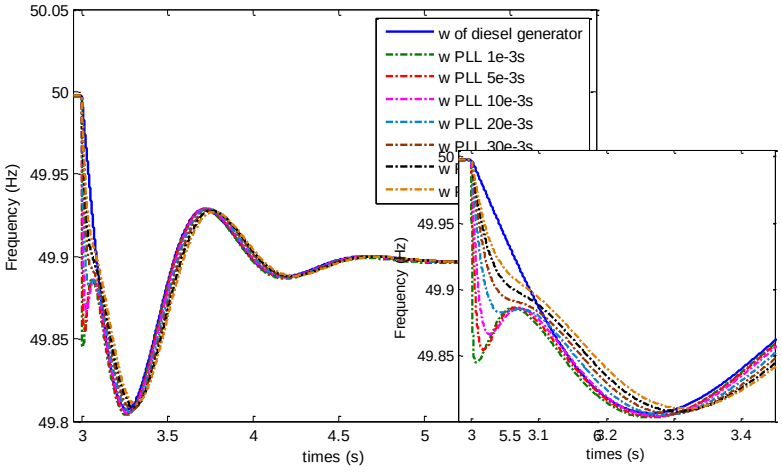

Figure 4.24 Measured frequency from PLL for various time constant of low pass filter

4.4 Simulation of energy storage system with droop characteristic

Energy storage system is added to the initial power system which consists of diesel generator (1.6MW, 400V), PV plant (250kW) and load (1MW, 400V) in Figure 4.25 for decreasing frequency

variation after active load power variation, meanwhile power of PV is assumed to be constant. Different energy storage control systems (1 to 3) are simulated with model topology of power system whose parameters are presented in Annex IV. Step time simulation is firstly elaborated, followed with the study of each energy storage control system according to load power variation (of 10kW for energy storage control # 1 and 100kW for energy storage control # 2 and 3). Consequently, all control systems are compared to each other. For all simulations, current in q-axis is controlled to zero. Therefore, energy storage does not produce or absorb reactive power.

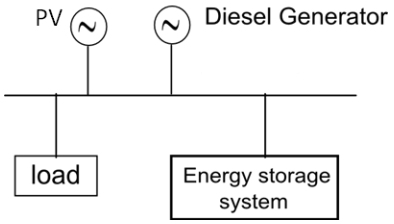

Figure 4.25 Simulated system representation

Step time around 50 µs is sufficient to simulate power system in MATLAB for steady state and transient analysis [66]. Indeed, simulations of system with renewable energy which has converter or inverter connected to power system needs very small step time. The step time depends on resonant frequency of filter and frequency of PWM. Frequency of simulation should be at least 20 times of resonant frequency and 50-100 times of PWM frequency. However, small step time takes very long simulation time.

Energy storage control #2 with RL filter is simulated for different step time simulations (50 µs and 10µs). The PWM frequency is equal to 5 kHz. Power of load increases by 0.1 MW at 3 seconds. Figure 4.26 illustrates AC current output of energy storage system from 4 seconds to 4.05 seconds. Small step time caused signal very different to sine wave in Figure 4.26 (step time 10µs). However, simulations with step time of 10 µs takes about 10 minutes. If step time decreases, time simulation is too long and may be out of memory.

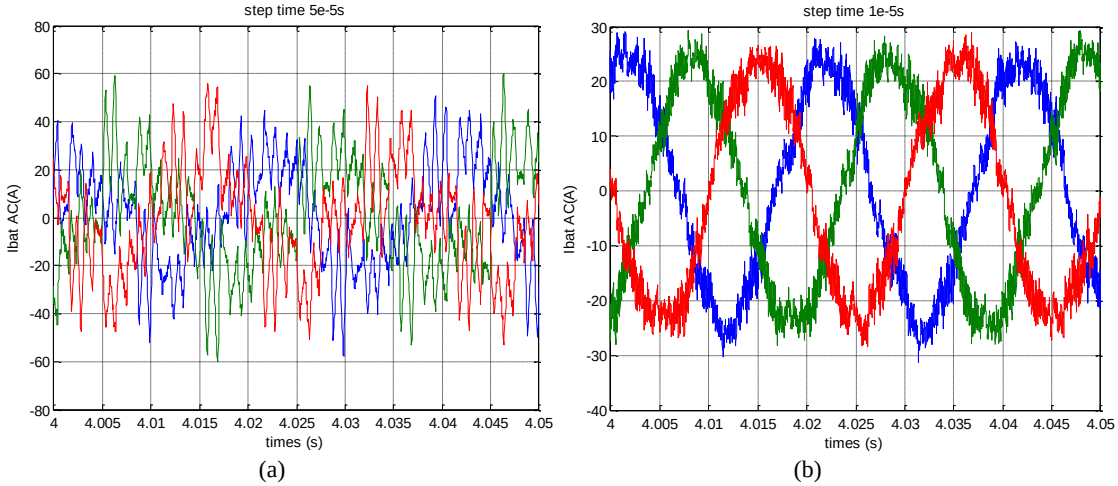

(a) (b)

Figure 4.26 AC current output of energy storage with sampling time simulation (a) 5e-5 seconds (b) 1e-5 seconds

Power system with renewable energy (with converter and/or inverter) can also be simulated with real time simulator as RTLAB©. In RTLAB simulation, the ratio of the simulated frequency to the PWM frequency decreases to a ratio of 5 to 10. The time simulation is shorter because of performance of the CPU processor. For example, for PWM frequency of 10 kHz, the needed step time simulation is at least equal to 10 to 20µs. The RTLAB can be used for off-line simulations (i.e. not connected to hardware) as the simulation in MATLAB in order to reduce time simulations. The RTLAB with hardware-in-the-loop (HIL) will be discussed in Chapter 7.

4.5.1 Simulation of ESS control #1

Energy storage with only inverter AC/DC in Figure 4.1 is connected to power system initial. Active power of load changes from 1MW to 1.01MW (active power of load increases 10kW) at 3 seconds. Frequency input of droop control of energy storage system is 50Hz from 0 to 2.5 seconds to wait diesel generator in steady state. And after 2.5 seconds; frequency input value is measured from PLL.

Parameters of PI controller are defined in (4.11) where ξ is 0.7 and time response of controller (t_r) is 7ms. The PWM frequency is 10 kHz and step time simulation is 2 μs. The energy storage system is connected to power system via filter RL.

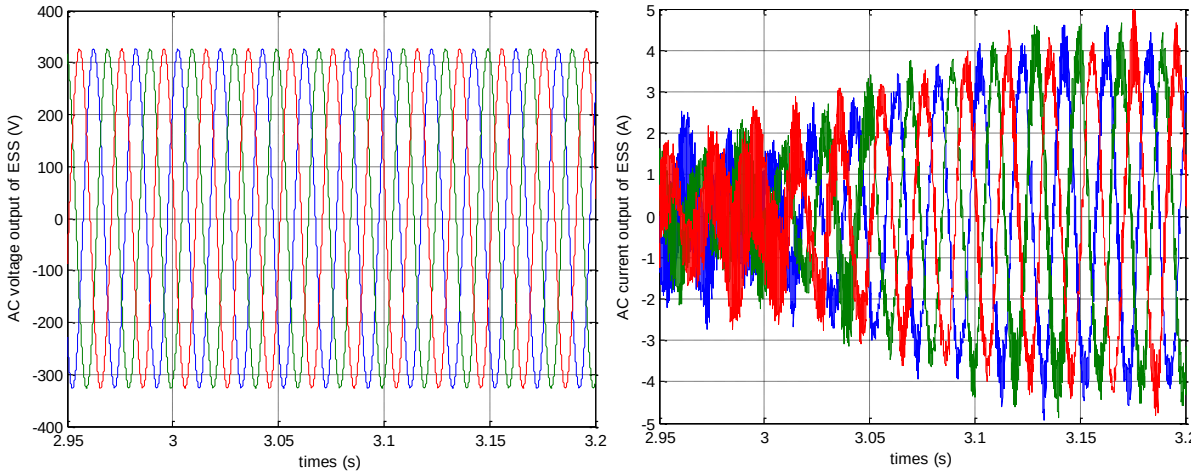

(a) (b)

Figure 4.27 (a) AC voltage output (b) AC current output of ESS according to increasing of load power 10kW

Voltage output of energy storage in Figure 4.27(a) is in sine signal. Current output of energy storage which is illustrated in Figure 4.27(b) is quite alike sine signal but there are some oscillations. The DC voltage of inverter which is shown in Figure 4.28(a) is quite constant. Furthermore, Figure 4.28(b) shows that current output of energy storage in d-axis follows its reference although there is an oscillation. If power variation of load is larger than 30kW, output current in d-axis is not able to follow its reference because of high variation of DC voltage and saturation by inductance. If this inductance is reduced, power variation can be larger but AC output current will come out with a really bad sine signal.

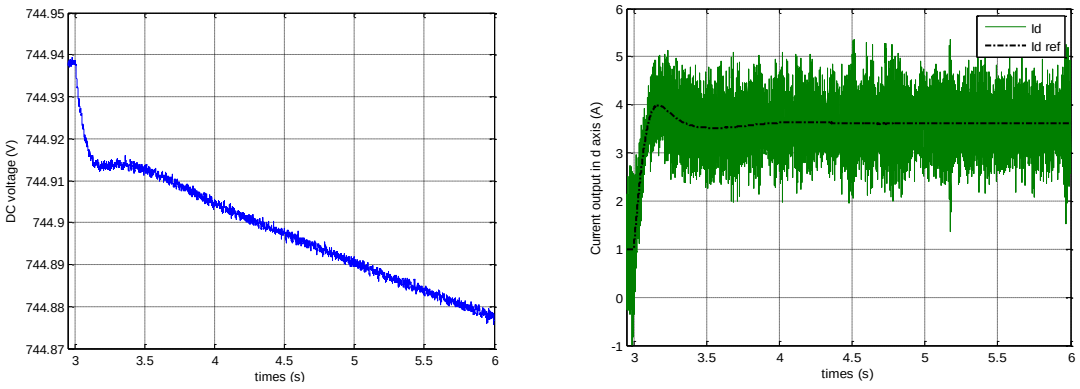

(a) (b)

Figure 4.28 (a) DC voltage of AC/DC (b) Current output in d-axis and its reference value according to increasing of load power 10 kW

Frequency response of system without and with energy storage is compared in Figure 4.29. Energy storage reduces frequency deviation in transient response and steady-state value. Angle velocity measured from synchronous machine in Figure 4.29(a) is quite similar to the measured frequency from PLL except in some fast dynamic response. However, this fast dynamic of measured

frequency PLL does not cause any effects on the control system of energy storage. Frequency deviation according to load power variation of system with energy storage is smaller than the initial system (without energy storage).

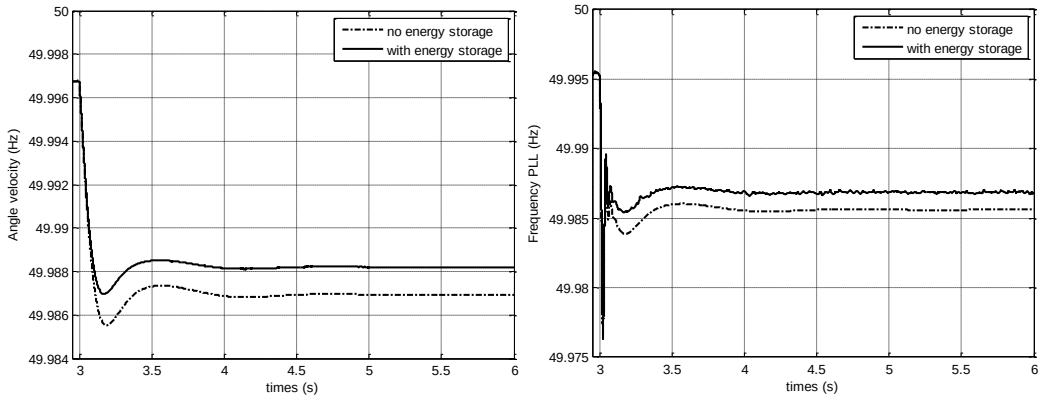

(a) (b)

Figure 4.29 Frequency response of system without and with ESS according to increasing of load power 10 kW (a) angle velocity of synchronous machine of diesel generator and (b) measured frequency by PLL

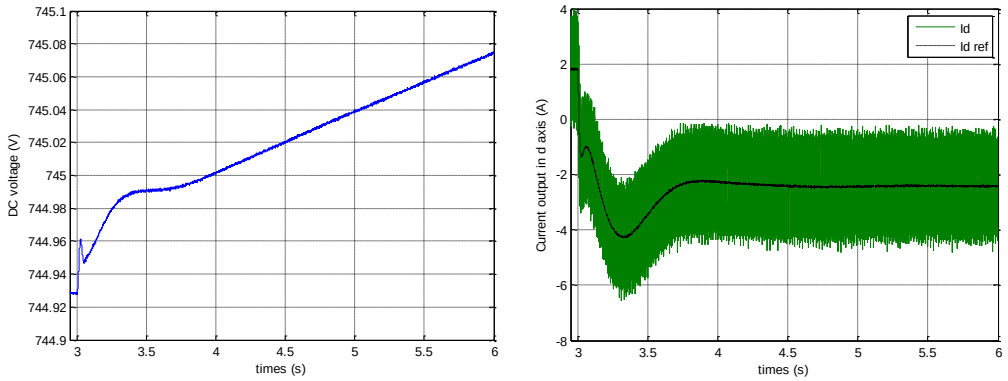

(a) (b)

Figure 4.30 (a) DC voltage of AC/DC (b) Current output in d-axis and its reference value according to decreasing of load power 10 kW

Furthermore, decreasing of load power -10kW is also simulated. AC voltage and current output of energy storage are quite similar to the increasing situation of load power in Figure 4.27(a) and (b). However, DC voltage or voltage output of energy storage barely increases in Figure 4.30(a) (it barely decreases for load power rising). While the current in d-axis and its reference is in negative value which signifies that current flow from power system to energy storage system or energy storage absorbs power (in charge mode). Nevertheless the current in d-axis is well followed its reference but with some oscillations.

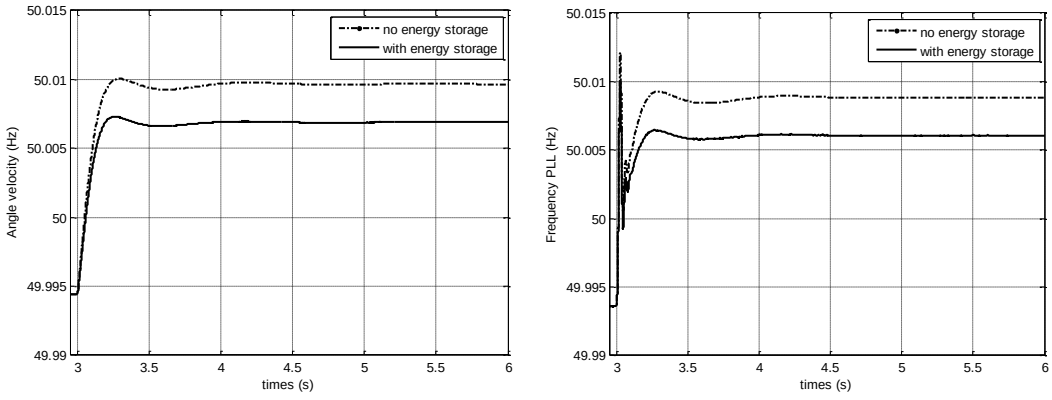

(a) (b)

Figure 4.31 Frequency response of system without and with ESS according to increasing of load power 10 kW

Finally, angle velocity of synchronous machine and measured frequency by PLL are plotted in Figure 4.31(a) and (b) respectively. Measured frequency by PLL has fast dynamic response similar to previous simulation. Frequency is increased after active power of load decreases. This is obviously indicated that energy storage can reduce frequency variation.

4.5.2 Energy storage control #2

Energy storage with DC/DC and AC/DC with controllers designed in 4.4.3.1 is validated with power system which consists of diesel generator and load. This simulation is similar to previous simulation of energy storage control system 1 except that the active power variation of load is 100kW at 3 seconds. Output AC voltage and current of energy storage (focus during load power variation 2.95 to 3.2 seconds) are illustrated in Figure 4.32(a) and (b). The AC voltage is constant. On the contrary, AC current of energy storage is increase at 3 seconds to inject active power to power system in order to limit the frequency deviation as shown in Figure 4.33(a).

The reduction of active power of load 100kW at 3 seconds is also simulated. Frequency response of system with and without energy storage in Figure 4.33(b) shows that energy storage is also relevant to the reduction of frequency deviation in this case.

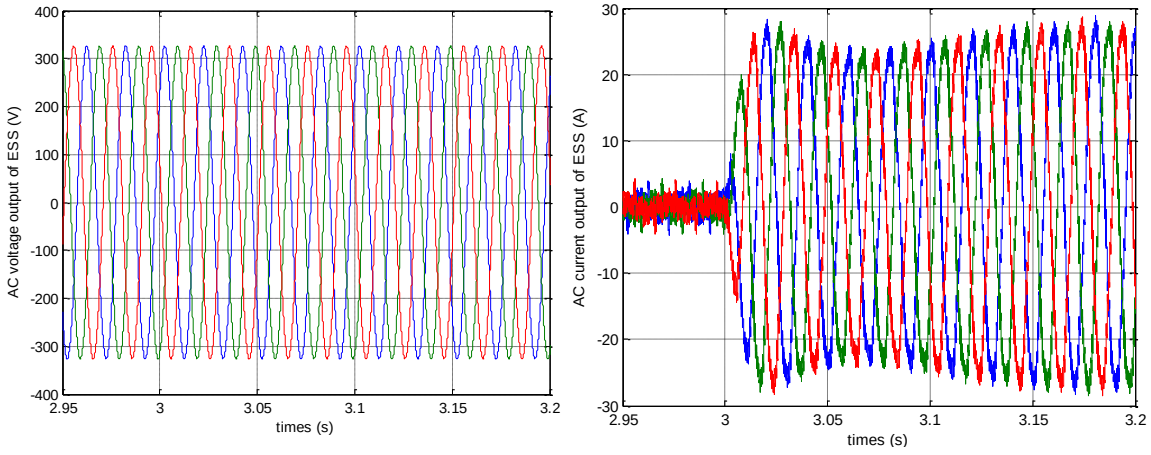

(a) (b)

Figure 4.32 (a) AC voltage output (b) AC current output of ESS system according to increasing of load power 100kW

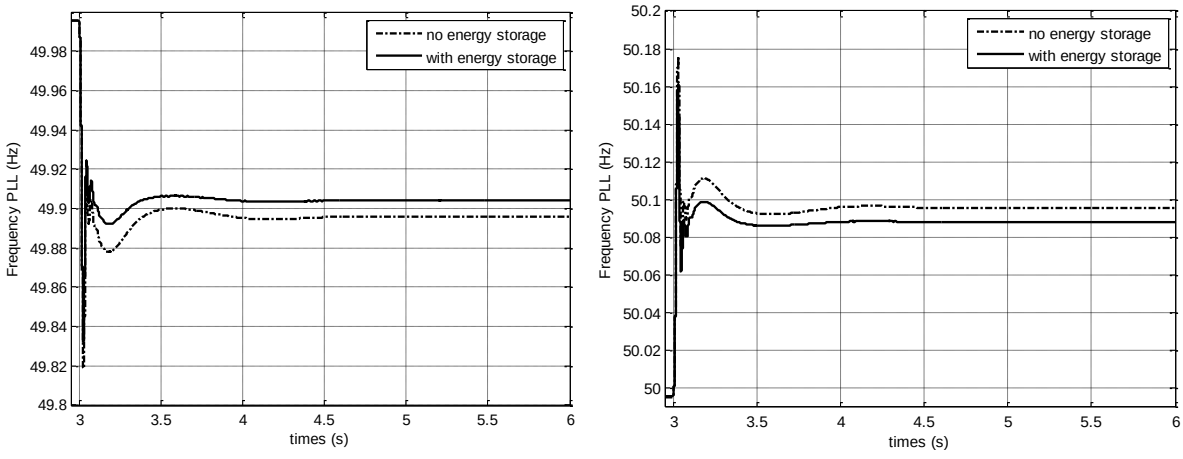

(a) (b)

Figure 4.33 Frequency response of system without and with ESS (a) increasing of load power 100kW (b) decreasing of load power 100kW

DC voltages of increasing and decreasing of load power which are illustrated in Figure 4.34(a) and (b) respectively have some variations after disturbance and return back to the reference value (1000V). For the increasing case, DC voltage response decreases from its reference value and turn back to reference value with rise time (80% of overshoot) of 0.019 second and settling time (+/-1% of steady state value) of 0.073 second. For the other case, DC voltage increases after the disturbance. Its

rise and settling times of DC voltage response are 0.017 and 0.059 second respectively. DC voltage variation according to rising of load power is larger than in decreasing case for the equivalent power variation.

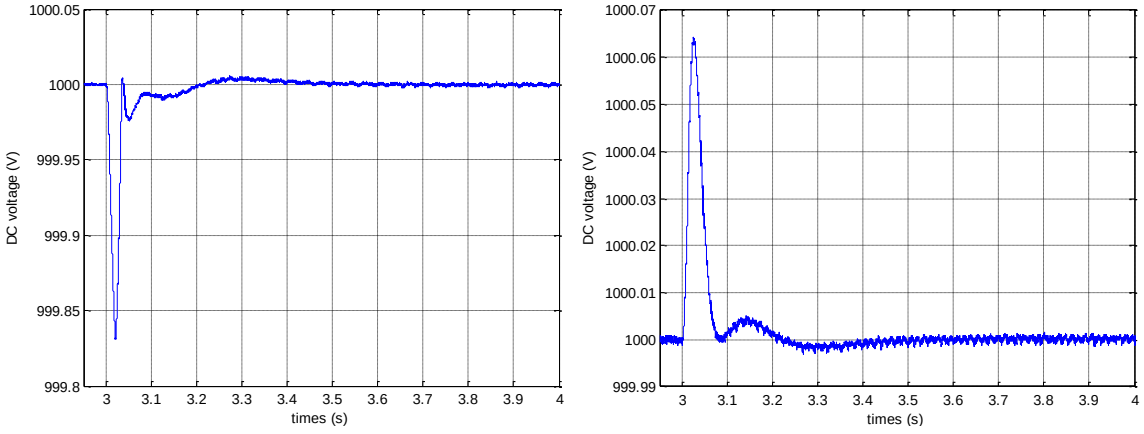

(a) (b)

Figure 4.34 DC voltage of AC/DC (a) increasing of load power 100kW (b) decreasing of load power 100kW

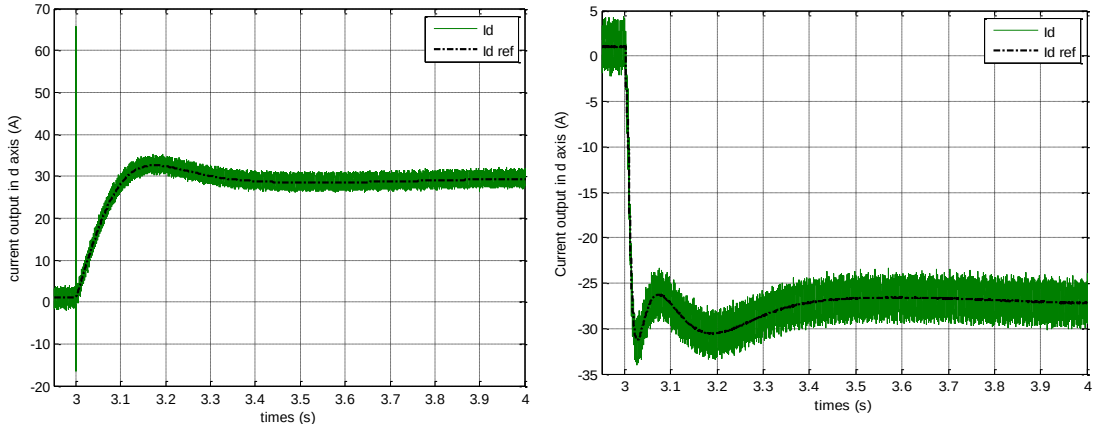

(a) (b)

Figure 4.35 Current output in d-axis and its reference value (a) increasing of load power 100kW (b) decreasing of load power 100kW

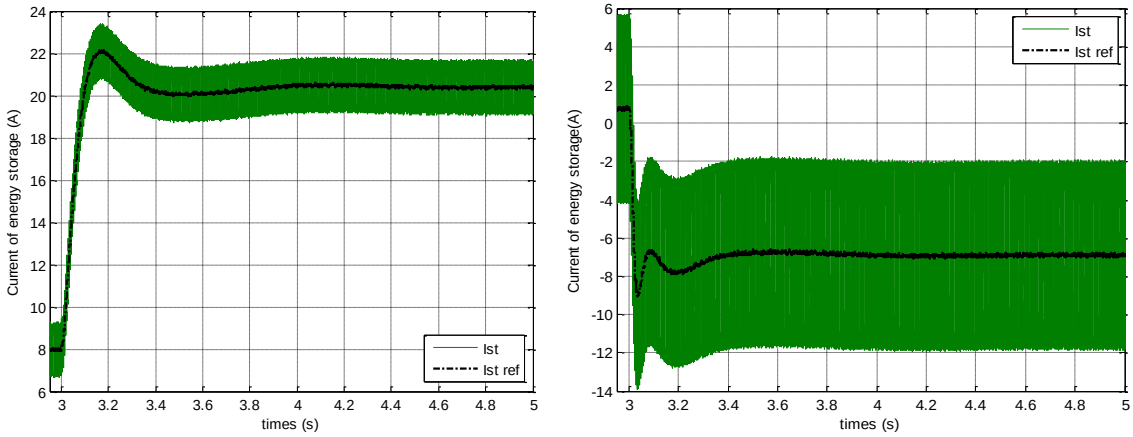

(a) (b)

Figure 4.36 Current of energy storage and its reference value (a) increasing of load power 100kW (b) decreasing of load power 100kW

The current output in d-axis and DC current of energy storage of these two different cases are also plotted in Figure 4.35 and Figure 4.36 respectively. All current responses follow their reference immediately because time response of three phase current controller and energy storage current controller are small (7ms). Currents is in positive value in load increasing case for the injection energy to power system and in negative value in load decreasing case for the absorption energy. Current

response of decreasing load power case has larger oscillation than in increasing case. The current of energy storage has large oscillation because its reference from DC voltage controller is not quite constant and has some oscillations.

4.5.3 Energy storage control #3

Energy storage system with controlling DC voltage by switching function in d-axis of inverter and power of energy storage (via current of energy storage) by switching function of inverter is simulated with an increasing and decreasing load power. AC voltage and current output of energy storage are illustrated in Figure 4.37(a) and (b).

Energy storage with this control system can also reduce frequency deviation according to load power variation in Figure 4.38. The frequency response of this control system is a slightly smaller than that of energy storage control #2. The overshoot of DC voltage by this control system is also smaller than the previous control system in Figure 4.39. The DC voltage response of energy storage control # 3 is the inverse of control system #2. DC voltage increases after the increasing of load power but it decreases in the previous control system. Rise and settling times of DC voltage in increasing of load case shown in Figure 4.39(a) are 0.017 second and 0.061 second, respectively and these values shown in Figure 4.39(b) are 0.017 second and 0.064 second, respectively. This shows that rise time and settling time of DC voltage by this control system are quite closed to the values of control system #2.

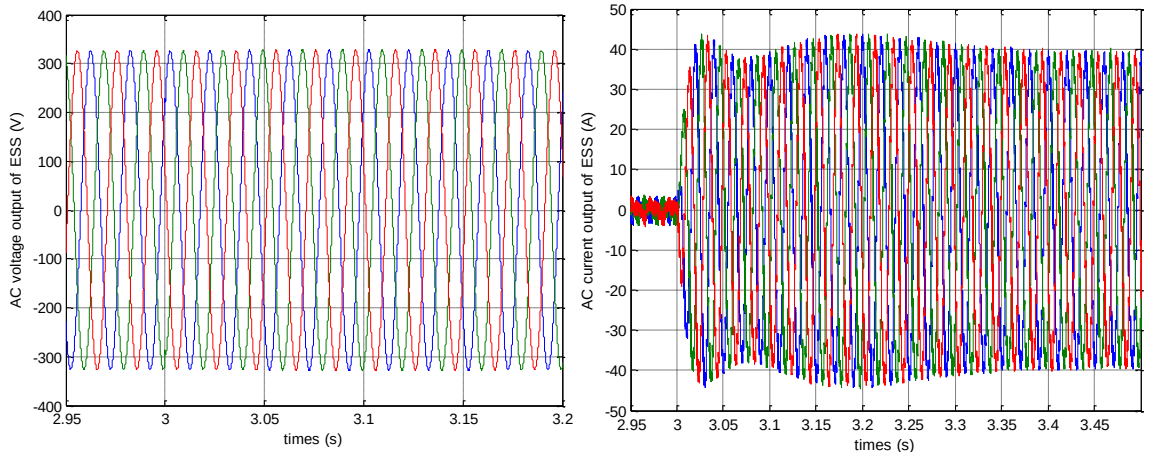

(a) (b)

Figure 4.37 (a) AC voltage output (b) AC current output of ESS system according to increasing of load power 100kW

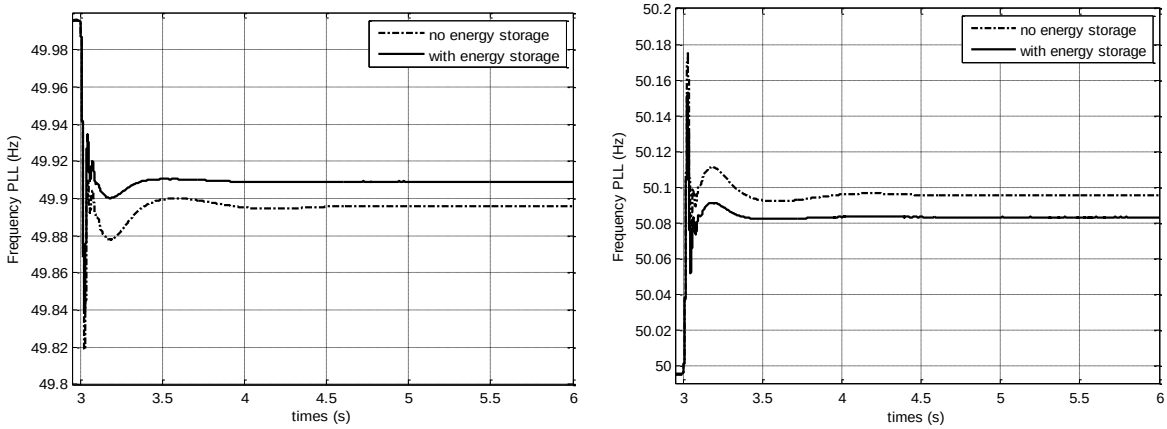

(a) (b)

Figure 4.38 Frequency response of system without and with ESS (a) increasing of load power (b) decreasing of load power 100kW

Output currents in d-axis and its reference (signal from DC voltage controller) of two different studied cases are illustrated in Figure 4.40(a) and (b). Reference signal presents more oscillation than measured current signal. Furthermore, current in d-axis of this control system is larger than current of

control system #2. Current of energy storage are presented in Figure 4.41. All current achieved correctly their reference value.

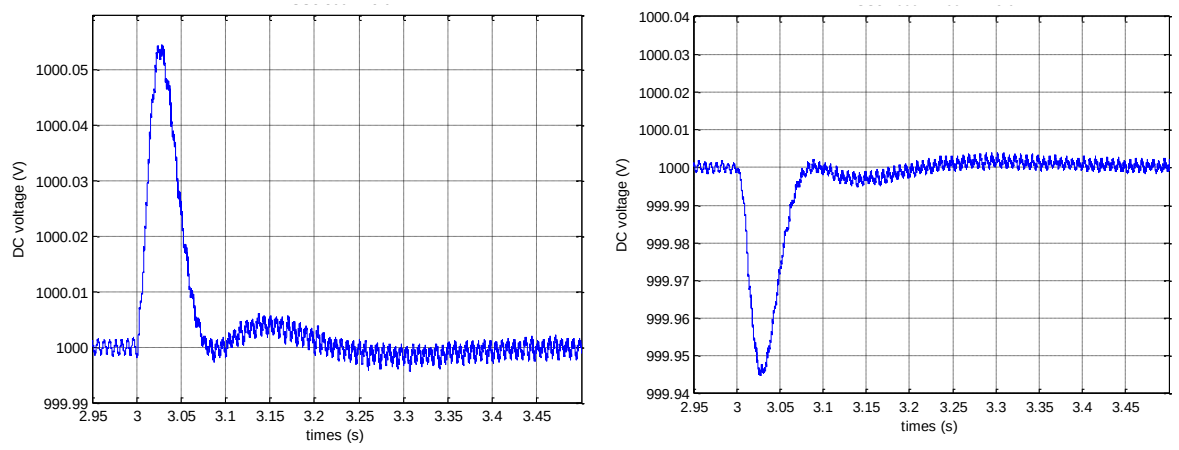

(a) (b)

Figure 4.39 DC voltage of AC/DC (a) increasing of load power 100kW (b) decreasing of load power 100kW

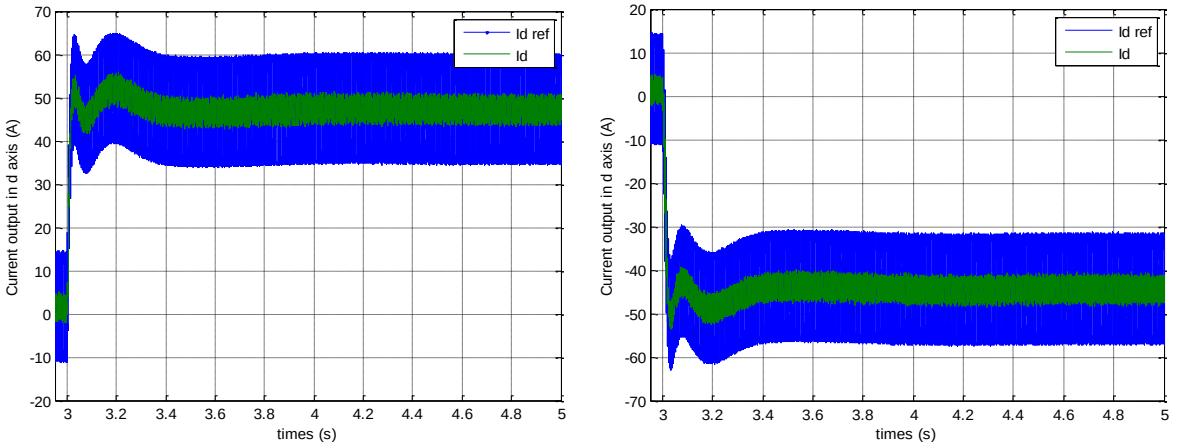

(a) (b)

Figure 4.40 Current output in d-axis and its reference value (a) increasing of load power 100kW (b) decreasing of load power 100kW

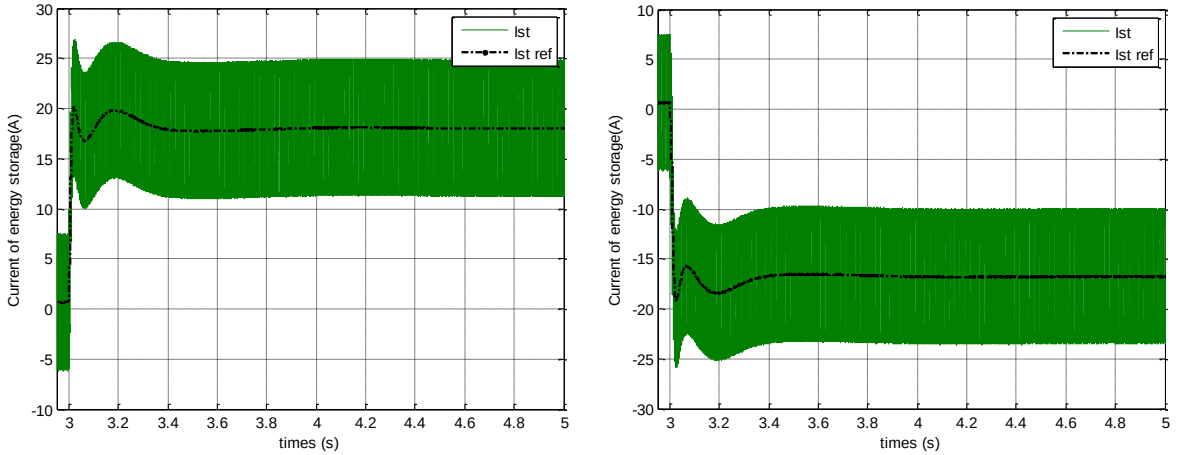

(a) (b)

Figure 4.41 Current of energy storage and its reference value (a) increasing of load power 100kW (b) decreasing of load power 100kW

4.5 Conclusion

In this chapter, electrical and control architectures of energy storage system have been studied and designed. Energy storage is connected to power system via interfacing system which consists of DC/DC converter and AC/DC converter and filter. Although, energy storage can be connected to only inverter AC/DC (no DC/DC) with the assumption that the DC voltage constant but this system is not robust to high power variation. Therefore, energy storage with DC/DC and AC/DC which facilitates to control DC voltage by switching function of DC/DC or switching function in d-axis of AC/DC is proposed. Energy storage control #2 (control V_{dc} by switching function of DC/DC) and control system #3 (control V_{dc} by switching function in d-axis of AC/DC) give similar results except that DC voltage overshoot by control system 3 is smaller than control system #2.

Chapter 5

Coordinated strategy for energy storage system participation to primary frequency control

5.1 Introduction

In isolated power system with high penetration of PV, the frequency is risky to be instable or its variations can be large and unacceptable. Energy storage can then be used to maintain the stability and/or improve the frequency response to avoid large perturbations. In literature reviewed, most studies have applied energy storage for primary frequency control to limit frequency deviation according to load variation which corresponds to instantaneous variations (like step signal). In this study, energy storage participates in primary frequency control in order to improve the frequency variation according to intermittency which is described by slower fluctuation than load variation. Frequency deviation according to slow fluctuation is then smaller than fast fluctuation for the same amplitude power deviation. However, these disturbances can be met frequently. Furthermore, energy storage can be used as the main source of frequency regulation. Droop control strategy is then applied to energy storage system while power of diesel generator is fixed at 60% of its nominal value [60] in order to limit variations around an efficient operating point.

For sudden power variation (load variation or loss of power source), the droop control is applied for energy storage to assist generator to balance active powers. However, the transient frequency response is not quite improved by droop control. It allows reducing the steady-state value of frequency response with an equivalent proportional controller. Many studies have tried to improve the transient response of the grid frequency. Then, in reference [19], the storage has to inject its rated power during a short time if the derivative time of frequency is over its reference. Although the frequency deviation in transient domain is reduced, it is not an optimal control. Besides, other power management of an ESS is proposed in [66], where the participation of the energy storage to frequency regulation is defined with a high pass filtering of wind power variations.

From the previous study on the impact of PV variation on grid frequency, a new strategy using the diagram of PV limitation presented in Figure 3.22 is proposed. The energy storage is then solicited to participate to frequency regulation if PV power variation is out of the acceptable limit. Moreover, from the study on the transfer function between frequency deviation and PV power deviation, a filtering strategy is also proposed. Energy storage with this second strategy will control the time-response of frequency for medium and high frequency band-widths of power fluctuation. These two strategies are elaborated and simulated with a real PV plant #1 (250kW) during 3 months. Results of their performance are compared to the classical droop control which has been already presented in chapter 4.

5.2 Indicator for comparison of strategy analysis

Studied isolated grid consists in diesel generator, photovoltaic plant, energy storage system modelled in chapter 4 and constant load as illustrated in Figure 5.1(a). It is assumed that at the beginning of simulation, the load power (0.6 per unit or 1.2 MW) equals to the summation of the initial power of diesel generator (0.5 per unit here or 1MW) and the initial power of PV (0.1 per unit or 0.2MW). The initial reference of power for the energy storage is then equal to zero; the frequency is equal to 50 Hz. The diesel generator has a primary frequency control with a droop (s_d) equal to 8%. The dynamic response of diesel is modelled by a first order transfer function, shown in (3.5). The grid frequency is calculated by (3.10). Equivalent control diagram of this power system is presented in Figure 5.1(b). In this chapter, active power of load remains constant. Energy storage is help to reduce frequency deviation and maintain stability according to power variation of PV.

Indicators to define performance of the different strategies are the maximal frequency deviation and the number of occurrences where grid frequency is over the acceptable limit. Moreover, participation of energy storage is also analyzed. The maximal active power of energy storage for charging and discharging modes are compared. The useful energy which is calculated as the difference between the maximal and minimum values of the stored energy along time duration is illustrated in Figure 5.2. Maximal power and useful energy will help us also to design the energy storage device. Furthermore, the maximal power and used energy of diesel generator are also analyzed in order to find out the extent that energy storage can reduce the participation of diesel generator.

Power of diesel generator (with primary and secondary controls) and energy storage in time domain will be also analyzed in the frequency domain by Fourier transform (as for PV power analysis in Chapter 2). The spectrum is analyzed by computing FHC indicator. Frequencies more than 1 Hz, between 0.01Hz to 1 Hz, and below 0.01Hz define high, medium, and low frequency regions respectively.

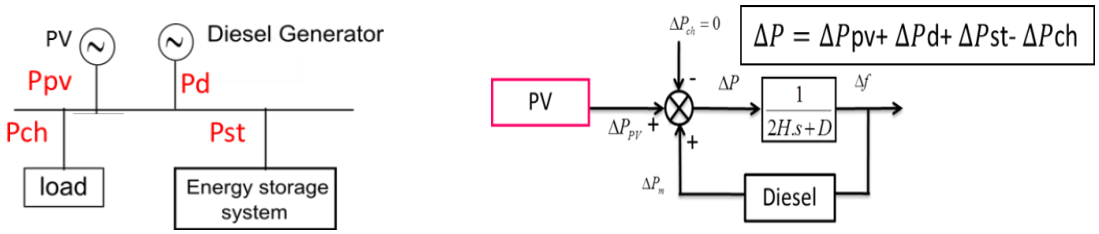

Figure 5.1 Simulated system

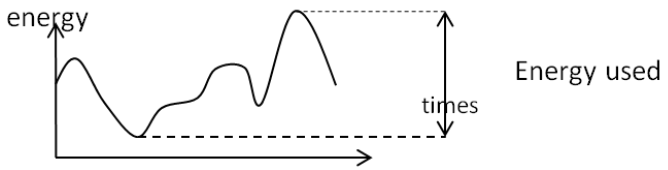

Figure 5.2 Energy used calculation

5.3 Strategy with limitation diagram on PV variation

The study on intermittency in the chapter 2 is used to define a new control strategy for energy storage device. From chapter 2, power signals of PV plant present many types of fluctuation: fast fluctuation, slow fluctuation, etc. as illustrated in Figure 5.3. The significant parameters used to define the different situations are the power variation (ΔP) and the duration of power change (Δt). The outcome reveals that each type of fluctuation causes different impact on the grid frequency.

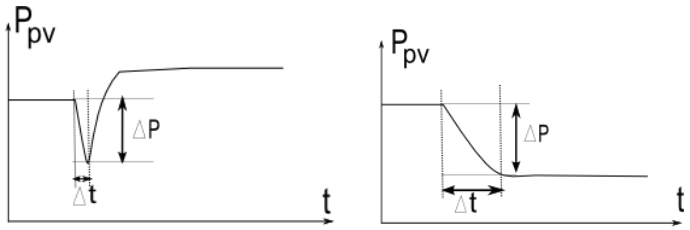

Figure 5.3 Different PV power signal with (a) fast fluctuation (b) slow fluctuation

PV power is assumed to evaluate as step and ramp signals. From chapter 3, the maximal frequency variation can be calculated from power variation and parameter K(Δt) in (3.28). Power variation and duration of power change which causes fixed maximal frequency deviation in (3.34) have been also defined. Then, the power limitation diagram is plotted in Figure 3.22. This is used to define different zones according to PV power deviation. Let us remember that the area below the limitation line is defined as the acceptable zone (the frequency variation remains in the acceptable limits) while, the area above this line corresponds to the inacceptable zone. The energy storage will participate to regulate frequency variation when the power deviation and the duration of power change are out of the acceptable limit. Finally, this *PV limitation diagram* will be used to size the energy storage device.

The energy storage is connected to power system via an interface with power electronics converters (DC/DC reversible converter and AC/DC inverter), and a RLC filter shown in Figure 5.4. The control architecture of this ESS has been already defined and designed in the chapter 4. In this study, the focus is put on the active power control and only energy storage power calculation part (blue box in Figure 5.4).

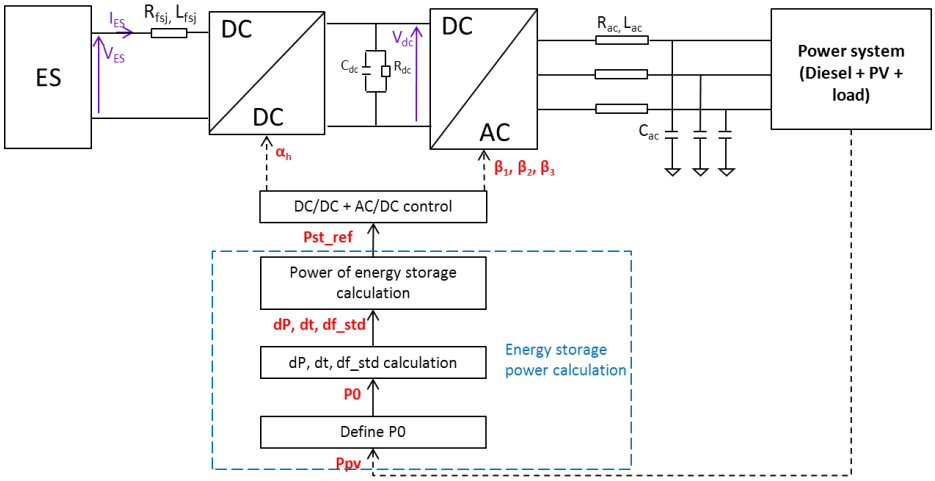

Figure 5.4 Energy storage systems

5.3.1 Control strategy algorithm

Dynamic parameters of power system (PI controller of frequency control of diesel generator, time response of diesel generator, equivalent inertia and load damping constant) and maximal acceptable frequency (Δf_{std}) are firstly defined in order to design the limitation of power variation (ΔP_{pv_limit}) versus the duration of power change (Δt_{limit}) as illustrated in Figure 3.22. The parameter K and K(Δt) of step signal and ramp signal from chapter 3 is used. However, the step signal (dt=0) cannot be detected in reality. It appears only at the beginning of simulation. The power variation for very small time different (dt) is considered as a step change, i.e. when time duration (dt) is equal to time resolution (t_s).

After defined the limitation curve, the power management for frequency regulation is presented in Figure 5.5, where n denotes the number of loops calculation.

The PV power is first measured, followed with the calculation of the power variation ($\Delta P_{pv}(t)$) and the duration of change ($\Delta t(t)$) for each time resolution (t_s) as illustrated in Figure 5.6. This power difference and the duration of change are then reported on the limitation curve. If the fluctuation of PV power remains in inacceptable zone (pink circle in Figure 5.6), the power reference of energy storage ($P_{es\_ref}(t)$) is then defined as the difference between the actual power variation ($\Delta P_{pv}(t)$) and the maximal acceptable power variation at specific duration of change ($\Delta P_{pv\_limit}(\Delta t(t))$) in (5.1). On the contrary, the power reference of energy storage is null if it is in the acceptable zone (orange circle in Figure 5.6). However, the power reference of energy storage does not change to zero immediately. The actual power reference of energy storage is 85% of its former value ($85\%*P_{es\_ref}(t-t_s)$) because the power variation just returns back to acceptable but still risky zone (green circle in Figure 5.6). Indeed, a fast change of storage power can cause a frequency variation. And if energy storage power reduce slowly (over 85%), energy needed of energy storage is high and power of energy storage is not near zero before the next PV power variation. Besides, the state of charge (SoC) of energy storage should be checked whether the energy storage.

$$P_{es\_ref}(t) = \Delta P_{pv}(t) - \Delta P_{pv\_limit}(\Delta t(t)) \quad (5.1)$$

Summarized calculation of power reference of ESS is divided into 3 cases:

1.) $P_{es\_ref}(t) = 0$ when State of Charge (SoC) is out of limit.

2.) $P_{es\_ref}(t) = 85\%$ of power reference before ($85\%*P_{ES\_ref}(t-t_s)$) when power difference and duration of change are in the acceptable zone or if active power of photovoltaic is stable.

3.) It is the difference between the power variation of PV and the limited power variation as when power difference and duration of change are in the unacceptable zone and the SoC is in acceptable limit.

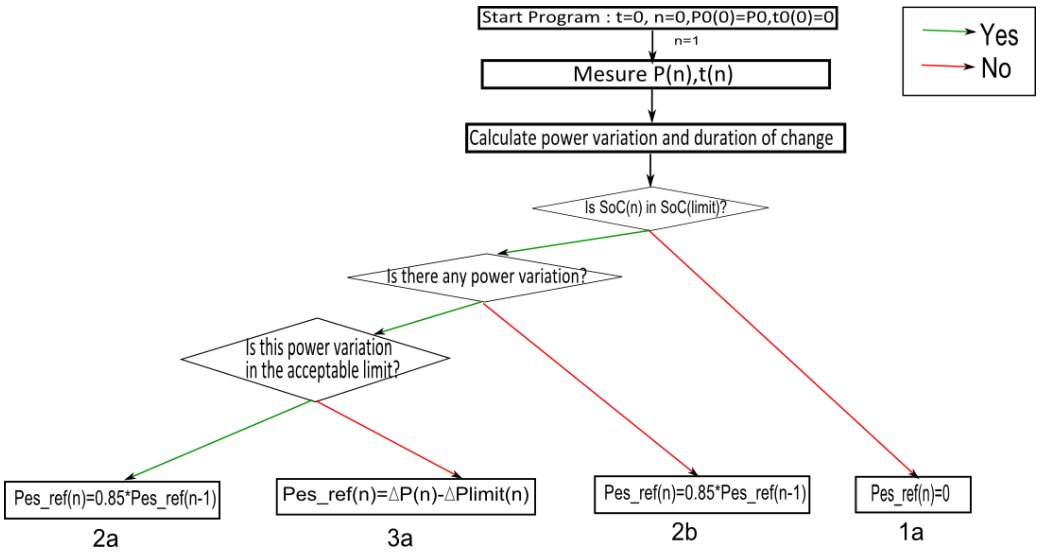

Figure 5.5 Power management algorithm for strategy with limitation diagram

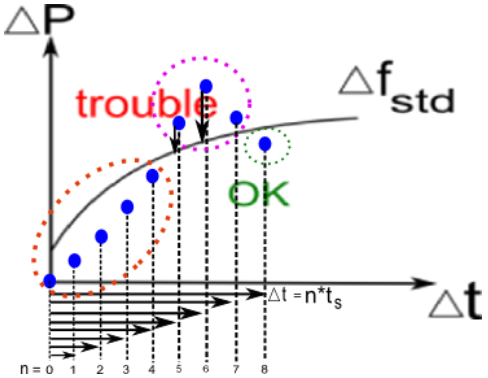

Figure 5.6 Control strategy

The important part is the power variation and the duration of change calculation. The power difference ($\Delta P_{pv}(t)$) is the difference between the actual power ($P_{pv}(t)$) and the reference power ($P_0(t)$) as shown in (5.2). The value of reference power ($P_0(t)$) is the initial power of PV (P_{ini}). This power is signified from the difference between the initial power reference of diesel generator (the power which causes the frequency to be equal to 50Hz) and the power of load (assumed to be constant). Only primary frequency control is considered in this study so the power reference of diesel generator is fixed. The duration of change (Δt) is the difference between actual time and reference time (time at power reference) (t_0) as presented in (5.3). However, it is not applicable for real power system because initial power is not fixed for an entire day. Therefore, diesel generator with primary and secondary frequency controls is investigated and power reference should be adapted according to secondary frequency control.

$$\Delta P_{pv}(t) = P_{pv}(t) - P_0(t) \tag{5.2}$$

$$\Delta t(t) = t - t_0 \tag{5.3}$$

5.3.1.1 Power system without secondary control

The fluctuation of PV can be separated into 3 situations as shown in Figure 5.7. The first situation is simple; the power decreases or increases continuously. The power reference (for a fixed brightness and temperature) keeps constant at initial power (P_{ini}). The time reference (t_0) is time at P_{o1} during the situation 1a and the beginning of situation 1b until the power of PV passes the power initial again at P_{o2}. The time reference (t_0) changes when PV power is equal to P_{o2}. Firstly, the power of PV decreases from P_{o1} to P_{o2}. The power variation (ΔP_1) and its duration of change (Δt_1) may be located in the acceptable zone (the green circle) in Figure 5.6.

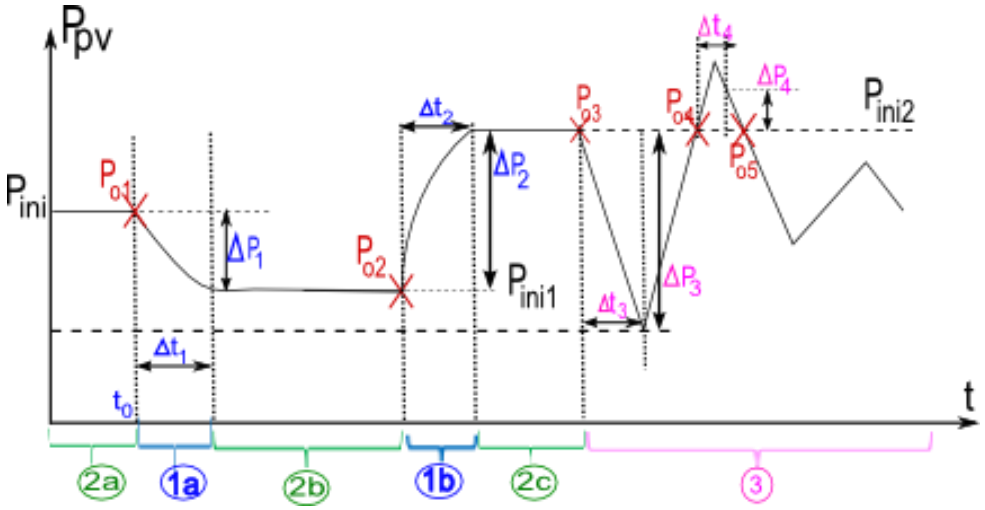

Figure 5.7 Power variation of PV for system without secondary control

The second case is the situation where active power keeps constant. This case is detected if the power variation is null (2a in Figure 5.7) or if the actual power variation equals to the previous power variation (2b and 2c in Figure 5.7) as shown in equation (5.4). The actual power reference of energy storage is then equal to 85% of its former value ($85\%*P_{es\_ref}(t-t_s)$). The power reference of energy storage decreases continuously to give some duration for the diesel generator to adapt its power.

$$\Delta P_{pv}(t) = \Delta P_{pv}(t - t_s) \quad \text{or} \quad \Delta P_{pv}(n) = \Delta P_{pv}(n-1) \tag{5.4}$$

The last case is the fluctuated power of PV situation. This situation is the same as the first situation. The time reference (t_0) is also changed when PV power passes at P_{o3} or P_{o4}. The major problem of this situation is that some fast fluctuations cannot be detected for the real signal of PV if the time resolution is not small enough.

An example of power difference (ΔP) according to duration of change (Δt) calculation is presented in Figure 5.8. The initial power is equal to 0.1 per unit. From this initial power at 5 seconds, the power difference and the duration of change are calculated from this point until the power of PV reached 0.1 per unit again at 25 seconds. The time reference (t_0) turns to 25 seconds. The time reference will be changed again if the power of PV equals to the initial power of 0.1 per unit.

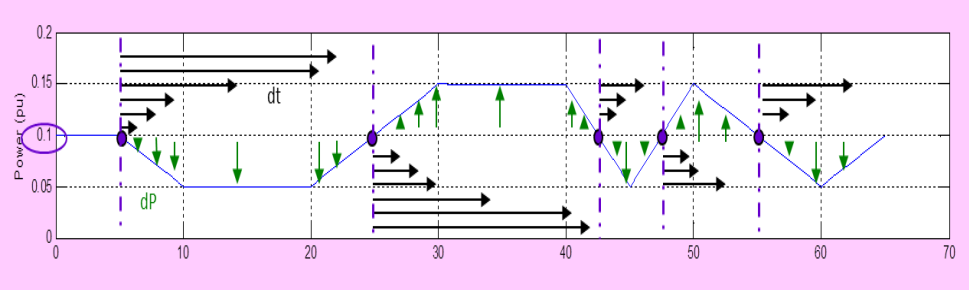

Figure 5.8 Calculation of power deviation of PV

5.3.1.2 Power system with secondary control

The fluctuation of PV power is also separated into 4 situations as illustrated in Figure 5.9. The first and second situations are similar as the previous case without secondary control and time reference is calculated with the same principle. Therefore, the power reference (keeping frequency at its nominal value) changes from P_{ini1} to P_{ini2}. Consequently, at the end of this situation, power reference of PV change to P_{o2} and P_{o3} thanks to an augmentation of brightness for instance. The time reference (t_0) changes when Ppv equals to P_{o2} or P_{o3}.

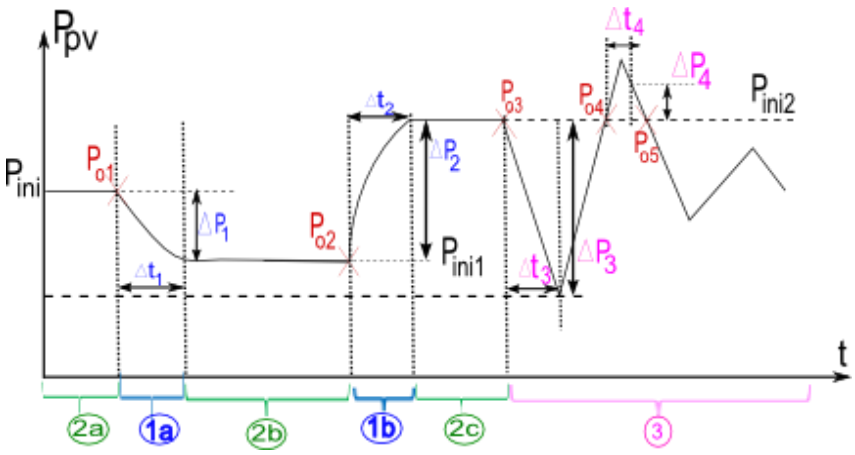

Figure 5.9 Power reference defined

The last case corresponds to fluctuated power of PV. It is quite equivalent to the first situation.

5.3.2 Validation of power management with simulation

The initial simulated system consists of diesel generator with droop frequency control (no secondary frequency control), a constant load and photovoltaic plant (as a disturbance of system frequency). The active power of PV varies with time. Energy storage system is then added to the system. The new control strategy explained above is applied and compared to the classical primary frequency control with droop characteristics. The simulated signal is used to validate the control algorithm. Then, the secondary control is studied according to PV power variation. Finally, a real PV signal measured at PV plant #1 is simulated to validate this control strategy.

5.3.2.1 Results with a simulated signal

Slow fluctuations of PV power in Figure 5.10 (a) are first simulated. The power of PV is constant and decreases continuously from 0.1 per unit at 5 seconds. Then, it is stable for several times at 0.05 per unit. After that, it increases again until reaches 0.15 pu at 30 seconds and is stable again

from this point. The frequency response of initial system (without energy storage) and system with energy storage are compared in Figure 5.10(c). The power of energy storage in Figure 5.10(b) is calculated with the algorithm. The power deviation and the duration of PV power change are calculated and compared to the limitation curve in Figure 5.10(d) and (f). The maximal acceptable frequency variation is fixed to 0.2 Hz.

From Figure 5.10, the system with energy storage is compared to the initial system (without energy storage) in 6 different situations.

Situation a: From t=0 to t=5 seconds, the power of PV is constant at 0.1 per unit. The power difference is null so the power reference of ESS should be 85% of former power reference ($85\%*P_{ES\_ref}(t-t_s)$) (condition 2b). The initial power reference of ESS is zero. Therefore, the power reference of ESS during this time remains to zero. The frequency keeps constant at 50

Situation b: From t=5 seconds, the power of PV decreases continuously from 0.1 pu to 0.05 pu at t=10s. In Figure 5.10 (d), it can be seen that the power difference (ΔP) in blue line is less than the limitation (ΔP limit) in green line from t=5 to t=7 seconds. Consequently, the power of energy storage is still null. Although the frequency decreases from 50 Hz, it is still in acceptable limit (more than 49.8 Hz). At t=7s, the power variation is upper than the limitation, so the power of energy storage is calculated by equation (5.1). We can observe in Figure 5.10 (c) that after 7 seconds the frequency in blue line (without energy storage) is less than 49.8Hz but the frequency in green line is still in acceptable value thanks to the participation of energy storage.

Situation c: From t=10 seconds to t=20 seconds, the PV power is constant at 0.05 per unit. The power of energy storage is continuously decreased while waiting the generator diesel participation to regulate the frequency variation. It can be seen that from 13 seconds, grid frequency of the initial system and the system with energy storage are identical because the power of energy storage is small and the frequency is mostly regulated by diesel generator.

Situation d: From t=20 seconds, the power of PV starts increasing again from 0.05 per unit and reaches 0.1 per unit at t=25 seconds. The power variation during this situation is always less than the limitation so the power of energy storage is still reduced. The frequency is also in acceptable range during this period.

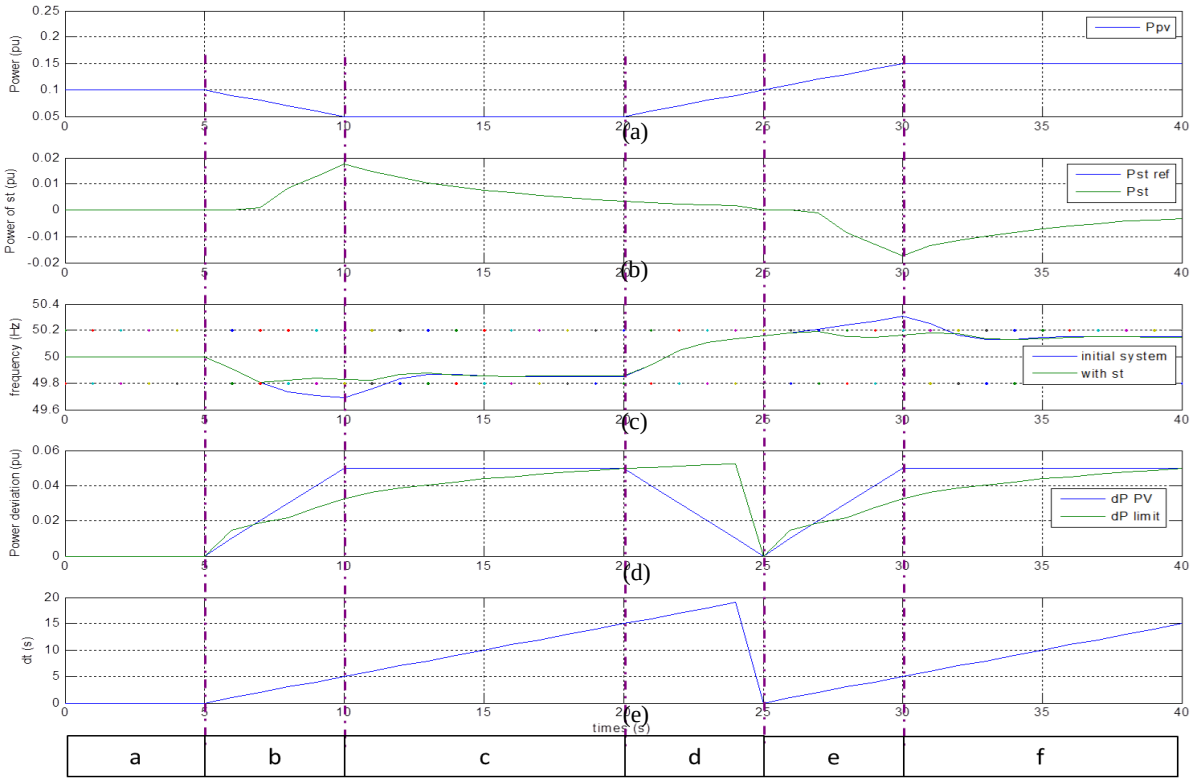

Figure 5.10 (a) Simulated power of PV (slow fluctuation) (b) Power of ESS (c) Frequency response of system without and with ESS (d) Calculated power variation of PV and limitation (e) Calculated duration of change

Situation e: At t=25 seconds, the power of PV is 0.1 per unit so the time reference (t_0) is change to 25 seconds here. This case is the same as the situation b.

Situation f: From t=30 seconds, the power of PV is stable again at 0.15 per unit. This case is the same as the situation c. However, in this case, the power of PV is upper than the initial power. It means that the power of source is more than the power of load. Therefore, the energy storage should absorb power (i.e. is in charging mode) and its power reference is negative.

5.3.2.2 Additional algorithm according to secondary control of diesel for real signal

As in real power system, for which the grid frequency returns to the nominal value with the secondary control; the power reference of PV (P0) has then to be changed along with time. Therefore, the determination of reference power (P0) is analyzed. P0 is defined as the initial power of PV (power of PV at t=0) which is the difference between power initial of diesel generator and load. As a matter of fact, this is the reference power which keeps frequency equal to 50Hz. After simulation, if P_{pv} fluctuates continuously, P0 and t0 will be updated as shown in Figure 5.11(a).

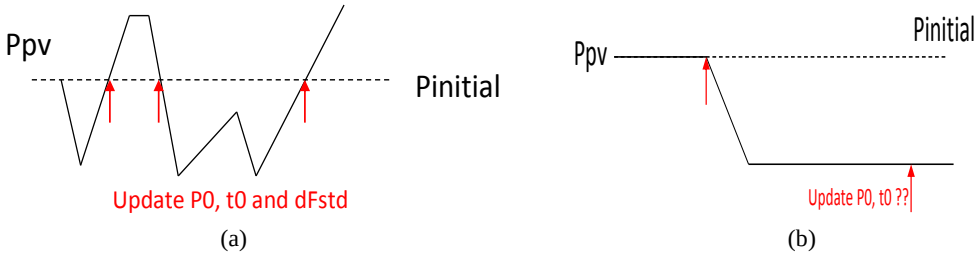

(a) (b)

Figure 5.11 Power PV signal (a) fluctuates continuously (b) decreases and is stable at new values

For only this algorithm of reference point detection, our control strategy works correctly for several minutes according to power variation of PV. For working in longer period, there are other points of view that have to be considered in defining the reference point; such as, the stable of power of PV in long period (more than 10 minutes), and the secondary control of diesel generator. The question is: which power reference (P0) is suitable for the calculation of power deviation (ΔP). If power of PV is stable for several minutes in Figure 5.11(b), the frequency is stable at a steady-state value and the secondary control of diesel generator turns on and allows frequency to come back over 50 Hz. The reference power of PV has to be changed. However, the big problem is when it has to be changed.

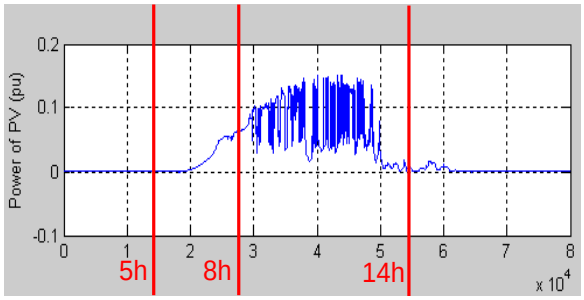

Figure 5.12 Power of PV 26/08/2011

The PV power of PV plant #1 on 26/08/2011 is illustrated in Figure 5.12, which has been separated into 4 periods. From 0 to 5 hours, power of PV remains constant at zero. In this first period, the frequency is stable at 50 Hz if there are no other disturbances in power system. Power is then increases slowly from 5 to 8 hours. In this period, the participation of energy storage is not necessary as the frequency changes slowly. The primary and secondary frequency control of diesel generator will take action in this period. From 8 a.m. to 2 p.m., power continuously fluctuates and presents sometimes stable periods for several minutes. This period may need the participation of energy

storage. Finally after 2 p.m., power of PV decreases slowly and remains stable at zero. Consequences are equivalent as periods 1 and 2.

Concentration has been put merely on the third period (8 to 14 hours) when the power of PV continuously fluctuates. When the power of PV is stable, the secondary control does not work during this period. The power reference is constant at power initial value. The reference time and the maximal frequency deviation are updated when the power equals to the initial power, the participation of energy storage being needless.

From Figure 5.13, it can be observed that the frequency response is improved according to the proposed control strategy; however, some frequencies are out of limit (more than 50.2Hz or less than 49.8Hz). Most of these frequencies occur when the absolute value of power deviation in one second is over 0.01 pu. This problem may be induced by approximation on the definition of power reference (P0) or the inability of the proposed control strategy to detect the fast fluctuations of PV power. According to this study, one of the most influent parameter is the power reference which is used to define the power deviation, and then have a huge impact on the control accuracy as well as on power and energy levels of energy storage.

The secondary control of diesel generator has been studied before adding another algorithm to improve the power reference determination. Finally, a new algorithm is added and completes this first one.

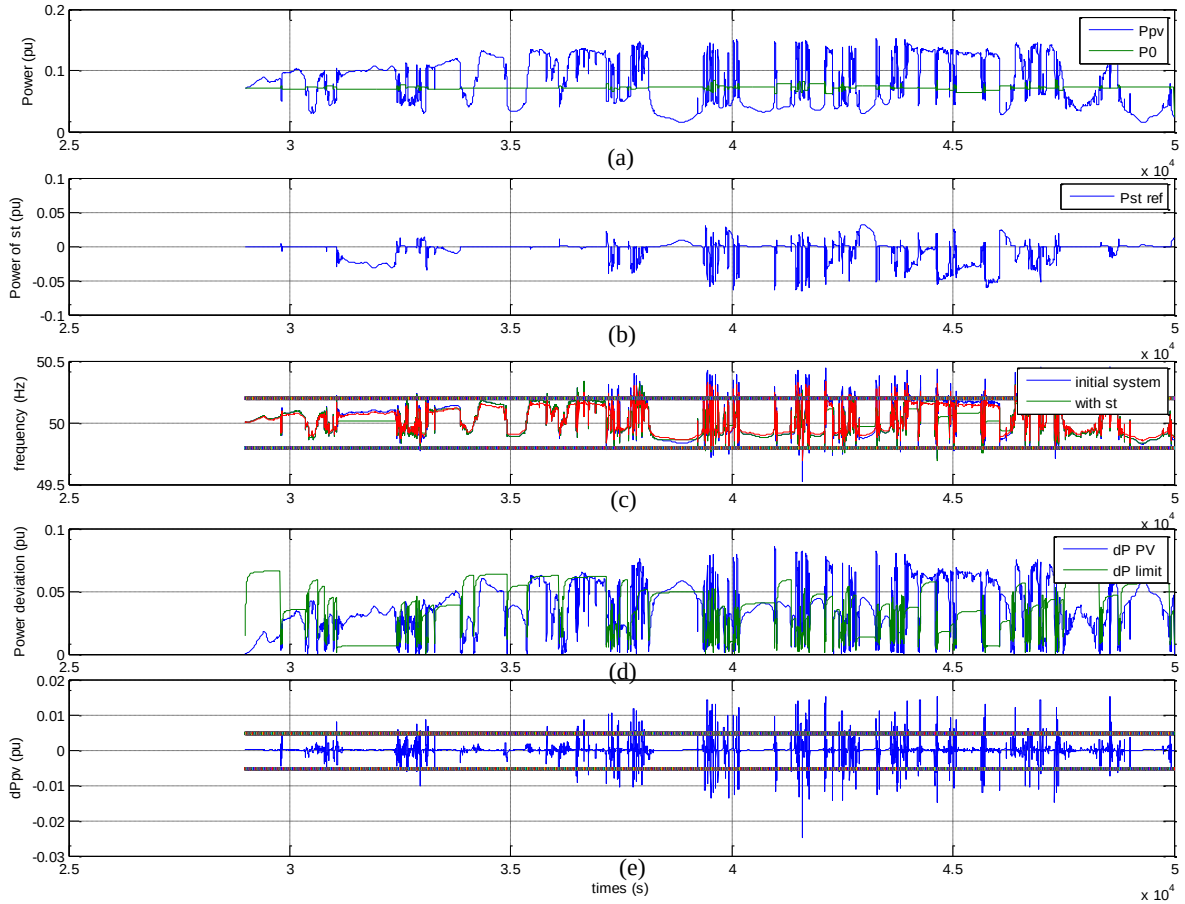

Figure 5.13 (a) Power of PV (b) Power of energy storage (c) Frequency response (d) Power deviation of PV from P0 and limitation (e) Power deviation of one step sampling time

a.) Secondary control study

The reference power of diesel is defined from frequency deviation and PI controller in (1.7). Parameter K_p is linked to the primary frequency control (K_p=1/R; where R denotes the droop value) and K_i defines the secondary control part. The power system that consists of diesel generator and load is simulated to study the secondary control of diesel. The frequency response according to power of

load variation illustrated in Figure 5.14(a) is for different K_i with a droop value of 6%. For the control without secondary control (K_i =0), frequency does not return back to 50Hz. If K_i increases, the time response of secondary control will decrease and the frequency returns to 50Hz faster but frequency response presents some oscillations. The power of diesel generator for K_i equals to 2 and 4, for a droop of 6%, are compared in Figure 5.14(b). Small K_i (large time response of secondary control) causes slower decrease of the primary control power and slower increase of power of secondary control.

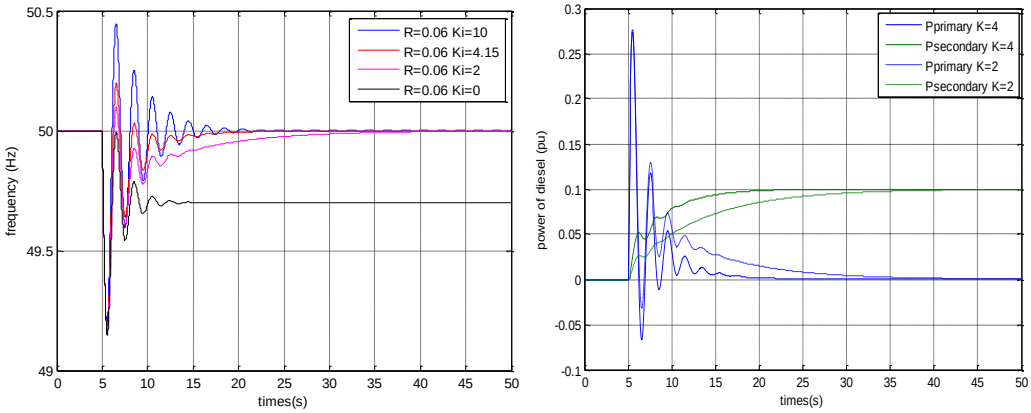

(a) (b)

Figure 5.14 (a) Frequency response (b) power of diesel generator according to increasing of load power with different K_i

The secondary control has an impact on power reference of PV (P0). When the power of PV is stable, the frequency is also stable and the secondary control turns on and brings frequency back to 50 Hz. It means that the initial power for diesel and PV turns to the new point. So the value of power reference has to be changed. The power of PV has to be stable for about 10-15 minutes in order to provide sufficient time for secondary control.

The significant questions are whether the power of PV is stable long enough for secondary control to finish its function, or whether the power reference has to be changed if the secondary control works but has not finished yet its action and when the power reference should be updated. To answer all these questions, real power signals recoded every 5 seconds of PV plant of 250kW at 26/08/2011 are studied. MATLAB facilitates to approximate the power from real power of PV (black point or red line in Figure 5.15) for each 0.1 second or 1 second (each blue line in Figure 5.15) by linear extrapolation. Droop value of diesel is equal to 8% and K_i is equal to 2.

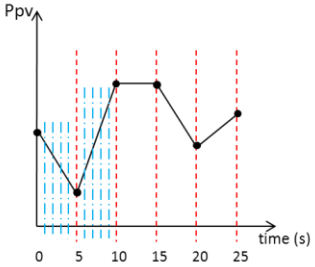

Figure 5.15 Linear extrapolation for power of PV

The power variation for one step time which is calculated by (5.5) corresponds to the difference of power between the blue lines where t_s is the sampling time. In this study, the power deviation (ΔPP) for one sampling time (t_s) is calculated for t_s of 0.1 second and the system frequency is plotted in Figure 5.16.

$$\Delta PP(t) = |P_{pv}(t) - P_{pv}(t-t_s)| \quad (5.5)$$

In Figure 5.16, the secondary control starts working when ΔPP is small. In order to observe the value of small ΔPP, the time period between $3.4x10^4$ to $3.6\ x10^4$ seconds (duration of 2000 seconds) of Figure 5.16 is zoomed and illustrated in Figure 5.17. It can be seen that at time 350 seconds that the

power of PV starts to be stable, the power deviation in one step time is about 0.016kW/0.1second and the secondary control starts working (the frequency turns to 50 Hz). During 350 to 850 seconds, the power of PV is stable and the power deviation is around 0.016kW/0.1second. Then, there are some variations before a new phase of stability at 930 seconds. After that, the power deviation decreases to be below than 0.1kW/0.1second and the secondary control brings the frequency back to 50Hz. It also turns on at 1420 seconds. During 1420 to 1800 seconds, the power deviation is less than 0.14kW/0.1second except that at time 1620 seconds the power deviation is about 0.16kW/0.1second with some frequency variations. However, it is quite small and can be neglected. Therefore, the power deviation for one step, which the secondary control turns on and the initial power (P0) is changed, is less than 0.16kW/0.1second ($1x10^{-4}$ per unit/0.1second or 0.064% of power rated of PV in 0.1 second). It can also be expressed that the secondary control starts working when the power deviation of PV (rate of change of PV power) is 1.6kW per second. If the sampling time is changed, this power ΔPP has to be adapted. For example, if sample time is 5 seconds, the secondary control starts working when ΔPP is less than 8 kW/5seconds ($5x10^{-3}$ per unit/5second or 3.2% of power rated of PV in 5 seconds).

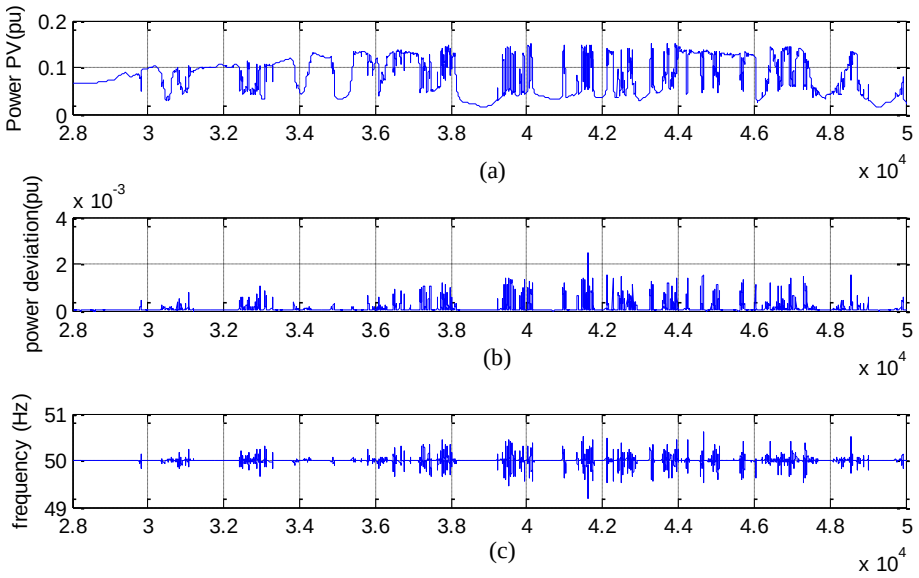

Figure 5.16 (a) Power of PV (b) Power variation for one sampling time (c) Simulated frequency signal between $2.8x10^4$ to 5 $x10^4$ seconds

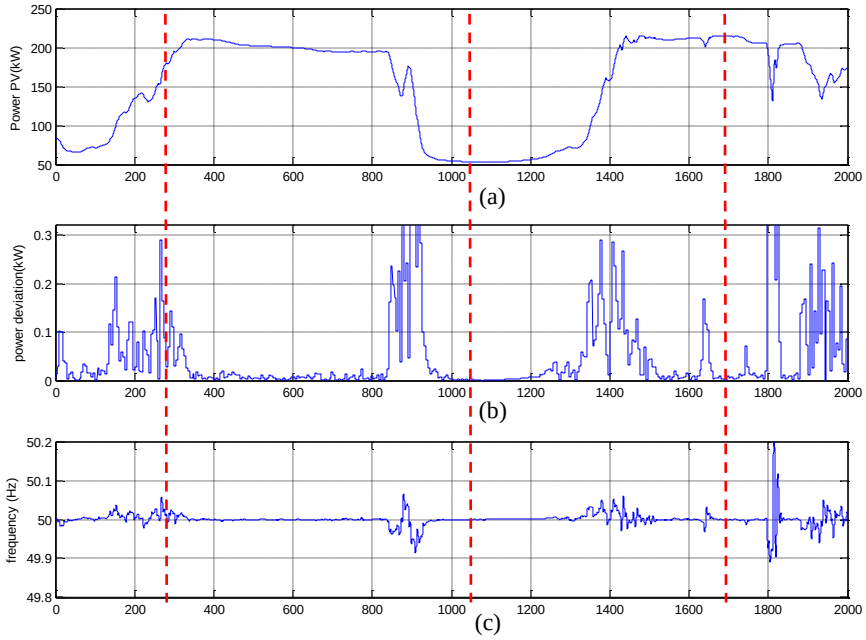

Figure 5.17 (a) Power of PV (b) Power variation for one sampling time (c) Simulated frequency signal during 3.4 $x10^4$seconds to $3.6x10^4$seconds (2000 seconds)

b.) New additional algorithm for power reference determination

The initial power of PV (P_0) has been decided to change when the frequency is stable at 50 Hz or closed to 50 Hz. The frequency turns to 50 Hz by the secondary control of diesel generator. Therefore, the reference power P0 is related to the secondary control. In the previous study, information of power variation ΔPP which causes starting of secondary control have been searched out. Therefore, in the definition of P0, the maximal power variation (dP_steady) has to be fixed. If ΔPP is less than dP_steady, the power of PV is set to be stable. Well, the period (t_steady) at which power is stable (ΔPP<dP_steady) has to be carefully defined. The initial power P0 is changed when ΔPP<dP_steady is upper than t_steady. This period should not be too long, because the energy storage should decrease its power as soon as the secondary control begins. P0 is changed in order to set power variation (ΔP=Ppv-P0) at zero and ΔP is in acceptable limit.

The parameters dP_steady and t_steady are then varied and the system with PV for one day is simulated. The system frequency is analyzed, followed by studies on the impact of the parameters of frequency control of diesel (droop, K_i) on dP_steady and t_steady is studied. Finally, parameters dP_steady and t_steady are validated for other PV signals.

i. Simulation 1 : Variation of dP_steady for fixed t_steady at 5 seconds

The power system that consists of diesel generator (with primary and secondary control), load (power constant), PV, and energy storage system is simulated in MATLAB – Simulink. The control power of energy storage system has different parameter dP_steady (use to define P0) and the period t_steady is fixed at 5 seconds. The period t_steady is selected at 5 seconds because the ESS should start to reduce its power as soon as possible when the secondary control starts working. It should not be too small in order to give enough time for detecting a stability of PV power.

The number of occurrences of frequency deviation which are more than 0.2 Hz of frequency of the system without ESS is 192. When dP_steady is larger than $2x10^{-3}$, power reference (P0) always changes (P0 equals to Ppv). Energy storage system does not participate to regulate frequency at all because power deviation ΔP is always zero. For dP_steady from $1x10^{-3}$ to $2x10^{-3}$, ESS participates sometimes but frequency is not in the acceptable limit. Energy storage system brings frequency back to the acceptable limit range (49.8-50.2Hz) when dP_steady is less than $1x10^{-3}$.

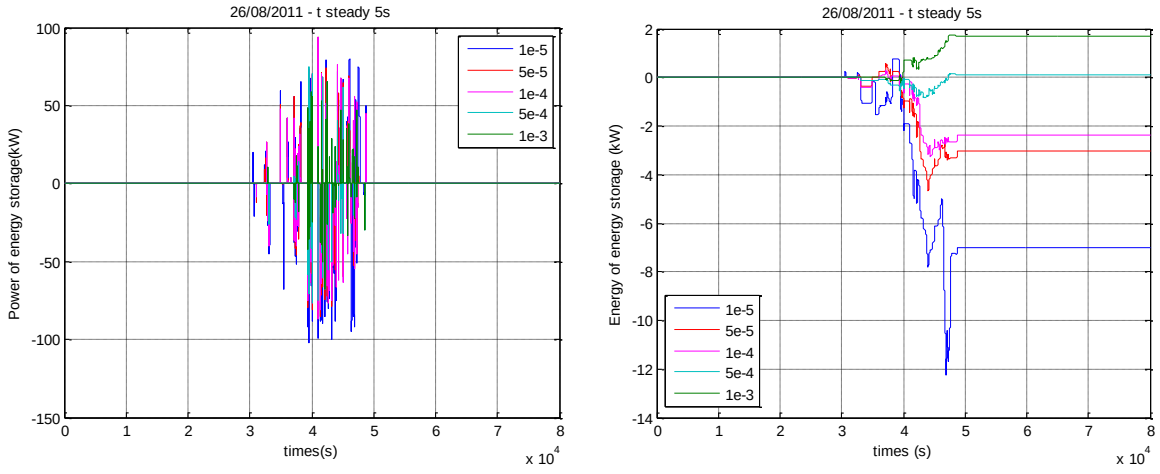

(a) (b)

Figure 5.18 (a) Power of energy storage (b) energy of energy storage for different dP_steady and t_steady 5 seconds

Power and energy of energy storage and diesel are calculated in this section. The energy storage device often participates to regulate frequency when the dP_steady decreases as shown in Figure 5.18(a). In Figure 5.18(b), stored energy of energy storage is negative for dP_steady equal to

$1x10^{-4}$, $5x10^{-5}$ and $1x10^{-5}$. It means that energy storage is mostly in a discharging mode. For dP_steady equal to $5x10^{-4}$and $1x10^{-3}$, the stored energy is upper than the initial state so energy storage is mostly in a charging mode. The minimal value of energy used occurs when dP_steady is of $5x10^{-4}$. Furthermore, the maximal power of primary power of diesel is reduced by energy storage in Figure 5.19. The maximal of primary power is minimal at dP_steady $5x10^{-4}$. The maximal power of primary power of $1x10^{-5}$ is larger than the others. Energy used of primary control of diesel is not quite different between the system with and without energy storage. The minimum energy used is obtained at dP_steady $5x10^{-5}$.

If dP_steady $5x10^{-4}$ is selected, the energy of energy storage is seldom used but it does not have any profound impacts on energy used of the primary control of diesel comparing to the situation without energy storage system. On the other hand, energy storage is too often used and energy used of primary control of diesel is reduced at dP_steady $5x10^{-5}$. Therefore, the selection of dP_steady will depend on the preference between, the minimum use of energy storage and the reduction of energy used for primary control of diesel. A dP_steady at $5x10^{-4}$ has been selected (to minimize energy used of energy storage with improve frequency performance) with a varying t_steady in the next section. However, this parameter has to be adapted if the parameter of frequency control of diesel changes.

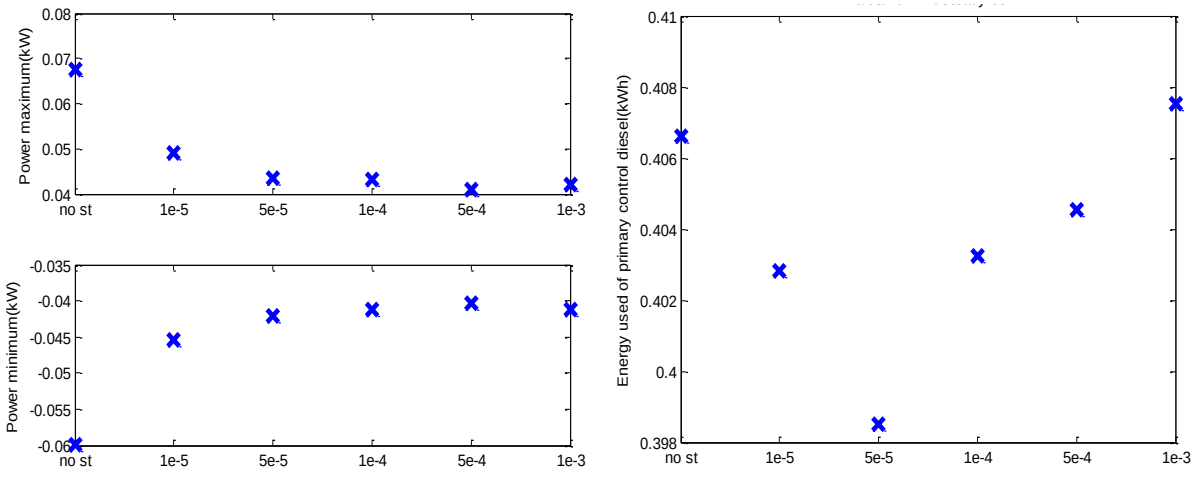

(a) (b)

Figure 5.19 (a) Maximal and minimal powers (b) useful energy of primary control of diesel for different dP_steady and t_steady of 5 seconds

ii. Simulation 2 : Varying of t_steady for dP_steady fixed to $5x10^{-4}$

In this simulation, the t_steady period is modified. Frequency is always in acceptable limit if t_steady is less than 60 seconds. When t_steady increases, energy storage participates less. Energy storage is more in discharge for t_steady of 30 and 60 seconds. It means that energy storage participates less to frequency control but it is in service for a long period. When t_steady increases or dP_steady decreases, the initial power (P0) does not often change. Therefore, energy storage should inject/absorb more energy. If the power deviation is still in the problem zone, it will be in this zone for a long time before P0 changes and power variation (ΔP) turns to zero.

Energy used of energy storage is minimal at t_steady equal to 5 seconds. Energy storage also reduces the maximal power of primary power of diesel. However, it does not have many impacts on energy used of primary control of diesel. Energy used for primary control is the smallest at t_steady 60s. The selected parameters are dP_steady $5x10^{-4}$ and t_steady 5 seconds. These parameters will also be validated with different PV signals.

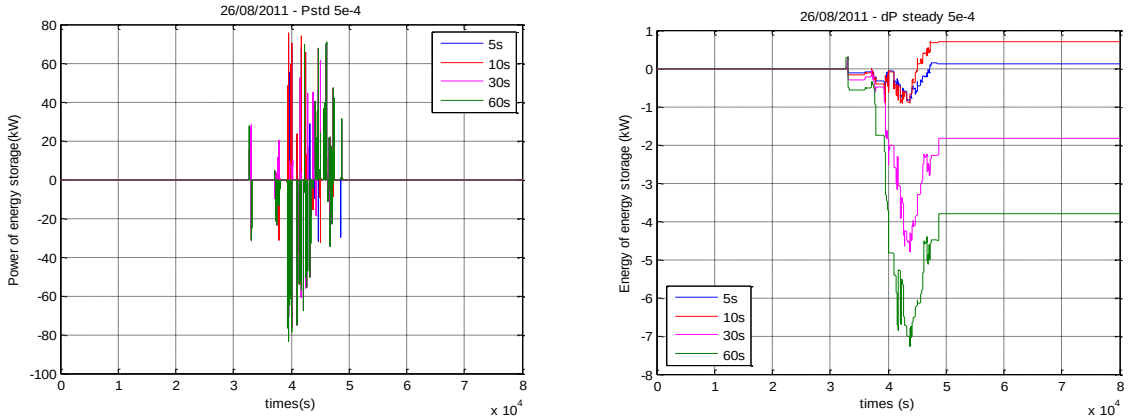

(a) (b)

Figure 5.20 (a) Power of ESS (b) energy of ESS for different t_steady and dP_steady $5x10^{-4}$

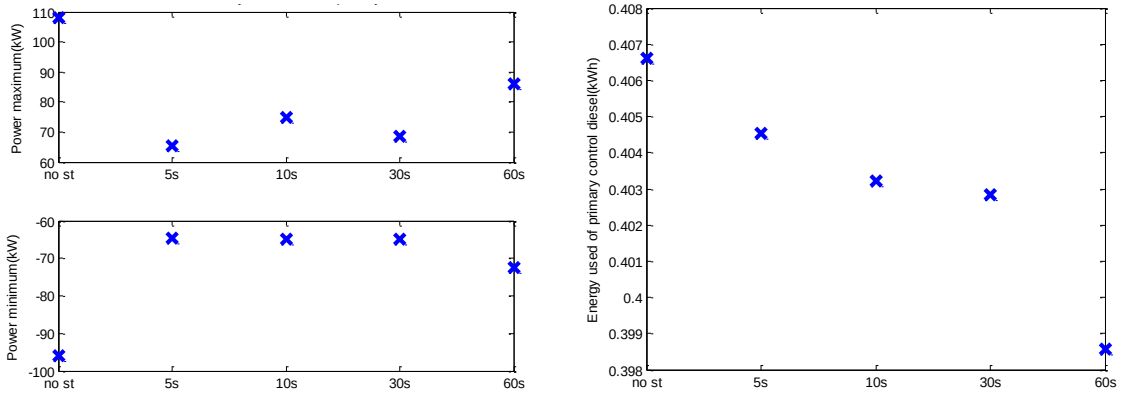

(a) (b)

Figure 5.21 (a) Minimal and maximal powers (b) energy used of primary control of diesel for different t_steady and dP_steady $5x10^{-4}$

iii. Simulation 3 : Varying parameter of frequency control for diesel

As having mentioned earlier, these two parameters: dP_steady and t_steady which have been used to define power reference (P0) are affected by the parameters of frequency control of diesel. When the droop value decreases, participation of diesel in primary frequency control increases. Frequency deviation is then reduced. Therefore, the frequency deviation will be small (or almost in acceptable range) if droop value of diesel is small. For the studied power system, if the droop value is smaller than 6%, there is no frequency problem.

For parameter K_i of the secondary control, time response of secondary control decreases when K_i increase. Diesel generator will then participate faster to the secondary control. Therefore, power and energy of diesel generator to regulate frequency is increased. The frequency deviation is decreased when K_i increases (time response reduces). Parameter dP_steady $5x10^{-4}$ and t_steady at 5 seconds can guarantee to maintain the frequency deviation at less than 0.2 Hz for K_i more than 2. If K_i decrease, these two parameters have to be modified to make frequency deviation within the acceptable limit. When K_i increases, energy storage has to participate more continuously for a long time. Therefore, dP_steady should be decreased while t_steady should be increased to cause less change on power reference. For example, if K_i is 1, dP_steady should be $1x10^{-6}$ and t_steady of 60 seconds to reduce frequency deviation according to power variation of PV.

c.) Validation of the complete control strategy with real PV power signal

The defined and complete algorithm is simulated with different real PV signals (with dP_steady and t_steady equal to $5x10^{-4}$ and 5 s respectively). The PV signals of PV plant #1 for all 3 months are simulated. Frequency is always in acceptable limit except in 20/10/2011 using the strategy with limitation diagram.

Six illustrations of power variation from more to less fluctuated signals, which are classified by their FHC in high frequency (see 2.4.3), are illustrated in Figure 5.22 (a) to (f) respectively. Frequency response of the initial system (without energy storage) according to fluctuated signal (20/10/2011, 26/08/2011, and 27/08/2011) (Figure 5.22 (a) to (c)) are out of limits and presented in Table 5.1. Small power variations on 11/09/2011, 31/08/2011 and 27/08/2011 have not caused any large frequency variations. The frequency of the initial system (with no energy storage) is always in the acceptable limit. Therefore, participation of energy storage is not needed in this situation of fluctuation. However, energy storage may seldom participate on 11/09/2011 because the minimum frequency is increased (frequency deviation from 50Hz decreases) as shown in Table 5.1.

System frequency according to all power fluctuation signals is always in the acceptable limits using our strategy with ΔPpv limitation except on 20/10/2011. However, the frequency response of system with energy storage, using this strategy, has evaluated out of limits twice, which it is not so far away from the acceptable range.

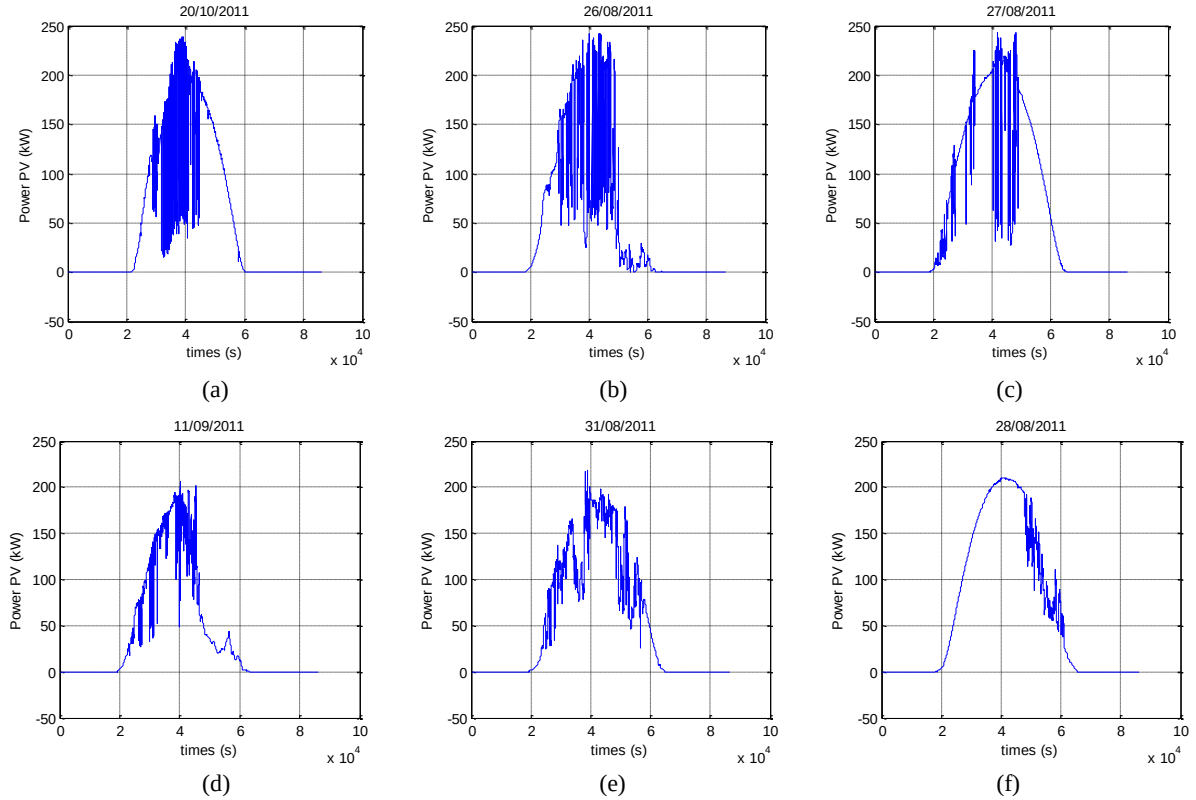

Figure 5.22 Power of PV signal (a) 20/10/2011 (b) 26/08/2011 (c) 27/08/2011 (d) 11/09/2011 (e) 31/08/2011 (f) 28/08/2011

Table 5.1: Frequency response analysis of system initial and system with ESS for six different PV signal

PV power signal	FHC in high frequency region (kW)	Initial system (without ESS)			System with ESS using limitation strategy		
		Number of occurrences with frequency out of limits	f_{max} (Hz)	f_{min} (Hz)	Number of occurrences with frequency out of limits	f_{max} (Hz)	f_{min} (Hz)
20/10/2011	18.4	1480	50.33	49.73	2	50.18	49.797
26/08/2011	12.5	208	50.24	49.73	0	50.16	49.84
27/08/2011	11.9	610	50.33	49.65	0	50.18	49.81
11/09/2011	4.35	0	50.09	49.865	0	50.09	49.873
31/08/2011	2.88	0	50.04	49.95	0	50.04	49.95
28/08/2011	0.975	0	50.02	49.98	0	50.02	49.98

Frequency response and power of energy storage in time domain of the most fluctuated signal (20/10/2011) are presented in Figure 5.23. Frequency variation of the initial system (without energy storage) is larger than frequency deviation of system with energy storage which is controlled by

limitation strategy in Figure 5.23(a). Energy storage helps mostly to keep frequency within the acceptable limit. Power of energy storage, as illustrated in Figure 5.23 (b), is quite large.

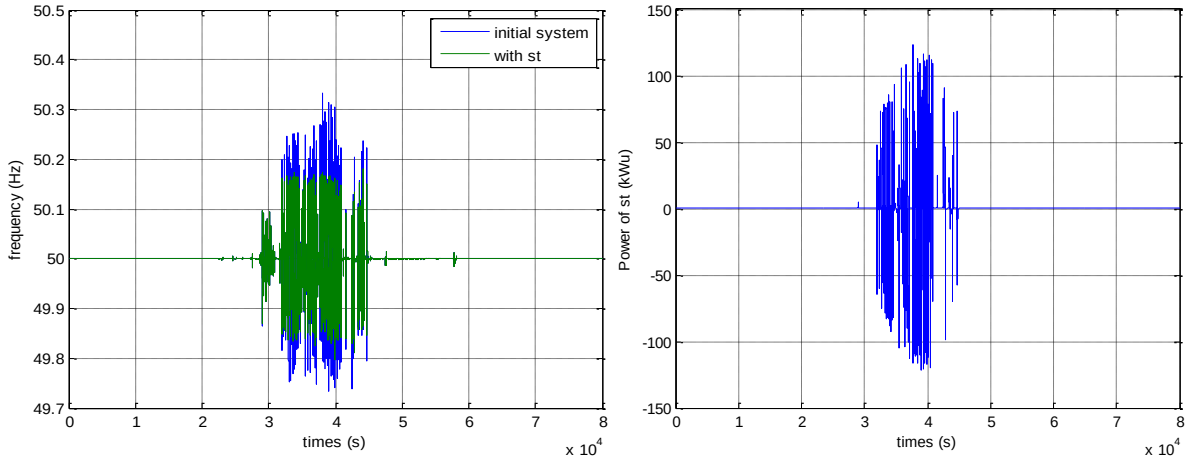

(a) (b)

Figure 5.23 Impact of our strategy on : (a) the frequency response (b) the power delivered by energy storage for power signal on 20/10/2011

5.3.3 Robustness analysis

Strategy with limitation diagram is approved with a lot of real PV power signals. However, performance of this strategy depends on the accuracy of limitation ΔP diagram, time of detection of deviation of energy storage, accuracy of measured PV power and accuracy of PV power reference (P0) determination.

5.3.3.1 Impact of limitation diagram

The limitation of power deviation (ΔPpv) and duration of change (Δt) are fixed by parameters which are supposed to be well-known, such as frequency deviation limitation and droop value of diesel generator, and approximate parameters, such as equivalent inertia, load damping constant and time response of diesel generator. In this study, each parameter is varied about ±50% and the limitation curves are plotted in Figure 5.24. Figure 5.24 (a) and (b) show that the known parameters (maximal frequency deviation and droop value of diesel generator) have a large impact on limitation curve. In the contrary, the approximate parameters have less impacts on limitation curve as shown in Figure 5.25 (c), (d), and (e).

5.3.3.2 Impact of error on PV measured power

Power reference calculation of energy storage is dependent to the PV measured power. An error between ±0-20 % is then added to the measured power of PV; the number of occurrence where frequency deviation is more than 0.2 Hz is then analyzed. Positive errors cause small impact on frequency because the power of energy storage is over estimated, so that frequency remains in acceptable limit. On the other hand, negative error causes large effect on frequency because the power of energy storage is under estimated in this case. With real PV power signals measured on 20/10/2011 which is the most fluctuated signal during three months, frequency is out of limit when error of measurement is more than 10%.

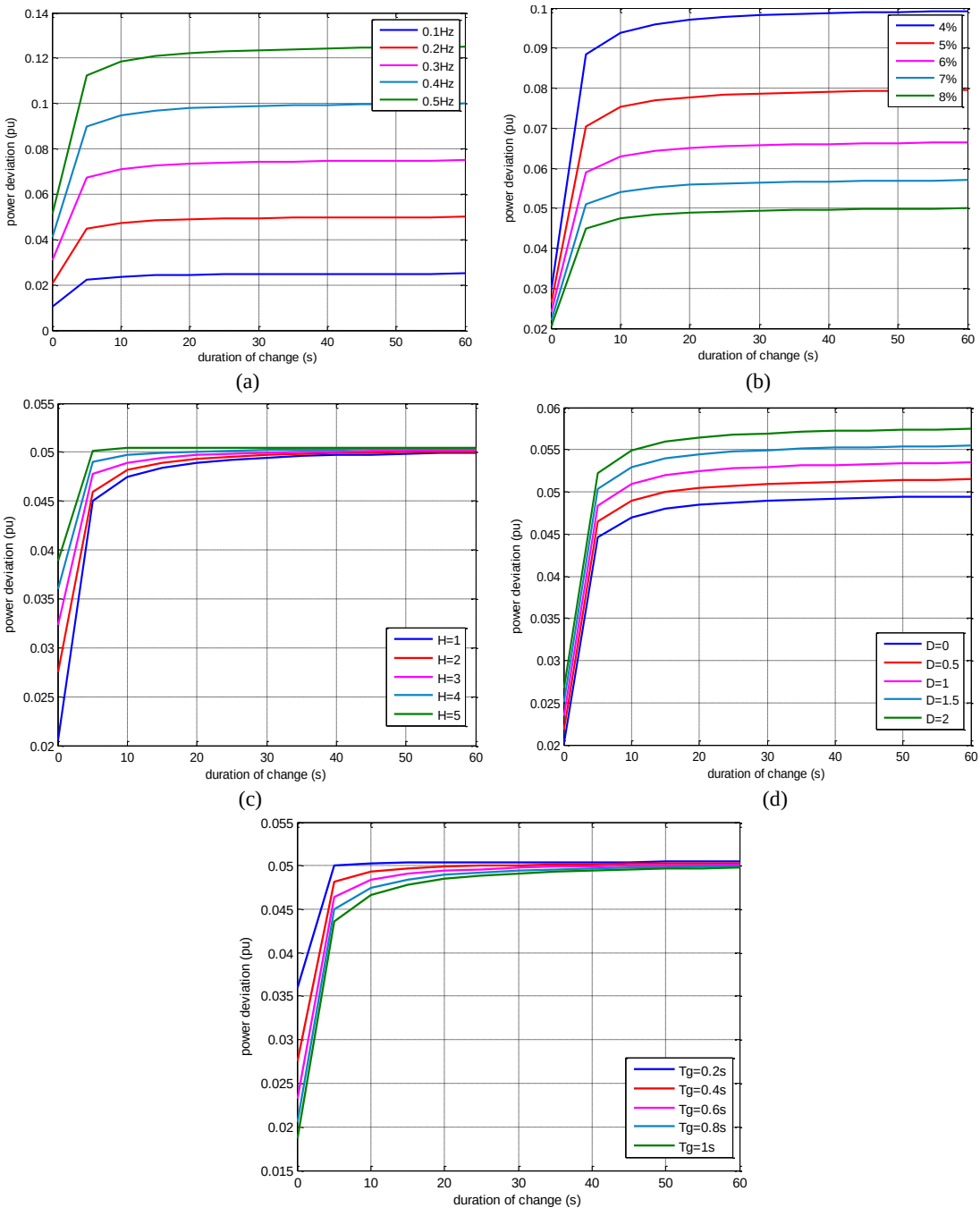

Figure 5.24 Limitations ΔPpv diagram with different (a) Maximal value of frequency deviation (b) Droop value of diesel generator (c) Equivalent inertia (d) Load damping constant (e) Time response of diesel generator

5.3.3.3 Impact of time for decision according to participation of energy storage

In our control strategy, 3 time parameters are used: the sampling time of measured PV power (denoted Ts_pv), time to take decision for participation of energy storage power (denoted Ts_st) and step time simulation (denoted Ts). Generally, time to take decision for energy storage participation has to be at least upper than the sampling time of measurement (Ts_st $\geq$ Ts_pv), because the reference of energy storage is defined from the PV power.

Time to take decision of 1 and 5 seconds is compared while sampling time of measured PV power of 0.1 second. Number of occurrences where frequency is out of limits increases when time to take decision of power of energy storage grows up but it is still smaller than number of occurrences of the initial system (without energy storage) as shown in Table 5.2. Time to take decision of power of energy storage every 5 seconds is too long. The problem will be detected too late. Frequency deviation is already over 0.2 Hz when the problem is detected (power deviation is over limitation diagram).

However, for larger system PV and larger power system, power fluctuation is more slowly so time to take decision of energy storage can be longer.

Table 5.2: Results of simulation with different time to take decision of power of ESS for PV power 20/10/2011

Number of occurrence dF > 0.2 Hz		f_{max} (Hz)	f_{min} (Hz)
For system without ESS	1480	50.33	49.73
For system Ts_st = 0.1s	2	50.18	49.797
For system Ts_st = 1s	86	50.23	49.76
For system Ts_st = 5s	1328	50.33	49.63

5.3.4 Strategy with limit power deviation diagram conclusion

This control strategy with limitation diagram can bring frequency to the acceptable limit with dP_steady of $5x10^{-4}$ and t_steady of 5 seconds for a rated power of diesel generator of 1.6MW, 2MVA. This strategy uses more power of energy storage compare to droop strategy. However, this strategy can save the use of energy storage for less fluctuation signals. This strategy will be compared to other strategies later. From robustness analysis, a good predication of parameters and an accurate measurement of PV power are needed in order to anticipate appropriated strategy.

5.4 Filtering strategy

According to the previous study of transfer function between frequency deviation and PV power deviation in Chapter 3, the frequency of PV signal fluctuation can be separated into 3 zones for low (<0.016Hz), medium (0.016-1.6Hz) and high frequencies (>1.6Hz). The secondary control of diesel generator takes action against power fluctuations in low frequency region; fluctuations in high frequencies are filtered by equivalent inertia of power system. The energy storage then assists diesel generator for primary frequency control. In this study, energy storage is also used for the same purpose. A new strategy based on filtering of PV profile is then proposed below.

5.4.1 Description of filtering approach

Various filter types (high pass, low pass, and band pass filters) are used on power variations (for load and PV) to define power of diesel and/or energy storage for their participation in frequency control. Four different filtering strategies are then proposed:

1. **Filter strategy #1:** Diesel with a low pass filter, Energy storage with a high pass filter. This strategy limits action of diesel generator to secondary control (i.e. low frequency region). Therefore, a low pass filter is applied. The energy storage device takes action for high frequency fluctuations (medium and high frequency region).
2. **Filter strategy #2:** Diesel with classical frequency control (primary and secondary controls), Energy storage with a high pass filter. Frequency control of diesel generator is classical in order to implement a feedback loop on frequency control. The energy storage assists diesel generator in primary frequency control by using high pass filter.
3. **Filter strategy #3:** Diesel with classical frequency control, Energy storage with a band pass filter. Band pass filter is used to replace the high pass filter of filter strategy #2. This filter limits energy storage action to medium frequencies. High frequency variations are filtered by equivalent inertia.
4. **Filter strategy #4:** Diesel with a low pass filter, Energy storage with a primary droop control. This strategy is the inverse of filter strategy #2. This strategy makes energy storage the main source of primary frequency control and limit diesel power to participate only to the secondary control.

These different filter strategies are analyzed and compared to system without energy storage in frequency domain, using Bode diagrams. Then, these strategies are simulated in time domain using MATLAB-Simulink.

5.4.2 Analysis filter strategy in frequency domain

The frequency response of the islanding grid is presented in Figure 5.1(b). The disturbance is the variation of both PV power and load power, which corresponds to the power deviation (ΔP_{diff}) in (5.6). In this study, power of charge is assumed to be constant so that the dominant power deviation ΔP_{diff} is the PV power variation (ΔP_{pv}). The low pass filter for diesel is modeled in (5.7) as illustrated in Figure 5.25(a). Moreover, the band pass and high pass filters for energy storage are defined in (5.8) and (5.9) respectively. Transfers function between frequency deviation (Δf) and power deviation (ΔP_{diff}) including filter strategies of energy storage are then analyzed.

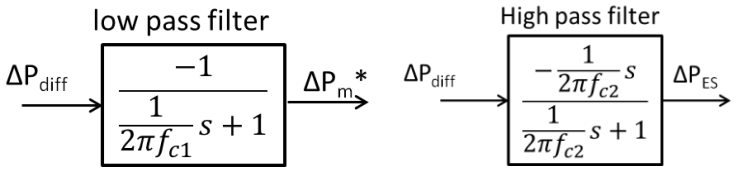

(a) (b)

Figure 5.25 (a) Low pass filter (b) High pass filter

$$\Delta P_{diff} = \Delta P_{pv} - \Delta P_{ch} \tag{5.6}$$

$$\frac{\Delta P_m^*}{\Delta P_{diff}} = \frac{-1}{\frac{1}{2\pi f_{c1}}s+1}; \frac{1}{2\pi f_{c1}} = \tau_1 \tag{5.7}$$

$$\frac{\Delta P_{ES}}{\Delta P_{diff}} = \frac{-\frac{1}{2\pi f_{c2}}s}{(\frac{1}{2\pi f_{c1}}s+1)(\frac{1}{2\pi f_{c2}}s+1)} \tag{5.8}$$

$$\frac{\Delta P_{ES}}{\Delta P_{diff}} = \frac{-\frac{1}{2\pi f_{c2}}s}{\frac{1}{2\pi f_{c2}}s+1}; \frac{1}{2\pi f_{c2}} = \tau_2 \tag{5.9}$$

5.4.2.1 Filter strategy #1

In this strategy, diesel generator takes action in low frequency region and energy storage participates in high frequency region. Transfer function between frequency deviation and power variation with energy storage is shown in (5.10). It can be seen that, if damping load constant (D) is zero, the frequency presents a steady-state error (it does not return to 50Hz). For instance, cut-off frequency of low pass and high pass filter is selected to be equivalent at 0.025Hz. Magnitude of Bode diagram is plotted for D equal to 0 and 1 in Figure 5.26. Magnitude of Bode diagram in Figure 5.26(a) is equivalent to system without secondary control and without filtering at low frequency. The steady-state error is not null. On the other hand, the low frequency region is filtered by load in Figure 5.26(b) if damping load constant (D) is not null. That means system frequency with this filter strategy does not return to 50Hz if damping load constant is null. System needs at least a closed-loop of the measured frequency, either with droop or damping load constant (or both droop and damping load constant).

This filter strategy, which does not return measured frequency in control loop (open loop system of frequency and power deviation), must be applied to power system with non-zero damping load constant. Although damping load constant is selected at zero in most articles, because it is the most critical problem against frequency, this parameter is different of 0 in real power system. For example, the islanding power system "Les Saints", has a damping load constant equal to 0.12. Therefore, for all following simulations, the damping load constant (D) will be taken at 0.12.

$$\frac{\Delta f}{\Delta P_{diff}} = \frac{\tau_1 t_g s^2 + (\tau_1 + t_g - \tau_2)s}{(2Hs+D)(\tau_1 s+1)(t_g s+1)} \cdot \frac{1}{(\tau_2 s+1)} \tag{5.10}$$

$$\tau_1 = \tau_2 = 1/(2 * \mathrm{pi} * 0,025) \tag{5.11}$$

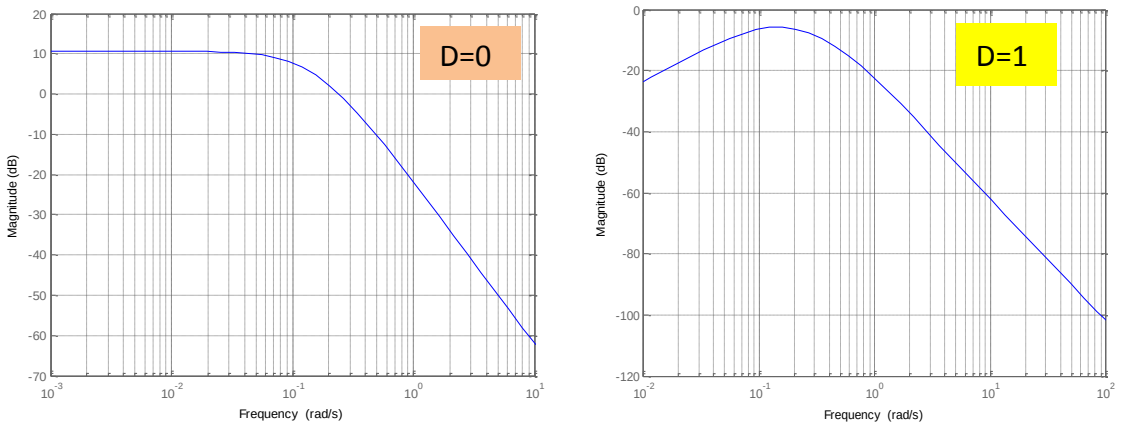

(a) (b)

Figure 5.26 Magnitude of transfer function between frequency variation and power variation of filter strategy #1 (a) load damping constant is zero (b) load damping constant is one

The cut-off frequency of the two filters is varied. In the reference case, active zones of diesel and energy storage are separated independently (cut-off frequencies are equivalent to 0.025Hz or 0.16 rad/s). Next, the cut-off frequency of low pass filter (fc1) is increased and causes a larger action region of diesel generator (it participates more in medium frequency). It means that medium frequency region is assumed by diesel and energy storage. Finally, action region of energy storage is increased to some low frequency region by reducing cut-off frequency of high pass filter (fc2). Magnitude of Bode diagrams for different cut-off frequencies is plotted in Figure 5.27.

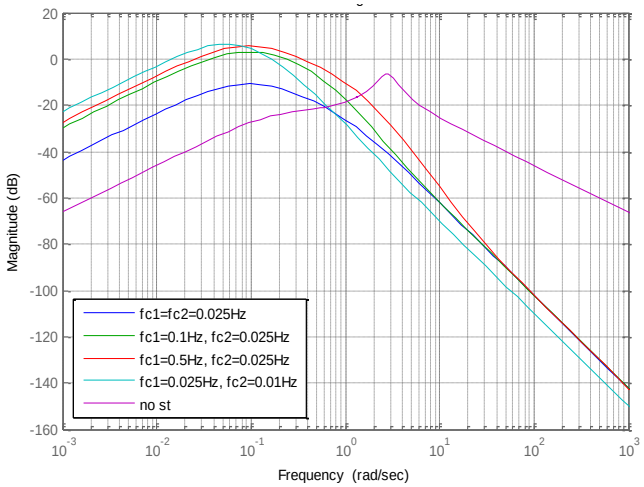

Figure 5.27 Magnitude of transfer function between frequency variation and power variation of filter strategy 1 with different cut-off frequencies

If cut-off frequency of low pass filter (fc1) is increased, the magnitude of df/dP in low and medium frequency will increase as shown in Figure 5.27. Therefore, the frequency deviation is larger for the same power deviation. When the cut-off frequency of high pass filter (fc2) is reduced, the magnitude of df/dP in high frequency region decreases. From these results, the cut-off frequencies of the two filters should be equivalents.

Equivalent cut-off frequency of two filters is then varied from 0.025Hz to 0.001Hz as illustrated in Figure 5.28. The magnitude of transfer function decreases in medium frequency region when cut-off frequency reduces. The frequency deviation in medium frequency fluctuation is improved according to system without energy storage. So that the cut-off frequency of two filters should be equivalent to a low value in order to enlarge the working band-width of frequencies for energy storage.

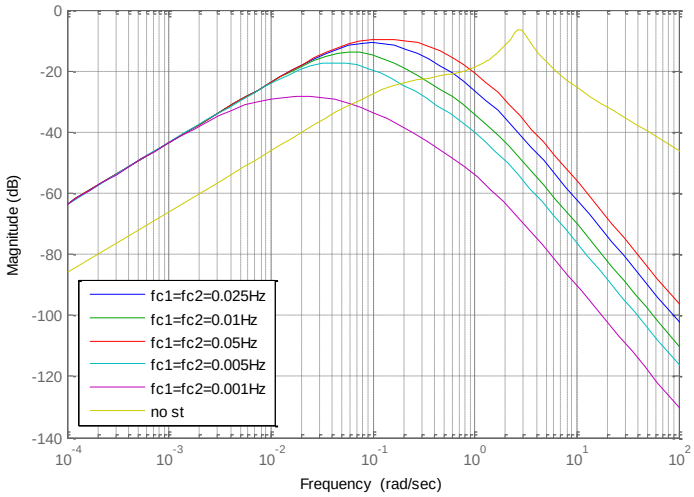

Figure 5.28 Magnitude of transfer function between frequency variation and power variation of filter strategy #1 with different cut-off frequency

The frequency deviation by the fluctuation of PV in some medium and low frequency regions of this filter strategy (all cut-off frequency) is higher than frequency deviation of system without energy storage for the same amplitude of power variation because this filter strategy does not return measured frequency value. This strategy can cause more frequency variation than system without energy storage if cut-off frequencies are not well defined.

5.4.2.2 Filter strategy #2

For this case, the energy storage system takes action in high frequency region and diesel is controlled by classical frequency control (with primary and secondary controls). The transfer function is given in (5.12). So that this strategy does not have steady-state error although damping load constant is zero. The cut-off frequency of high pass filter for energy storage system is then varied. The magnitude of Bode diagram is illustrated in Figure 5.29.

$$\frac{\Delta f}{\Delta P_{diff}} = \frac{t_g s+1}{(2Ht_g)s^3+(2H+t_g D)s^2+(K_p+D)s+K_i} \cdot \frac{1}{(\tau_2 . s+1)} \tag{5.12}$$

When the cut-off frequency of high pass filter is risen up, energy storage system will participate less in medium frequency so that the frequency deviation in this frequency region is larger for the same amplitude of power variation. The fluctuation in high frequency region is more filtered with energy storage, which can be interpreted that energy storage is coordinated with equivalent inertia of system to regulate frequency. However, there is no variation of PV power in high frequency, upper then 1 Hz (cf. chapter 2).

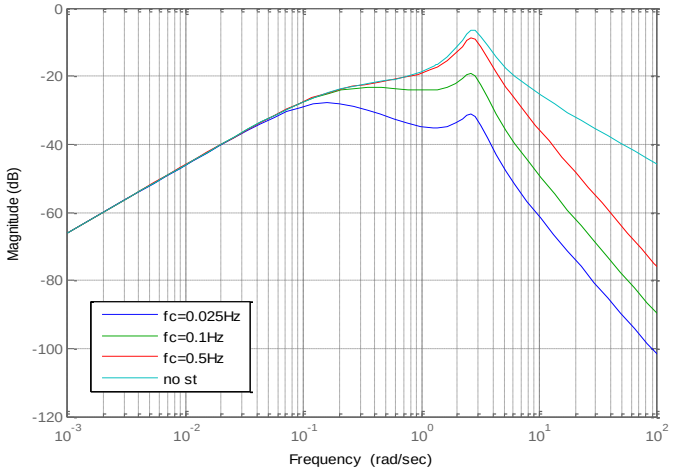

Figure 5.29 Magnitude of transfer function between frequency variation and power variation of filter strategy #2 with different cut-off frequency

5.4.2.3 Filter strategy #3

This filter strategy is quite similar to filter strategy #2 except that energy storage is limited to work in the medium frequency zone. There is no coordination with equivalent inertia to filter fluctuations in high frequency. The band-pass filter is illustrated in Figure 5.30. The cut-off frequency at high frequency (fc1) is for low pass filter and cut-off frequency at low frequency (fc2) is for high pass filter. Transfer function in (5.13) show that there is no steady-state error. Furthermore, Bode diagram of this transfer function (for fc1=1.2Hz, fc2=0.025Hz) is plotted in Figure 5.31, comparing to system without energy storage. The magnitude of df/dP is equivalent for system with and without energy storage in low and high frequency regions. Magnitude of df/dP of system with energy storage is the lowest at frequency around 1.1 rad/s (0.21 Hz) that is approximately around the frequency at the maximal gain (wo = $\sqrt{1/\tau_1.\tau_2}$) of band pass filter (0.99 rad/s).

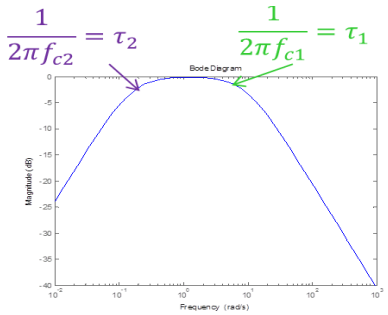

Figure 5.30 Band pass filter

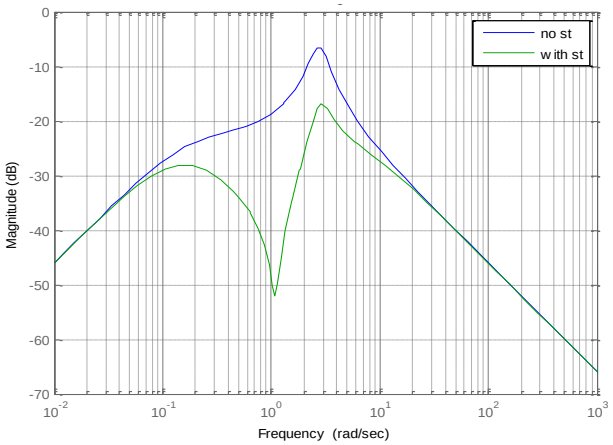

Figure 5.31 Magnitude of transfer function between frequency variation and power variation of filter strategy #3

$$\frac{\Delta f}{\Delta P_{diff}} = \frac{t_g s+1}{(2Ht_g)s^3+(2H+t_g D)s^2+(K_p+D)s+K_i} \cdot \frac{\tau_1.\tau_2 s^2+\tau_1 s+1}{(\tau_2.s+1)(\tau_1.s+1)} \quad (5.13)$$

From the Hurwitz criterion and equation (5.12) and (5.13), the system is stable if summation of K_p and D is strictly greater than 0 (K_p+D>0). Therefore, the droop value and the load damping constant cannot be null at the same time.

5.4.2.4 Filter strategy #4

The control system of diesel and energy storage is taken turns. The low pass filter is applied for diesel generator to participate only to the secondary control. Classical primary frequency control (with droop value) is applied to energy storage. This makes the system to be a closed loop system without any steady-state error. The cut-off frequency of low pass filter for diesel is varied (droop for storage is equal to 6%) and magnitude df/dP is plotted in Figure 5.32. When the cut-off frequency increases (i.e. diesel participates more), the magnitude of transfer function is more filtered in low and medium frequency regions but it is not affected in high frequency regions. Then, magnitude of df/dP is equivalent for system with and without energy storage and for all cut-off frequencies because this frequency region is regulated by equivalent inertia of system.

$$\frac{\Delta f}{\Delta P_{diff}} = \frac{1}{2H.s+(D+K_{p_{st}})} \cdot \frac{\tau_1 t_g s^2+(\tau_1+t_g)s}{(t_g.s+1)(\tau_1.s+1)} \quad (5.14)$$

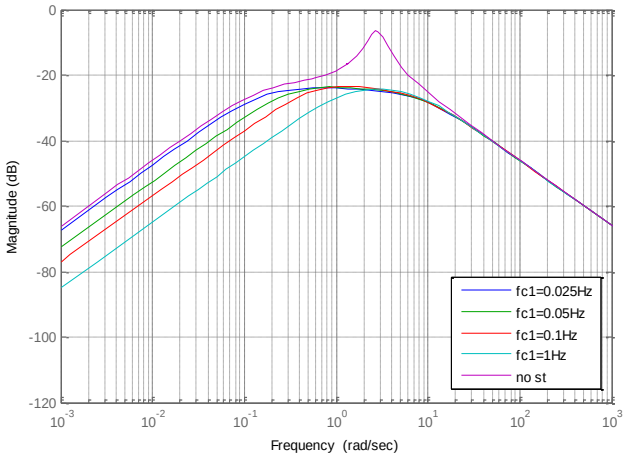

Figure 5.32 Magnitude of transfer function between frequency variation and power variation of filter strategy #4 with different cut-off frequency

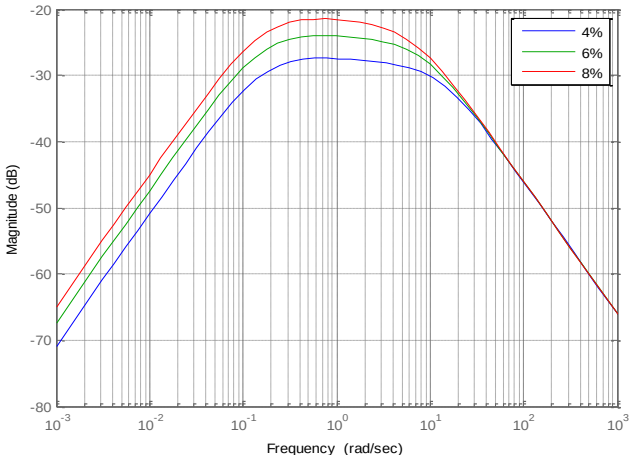

Figure 5.33 Magnitude of transfer function between frequency variation and power variation of filter strategy #1 with different droop values of ESS

The droop for energy storage is varied for cut-off frequency of 0.025Hz in Figure 5.33. Droop value of energy storage does not impact the magnitude of df/dP in high frequencies. When droop value for storage increases, magnitude of df/dP in low and medium frequency increases so frequency deviation is larger for the same amplitude of power deviation.

5.4.2.5 Comparison of different filtering strategies

Finally, all filter strategies are compared to system without any energy storage as illustrated in Figure 5.34 (with a damping load constant 0.12). The cut-off frequencies of low and high pass filter of strategy #1, and of high pass filter of strategy #2 are at 0.025Hz. Cut-off frequencies of low and high pass filter of strategy #3 are 0.025Hz and 1.2 Hz respectively. Cut-off frequency of strategy #4 is 0.025Hz with a droop value for energy storage of 6%.

The first strategy (in red line), which corresponds to an open-loop system, is worse than the others in low frequency region (<0.016Hz or 0.1rad/s). In high frequency region (>1.6Hz or 10rad/s), the first and second strategies which apply high pass filter for energy storage have less magnitude of $\Delta f/\Delta P_{diff}$. Therefore, the frequency deviation is less than the other cases for the same magnitude of power variation. Energy storage participates to regulate frequency in equivalent inertia zone. In medium frequency zone (0.016-1.6 Hz or 0.1-10rad/s), filter strategies 2, 3, and 4 have less magnitude $\Delta f/\Delta P_{diff}$ than system without energy storage. Magnitude $\Delta f/\Delta P_{diff}$ of filter strategy #1 is also smaller

than system without energy storage in the same medium frequency region. This indicates that energy storage can coordinate to reduce frequency deviation in this zone (for the same amplitude of power variation). The filter strategy #4 cannot reduce frequency deviation as much as strategy #1 (in some frequency range), 2 and 3. To improve the strategy #4, droop value for energy storage has to be decreased (energy storage have to participate more).

In summary, the grid frequency can be unstable if damping load constant is zero and if there is no primary control (no droop) at the same time for diesel, which is controlled by a classical frequency control system (primary and secondary control). For control system of diesel by filtering, grid frequency does not return to 50Hz if damping load constant is null. System needs the return of frequency to form a closed-loop system, either droop or damping load constant. Performance of filter strategy depends on the cut-off frequency of filter. All filter strategies are then simulated in time domain in MATLAB-Simulink.

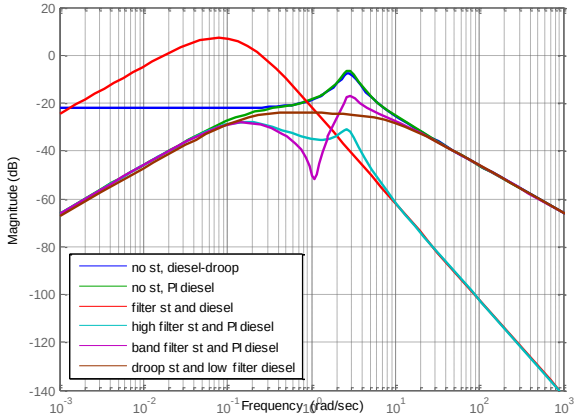

Figure 5.34 Magnitude of transfer function between frequency variation and power variation of different filter strategies of energy storage system

5.4.3 Analysis of filtering strategies in time domain

The system in Figure 5.1(b) is simulated. The PV signal of 26/08/2011 is studied as a disturbance of system. Firstly, grid frequency response is analyzed to define the performance of each strategy. Next, the power and energy of energy storage and diesel generator are analyzed. The droop value of diesel is fixed at 8% and K_i is equal to 2.

5.4.3.1 Filter strategy #1

From system analysis in frequency domain in previous sections, this strategy can cause more frequency deviations than system without energy storage. Filters with a cut-off frequency of 0.025Hz are firstly used. Frequency response of power signal on 26/08/2011 (in Figure 5.22(b)) in Figure 5.35(a) shows that frequency deviation of system with this filter strategy is larger than system without energy storage (diesel is controlled by classical control loops). The cut-off frequency is then reduced. Frequency deviation of system with this strategy is always large until a cut-off frequency of 0.001Hz; the frequency deviation of initial system is then improved as illustrated in Figure 5.35(b). This frequency response is always in acceptable limit (49.8-50.2Hz). The cut-off frequency of 0.001Hz is also used to simulate the most fluctuated signals during 3 months, e.g. on 20/10/2011 (see Figure 5.22(a)). The frequency response in Figure 5.36(b) shows that cut-off frequency 0.001Hz of this filter strategy can reduce frequency deviation of initial system.

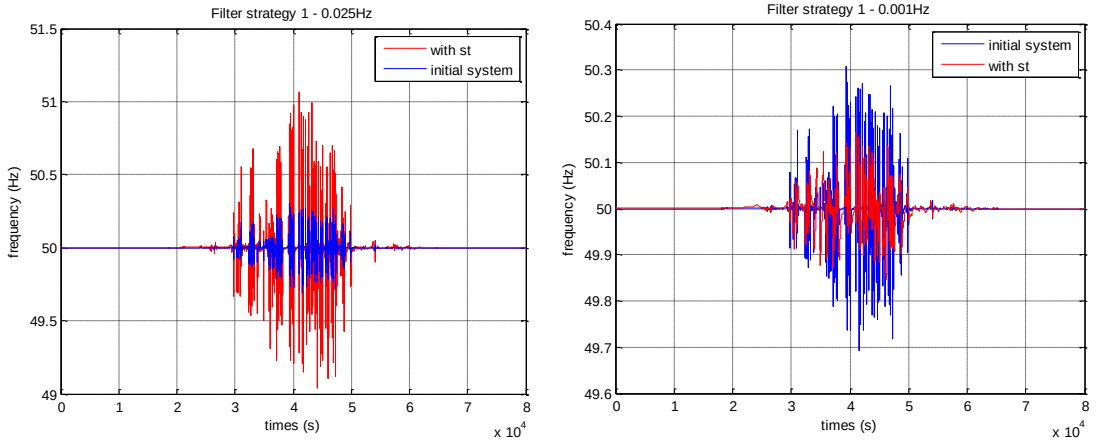

(a) (b)

Figure 5.35 Frequency response of system with filter strategy #1 for cut-off frequency (a) 0.025Hz (b) 0.001Hz in 26/08/2011

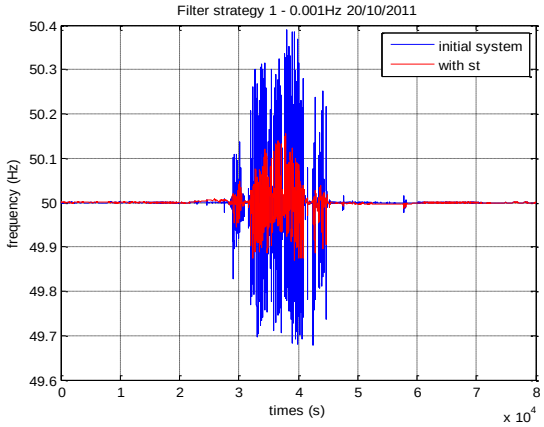

Figure 5.36 Frequency response of system with filter strategy #1 for cut-off frequency 0.001Hz in 20/10/2011

From Figure 5.27 and results in time domain simulation, it can be noticed that the frequency of the initial system has been improved and frequency remains within the acceptable limits, if magnitude of transfer function $\Delta f/\Delta P_{diff}$ of system with filter strategy is less than the initial system for frequency more than 0.06rad/s or 0.0095 Hz.

Power of energy storage and diesel generator on 26/08/2011 and 20/10/2011 are illustrated in Figure 5.37 and Figure 5.38. With this strategy, the energy storage works as the main source of primary frequency control and diesel generator takes action only in secondary control.

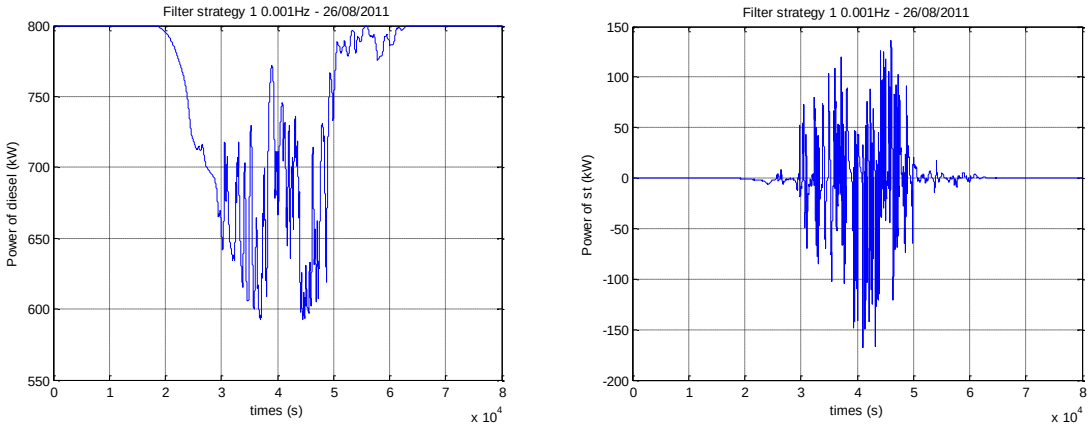

(a) (b)

Figure 5.37 (a) Power of diesel generator (b) Power of ESS in 26/08/2011

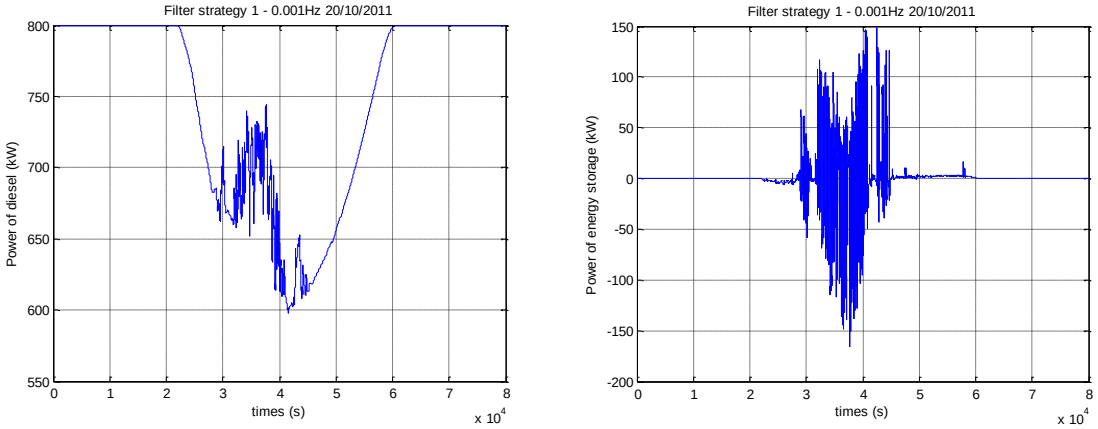

(a) (b)

Figure 5.38 (a) Power of diesel generator (b) Power of ESS in 20/10/2011

5.4.3.2 Filter strategy #2

High pass filtering of PV power is applied to energy storage. Cut-off frequency of filter is then varied from 0.001Hz to 0.1Hz. Grid frequency, power of energy storage, primary power of diesel, and secondary power of diesel are compared and shown in Figure 5.39. Energy storage of this strategy can reduce frequency deviation of system without energy storage for all cut-off frequencies, but frequency response with cut-off frequency more than 0.05Hz is out of the acceptable limit as illustrated in Figure 5.39(a). Cut-off frequency of 0.001Hz (like in strategy #1) causes very small frequency variations because all fluctuations are assumed by fast energy source like energy storage. The power of energy storage with 0.001Hz cut-off frequency is the largest in Figure 5.39(b). When the cut-off frequency is decreased (i.e. band-width of energy storage is increased), power of energy storage increases as shown in Figure 5.39(b), but the primary power of diesel decreases in Figure 5.39(c). The secondary power of diesel for cut off frequencies of 0.025, 0.05, and 0.1Hz are quite equivalent to secondary power without energy storage shown in Figure 5.39(d). The cut-off frequency of 0.001Hz reduces secondary power of diesel.

Therefore, if energy storage is needed to be used as the main source of primary frequency control, cut-off frequency of high pass filter should be very small. However, if energy storage is required just to participate only when frequency is critical (optimum use of energy storage), cut-off frequency should be around 0.025Hz.

Energy used of energy storage and diesel generator is calculated. Energy used of energy storage for each cut-off frequency is illustrated in Figure 5.40(a) with the primary control of diesel generator in Figure 5.40(b). Energy of energy storage by filter 0.001Hz is much larger than the others. On the contrary, the energy used for primary control of diesel is smaller than the others.

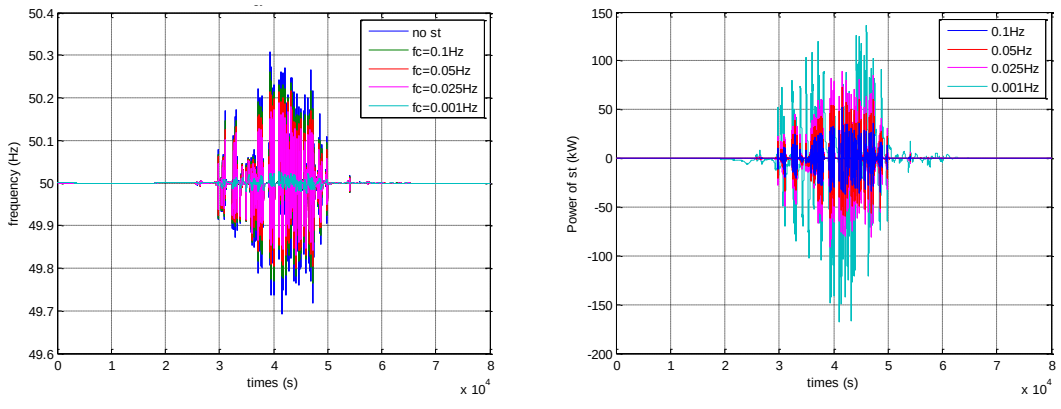

(a) (b)

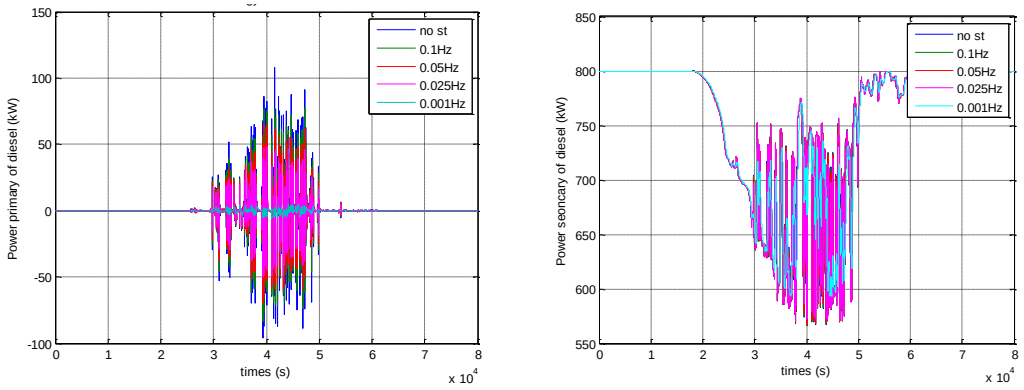

(c) (d)

Figure 5.39 (a) Frequency response (b) Power of ESS (c) Power of primary control of diesel generator (d) Power of secondary control of diesel generator of power system with filter strategy #2 in 26/08/2011

Furthermore, power of energy storage and primary power of diesel in time domain shown in Figure 5.39(b) and (c) respectively; are analyzed according to their variations by standard deviation calculation in Figure 5.41(a) and (b). When cut-off frequency rises up, standard deviation of power of energy storage decreases (less variation) but that of diesel increases (more variation) as illustrated in Figure 5.41 (a) and (b) respectively. However, standard deviation of primary power diesel of system with energy storage is smaller than the system without energy storage.

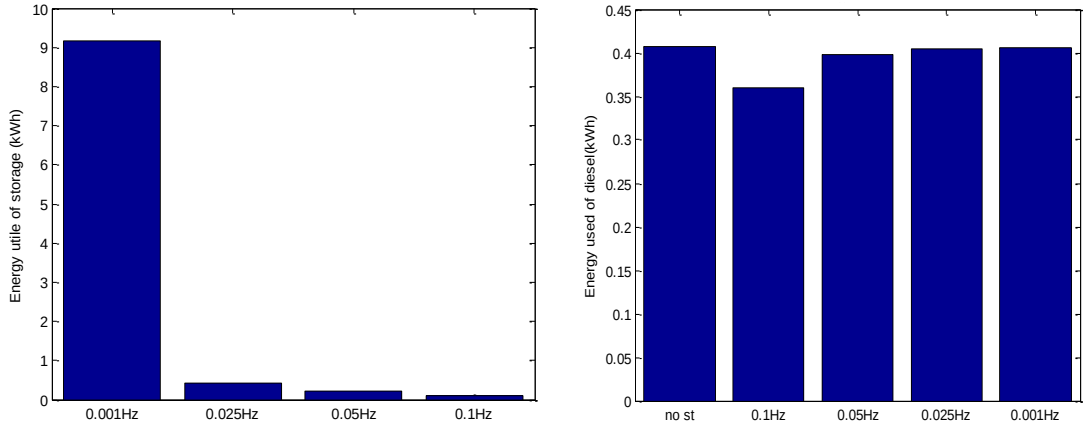

(a) (b)

Figure 5.40 (a) Energy used of ESS (b) Energy used of diesel generator of power system with filter strategy #2 in 26/08/2011

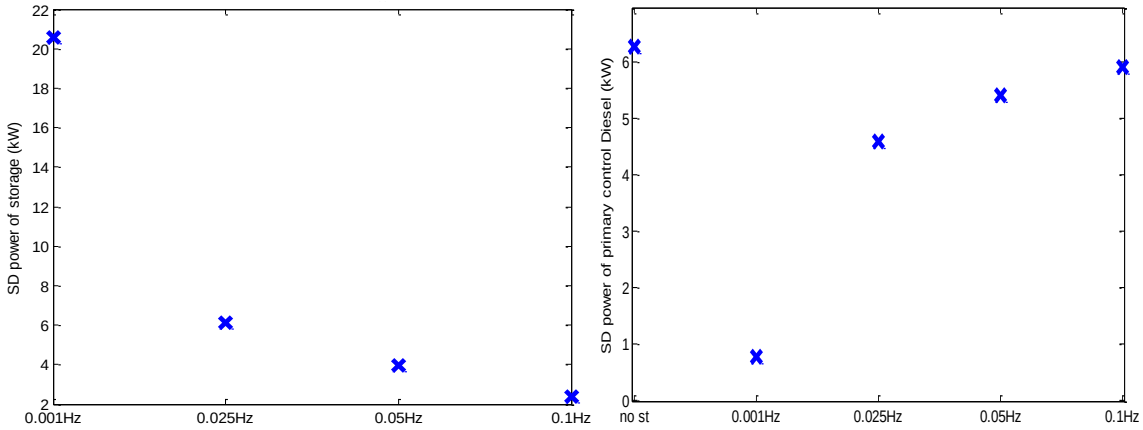

(a) (b)

Figure 5.41 Standard deviation of (a) power of ESS (b) power of primary control of diesel generator for different cut-off frequency of filter strategy #2 in 26/08/2011

Power of energy storage and power of primary control of diesel generator in time domain are transformed to frequency domain by Fourier Transform as shown in Figure 5.42(a) and Figure 5.43(a). Spectrum of power of energy storage with cut-off frequency 0.001Hz is quite different from the

others. From spectrum of these powers, FHC (by equation (2.21) in chapter 2) is calculated to signify variation of signal in each frequency range regions as illustrated in Figure 5.42(b) and Figure 5.43(b).When cut-off frequency decreases, energy storage participates more in low and medium frequency regions. The primary power of diesel is reduced in high and medium frequency regions but it decreases in low frequency only with cut-off frequency of 0.001Hz.

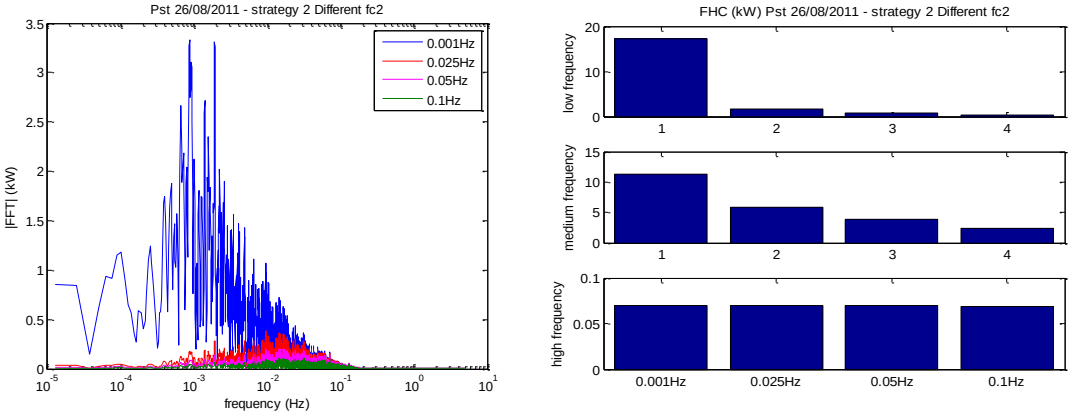

(a) (b)

Figure 5.42 (a) Spectrum (b) FHC in each frequency region of power of ESS for different cut-off frequency of filter strategy #2 in 26/08/2011

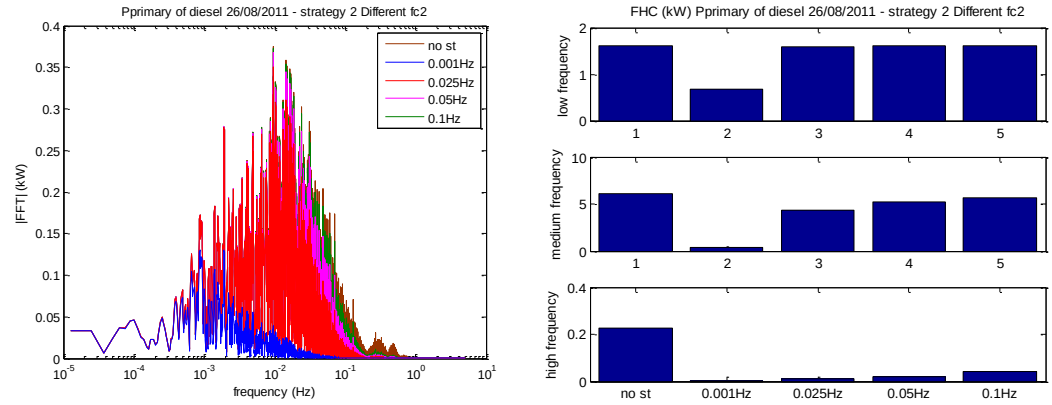

(a) (b)

Figure 5.43 (a) Spectrum (b) FHC in each frequency region of power of primary control of diesel generator for different cut-off frequency of filter strategy #2 in 26/08/2011

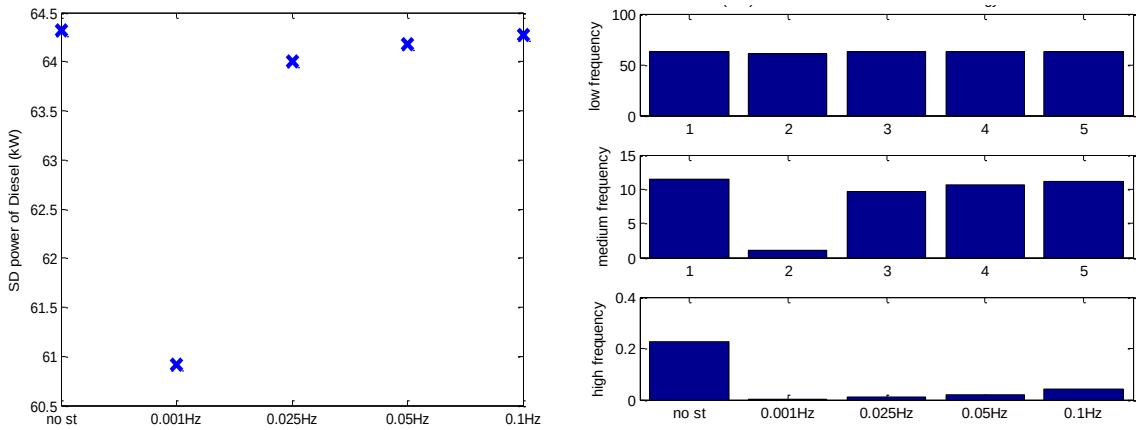

(a) (b)

Figure 5.44 (a) Standard deviation (b) FHC of spectral of power total of diesel generator for different cut-off frequency of filter strategy #2 in 26/08/2011

The total power of diesel (primary and secondary) is analyzed in time and frequency domain. Figure 5.44(a) Figure 5.52 shows that cut-off frequency 0.001Hz can reduce variation of power of

diesel. The total power of diesel in medium and high frequency regions; are reduced by energy storage as shown in Figure 5.44(b).

As having mentioned above, if the objective of energy storage system is merely to limit frequency deviation and save the use of ESS, cut-off frequency 0.025Hz has to be used. In the case that the power of diesel generator has to be also reduced, cut-off frequency selected has to be very low like 0.001Hz.

5.4.3.3 Filter strategy #3

This strategy is quite similar to filter strategy #2 except that it limits working of energy storage in high frequency region (energy storage only participate for medium frequency of fluctuation). The low cut-off frequency (fc2) is firstly fixed at 0.025Hz and high cut-off frequency (fc1) is varied from 0.5 to 1.2 Hz. Frequency responses for all cut-off frequency of this strategy is quite similar to frequency response of strategy #2. Primary and secondary power of diesel and power of energy storage is also quite identical to strategy #2. The energy used of energy storage and primary power of diesel is compared in Figure 5.45. Energy used of primary control of diesel and energy storage by this filter strategy is smaller than strategy #2. When high cut-off frequency of band pass filter increase, working region of energy storage also increase so it will participate more. Figure 5.45 shows that energy used of energy storage increases when fc1 increases but in small value of difference. Energy storage reduces the energy used of primary control of diesel in Figure 5.45 (b). Increasing of high cut-off frequency (fc1) does not cause any effect on energy used of primary control of diesel.

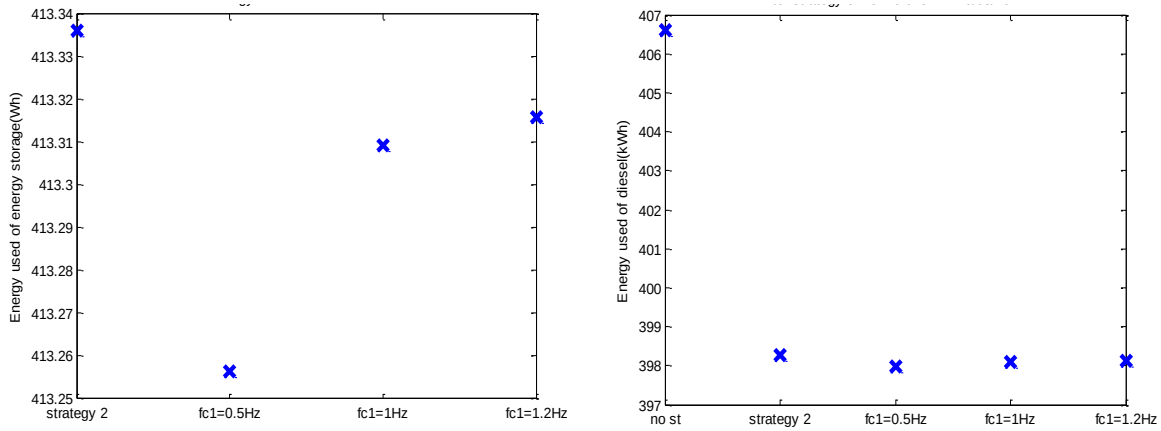

(a) (b)

Figure 5.45 (a) Energy used of ESS (b) Energy used of diesel generator of power system with filter strategy #3 in 26/08/2011

5.4.3.4 Filter strategy #4

In case that energy storage works as the main source of primary frequency control. The frequency returns to make closed loop system by droop control for energy storage. Low pass filter of PV power is applied for diesel generator to mainly coordinate for secondary control. Droop for energy storage is firstly fixed at 4% and cut-off frequency of low pass filter is varied from 0.001Hz to 1.5Hz. Frequency response and power of energy storage have been illustrated in Figure 5.46. This strategy with cut-off frequency 0.001Hz and 0.025Hz causes more frequency deviation than system without energy storage in Figure 5.46(a). If cut-off frequency increases (diesel works in medium frequency region or in primary control), frequency deviation is then decreased. However, it is not all in acceptable limit. To improve the frequency response, the rated power of energy storage should be increased or droop value for energy storage is decreased to let energy storage participate to regulate frequency longer. Referring to the sizing of energy storage, it needs diesel generator to participate in primary control. It can be seen in Figure 5.46(b) that power of energy storage decreases when cut-off frequency rises up.

The objective of this strategy is to limit diesel to work only in secondary control in which cut-off frequency of low pass filter should be less than 0.025 Hz (cut-off frequency of power system shown in Figure 3.4). Therefore, energy storage has to be redesigned for filter 0.025Hz and 0.001Hz. Frequency is in acceptable limit if power rated of energy storage is increases from 0.3MW to 1MW with cut-off frequency 0.025Hz and droop for energy storage 4%. For cut-off frequency 0.001 Hz, power rated of energy storage should be 1MW and droop for storage should be 2% to make frequency in acceptable limit.

The standard deviation of power of energy storage decreases when cut-off frequency decreases as shown in Figure 5.47. Therefore, power of energy storage has less variation for high cut-of frequency. Besides, cut-off frequency 0.001 Hz for diesel generator makes energy storage participate more than energy storage with classic primary control of diesel generator and vice versa for other cut-off frequencies. Spectral of power of energy storage in Figure 5.46(b) is presented in Figure 5.48(a). Spectral of energy storage with cut-off frequency 0.001Hz for diesel generator is dominating others. FHC of spectral in Figure 5.48(b) shows that cut-off frequency 0.001Hz causes energy storage participate more in low and medium frequency region. But in high frequency region, all cases are quite identical.

The total power of diesel is analysed. The variation of the total power of diesel is reduced by energy storage. Cut-off frequency 0.001Hz causes the smallest variation in Figure 5.49(a). The variation in medium and high frequency regions are also decreased by energy storage. And cut-off frequency 0.001Hz causes more reduce in medium frequency region as illustrated in Figure 5.49(b).

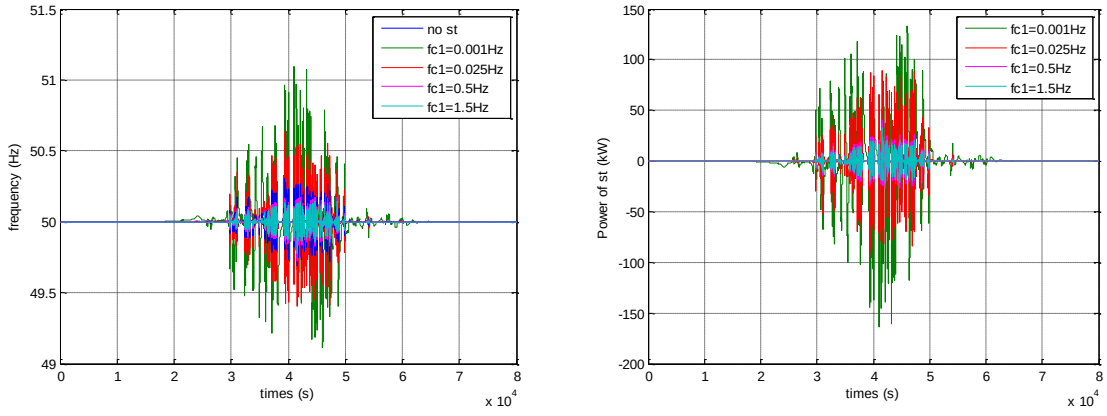

(a) (b)

Figure 5.46 (a) Frequency response (b) Power of ESS of power system with filter strategy #4 with different cut off frequency in 26/08/2011

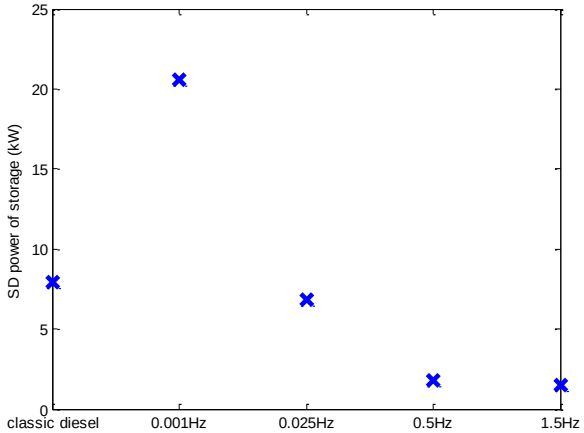

Figure 5.47 Standard deviation of power of ESS with filter strategy #4 with different cut off frequency in 26/08/2011

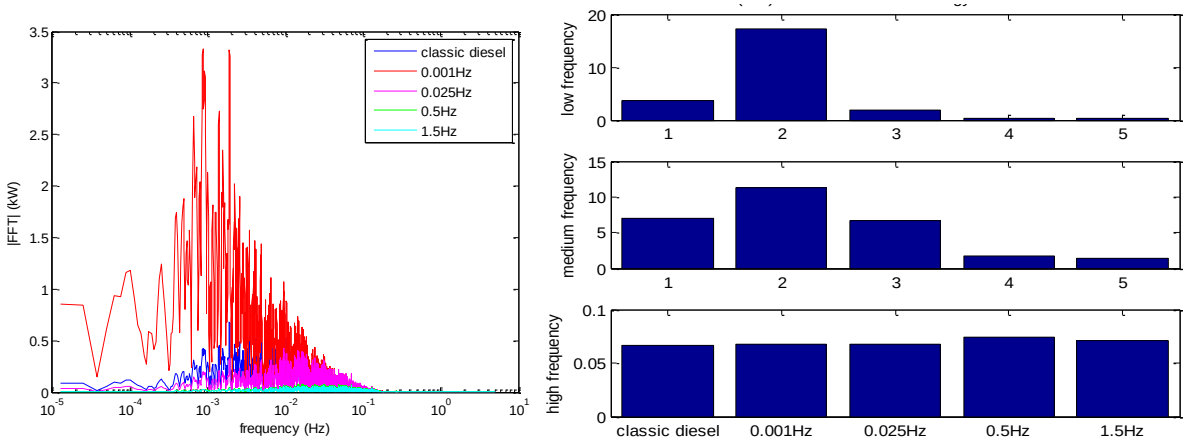

(a) (b)

Figure 5.48 (a) Spectral (b) FHC in each frequency region of power of ESS for different cut-off frequency of filter strategy #4 in 26/08/2011

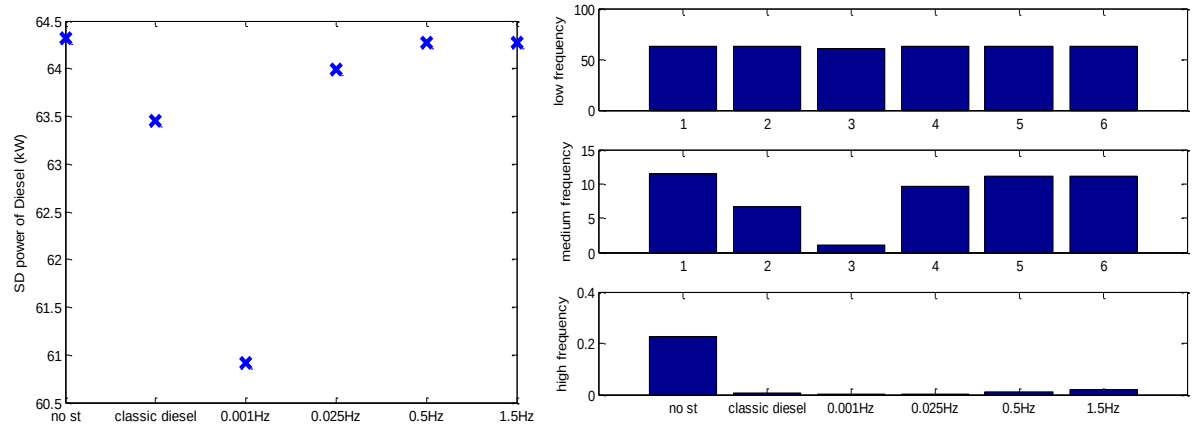

(a) (b)

Figure 5.49 (a) Standard deviation (b) FHC in each frequency region of power total of diesel generator for different cut-off frequency of filter strategy #2 in 26/08/2011

Cut-off frequency is then fixed at 1.5Hz and droop for energy storage is varied by decreasing from 4% to 2%. Frequency deviation is reduced to be all in the acceptable limit by droop for energy storage 2% as shown in Figure 5.50.

In the case that the ESS is designed to work as the main source of primary frequency control, cut-off frequency of low pass filter should be very low like 0.001Hz but power rated of energy storage (sizing) have to be large in order to guarantee frequency performance.

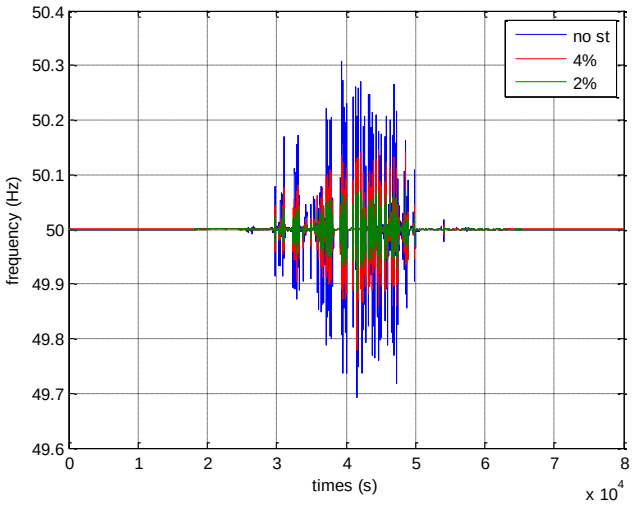

Figure 5.50 Frequency response of power system with filter strategy #4 with different droop of ESS in 26/08/2011

5.4.3.5 Comparison of different filtering strategies

In this topic, different filter strategies are compared. Frequency response, power and energy of ESS, and power and energy of diesel generator are analyzed. The parameter of each strategy have been defined and shown in Table 5.3.

Table 5.3: Parameter of filter strategies

Filter strategy	Diesel generator	Energy storage system
1	Low pass filter with fc1=0.001Hz	High pass filter with fc2=0.001Hz
2	Primary and secondary control	High pass filter with fc2=0.001Hz
3	Primary and secondary control	Band pass filter with fc1=0.5Hz fc2=0.001Hz
4	Low pass filter with fc1=0.001Hz	Primary control by droop with Pes_rated 1MW and droop 2%

Parameters selected in Table 5.3 have been chosen according to the fact that all system frequencies are in the acceptable limit and frequency band-width of action for energy storage is quite similar. Rated power of energy storage does not induce any impact on control algorithm of filtering strategies #1 to #3 but it has an effect on strategy #4. All strategies are simulated with PV power signal of PV plant#1 in 28/08/2011 and 20/10/2011 and compared to system without energy storage. From Figure 5.51(a) and Figure 5.52(a), energy storage reduces frequency deviation of the initial system (without energy storage). Moreover, the frequency deviation of filtering strategy #2 is always minimal. Maximal, minimal power and energy used of energy storage system of different strategies are quite similar as illustrated in Figure 5.51 (b) and (c), and Figure 5.52 (b) and (c).

Used energy of diesel with system including energy storage is greater than system without energy storage as shown in Figure 5.51 (d) and Figure 5.52 (d). Figure 5.51 (e) and Figure 5.52 (e) indicate that primary power of diesel of the initial system (no energy storage) is reduced by strategy #2 and #3 (strategy #1 and 4 no primary control). Therefore, the energy used for primary control of diesel also decreases with energy storage device.

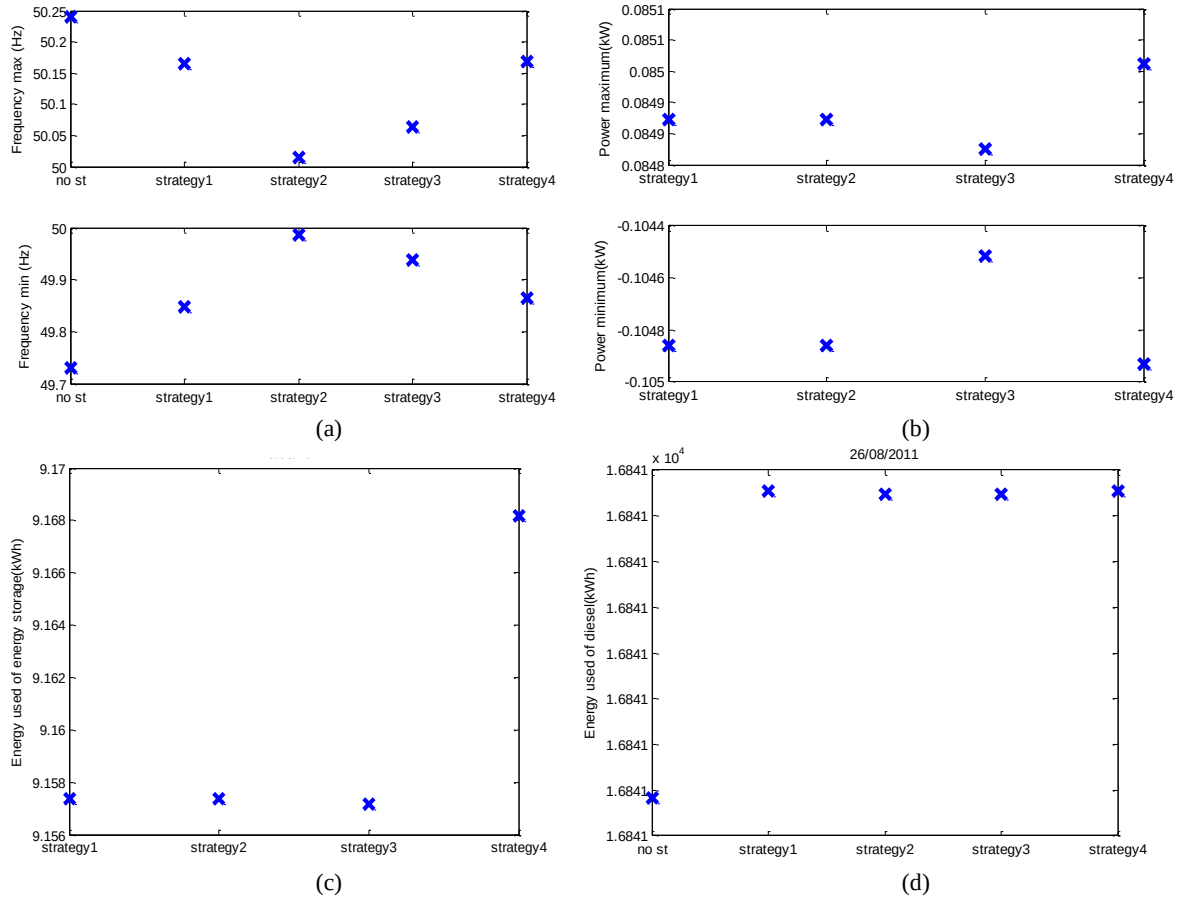

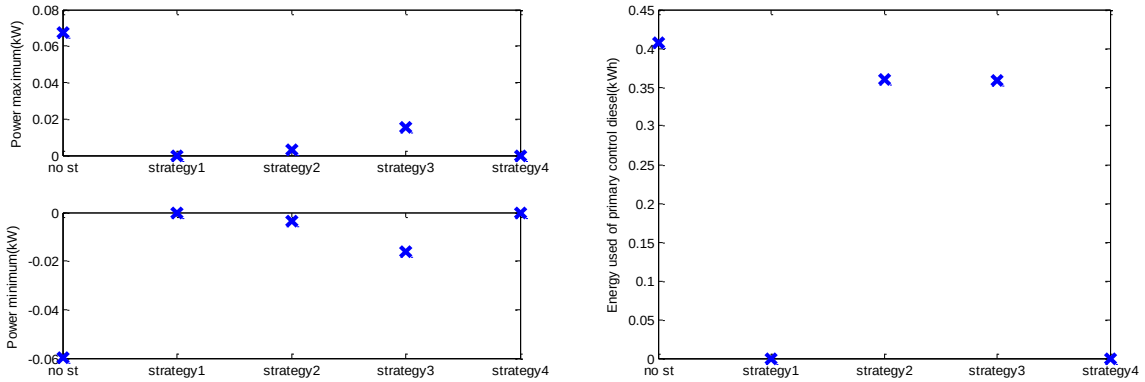

(e) (f)

Figure 5.51 Data analysis of PV signal 26/08/2011 (a) Frequency maximal and minimal (b) Power maximal and minimal of energy storage (c) Energy used of energy storage (d) Energy used of diesel generator (e) Power of primary control of diesel (f) Energy used of primary control of diesel

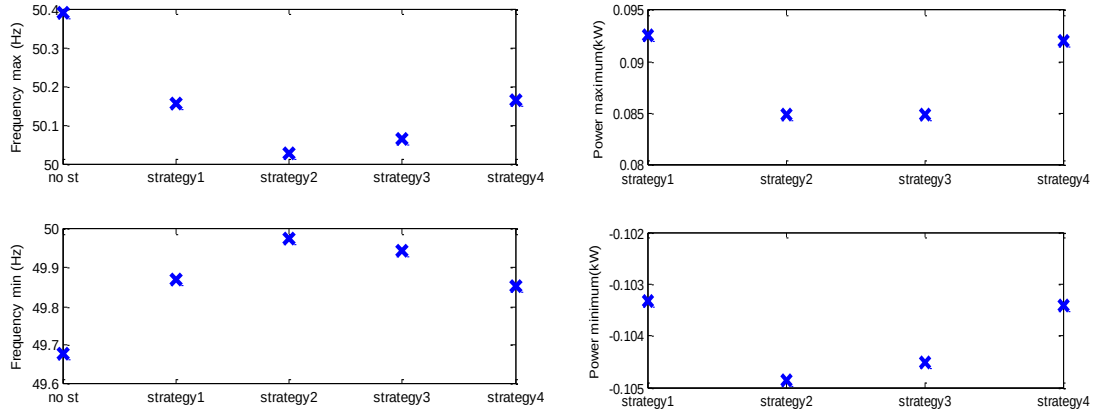

(a) (b)

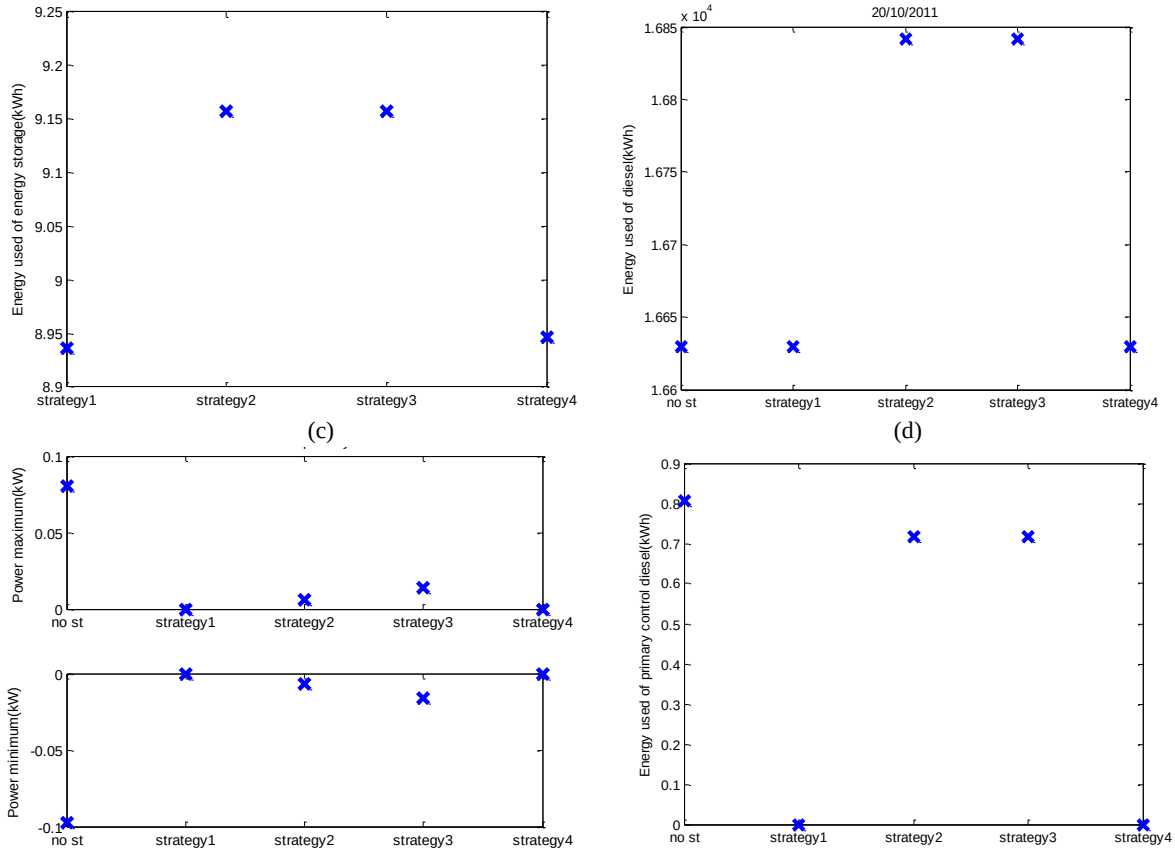

(c) (d)

(e) (f)

Figure 5.52 Data analysis of PV signal 20/10/2011 (a) Frequency maximal and minimal (b) Power maximal and minimal of energy storage (c) Energy used of energy storage (d) Energy used of diesel generator (e) Power of primary control of diesel (f) Energy used of primary control of diesel

5.4.3.6 Sensitivity on parameters of Diesel frequency control

If Ki decreases, time response of secondary control of diesel will increase. Energy used for primary control is also increased because frequency returns to 50Hz quite slow. For the system with energy storage by all filter strategies with cut-off frequency 0.001Hz, frequency is always in the acceptable limit when Ki decreases to 1. Power of energy storage and diesel do not change too but the energy used for primary control of diesel increases. However, if cut-off frequency becomes larger (0.025Hz), when K_i decreases, cut-off frequency has to be decreased as in the Bode diagram with different K_i as shown in Figure 5.53.

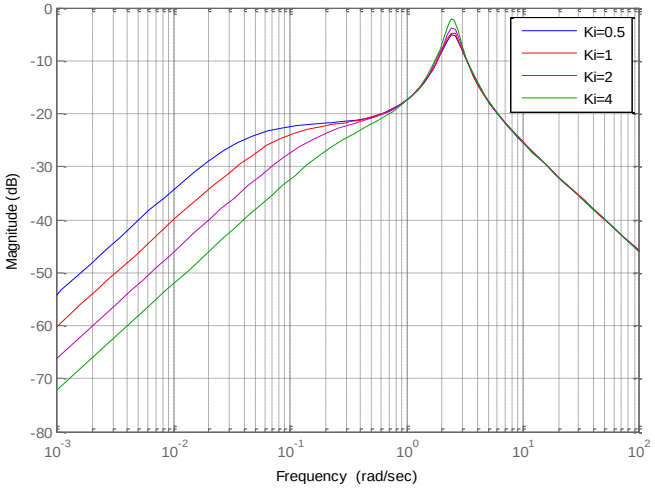

Figure 5.53 Magnitude of transfer function between frequency variation and power variation with different integral gain of secondary control of diesel generator

5.4.4 Filtering strategy conclusion

Filtering strategy for energy storage can reduce frequency deviation of initial system without energy storage. Performance of filter strategy depends on its cut-off frequency. If cut-off frequency of high pass filter for energy storage is very low (0.001Hz), energy storage can turn to be the main source of primary frequency control.

Strategies 1 and 4 have risk to cause more frequency variations than initial system. For filter strategy #1, cut-off frequencies of two filters should be equivalent and small (below 0.001 Hz) in order to improve frequency response of the initial system. In case of strategy #4, rated power of energy storage, droop for energy storage and cut-off frequency of low pass filter have to be well defined.

5.5 Simulation and comparison of different strategies

Power system in Figure 5.1 with the most fluctuated PV power signal (20/10/2011) is simulated in MATLAB-Simulink with different strategies of energy storage system. Power of ESS (ΔP_{ES}) is defined by different strategies as presented in Table 5.4. The first system is an initial system without ESS. The second strategy is the classical primary frequency control which is applied to energy storage system. Others are strategies those presented in topic 5.3 and 5.4.

Cut-off frequency of all filter strategies is selected at very low value because filter strategy #1 needs very low cut-off frequency to improve the frequency response. Power rated of energy storage does not cause any impact on control algorithm of strategy with limitation diagram and filter strategy #1 to #3. However, it has an effect on droop for storage and filter strategy #4. Energy storage system by filter strategy becomes the main source of primary control. Therefore, its power rated should be grown up and droop value should be low.

Table 5.4: Parameter of different strategies

Strategy	Diesel generator	Energy storage system
Initial	PI controller	No
Droop for ESS	PI controller	Droop control with Pes_rated 0.3MW and droop 6%
Limitation diagram	PI controller	Power deviation limit line
Filter strategy #1	Low pass filter with fc1=0.001Hz	High pass filter with fc2=0.001Hz
Filter strategy #2	PI controller	High pass filter with fc2=0.001Hz
Filter strategy #3	PI controller	Band pass filter with fc1=0.5Hz fc2=0.001Hz
Filter strategy #4	Low pass filter with fc1=0.001Hz	Droop control with Pes_rated 1MW and droop 2%

5.5.1 Time domain analysis

Frequency response and maximal/minimal values of frequency of each strategy are plotted in Figure 5.54and Figure 5.55respectively. Frequencies of all systems with energy storage (except for the droop control of energy storage) are in the acceptable limit (49.8-50.2Hz). For droop control, frequency performance (frequency variation) depends on the frequency sensitivity coefficient (K in W/Hz), that is defined as a function of droop value, nominal frequency and rated power of energy storage. Power rated of energy storage (Pst_rated) is firstly fixed at 0.3 MW, and droop value of energy storage at 6%; K is then equal to 10^5 W/Hz. Rated power of energy storage should be around 0.75 MW (increase K to $2.5x10^5$ W/Hz) to make frequency remains in the acceptable limits with this strategy

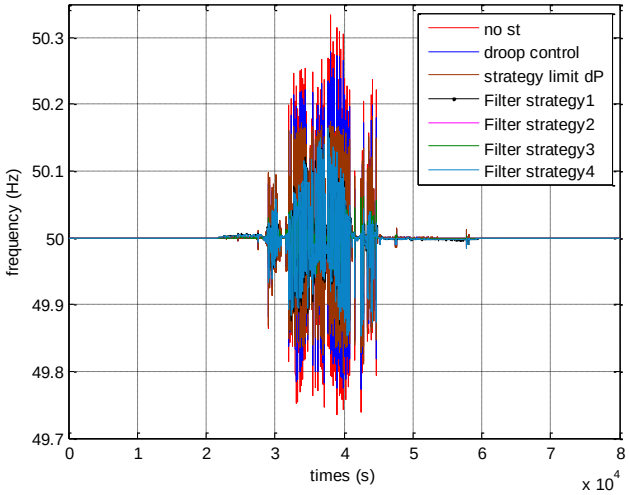

Figure 5.54 Frequency response of different strategies for ESS in 20/10/2011

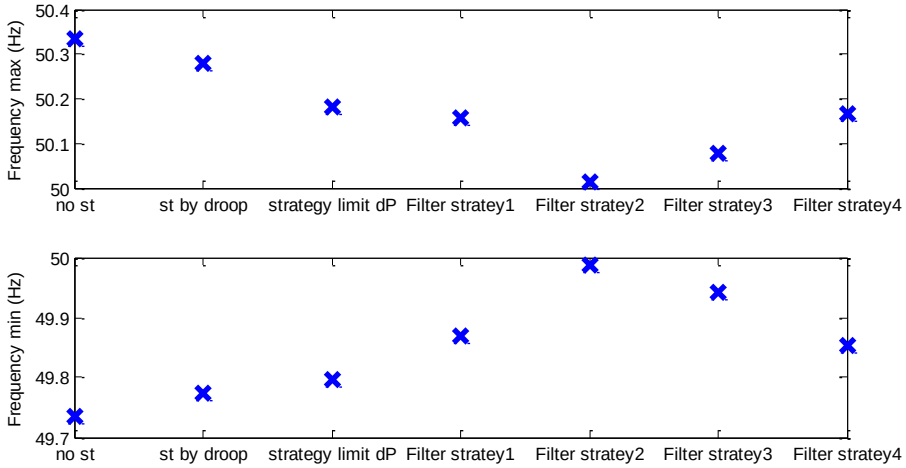

Figure 5.55 Frequency maximal and minimum of different strategies for ESS in 20/10/2011

Power of energy storage of filter strategies is higher than other strategies in Figure 5.58(a). Furthermore, its standard deviation is also higher but the primary power of diesel and its standard deviation of the initial system are reduced by filter strategies 2 and 3 as shown in Figure 5.59. Filter strategies 1 and 4 have no power of primary control by diesel. Filter strategies can reduce power and energy used of primary control more than droop strategy and limit ΔP_{pv} strategy. However, the energy used of energy storage is larger. In the case that the main target is to be replaced diesel generator with energy storage; filter strategies with low cut-off frequency (0.001Hz) is a promising strategy. The energy storage of strategy limitation diagram shown in Figure 5.58; participates less often than the others but it can keep frequency within the acceptable limit. Furthermore, power of primary control of diesel is also reduced by this strategy as shown in Figure 5.59 although it is not as large as the filter strategies. Strategy limitation diagram seems to be the optimal use of energy storage.

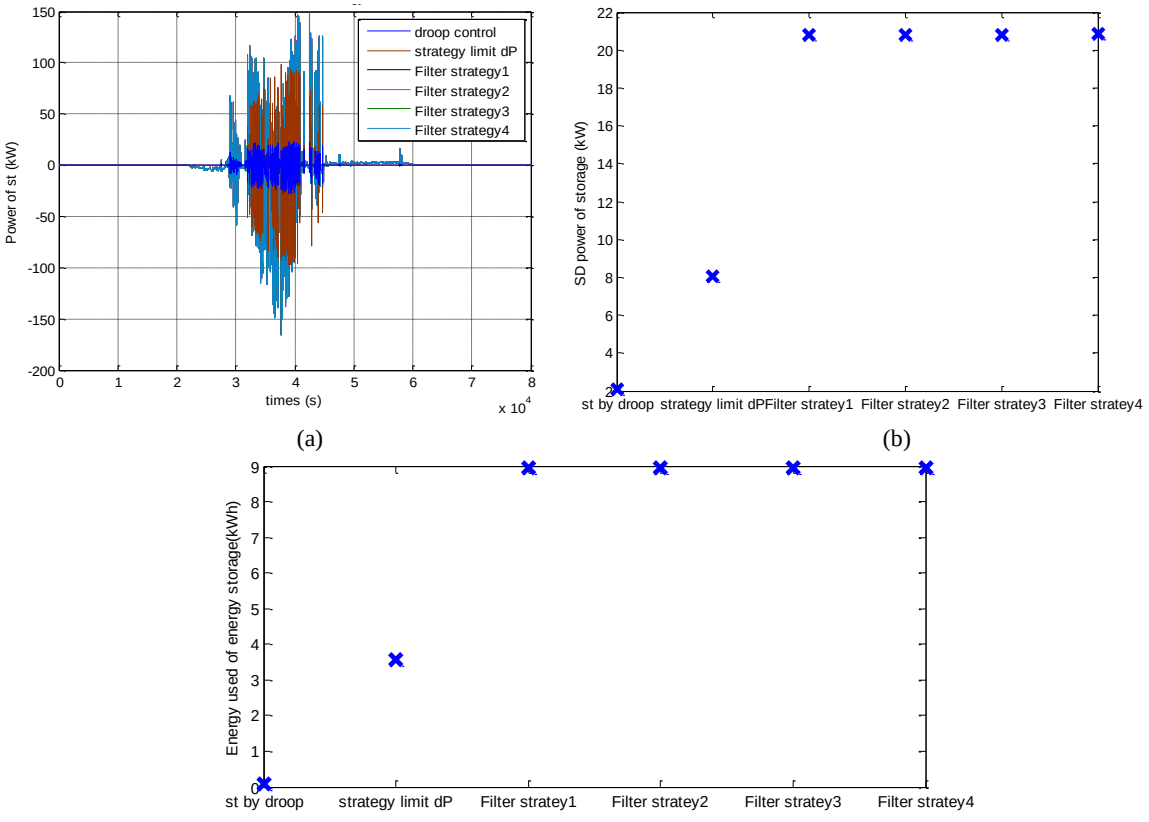

(a) (b)

(c)

Figure 5.56 (a) Power of ESS (b) Standard deviation of power of ESS (c) Energy used of ESS for different strategies in 20/10/2011

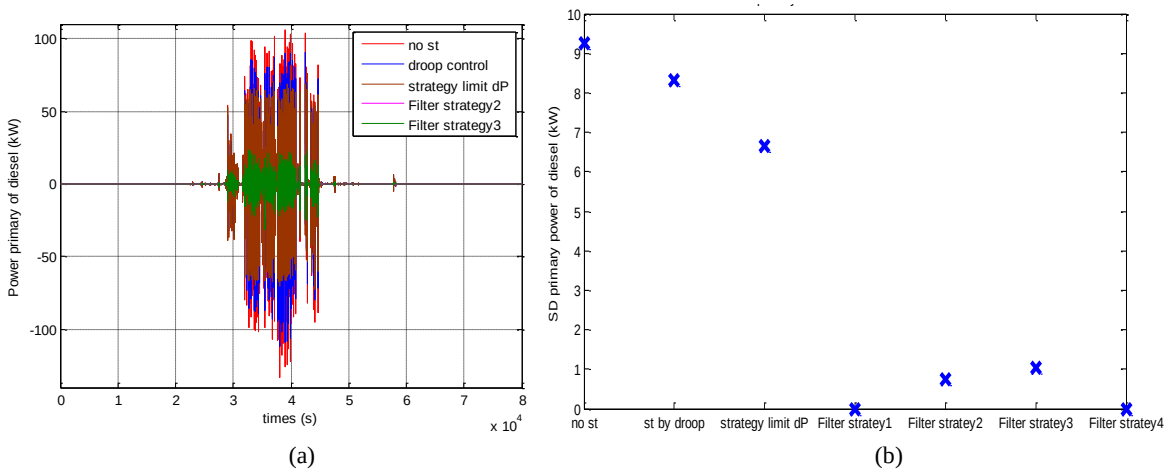

(a) (b)

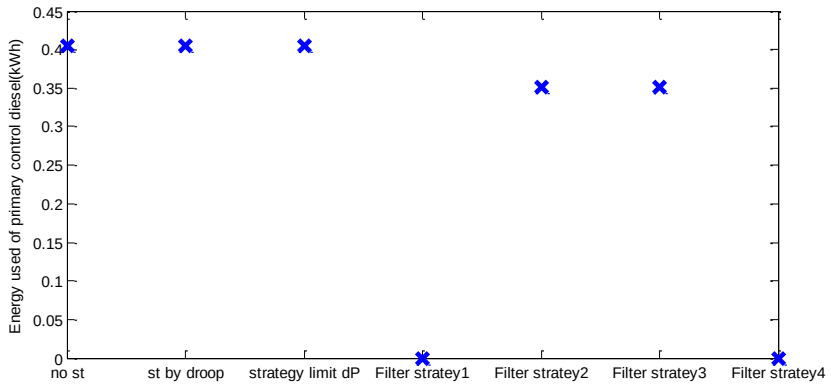

(c)

Figure 5.57 (a) Power of (b) Standard deviation of power of (c) Energy used of primary frequency control of diesel generator for different strategies in 20/10/2011

For filter strategies 2 and 3, the energy storage is overused if objective is only to improve frequency response. Cut-off frequency of high pass filter (f_{c2}) can be increased to 0.025Hz and frequency response is always in the acceptable limit as illustrated in Figure 5.60(a). Although the maximal frequency deviations of strategy #2 and #3 shown in Figure 5.58 are larger than that of in Figure 5.55, it is always in the acceptable limit. Standard deviation of power of energy storage and its stored energy of strategies 2 and 3 shown in Figure 5.59 are reduced. However, standard deviation of primary control of diesel and its energy used of primary control is increased and near the value of the initial system.

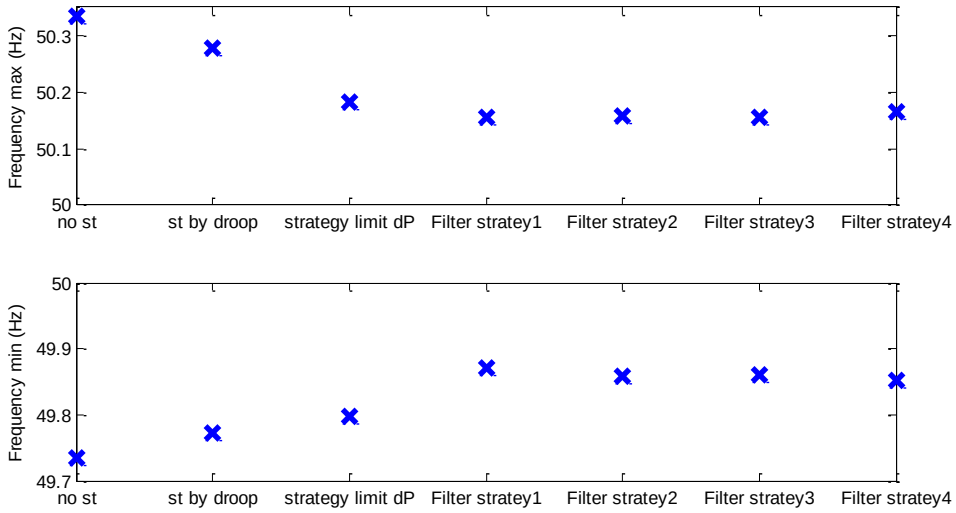

Figure 5.58 Frequency maximal and minimum of different strategies for ESS with cut-off frequency 0.025Hz for filter strategy #2 and #3 in 20/10/2011

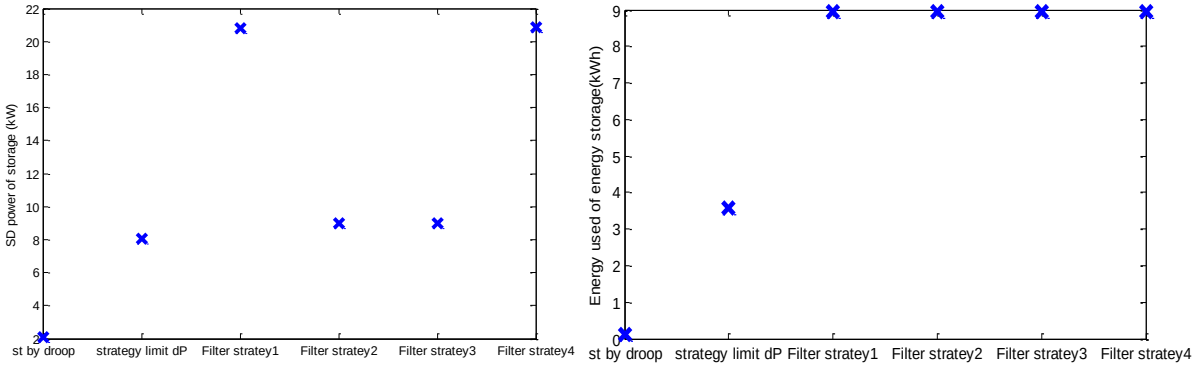

(a) (b)

Figure 5.59 (a) Standard deviation of power of (b) Energy used of ESS of different strategies for ESS with cut-off frequency 0.025Hz for filter strategy #2 and #3 in 20/10/2011

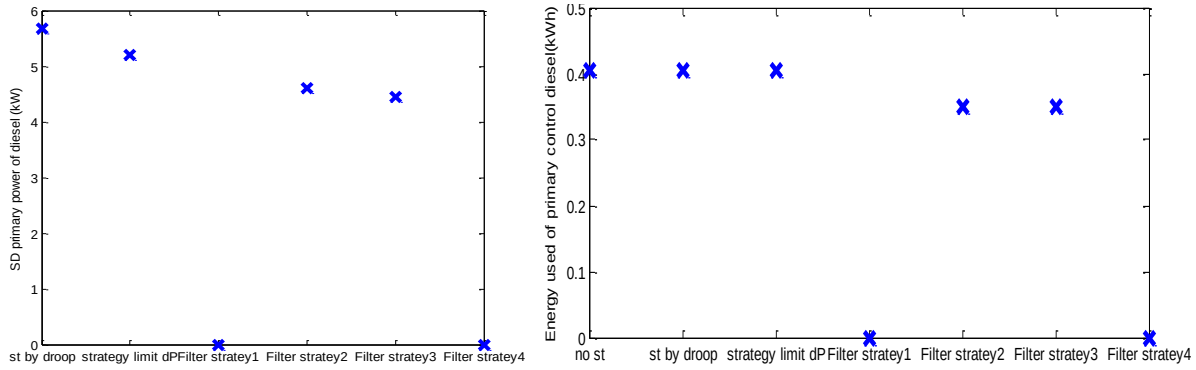

(a) (b)

Figure 5.60 (a) Standard deviation of power of (b) Energy used of primary frequency control of diesel generator of different strategies for ESS with cut-off frequency 0.025Hz for filter strategy #2 and #3 in 20/10/2011

5.5.2 Analysis in frequency domain

Powers of energy storage and diesel generator of each strategy are compared. Spectral of power of energy storage for each strategy is shown in Figure 5.61(a) and its variation for each frequency range (FHC) is illustrated in Figure 5.61(b). Concerning the energy storage with droop control and limitation diagram strategies, both participate less in medium and low frequency than with the filter strategy. Power of energy storage by limitation diagram strategy is larger than the others in high frequency region.

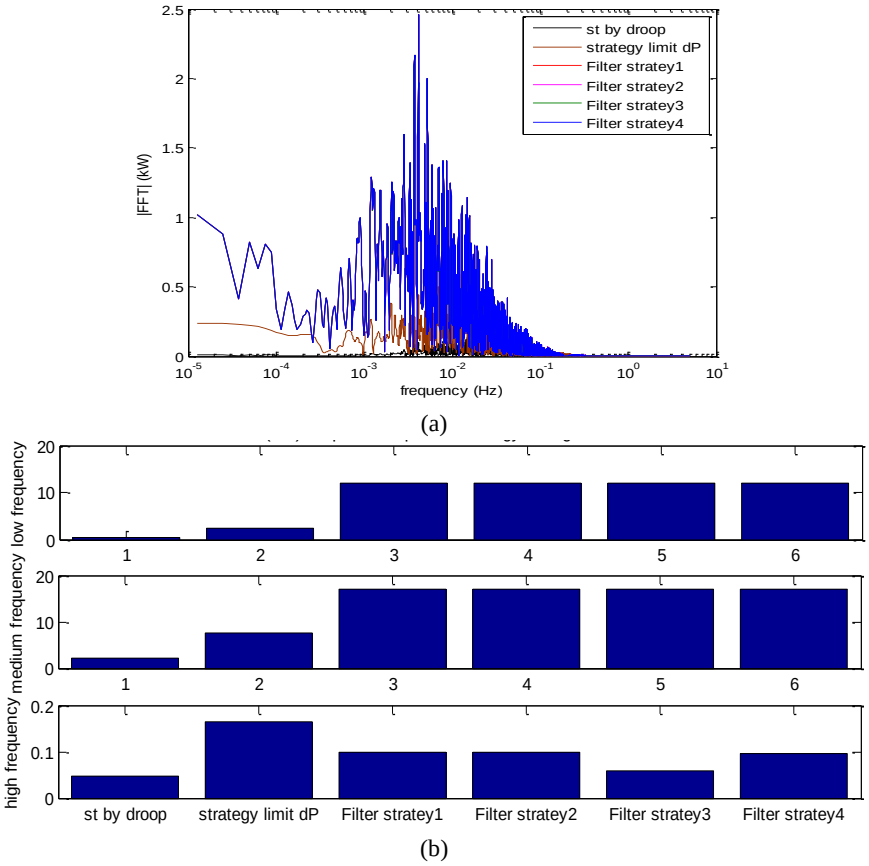

(a)

(b)

Figure 5.61 (a) Spectral (b) FHC in each frequency range of power of energy storage system

Power of primary control for diesel in frequency domain and its FHC for each frequency range are illustrated in Figure 5.62(a) and Figure 5.62(b) respectively. Filter strategies 1 and 4 do not have primary power because low pass filter is used to control the diesel. Energy storage by all strategies can reduce primary power of diesel in medium frequency region. Filter strategies 2 and 3 can also reduce primary power of diesel in low frequency region. FHC of primary power by filter strategy #2 (high pass filter for energy storage and classical frequency control for diesel) is less than the others in all

frequency regions. Filter strategy #3 causes less reduction in high frequency region, but in this region, primary power is increased by strategy with limitation diagram.

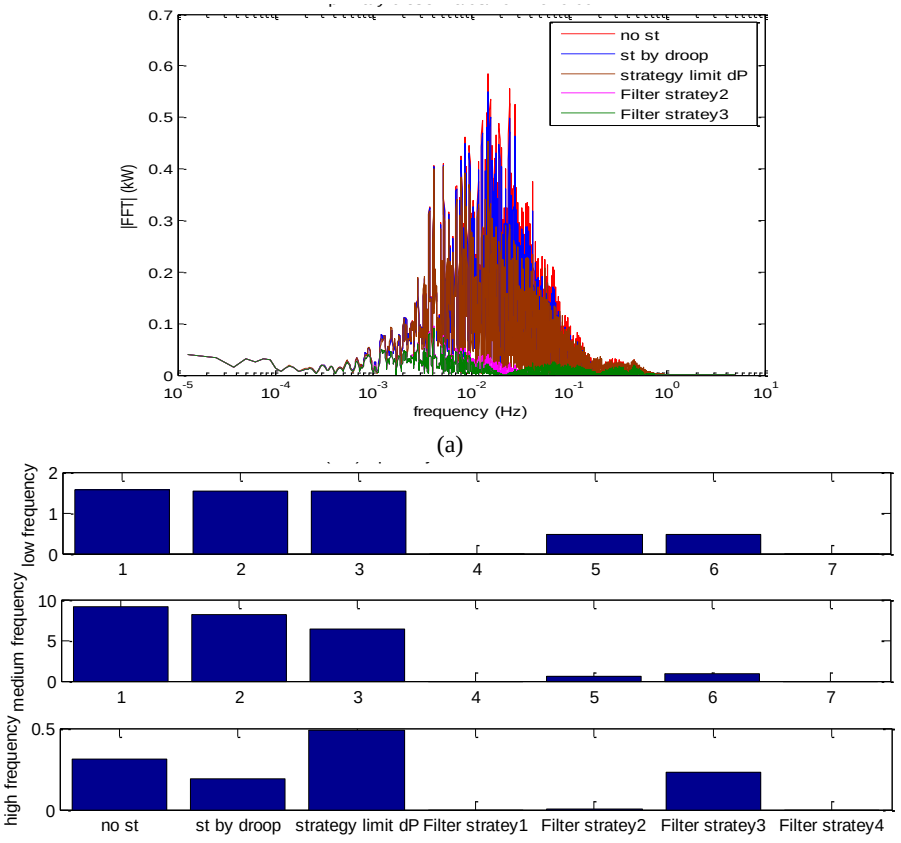

Figure 5.62 (a) Spectral (b) FHC in each frequency range of power of primary frequency control of diesel generator

Standard deviations of the total power of diesel and its FHC for each frequency range are illustrated in Figure 5.63(a) and (b) respectively. Energy storage can reduce the variation of power of diesel especially by filter strategy. The total power of diesel in low frequency region is identical for all strategies. Energy storage by all strategies can also reduce the total power of diesel in medium frequency region. Filter strategy causes more reduction in this frequency region. There is no power required for diesel in high frequency region for filter strategies 1, 2, and 4. Strategy with limitation diagram causes more variation in high frequency region.

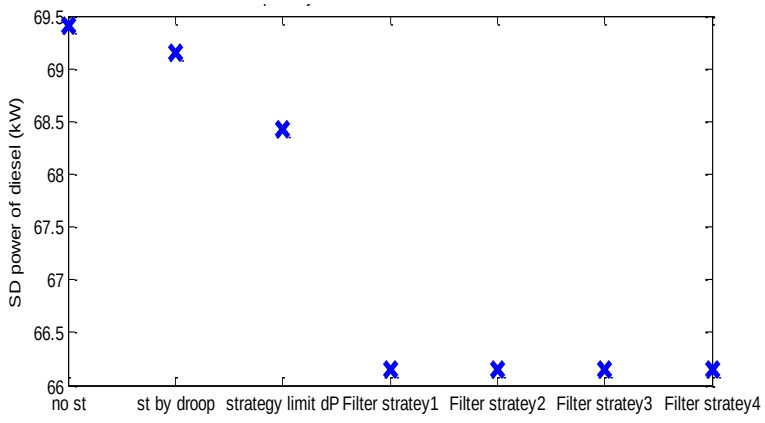

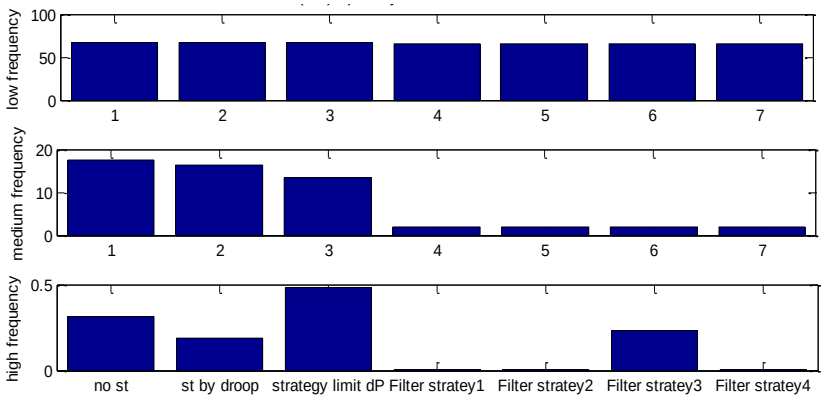

(b)

Figure 5.63 (a) Spectral (b) FHC in each frequency range of power total of diesel generator

5.5.3 Participation of energy storage system for each strategies

In this section, participation of energy storage in one day is studied. Time, power, and energy during charge and discharge during one day are separated as illustrated in Figure 5.64. Time of discharge is plotted versus maximal power during each discharge. Furthermore, maximal power during discharge and total energy of each discharge during one day are plotted for each strategy. Discharge power of energy storage by droop control is less than the others and spreads in wide range of small values as shown in Figure 5.65(a). Energy storage by strategy with limitation diagram participates less often than the other strategies (see Figure 5.65(b)). Time discharge of energy storage by limitation diagram is also shorter than the other strategies. Time, power, and energy discharges of filter strategies #1, #2, #3, and #4 are quite identical.

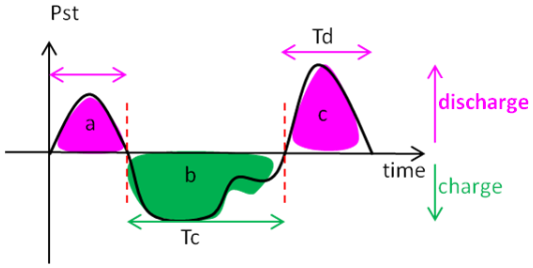

Figure 5.64 Power of energy storage during charge and discharge

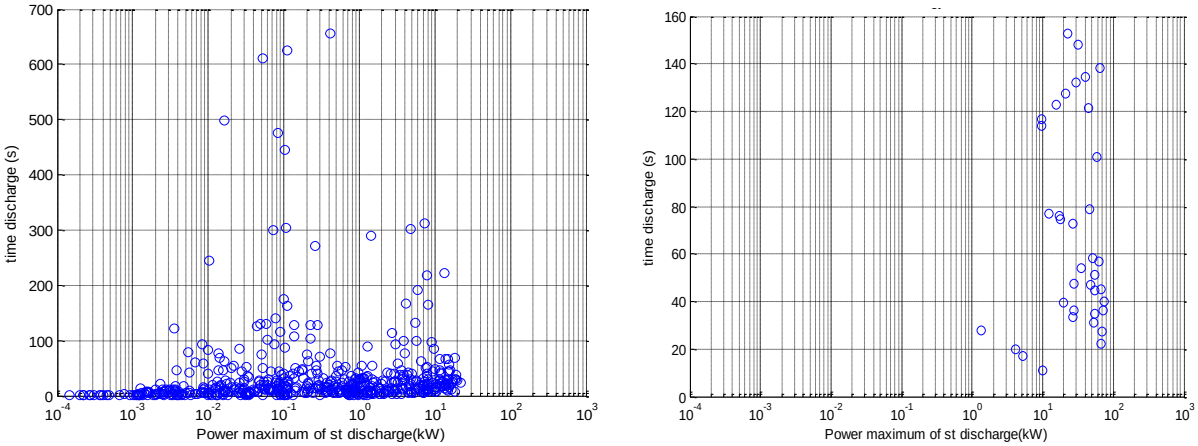

(a) (b)

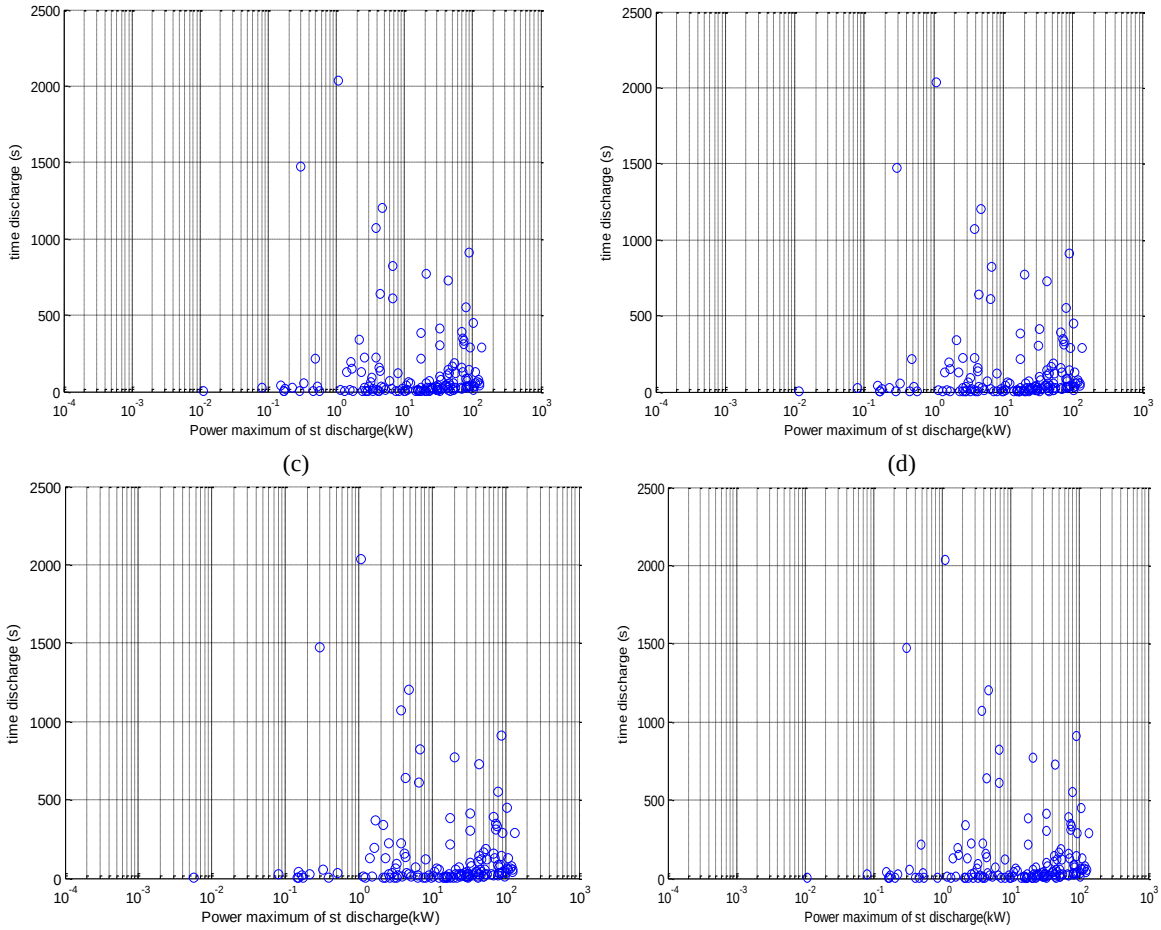

Figure 5.65 Discharge power and time of energy storage during one day by (a) Droop control strategy (b) Strategy with ΔP_{pv} diagram for ESS (c) Filter strategy #1 (d) Filter strategy #2 (e) Filter strategy #3 (f) Filter strategy #4

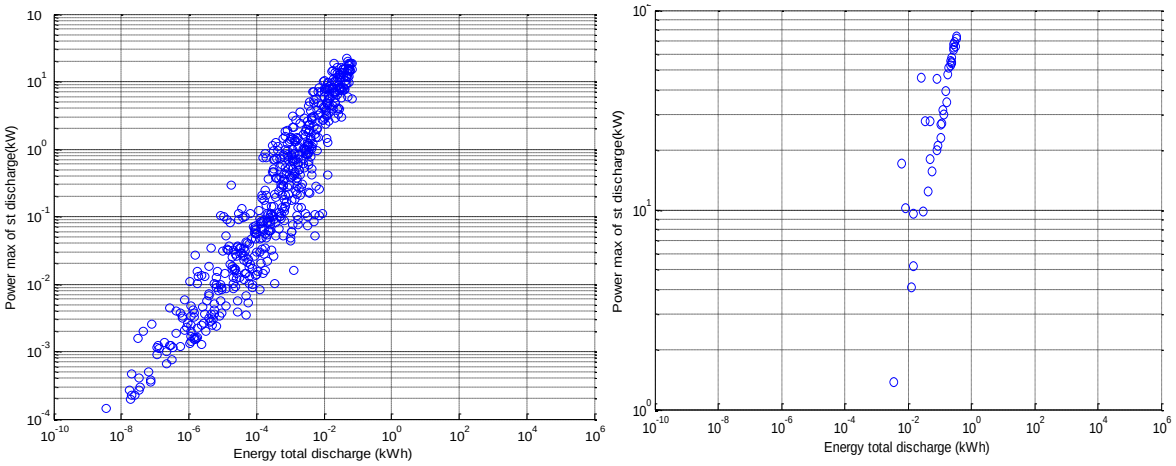

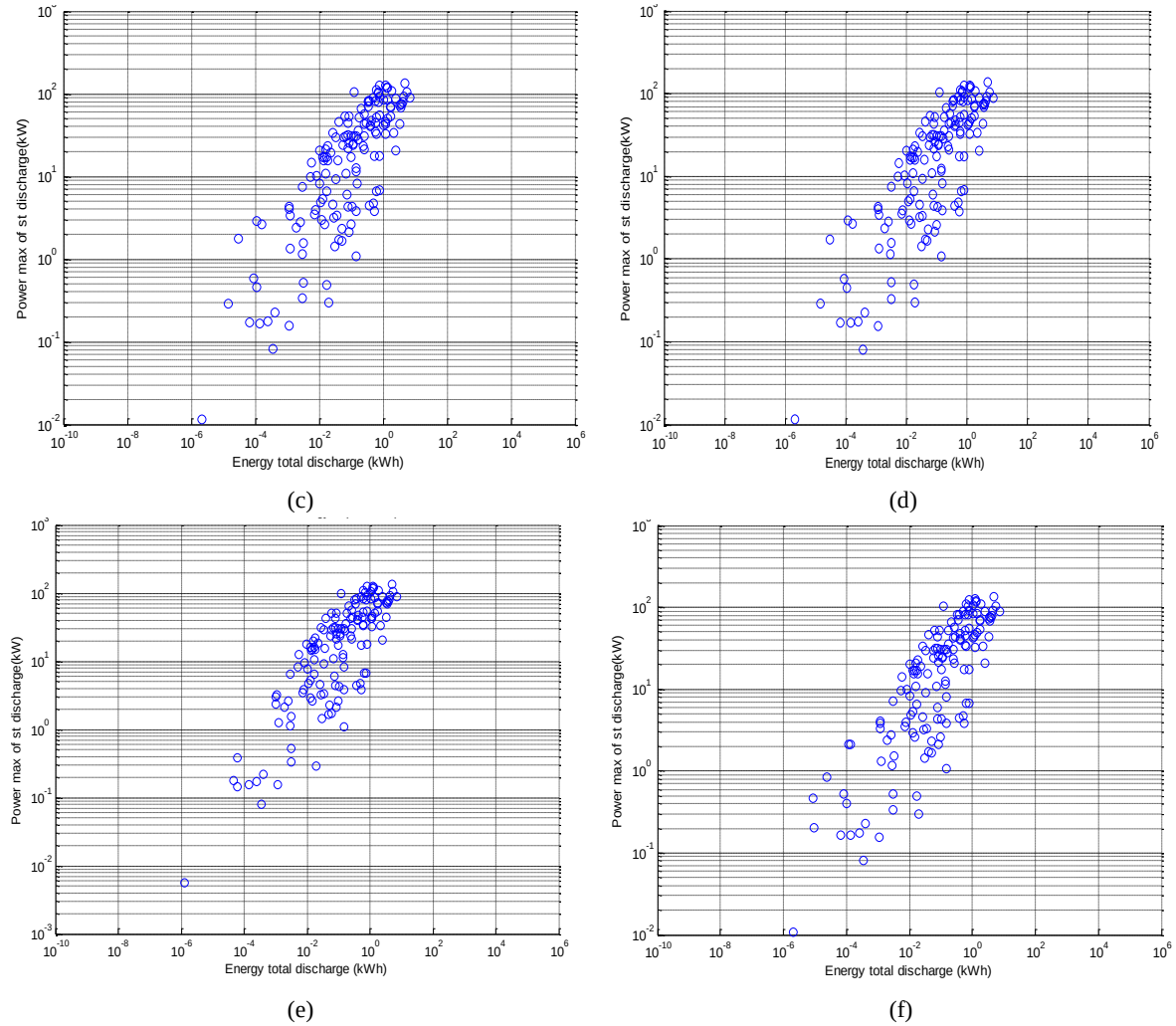

Figure 5.66 Maximal power during discharge and total energy of each discharge during one day (a) Droop control strategy (b) Strategy with ΔP_{pv} diagram for ESS (c) Filter strategy #1 (d) Filter strategy #2 (e) Filter strategy #3 (f) Filter strategy #4

From Figure 5.66 (a) to (f), energy of the maximal discharge and power at this point are plotted in the Ragone diagram in Figure 5.67 [44]. Maximal values of discharge power and energy of all filter strategies are larger than strategy with limitation diagram and droop control and correspond to technological choice as flywheel (all couples of data (energy, power) are quite included in the flywheel zone of normal operation). Strategy with limitation diagram is included in the zone of double layer capacitor or flywheel actions. The maximal discharge time of each strategy in Figure 5.65 (a) to (f) and power at this point are also plotted in Figure 5.68(a). The maximal power discharge and its time discharge are shown in Figure 5.68(b).

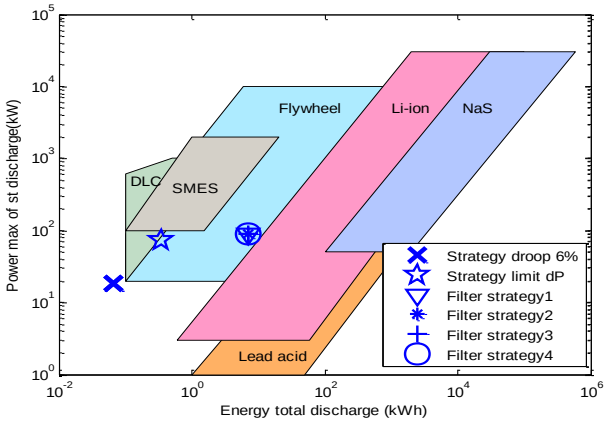

Figure 5.67 Power discharge and energy total discharge maximal 26/08/2011

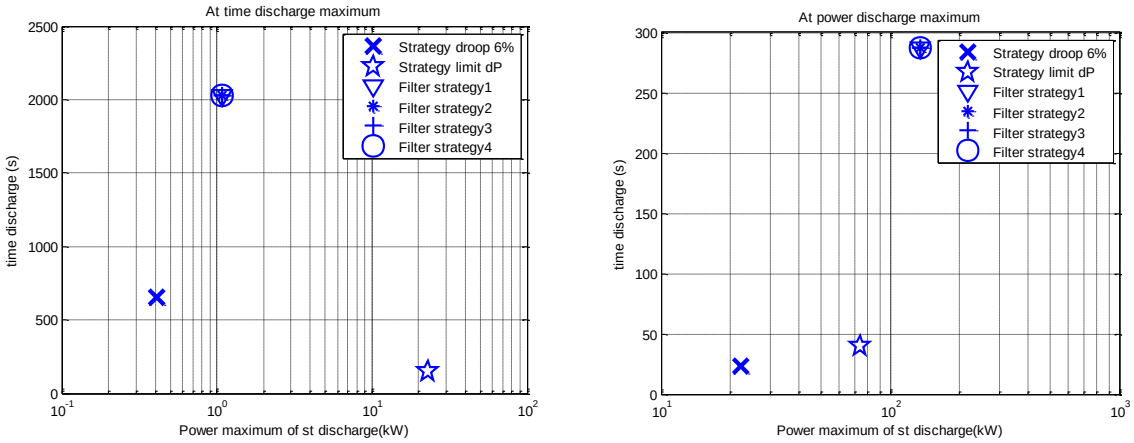

(a) (b)

Figure 5.68 (a) Maximal time discharge and power discharge at this time discharge (b) The maximal power discharge and time discharge at this power discharge

PV power signal on 20/10/2011 which is the most fluctuated signal is also analysed. The maximal energy discharge and its discharge power of all strategies are plotted on Ragone diagram in Figure 5.69. In the same way, the maximal time discharge and its discharge power are illustrated in Figure 5.70(a) and the maximal power discharge and its time discharge are shown in Figure 5.70(b). Filter strategies are included in the "battery" zone (as Li-ion). Strategy with limitation diagram is in the zone of flywheel and SMES. The maximal time discharges of all filter strategies are larger than the others for all two days in Figure 5.68(a) and Figure 5.70(a). Maximal power discharges of different filter strategies are larger than the others for two days in Figure 5.68(b) and Figure 5.70(b). At the point of the maximal time discharge, discharge power of energy storage by strategy with limitation diagram is larger than the others.

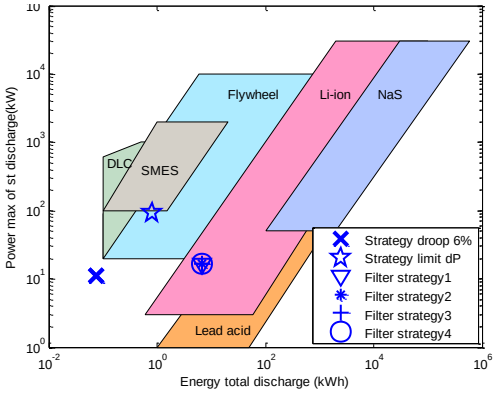

Figure 5.69 Power discharge and energy total discharge maximal 20/10/2011

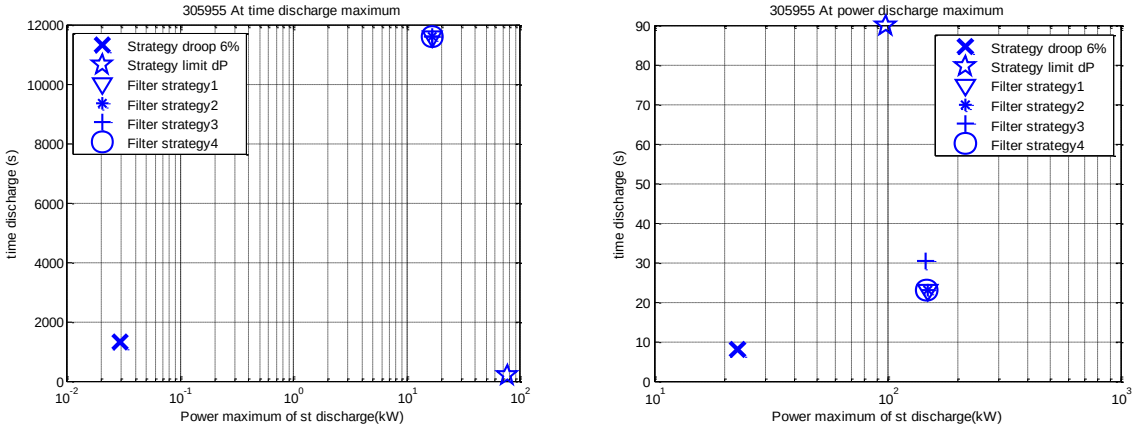

(a) (b)

Figure 5.70 (a) Maximal time discharge and power discharge at this time discharge (b) The maximal power discharge and time discharge at this power discharge

In the following section, impact of cut-off frequency of high pass filter of strategy #2 is studied. When cut-off frequency increases, maximal power discharge is quite identical but energy discharge decreases as shown in Figure 5.71 because energy storage participates less. For cut-off frequency 0.001 Hz, power and energy is in battery zone but for other cut-off frequencies they are in capacitor or flywheel zone. For low cut-off frequency, energy storage should have high energy density. In Figure 5.72(a), maximal time discharge of cut-off frequency 0.001 Hz is much larger than the others. And power discharge at this time discharge is also very high. The maximal power discharge in Figure 5.72(b) of all cut-off frequencies does not have too much different. The maximal power discharge of cut-off frequency 0.001 Hz is always the highest.

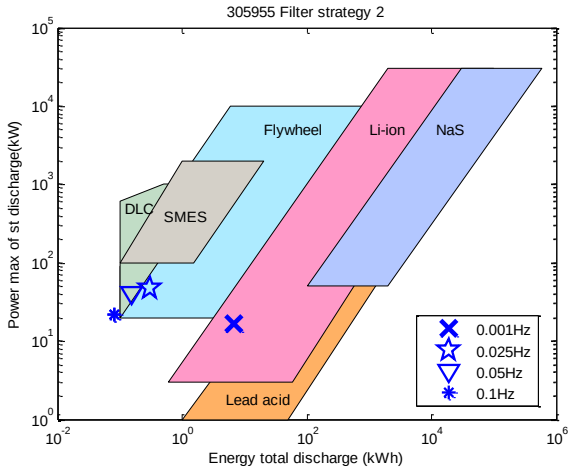

Figure 5.71 Power discharge and energy total discharge maximal with strategy #2 on 20/10/2011

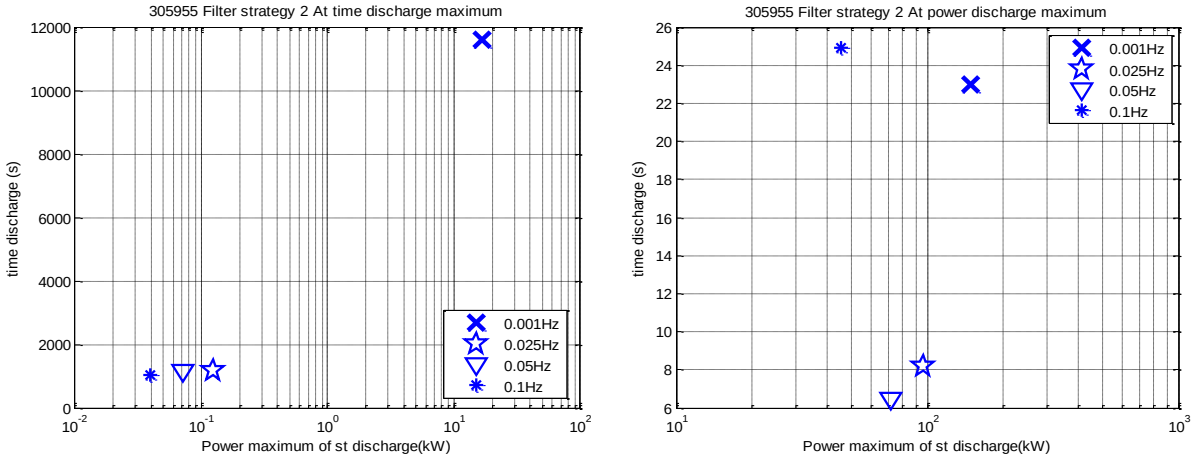

(a) (b)

Figure 5.72 (a) Maximal time discharge and power discharge at this time discharge (b) Maximal power discharge and time discharge at this power discharge

5.5.4 Impact of PV penetration rate (version provisoire)

Rate penetration PV is the proportional between power installed of photovoltaic and summation of power of all production units. All previous simulations, power rated of diesel and PV are 1.6MW and 250 kW respectively, and rate of penetration is about 16%. Power rated of PV is increased to rising rate penetration of PV. On the other hand, rate penetration of PV is reduced by decreasing of power installed of PV shown in Table 5.5. Power PV signal on 20/10/2011, which is the most fluctuated signal, is then defined as the source of disturbance in this simulation. Firstly, each strategy is studied. Power rated of energy storage is 0.3MW for the first three strategies except the last filter strategy 4 which is 1MW of energy storage.

Table 5.5: Power rated of diesel and PV penetration rate

Power rated of diesel (kW)	Power installed of PV (kW)	Rate penetration PV (%)
	133.33	8.33%
	160.00	10.00%
	200.00	12.50%
	250.00	**15.63%**
1600	333.33	20.83%
	400.00	25.00%
	533.33	33.33%
	666.67	41.67%
	800.00	50.00%

5.5.4.1 System initial (without energy storage system)

System without energy storage system is simulated with different power rated of PV. Their frequency response and power of primary control of diesel is illustrated in Figure 5.74(a) and (b). Frequency deviation increases when PV penetration rate increases (power rated of diesel reduces). Power of primary control of diesel is increased with the increase of penetration rate of PV because the frequency variation has been raised up. Small diesel generator with droop 8% cannot guarantee frequency performance. Droop value of primary control should be reduced or energy storage system should be installed in order to improve frequency response of system with high PV penetration rate.

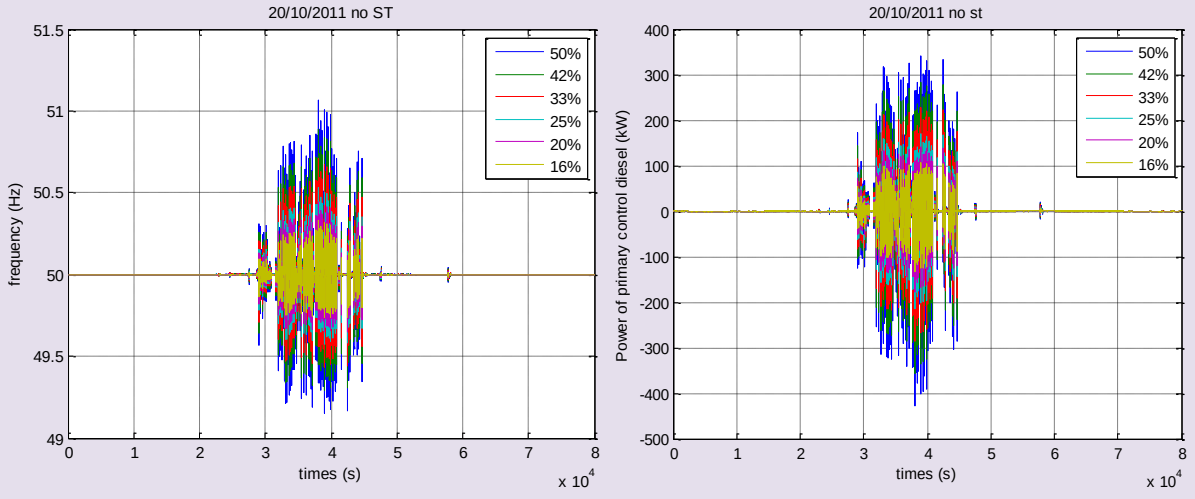

(a) (b)

Figure 5.74 (a) Frequency response (b) Power of primary control of diesel generator of power system without energy storage system for various penetration rates of PV on 20/10/2011

5.5.4.2 Droop control strategy for energy storage system

In this study, energy storage system is controlled by classical primary frequency control to coordinate with the diesel generator in frequency regulation. Firstly, droop value 6% is selected for the study with various PV penetration rates. Frequency deviation; shown in Figure 5.75(a), increases with the increase of penetration rate of PV which is similar to the system without energy storage system. Furthermore, power of ESS also rises up when PV penetration rate increases as shown in Figure 5.75(b). Power of primary control of diesel generator which is illustrated in Figure 5.75(c) will decrease when penetration rate of PV grows up which is opposite to the system without ESS. Droop value or power rated of energy storage has to be adapted when penetration rate increases.

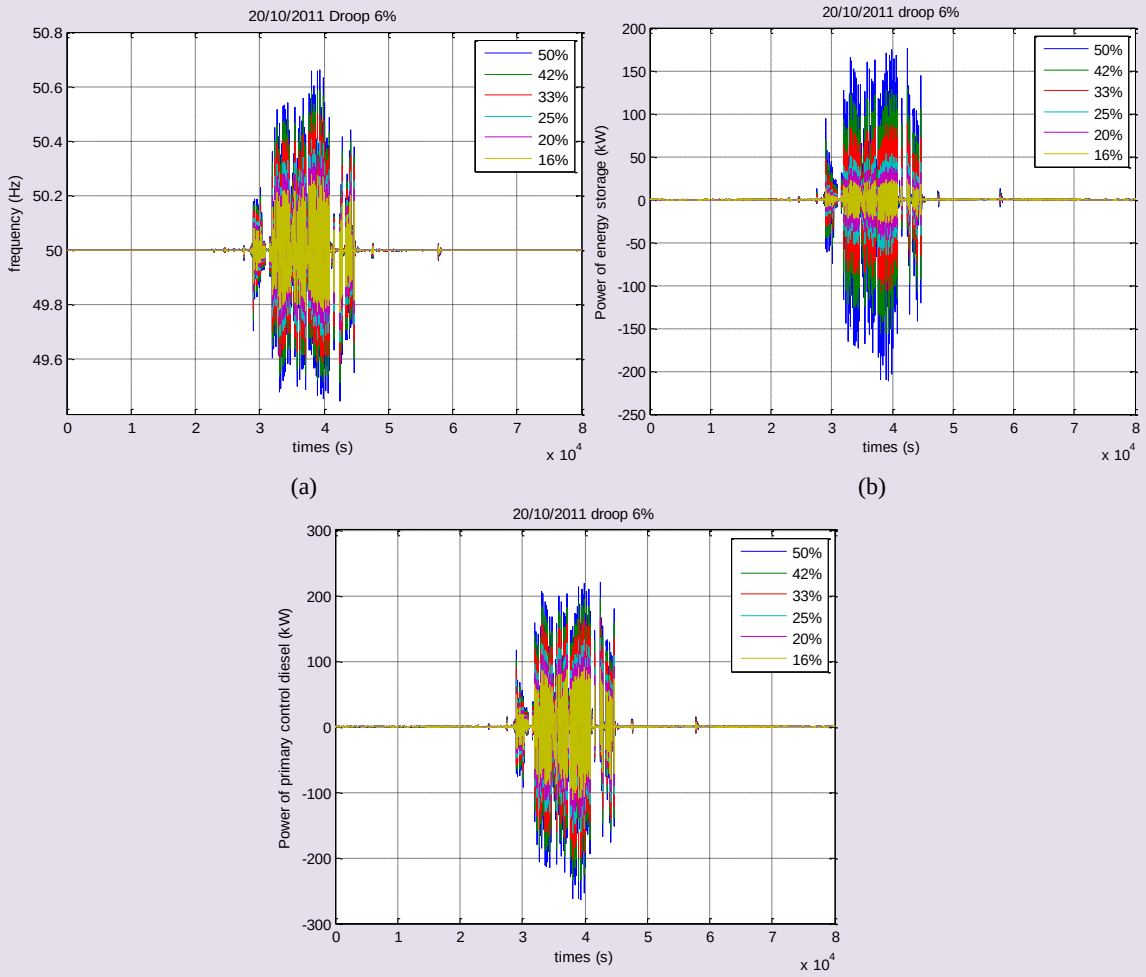

Figure 5.75 (a) Frequency response (b) Power of ESS (c) Power of primary control of diesel generator of power system with ESS by droop control for various penetration rates of PV

5.5.4.3 Strategy with limit ΔP_{pv} diagram

This strategy causes some large frequency variation in large high penetration rate of PV as illustrated in Figure 5.76(a) which could be a problem of determination of power reference (P0). Parameters of algorithm of this strategy will be adapted later in 5.5.4.6 according to the penetration rate of PV. Power of ESS is larger when PV penetration rate increases in Figure 5.76(b) but power of primary control of diesel decreases in Figure 5.76(c).

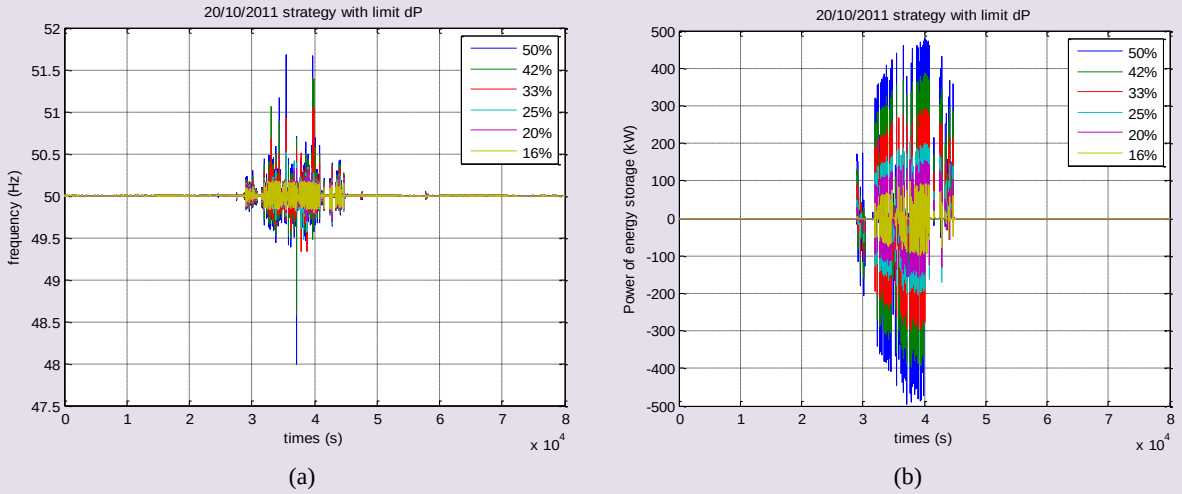

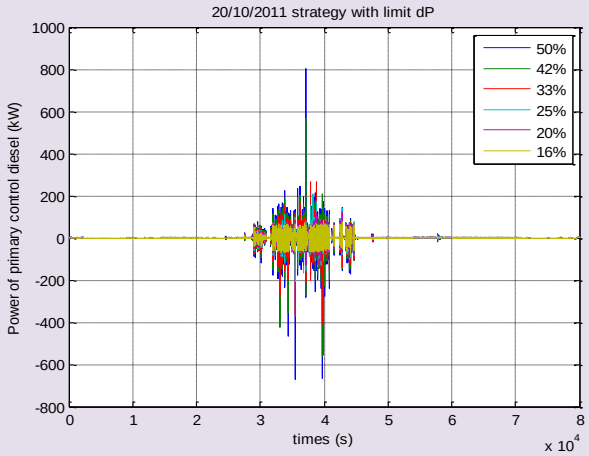

(c)

Figure 5.76 (a) Frequency response (b) Power of ESS (c) Power of primary control of diesel generator of power system with ESS by strategy with limit ΔPpv diagram for various penetration rates of PV

5.5.4.4 Filter strategy 1 to 4

The filter strategy 2 is the representative of all filter strategies. For cut-off frequency 0.001Hz, frequency variation in Figure 5.77(a) is very small for all rate penetration PV and is always in the acceptable limit (49.8-50.2Hz). On the contrary, frequency variation is very large for cut-off frequency 0.025 Hz, and larger than the acceptable limit for PV penetration rate over 25% in Figure 5.77(b).

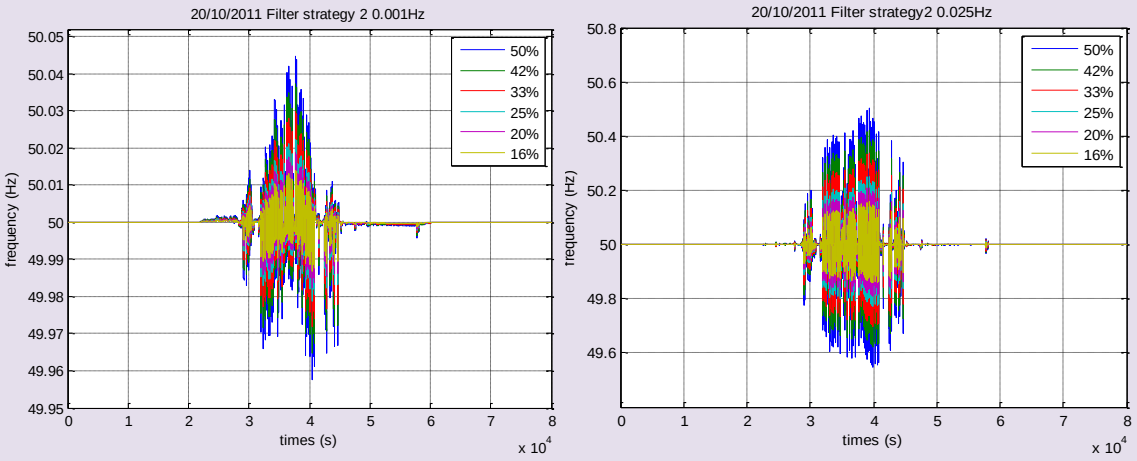

(a) (b)

Figure 5.77 Frequency response with cut-off frequency (a) 0.001Hz (b) 0.025Hz of power system with ESS by filter strategy 2 with various penetration rates of PV

5.5.4.5 Comparison of all strategies

Number of occurrences which frequency is out of limit (over 50.2 or less than 49.8) with different rate of penetration PV for each strategy shown in Table 5.4 are plotted in Figure 5.78. Number of occurrences which frequency deviation is more than 0.2 Hz increase when penetration rate of PV rises up as shown in Figure 5.78. For very low PV penetration rate (less than 8%), energy storage system is needless because frequency is always in the acceptable limit because frequency control of diesel generator can guarantee frequency performance.

Droop control for energy storage system can reduce frequency deviation but it cannot retain all frequencies in the acceptable limit for high penetration PV. Droop 6% can guarantee frequency performance (frequency in the acceptable limit) until the penetration rate touches 10% (power rated of PV 160kW). For high penetration PV, droop value for ESS has to be decreased or power rated of ESS should be increased to guarantee frequency performance.

Filter strategy 2 and 3 with cut-off frequency 0.001Hz can guarantee frequency performance for all power rated of PV (133kW to 800kW). However, for PV penetration rate over 40%, some frequencies deviation of filter strategy 3 is larger than the acceptable limit. Frequency is always in the limit because cut-off frequency is very small and working window of ESS (fast response source) is very large. Power of primary frequency control of diesel for penetration rate of PV 16% (power rated of PV 250kW) is very small. Therefore, it can be cited that cut-off frequency of 0.001Hz of filter strategies 2 and 3 can guarantee frequency performance for all rates of penetration less than 50%. If the reduction of power of the diesel generator is the purpose, low cut-off frequency (like 0.001Hz) is suitable. However, for low penetration rate of PV, energy storage is over sizing for this low cut-off frequency. The cut-off frequency has to be designed in relation to rate of penetration of PV which will be elaborated later.

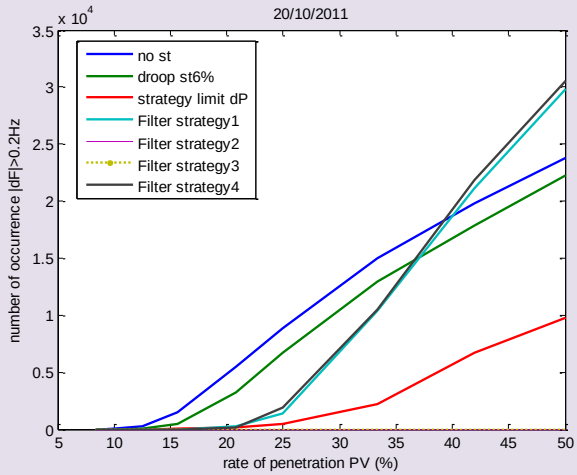

Figure 5.78 Number of occurrence of over limit frequency variation versus penetration rates of PV for different strategies

Strategy limit ΔPpv diagram causes less number of occurrences than frequency which is out of the limit than filter strategies 1 and 4 when rate of penetration of PV increases. However, it causes worse frequency problem than system without energy storage system for PV penetration rate over 40%. Performance of filter strategies 1 and 4 depend on the cut-off frequency. Therefore, for high penetration PV, cut-off frequency has to be reduced. For strategy limit ΔPpv diagram, parameter dP_steady which is used to define power reference (P0) has to be adapted.

The maximum power of ESS and its energy used with different rate of penetration PV are illustrated in Figure 5.79. Power maximum and energy used of ESS of droop control 6% are always smaller than the others and increase when rate penetration PV rises up. Furthermore, their values by all filter strategies are quite identical and constant for all PV penetration rates. They also rise up quite rapidly in low penetration rate of PV but will be slow for rate of penetration higher than 30%. For PV rate of penetration over 30 %, energy used of ESS by strategy with limit ΔPpv diagram is larger than by filter strategies.

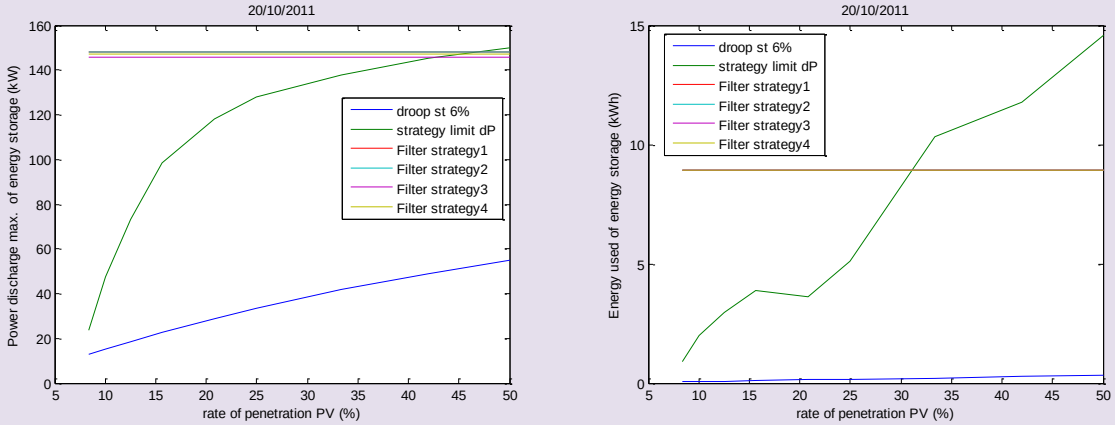

(a) (b)

Figure 5.79 (a) Power discharge maximum (b) Energy used of ESS versus penetration rates of PV for different strategies

Power maximum and energy used of primary control of diesel are analyzed. Power maximum and energy used of primary control of diesel of no energy storage system, filter strategy 2, and 3 is constant for all penetration rates of PV in Figure 5.80. Power maximum of primary control of strategy with limit ΔPpv diagram is higher than the others for rates of penetration over 25%. Power and energy of filter strategies 2 and 3 are much smaller than the others. For droop strategy, power falls down when rate penetration PV increases.

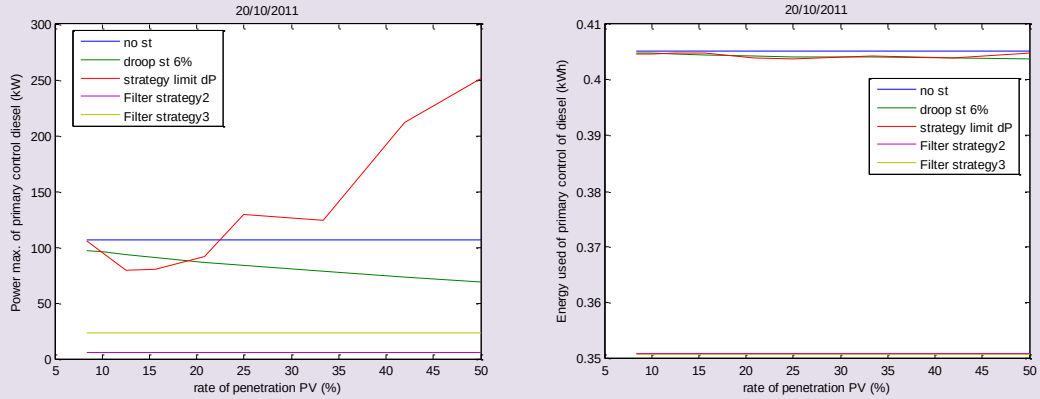

(a) (b)

Figure 5.80 (a) Power maximum (b) Energy used of primary control of diesel versus penetration rates of PV for different strategies

5.5.4.6 Improve control strategy according to rate penetration PV

According to previous topic, rate penetration of PV has an influence on control strategy of energy storage system. Objective of this study is to find out how to determine the parameters of control strategies for high penetration PV while frequency performance will be guaranteed.

a) Droop control strategy

To guarantee frequency performance for high penetration PV, droop value of energy storage system should be low and/or power rated of energy storage should be increased. Number of occurrence over the limit frequency variation is lessen when the droop decreases as illustrated in Figure 5.81(a). Small droop value for energy storage can guarantee frequency performance for high penetration rate of PV. Power maximum of primary control of diesel is very small for low droop value of energy storage as shown in Figure 5.81(b). Nevertheless Figure 5.82 shows that power and energy of energy storage for smaller droop is larger than the others.

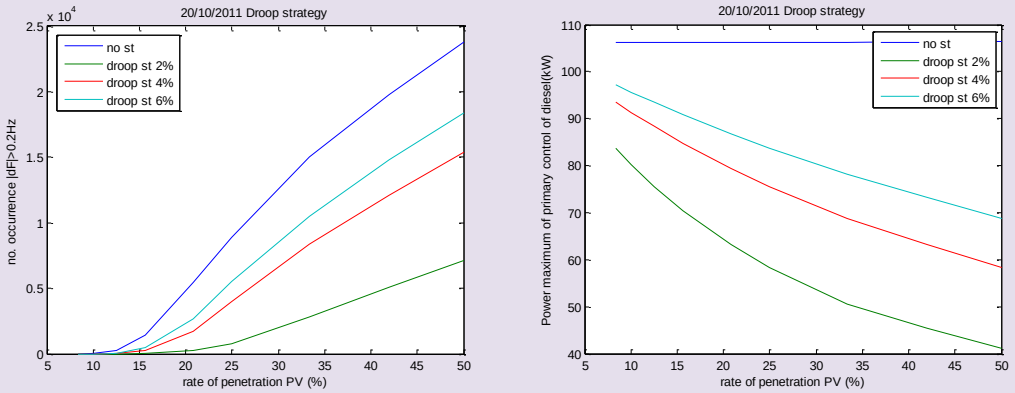

(a) (b)

Figure 5.81 (a) Number of occurrence of over limit frequency variation (b) Power maximum of primary frequency control of diesel generator versus penetration rates of PV of droop control strategy for ESS

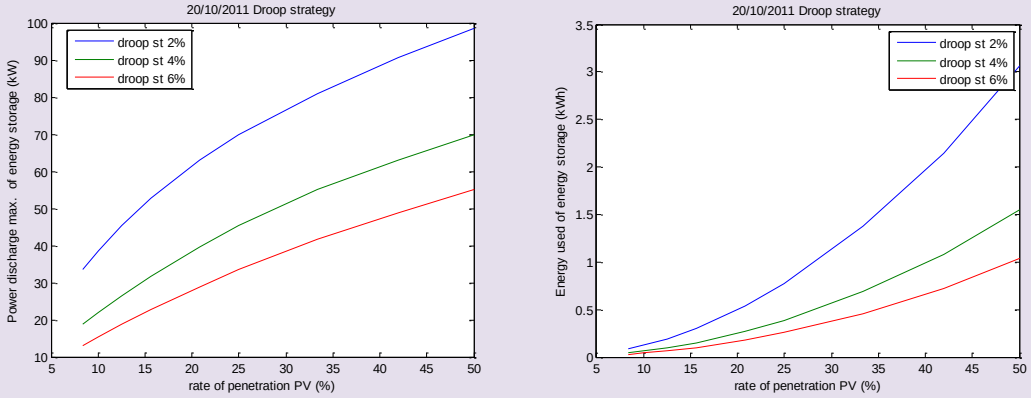

(a) (b)

Figure 5.82 (a) Power discharge maximum (b) Energy used of ESS versus penetration rates of PV of droop control strategy for ESS

Various droop values for ESS are compared to the other strategy and are illustrated in Figure 5.83. Droop for ESS should be 2% in order to have number of occurrence less than strategy with the limit ΔP_{pv} diagram. For high penetration of PV, only small droop value is not sufficient to decrease frequency deviation. Power rated of energy storage should be increased too.

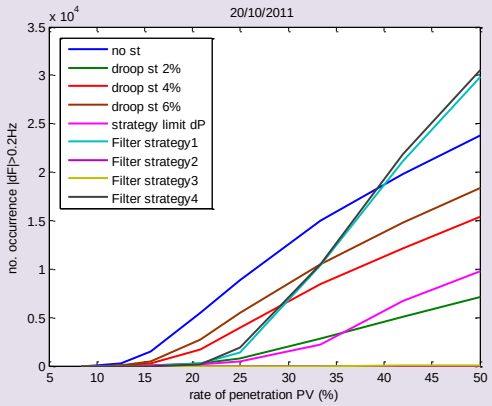

Figure 5.83 Number of occurrence of over limit frequency variation versus penetration rates of PV for different droop values of ESS (comparing to other strategies)

Power rated of energy storage is then increase to 0.5MW (initial power rated is 0.3MW) with droop 2% for different penetration rates of PV. Number of occurrence which frequency deviation over 0.2 Hz is decreased by rising power rated of energy storage in Figure 5.84.

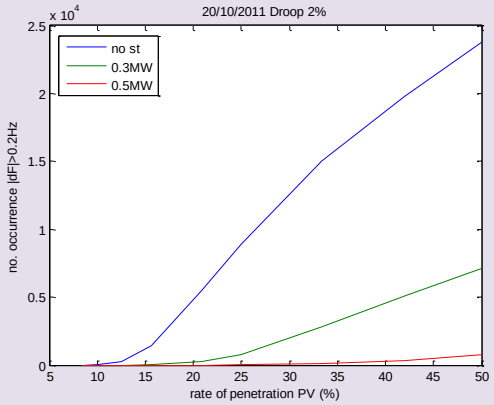

Figure 5.84 Number of occurrence of over limit frequency variation versus penetration rates of PV of droop control strategy for ESS (with different power rated of energy storage)

b) Filter strategies

Figure 5.78 shows that filter strategies 1 and 4 cannot guarantee frequency performance in high penetration of PV. Droop and/or power rated of energy storage have to be adapted similar to the droop control strategy which has been presented in the previous topic for filter strategy 4. In case of filter strategy 1, cut-off frequencies of two filters have to be very small in high penetration rate of PV (in case of similar cut-off frequency for two filters). Besides, cut-off frequency of high pass filter for energy storage system should be small; but that of low pass filter for diesel generator should be large in order to increase the working band of each power source. In this topic, cut-off frequency of filter strategies 2 and 3 are redesigned. Frequency response of power system with energy storage system by filter strategy 2 is always in the acceptable limit for cut-off frequency 0.001Hz when PV penetration rate grows up as shown in Figure 5.78. Cut-off frequency 0.01Hz can bring frequency into the acceptable limit until the rate is approached 34% as illustrated in Figure 5.85. Large cut-off frequency can also guarantee frequency performance in small rate of penetration. Therefore, cut-off frequency should be selected in relation to power rated of diesel or penetration rate of PV. Although small cut-off frequency such as 0.001Hz can guarantee frequency performance in large window of penetration rate of PV, ESS is over used in low penetration rate.

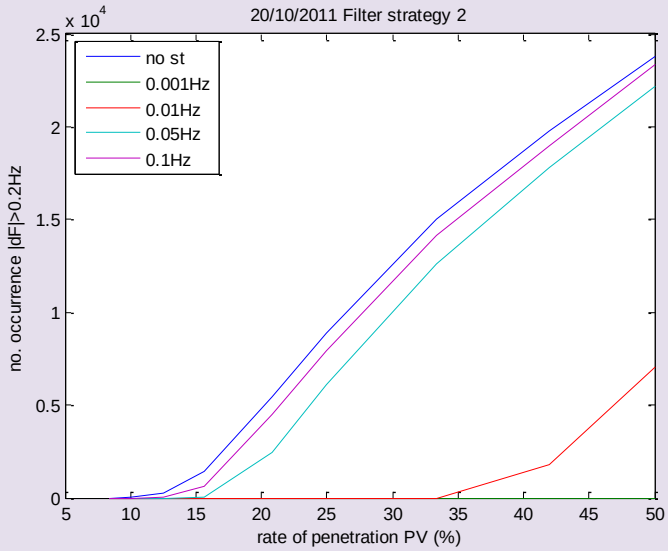

Figure 5.85 Number of occurrence of over limit frequency variation versus penetration rates of PV of filter strategy 2 with various cut-off frequencies

Power maximum and energy used of ESS are illustrated in Figure 5.86. Power of ESS is constant for all rates of penetration as shown in Figure 5.86(a) and it is maximal at cut-off frequency

0.001Hz. Energy used as illustrated in Figure 5.86(b) increases when penetration rate of PV increases and energy used of cut-off frequency 0.001 Hz is always higher than the others.

Power maximum and energy used of primary control of diesel are shown in Figure 5.87. Power maximum is always constants for all PV penetration rates. It is obvious that ESS can reduce power maximum of the initial system (without energy storage system). Power maximum of cut-off frequency 0.001Hz is less than the others. Energy used shown in Figure 5.87(b) is quite identical for cut-off frequency 0.01-0.1Hz but energy used of cut-off frequency 0.001Hz is much less than the others.

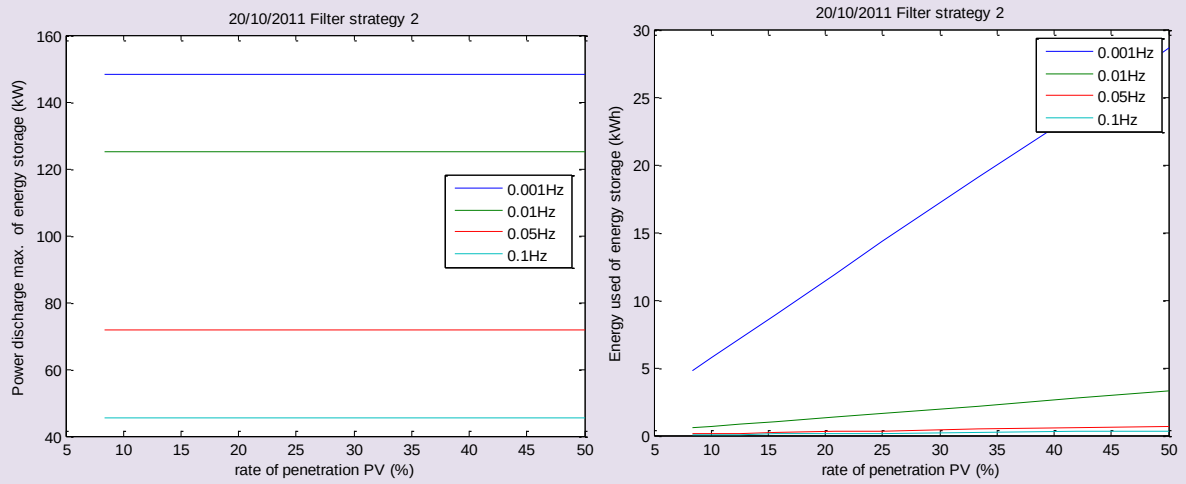

(a) (b)

Figure 5.86 (a) Power discharge maximum (b) Energy used of ESS versus penetration rate of PV of filter strategy 2 with various cut-off frequencies

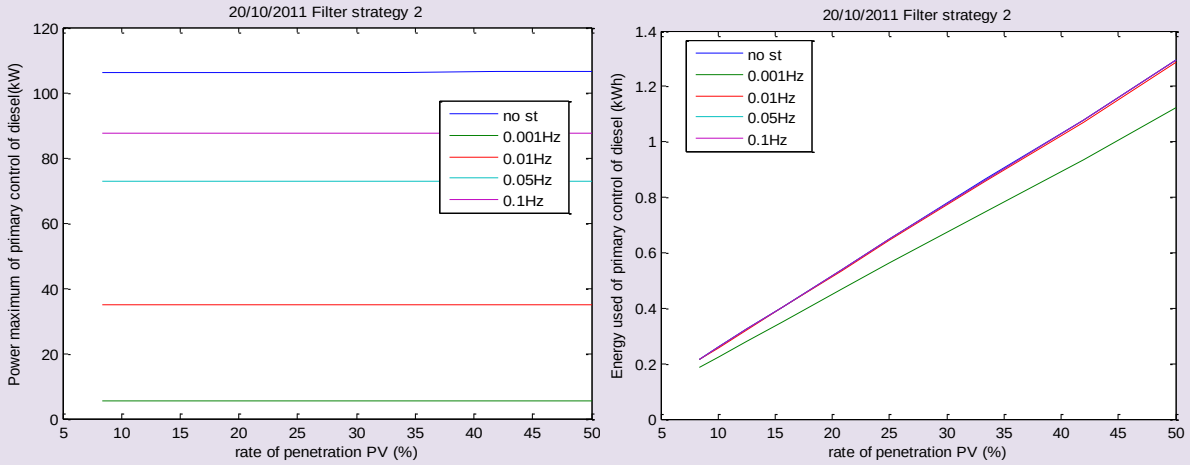

(a) (b)

Figure 5.87 (a) Power maximum (b) Energy used of primary frequency control of diesel generator versus penetration rate of PV of filter strategy 2 with various cut-off frequencies

All cut-off frequencies of filter strategy 2 are then compared to the other strategies and illustrated in Figure 5.88. For penetration rate of PV over 15%; filter strategy 2 with cut-off frequency 0.05 and 0.1Hz has more number of occurrence which frequency is out of limit more than droop control strategy (droop 6%). For cut-off frequency 0.001 and 0.01Hz have better frequency performance than the others (but similar to filter strategy 3) for all PV penetration rates.

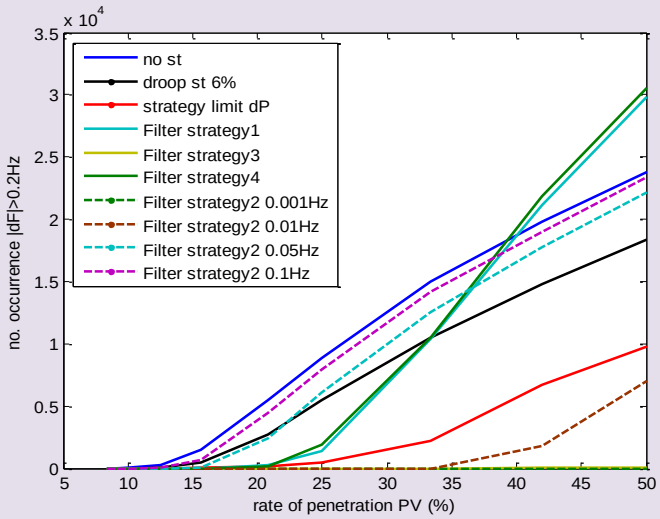

Figure 5.88 Number of occurrence of over limit frequency variation versus penetration rate of PV for different cut-off frequencies of filter strategy 2 (comparing to other strategies)

As having mention earlier, cut-off frequency of filter strategy 2 can be selected relying on the penetration rate of PV. Defining cut-off frequency from different penetration rates can be done as follows:

1. Define frequency deviation acceptable (dF_std)
2. Define power variation maximum of PV (dPmax)
3. Calculate Amp_bode_max in (5.15)
4. Read frequency cut-off maximal (F_cut_max) at Amp_bode_max from Bode diagram in Figure 5.89. Consequently, cut-off frequency can be selected as less than or equal to this frequency cut-off maximal.

$$\textbf{Amp\_bode\_max} = \textbf{20*log(|dF\_std|/|dPmax|)} \quad (5.15)$$

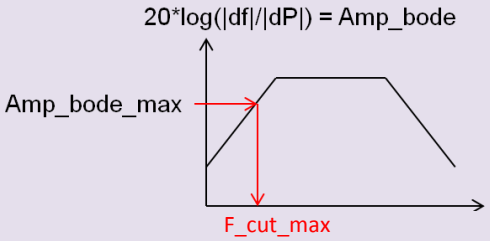

Figure 5.89 Cut-off frequency maximum selected for filter strategy 2 from Magnitude of Bode diagram of transfer function between frequency variation and power variation

For example, dF_std is selected at 0.2Hz (0.2/50 per unit) and dPmax is 50% of power rated PV (0.5*250/1600 per unit) for power rated of diesel 1600kW and the Amp_bode_max is -25.82dB. From bode diagram in Figure 5.90; F_cut_max is 0.3rad/s or 0.05Hz. It then can be seen from Figure 5.88 that number of occurrence of cut-off frequency 0.05Hz is always zero until the penetration rate gets to 16% (power rated of PV 250kW).

If rate penetration is 25% (power rated of PV 400kW), F_cut_max will be 0.012Hz which can be seen from Figure 5.88. The cut-off frequency 0.01Hz can keep frequency in the acceptable limit for penetration rate of 25%.

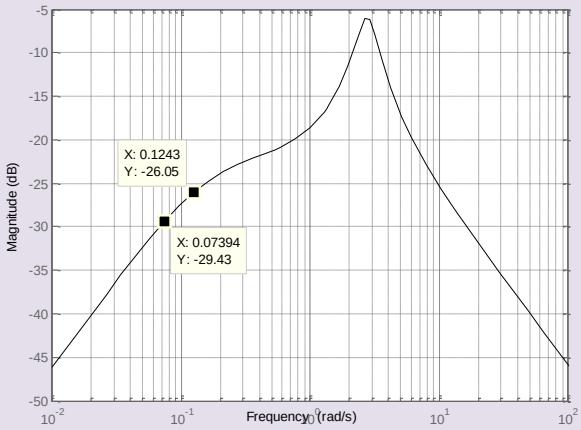

Figure 5.90 Magnitude of Bode diagram of transfer function between frequency and power variations

For filter strategy 3 (band pass filter for ESS), low cut-off frequency has been selected as the same as the filter strategy 2 mentioned above. High cut-off frequency should be adapted for high penetration rate. To select high cut-off frequency, Amp_bode_max is used and read maximal of high cut-off frequency (F_cut_max2) which is higher than the previous cut-off frequency maximal (F_cut_max) shown in Figure 5.91.

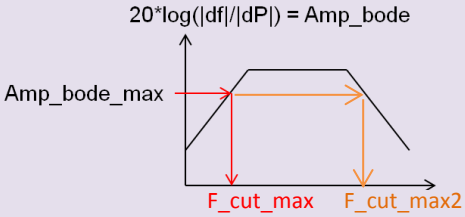

Figure 5.91 Cut-off frequency maximum selected for filter strategy 3 from Magnitude of Bode diagram of transfer function between frequency and power variations

c) Strategy with limit ΔPpv diagram

Finally, control parameters of strategy with limit ΔPpv diagram have to be adapted. Parameter dP_std and t_std which are used to define or change power reference (P0) should be modified when penetration rate of PV increases. For PV penetration rate 20% (power rated of PV 320kW), number of occurrence which frequency is out of limit of strategy with limit ΔPpv diagram (dP_std 5e-4 per unit, t_std 5 seconds) is 190. If dP_std is 1e-7 per unit and t_std is 30 seconds, frequency is always in the acceptable limit. However, in the same situation but with power rated of PV 400kW (25% penetration rate), number of occurrence is reduced from 509 to 9. Therefore, parameter dP_std should be decreased and t_std should be increased when PV rate of penetration increases. Although parameter dP_std 1e-7 and t_std 30 seconds causes less frequency variation, it makes energy storage always in charge mode. Furthermore, energy storage system also participates in secondary control. Therefore, energy storage system in high penetration rate of PV should participate in secondary control. As slow fluctuation (large duration of charge dP) causes more impact on frequency than low penetration rate of PV. This means that energy rated (maximum) of energy storage should be high.

5.5.5 Sizing of energy storage

Energy storage installed in isolated micro power system generally is designed according to its control strategy and/or cost and/or power system. Generally, energy storage is installed to coordinate with diesel generator in frequency regulation. Power rated of energy storage by droop control depends on primary frequency control parameters of thermal plant (droop and power rated) and droop value of energy storage [38]. Referring to the sizing of energy storage by [19] which has concerned with improving transient response of frequency after load disturbance by injecting power at power rated of energy storage. The optimal sizing of energy storage is also proposed in [65] with new algorithm

which has used overloading characteristics of BESS including characteristics overloading capacity and permissible overloading duration.

Furthermore, energy storage is installed to system with renewable energy to maintain the stability or reduce frequency variation. Power rating of energy storage connected to wind farm is designed according to spreadsheets developed on the basis of the probabilistic approach [59]. Energy storage can also be designed by power variation of wind energy [66].

Energy storage installed to this studied system with photovoltaic is designed according to two control strategies presented in 5.3 and 5.4 which can be elaborated as follows.

5.5.5.1 Strategy with limit ΔP_{pv} diagram

Power of energy storage by strategy with limit ΔP_{pv} diagram depends on power measured of PV and power variation maximal (from limitation diagram in Figure 3.22). To design power and energy installed of energy storage, the recorded power variation of PV should be preliminarily known. In 2.4.2 of Chapter 2 (Study characteristics of power fluctuation of photovoltaic), the distribution of power variation (ΔP) for different time differences (Δt) have been founded.

The duration of power change (Δt_d) and the amplitude of power fluctuation (ΔP) which are illustrated in Figure 5.92; are the key parameters which will link data recorded and limitation diagram to sizing the energy storage. It has been assumed that the duration of change (Δt_d) in this chapter equals to the time different (Δt) which is used to calculate the power deviation in 2.4.2 of Chapter 2. The power deviations limited have been known for each duration change. Furthermore, the number of occurrence of power deviation which is larger than the limited power deviation has also been found by 2.4.2 of Chapter 2. Therefore from all these information, the necessity of the installation of energy storage can be finalized with its optimal power and energy rated.

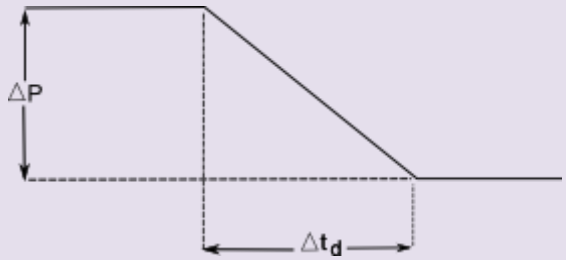

Figure 5.92 Calculation of power variation

From the limitation diagram illustrated in Figure 3.22, the maximum power deviation for each time difference is defined; followed by the recording of the distribution of power deviations in order to find out the number of occurrence which the power deviation is more than the selected limit (in both negative and positive value of power deviation). The power deviation which needs to be regulated for each time difference will then be selected. For example, the limited power deviation of studied system for time difference 10 seconds is 0.08 per unit or 128kW. From the distribution of power deviation for time different 10 seconds of photovoltaic 250kW shown in Figure 5.93, power deviation 128kW (pink line) is the acceptable maximum frequency variation. Power deviation over 128kW can cause frequency variation over the selected acceptable limit. The energy storage in this issue will take part to change power deviation characteristic which will affect to the frequency variation. Power deviation problem selected 150kW (red line) is brought back to the limitation (bring red line to pink line) by energy storage. Furthermore, the new acceptable point can be power in the acceptable zone (green line) to assure the stability of optimal frequency performance (bring red line to green line). In this case, power rated and energy installed of energy storage should be higher.

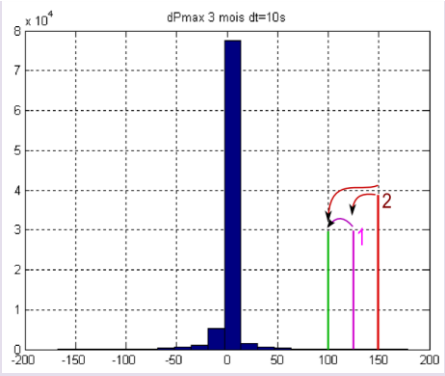

Figure 5.93 Distribution of power deviation maximal in 3 months for time different 10 seconds with different case study

If the purpose is to bring the power deviation problem (power deviation that needed to be regulated) to the limited line (first case), there will be three choices of regulation. The first choice or choice A as shown in Figure 5.94(a); the power deviation is kept constant but the duration of change is longer which is illustrated in red line in Figure 5.94(b). This case the energy storage works to smooth down the power deviation of photovoltaic. The new duration of change is turned to Δt_{d1} as shown in Figure 5.94(b). The second choice B; the duration of change is kept constant but the power deviation falls down which is presented in green line in Figure 5.94(b). The new power deviation after being regulated by energy storage is ΔP_1. Finally, the power deviation decreases and the duration of change increases which is the last choice C. This choice has many paths because the power deviation and duration of change can be many values. The power duration changes to ΔP_2 and the duration of change turns to Δt_{d2} as shown in Figure 5.94(b). If choice B is selected, there will then have new power deviation ΔP_1 for duration of change Δt_d; followed by the calculation of power and energy of installed energy storage.

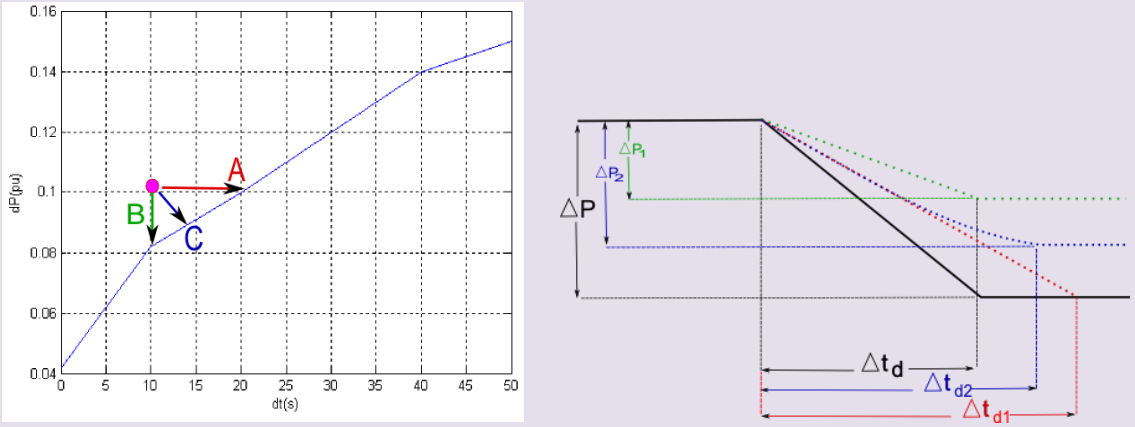

(a) (b)

Figure 5.94 (a) Limitation ΔPpv diagram (b) Power deviation response with different cases of new power deviation

Figure 5.95 illustrates the new power deviation of choice B. The power rated can be defined as the difference between power deviation problem of PV (ΔP_{pv}) and power deviation limit (ΔP_{limit}) as presented in (5.16). The energy of energy storage is the area between the power deviation limit (ΔP_{limit}) for duration of change (Δt_d) and the power deviation (ΔP_{pv}) as shown in Figure 5.95. It has been assumed that energy storage will participate only in transient response (during variation of power PV). While power of PV remains stable (no power variation); frequency response is stable too. Energy storage by strategy with limit ΔP_{pv} diagram will reduce its power (as having mention in 5.3.1 situation 2b in Figure 5.5). Diesel generator which has larger time response will take action in this steady-state response and after that the secondary control of diesel generator will bring frequency back to the nominal value. The energy of energy storage will therefore be at half of the multiple of duration of change and the power of energy storage presented in (5.17).

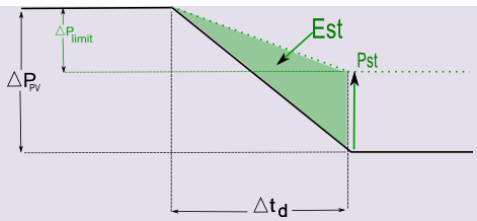

Figure 5.95 Power deviation response of situation B (in green line) comparing to the initial power deviation (in black line)

$$P_{st} = \Delta P_{PV} - \Delta P_{limit} \tag{5.16}$$

$$E_{st} = \frac{1}{2}\Delta t_d (\Delta P_{PV} - \Delta P_{limit}) \tag{5.17}$$

According to the proposed method to sizing the energy storage, this method is applied to studied power system in order to calculate the power rated and energy of energy storage. The power system consists of diesel generator 1.6MW and load. Photovoltaic 250kW is also installed in this power system (PV penetration rate is 16%). The power of this PV is recorded every 5 seconds for 3 months (August to October 2011).

The first step is to analyze whether the energy storage is needed. Figure 5.96 shows the limitation of power deviation (ΔP) of PV for each duration of change (dt). For 5 seconds duration of change, the power deviation limit is 0.04503 per unit or 90kW. Figure 5.97 shows the histogram of the maximum power deviation for 5 seconds duration of change (from intermittent study); some occurrences which the power deviation is larger than 90kW have been observed. Therefore, the energy storage is needed to be installed in this power system.

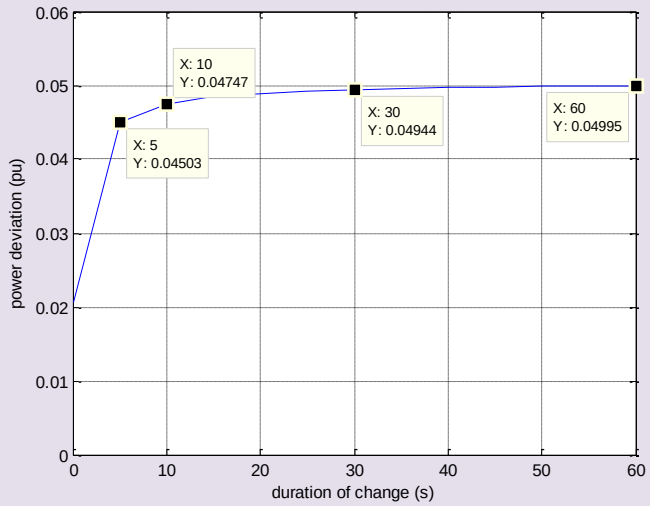

Figure 5.96 Limitation curve of power deviation (ΔP) for different duration of change (dt)

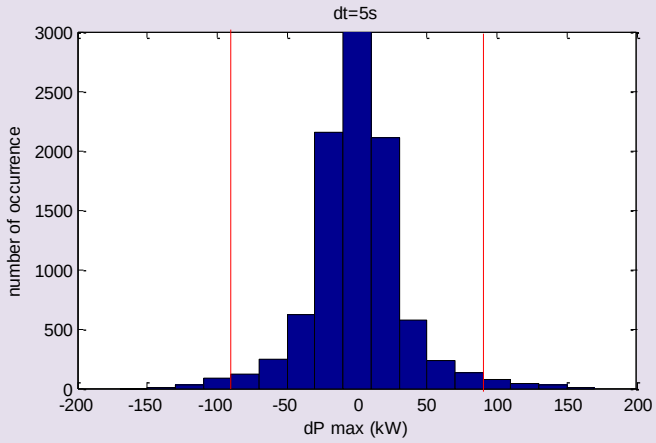

Figure 5.97 Histogram of ΔPmax for dt 5 seconds

Sizing of the energy storage is undertaken. The power and energy of energy storage are calculated for different durations of change (5, 10, 30, and 60 seconds). The power of energy storage presented in (5.16) is the difference between the absolute power deviation of PV (ΔP_{pv}) (in Figure 5.97) and the limit power deviation from curve (ΔP_{limit}) in Figure 5.96. The negative power of energy storage signifies that the energy storage is in charge mode. On the contrary, the energy storage is discharging when the power of energy storage is positive. Consequently, the power of energy storage for each power deviation (ΔP_{pv}) and the number of occurrence of each Pes are defined. The total energy is the multiple of energy storage for one time (in (5.17)) and the number of occurrence.

From Figure 5.97, the power deviation which is more than the limit power deviations (ΔP_{limit}; 90kW in Figure 5.96) for 5 seconds duration of change is presented in Table 5.6 with their number of occurrence. The maximum amplitude of power deviation is +160kW (increase power) and -140kW (decrease power). The mean value of maximum power deviation is used for each power deviation range to calculate the power of energy storage.

The power and energy of energy storage which are calculated from (5.16) and (5.17) are presented in Table 5.6. Energy total is the multiple of energy in kW.s with number of occurrence. The maximum needed powers of energy storage are 50kW and -70kW in charge and discharge modes respectively. While the maximum energy values are 125kWs and 175kWs in charge and discharge modes respectively.

Table 5.6: Data from Figure 5.97 for power deviation which out of limit and Sizing of energy storage for dt 5 seconds

ΔPmax (kW) mean value	-160	-140	-120	-100	100	120	140	160
ΔPmax (kW) range	<-150	-150 to -130	-130 to -110	-110 to -90	90 to 110	110 to 130	130 to 150	>150
no. Occurrence	0	9	26	88	74	44	30	8
Power of energy storage (kW)	70	50	30	10	-10	-30	-50	-70
Energy (kWs)	175	125	75	25	-25	-75	-125	-175
Total Energy (kWh)	0.00	0.31	0.54	0.61	-0.51	-0.92	-1.04	-0.39

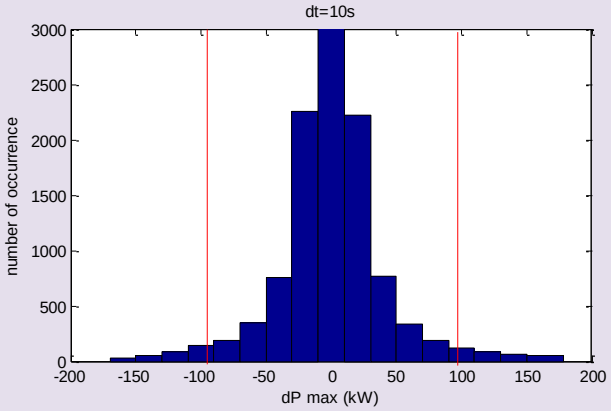

Figure 5.98 Histogram of ΔPmax for dt 10 seconds

Table 5.7: Data from Figure 5.98 for power deviation which out of limit and Sizing of energy storage for dt 10 seconds

ΔPmax (kW) mean value	-180	-160	-140	-120	-100	100	120	140	160	180
ΔPmax (kW) range	<-170	-170 to -150	-150 to -130	-130 to -110	-110 to -90	90 to 110	110 to 130	130 to 150	150 to 170	>170
no. Occurrence	0	23	50	86	142	119	84	68	44	6
Power of energy storage (kW)	85	65	45	25	5	-5	-25	-45	-65	-85
Energy (kWs)	425	325	225	125	25	-25	-125	-225	-325	-425
Total Energy (kWh)	0.00	2.08	3.13	2.99	0.99	-0.83	-2.92	-4.25	-3.97	-0.71

From Figure 5.96, the maximum power deviation is 95kW for 10 seconds duration of change. Power of energy storage for each power deviation of PV which is over limit is presented in Table 5.7. The maximum power of energy storage needed is 65kW and -85kW in charge and discharge modes respectively and are 325kWs in charge and 425kWs in discharge modes for the maximum energy.

Furthermore, energy storage is sized for duration of change 30 and 60 seconds as presented in Table 5.8 and Table 5.9 respectively. Power deviation maximal of time differences 30 and 60 seconds from Figure 5.96 are 99kW and 100kW respectively. Power maximal of energy storage both in charge and discharge modes with energy and total energy for different durations of change are summarized in Table 5.10.

Table 5.8: Data from histogram of power deviation which out of limit and Sizing of energy storage for dt 30 seconds

ΔPmax (kW) mean value	-180	-160	-140	-120	-100	100	120	140	160	180
ΔPmax (kW) range	<-170	-170 to -160	-150 to -130	-130 to -110	-110 to -90	90 to 110	110 to 130	150 to 170	131 to 150	>170
no. Occurrence	18	65	87	122	171	175	114	82	57	27
Power of energy storage (kW)	81	61	41	21	1	-1	-21	-41	-61	-81
Energy (kWs)	1215	915	615	315	15	-15	-315	-615	-915	-1215
Total Energy (kWh)	6.08	16.52	14.86	10.68	0.71	-0.73	-9.98	-14.01	-14.49	-9.11

Table 5.9: Data from histogram of power deviation which out of limit and Sizing of energy storage for dt 60 seconds

ΔPmax (kW) mean value	-200	-180	-160	-140	-120	120	140	160	180	200
ΔPmax (kW) range	<-190	-190 to -150	-170 to -150	-150 to -130	-130 to -110	110 to 130	150 to 170	130 to 150	170 to 190	>190
no. Occurrence	0	29	55	84	120	117	86	60	29	2
Power of energy storage (kW)	100	80	60	40	20	-20	-40	-60	-80	-100
Energy (kWs)	3000	2400	1800	1200	600	-600	-1200	-1800	-2400	-3000
Total Energy (kWh)	0.00	19.33	27.50	28.00	20.00	-19.50	-28.67	-30.00	-19.33	-1.67

Table 5.10: Data summary of power and energy total of energy storage for each duration of change

dt (s)	**Charge**			**Discharge**		
	Pes_max (kW)	**Energy (kWh)**	**Energy total (kWh)**	**Pes_max (kW)**	**Energy (kWh)**	**Energy total (kWh)**
5	50	0.035	0.31	70	0.049	0.39
10	65	0.090	2.08	85	0.118	0.71
30	81	0.338	6.08	81	0.338	9.11
60	80	0.667	19.33	100	0.833	1.67

Power of energy storage in charge mode is maximal at 80kW to 81kW for 30 and 60 seconds duration of change. Energy climbs up when time difference increases because energy storage participates with high power for long period. The maximal of energy total in charge mode is 19.33 kWh at 60 seconds duration of change because energy storage has to absorb high power for long duration and number of occurrence at this high power is large as presented in Table 5.9. For discharge mode, power maximal is 100kW and energy is 1.67kWh at time difference of 60 seconds. However, the maximal energy total at 30 seconds duration of change is 9.11 kWh which is quite larger than at time difference of 60 seconds. Energy total of energy storage in discharge mode of time difference 60 seconds is small because number of occurrence at this high power is only two as shown in Table 5.9. It can be assumed that this fluctuation can be neglected. Therefoer, power deviation needed to regulate

of time difference 60 seconds can be reduced from 200kW to 180kW which causes power of energy storage is 80kW, energy is 325kW.s and 0.67 kWh similar to charge mode.

In conclusion, power rated of energy storage and its energy are selected at is 80kW and 0.67kWh respectively.

5.5.5.2 Filter strategy 2

Energy storage with high pass filter strategy has been sizing in [66] according to wind power variation. In our study, their methodology is modified for power variation of PV. Effective storage capacity (A_{ESS}) in Watt.s can be defined by (5.18) where τ_2 is time constant of high pass filter (inverse of cut-off frequency) and P_{pv_max} is power rated of PV with the assumption that power of PV varies with its entire power. However, this design is not optimal because power variation of PV does not equal to its power rated. Equation (5.19) is proposed where $c_{0(max)}$ is coefficient of power fluctuation of PV.

From 2.4.2 in Chapter 2, power variation maximal of PV has been defined to be 180 kW (few occurrences of power variation over 180kW and has been neglected a having mentioned in previous topic) and $c_{0(max)}$ equals to 72% where power rated of PV is 250kW. For cut-off frequency 0.001 Hz, capacity storage is 7.96kWh but 0.32kWh is need for cut-off frequency 0.025 Hz. Increasing cut-off frequencies will reduce the effective storage capacity because the working band of energy storage is decreased.

$$A_{ESS} = \tau_2 . P_{pv\_max} \; ; \quad \tau_2 = 1/(2*pi*f_{c2})) \tag{5.18}$$

$$A_{ESS} = \tau . c_{0(max)} . P_{pv\_max} \tag{5.19}$$

Energy storage by limit ΔP_{pv} diagram and by filter strategy 2 with cut-off frequency 0.025Hz cause quite the same frequency performance and participation of diesel generator. However, energy or effective storage capacity of filter strategy 2 is half of strategy with limit ΔP_{pv} diagram. Therefore, energy storage by filter strategy 2 is not suitable as strategy with limit ΔP_{pv} diagram (60 seconds) for long period frequency regulation.

5.5 Conclusion

Two strategies; limit ΔP_{pv} diagram and filter, are proposed with coordination with power PV variation. These two strategies are validated with real power PV. Energy storage system by limit ΔP_{pv} diagram can reduce frequency variation according to power variation of PV. This strategy depends on the measured power of PV and determination of power reference which is used to define the power variation. Filter strategy 1 to 4 can also be guarantee frequency performance but with some limitations. For instance, filter strategies 2 and 3 with low cut-off frequency (0.001 Hz) can reduce power of primary frequency control of diesel generator but with larger power and energy used of ESS. Therefore, strategy with limit ΔP_{pv} diagram happens to be the optimum use of ESS. Power participation of ESS by this strategy is quite large but with less frequently. On the other hand, filter strategies with low cut-off frequency can optimize the use of diesel generator in primary frequency control. In spite of higher power participation of ESS by filter strategies than the others, its power of primary control of diesel generator is small.

Finally, frequency variation in high penetration PV can be guaranteed by filter strategy 2 and 3. Strategy with limit ΔP_{pv} diagram has to be adapted the power which signifies the stable power PV (dP_steady). In case of filter strategy 1; its cut-off frequency should be reduced but droop value and power rated of energy storage should be increased for droop strategy and filter strategy 4 in high penetration PV.

Chapter 6

Design of an H infinity controller for energy storage system

6.1 Introduction

The control architecture of an energy storage system (ESS) consists in two main parts, one concerning the generation of a power reference, and the other, the control of inverter currents. Inverter interfacing the energy storage system can be used to control power participation of ESS to primary regulation frequency and/or control of DC voltage. The reference of ESS can be defined by droop control (described in Chapter 4) or another strategy based on a limitation diagram or a filtering strategy presented in Chapter 5.

Classical primary frequency control with a simple structure of ESS (storage device associated with an AC/DC inverter) has been represented in Figure 4.12. But the control architecture and design become more complex for ESS consisted with two converters (a chopper and an inverter as seen in Figure 4.15 and Figure 4.22). All parameters of controllers have then to be carefully defined. They depend on parameters of energy storage system such as its state-of-charge, its internal resistance, the capacitor of the DC bus, and parameters of filter. The sensitivity of such parameters must be included into the design of controllers as uncertainties on modelling and measurements (on grid frequency or PV production for instance). Moreover, it should be interesting to design multivariable controllers for integrated systems of production, including PV and storage devices connected to a DC bus before any connection to the grid, solution proposed by a lot of manufecturers (site [ATAWEY, SINTEO, SIEMENS, ….])

In this study, we have thus designed a robust control of grid frequency, based on H infinity control theory. After a short description of the methodology used for designing a robust controller, the state-space modelling of the ESS is presented and linearized for the steady-state operating points. Then, the desired dynamic performances are expressed in the frequency domain, before synthetizing the H infinity controller. Finally, the dynamic performances of the energy storage system are analyzed according to robustness.

6.2 H infinity (H_∞) controller

Generally, a controlled system with closed-loop control should keep a stable behavior while following a given reference with desired performances. This behavior is characterized by a nominal stability (NS) and nominal performance (NP). Controller should be able to guarantee desired performances even in presence of model uncertainties, parameter uncertainties or low variations of operating points. If control system with uncertainties remains stable, system is characterized by a robust stability (RS) or robust performance (RP) when the system response with uncertainties achieves the desired performance.

Control system consists of plant (G(s)) and controller (K(s)) is illustrated in Figure 6.1, where y(t) and u(t) are output and input of plant respectively. G(s) can model either a single input single output (SISO) system or a multi inputs multi outputs (MIMO) one. Besides, there are many possible disturbances of system such as reference (r(t)), input disturbance ($d_i(t)$), output disturbance ($d_y(t)$), measurement noise (n(t)), etc. Controller K(s) is designed to achieve desired objectives and performances such as attenuating the effects of disturbances or measurement noises, or to avoid actuators saturation.

To evaluate the performance of a complete control of a MIMO system, five sensitivity functions can be defined: output sensitivity (S_y), output complementary sensitivity (T_y), input complementary sensitivity (T_u), plant sensitivity (S_yG), and controller sensitivity (KS_y) which represent the relationship between output (y(t)) or control input (u(t)) and several inputs (output disturbance, reference, input disturbance, and noise). For single input single output system (SISO), output sensitivity and input sensitivity are identical because G(s). K(s) equals to K(s).G(s). Complementary sensitivity functions of input and output are also equivalent for SISO case.

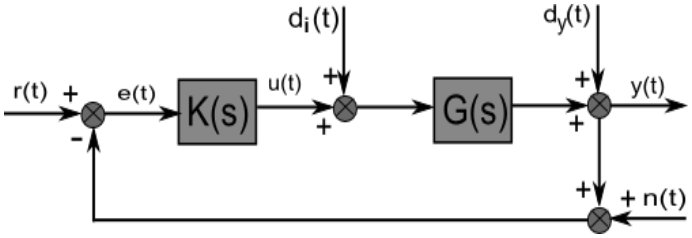

Figure 6.1 Classical control architecture

Output sensitivity function (S_y) models the transfer function between the output (y(t)) and the output disturbance ($d_y(t)$) in (6.1); the output complementary sensitivity function (T_y) is the transfer function between the output (y(t)) and the reference (r(t)) or negative of noise (-n(t)) as presented in (6.2). Plant sensitivity function (S_yG) in (6.4) represents the relation between the output (y(t)) and the input disturbance ($d_i(t)$). Furthermore, the relation between control input and inputs and the transfer function between control signal (u(t)) and input disturbance ($d_i(t)$) are negative of input complementary sensitivity function (T_u) as shown in (6.3). Finally, controller sensitivity (KS_y) in (6.5) presents the transfer function between control signal (u(t)) and negative of output disturbance ($-d_y(t)$), or reference (r(t)) or negative of noise (n(t)) [112].

$$\mathbf{S}_{\boldsymbol{y}} = \frac{\boldsymbol{y(t)}}{\boldsymbol{d_y(t)}} = \left(\boldsymbol{I_p} + \boldsymbol{GK}\right)^{-1} \tag{6.1}$$

$$\mathbf{T}_{\boldsymbol{y}} = \frac{\boldsymbol{y(t)}}{\boldsymbol{r(t)}} = -\frac{\boldsymbol{y(t)}}{\boldsymbol{n(t)}} = \left(\boldsymbol{I_p} + \boldsymbol{GK}\right)^{-1}\boldsymbol{GK} \tag{6.2}$$

$$\mathbf{T}_{\boldsymbol{u}} = -\frac{\boldsymbol{u(t)}}{\boldsymbol{d_i(t)}} = \boldsymbol{KG}(\boldsymbol{I_m} + \boldsymbol{KG})^{-1} \tag{6.3}$$

$$\boldsymbol{S_y}\mathbf{G} = \frac{\boldsymbol{y(t)}}{\boldsymbol{d_i(t)}} = \mathbf{S}_{\boldsymbol{y}}(\boldsymbol{s}).\boldsymbol{G}(\boldsymbol{s}) \tag{6.4}$$

$$\mathbf{KS}_{\boldsymbol{y}} = \frac{\boldsymbol{u(t)}}{\boldsymbol{r(t)}} = -\frac{\boldsymbol{u(t)}}{\boldsymbol{n(t)}} = -\frac{\boldsymbol{u(t)}}{\boldsymbol{d_y(t)}} = \mathbf{K}(\boldsymbol{s}).\mathbf{S}_{\boldsymbol{y}}(\boldsymbol{s}) \tag{6.5}$$

Each sensitivity function relates to different objectives controller design. For example, if objective of the controller design is a noise attenuation, output complementary sensitivity function (T_y) and controller sensitivity function (KS_y) have to be taken into consideration. On the other hand, output sensitivity function and controller sensitivity function are the main influencing factors to be analyzed for reject disturbance objective. Furthermore, controllers can be designed to respond to many objectives such as tracking reference and robustness against noise measurement, or reject output disturbance and noise attenuation, etc. However, it is difficult to achieve all objectives in the controller design, compromising between each objective is inevitable.

The H infinity controller is introduced as an optimization and robust control problem. In 1960s, linear quadratic Gaussian (LQG) which is a multivariable design technique has been developed to solve multiobjectives design of controller. Although it could achieve some good performances, robustness of closed-loop system is quite poor. Therefore, H infinity control theory which can take robustness issue into account in feedback design has been introduced by Zames and Francis in the early 1980s [113].

The closed loop system of an H infinity problem is described in Figure 6.2, with the transfer function of plant P(s) which is controlled by optimal controller K(s). The initial transfer function (G(s) is then completed with some weighting functions (W(s)) expressing the desired dynamic performances in order to form P(s). P(s) is defined as a state space system presented in (6.6) to (6.9). Inputs of plant system P(s) consist in input disturbance (w) and control input (u) which is generated from controller K(s) as shown in Figure 6.2. Outputs of plant system P(s) are the measured outputs (y), which are sent to the controller K(s).

The H infinity control objective is to find a stabilizing controller K(s) that minimizes the H-infinity norm of the closed-loop transfer matrix T_{zw} from disturbance w to output z for a given open loop plant P(s) as presented in (6.10), where $F_l(P,K)$ is the "lower" linear-fractional representation [112]. However, in practice, an optimal controller is not necessary to solve a H infinity problem (global minimization of $\|T_{z\omega}(s)\|_\infty$ [112], [114]. A Suboptimal controller is often computed instead. According to global minimal value γ, the H infinity suboptimal control problem is to define the limitation of minimal value $\gamma_\infty > \gamma$. Therefore, H infinity suboptimal controller is designed to ensure constraints shown in (6.10) where γ_∞ is the minimum bound of the H infinity suboptimal control problem.

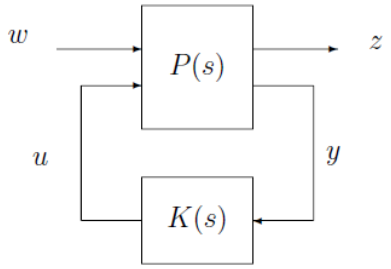

Figure 6.2 System of H infinity controller

$$P(s) = \left[\begin{array}{c|cc} A & B_1 & B_2 \\ \hline C_1 & D_{11} & D_{12} \\ C_2 & D_{21} & D_{22} \end{array}\right] \tag{6.6}$$

$$\dot{x}(t) = A.x(t) + B_1.w(t) + B_2.u(t) \tag{6.7}$$

$$z(t) = C_1.x(t) + D_{11}.w(t) + D_{12}.u(t) \tag{6.8}$$

$$y(t) = C_2.x(t) + D_{21}.w(t) + D_{22}.u(t) \tag{6.9}$$

$$\|\boldsymbol{T_{zw}(s)}\|_\infty = \|\boldsymbol{F_l(P(s), K(s)}\|_\infty < \boldsymbol{\gamma}_\infty \tag{6.10}$$

There are a lot of numerical methods to find and design the controller K. One of the most familiar methods consists in resolving LMI (Linear matrix inequalities) formulation. LMI is then a powerful tool in robust control optimization theory. The solution of LMIs means solving a convex optimization problem [115]. The optimal design of controllers for MIMO systems with multi-objective performances is the main interest of this methodology. Conversely, the order of controller may be high even if some methods of order reduction are possible and proven. It must also be noticed that this robust control is adapted to linear system, and then to small-signal disturbances. H infinity controller has been ever used to to control power electronic converters (inverter DC/DC and AC/DC) [116], and

power generation (diesel generator, energy storage, etc.) [117], [72], but not ever on grid frequency regulation.

6.2.1 Weighting function design

One of the more important steps of H infinity controller design is the definition of dynamic performance of the system. The desired robustness and performances specification are implemented in plant P as weighting functions on the characteristics of the sensitivity transfer function [112]. Weighting functions are then used in the design and analysis of controller. In the following, the S/KS mixed sensitivity problem is considered; this problem corresponds to a rejection of perturbance and to reach performances. Weighing function expressed in frequency domain can then represent specifications on system response in time domain [116], [117].

Output sensitivity function presented in (6.1) is weighted by a function of output performance (W_e) represented in Figure 6.3 and defined in equation (6.11), where ω_B is linked to the band-width and then, to the time response, A_ε is the steady-state error and M_s has an impact on system overshoot and stability margins. Rise time is approximated to be equal to $2.3/\omega_B$. Furthermore, M_s should be less than 2 (6dB) to guarantee a sufficient module margin. High cut-off frequency of weighting function (ω_B) cause high closed loop bandwidth, fast time response, fast rejection of the disturbance, and good robustness to parametric uncertainties. Furthermore, the settling time can be approximated from ω_B and A_ε (i.e. $2.3/A_\varepsilon.\omega_B$).

Dynamic performance of control input is designed by weighting function of control input (W_u) shown in (6.12) on controller sensitivity (KS) (in (6.5)). In Figure 6.4, M_u is designed according to system behaviour at low frequency and some limitation of control input [117]. Frequency parameter (ω_{bc}) which is related to close loop bandwidth has an influence on robustness and can be designed to achieve good robust performance (RP). For example, low ω_{bc} can be better to limit measurement noises and reduce effects of model uncertainties.

$$\frac{1}{W_e(s)} = \frac{s+\omega_B.A_\varepsilon}{\frac{s}{M_s}+\omega_B} \tag{6.11}$$

$$\frac{1}{W_u(s)} = \frac{A_u.s+\omega_{bc}}{s+\frac{\omega_{bc}}{M_u}} \tag{6.12}$$

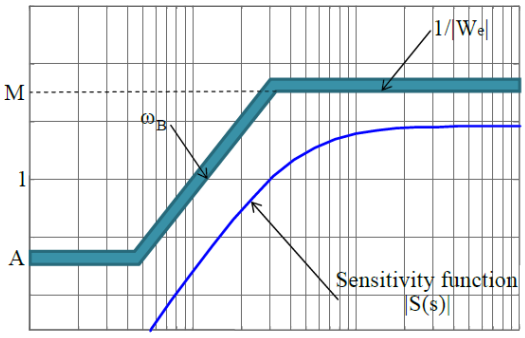

Figure 6.3 Weighting function design for output performance

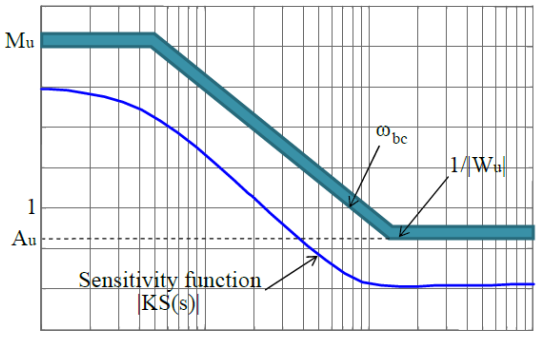

Figure 6.4 Weighting function design for control input

All weighting functions are integrated in the H infinity formulation; this becomes:

$$\left\| \begin{matrix} W_e.S \\ W_u KS \end{matrix} \right\|_\infty \leq \gamma_\infty \tag{6.13}$$

Methodology to study H infinity problem can then be detailed [116]:

1. Analyze and model the initial system G(s) to select objective of control, such as: a good reference tracking, best disturbance rejection, robustness against noise, etc.
2. Define control inputs and measured outputs, and express output performance
3. Dynamic performances of system (bandwidth, rise time, overshoot, and stability margins) are defined and expressed into frequency domain. Consequently, one or several weighting functions (W(s)) are obtained according to the number of objectives.
4. Design of robust controller (K) :
   - 4.1. Design of the full order controller
     - 4.1.1. The plant P(s) is defined from G(s) and W(s)
     - 4.1.2. Design the controller K(s) (Receive the full order controller K which is the order of system plus the order of weighting function). The H infinity norm γ_∞ is calculated using dedicated Matlab functions (Yalmip interface and Sedumi solver [118]).
   - 4.2. Reduce order controller such as PI controller [119]
     - 4.2.1. Transform the P(s) (from full order) in form of PI study
     - 4.2.2. Calculate the initial PI
     - 4.2.3. Design the controller K(s) with PI from 4.2.2 and H infinity norm γ defined.
5. If there is no solution for LMI resolution, the performance (weighting function) or objectives of control have to be changed. On the other hand, if the controller is found, the controller is optimal and then, the robustness of system with controller has to be analyzed for stability and performances.
6. Analyze the robustness of (P, K) system using the μ-analysis (cf. the following section).

According to the problem of droop control, the H infinity controller is firstly designed and applied to a storage energy system to improve the transient response of frequency against power variation of load and PV production, and robustness against parameter uncertainties.

6.2.2 Robustness analysis: μ-analysis

Any controller is designed from an approximated mathematical model of the system. Although represented model has dynamic (physical) response almost similar to the real system, some physical dynamics are commonly neglected due to the limitation of knowledge and the presentation of these dynamics into a mathematical model. For instance, a complex model of non-linear time-varying system is often linearized and its order reduced to simplify mathematical model and elaborate linear either non-linear control architectures. In controller design, a very complex and high order model, which is quite closed to a real system, can bring about a high robust controller against model uncertainties. Robust controller should be obtained but it will be quite difficult to achieve this controller. As the parameters of a mathematic model of plant are approximated and fixed, these can be deviated from the real system. Furthermore, effects of measurement imperfection (such as sensor noise) are classically neglected in simulated system. Differences between the actual system and the mathematical model (for controller design) may have effects on the stability and performance of a controlled system [113]. Therefore, the analysis of robustness has to be carefully carried out in order to avoid issues link to uncertainties.

Robustness in the aspect of control system is an ability of a system to resist to the disturbance or any dynamic perturbation. Previously, controller K(s) is designed according to desired performance. In this topic, its robustness property is analyzed with the help of a special tool dedicated to H-infinity

control theory: the μ-analysis [112], [114]. Uncertainties are firstly modelled as a mathematical representation. Then, two robust properties, i.e. Robust Stability (RS) and Robust Performance (RP) are analyzed. If desired controller cannot achieve these two robust properties, this controller would be redesigned including model uncertainties.

Uncertainties in robust control are separated into two groups: unstructured and structured uncertainties. The first group represents unknown structure and model order in high frequencies, nonlinearities of modelling, etc. The structured uncertainties represent variations of system parameters which have impacts on low frequency performance [120].

According to the closed loop system illustrated in Figure 6.2, uncertainties are represented as Linear Fractional Representation (LFR) as shown in Figure 6.5. The plant (P) and controller (K) in Figure 6.5(a) are combined to the initial closed loop system with uncertainties (N) as presented in Figure 6.5(b). This LFR will be used to define transfer function from w to z as upper Linear Fractional Transformation (LFT) as presented in (6.14). The conditions defining robustness for stability or performances can be defines as [112]:

Nominal stability (NS) $\leftrightarrow$ N is internally stable

Nominal performance (NP) $\leftrightarrow$ $\|N_{22}\|_\infty < 1$ and condition of NS is checked

Robust stability (RS) $\leftrightarrow$ $\mathbf{F_u}(\boldsymbol{N},\Delta)\ is\ stable\ for\ \forall\Delta, \|\Delta\|_\infty < 1$ and condition of NS is checked

Robust performance (RP) $\leftrightarrow$ $\|\mathbf{F_u}(\boldsymbol{N},\Delta)\|_\infty < 1\ \ \forall\Delta, \|\Delta\|_\infty < 1$ and condition of NS is checked

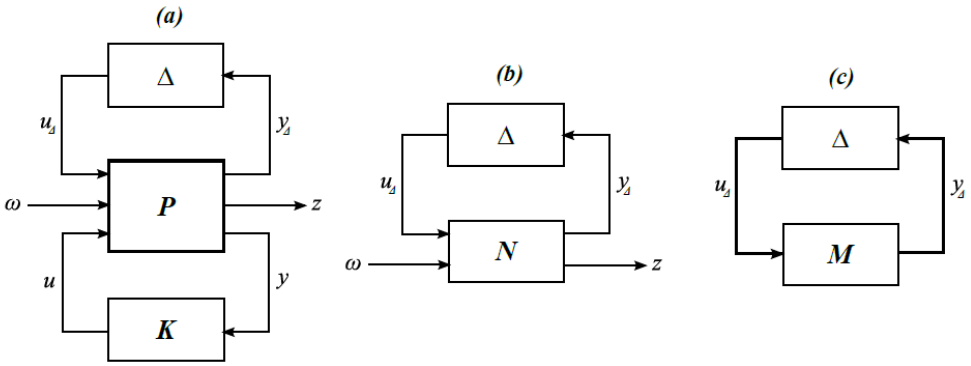

Figure 6.5 Complete system control with uncertainties

$$\mathbf{F_u}(\boldsymbol{N},\Delta) = \boldsymbol{N_{22}} + \boldsymbol{N_{21}}\Delta(\boldsymbol{I} - \boldsymbol{N_{11}}\Delta)^{-1}\boldsymbol{N_{12}} \tag{6.14}$$

The block Δ, which takes into account of all uncertainties of a closed loop system, is called the unknown matrix. The purpose is to find the maximum uncertainty for which the system remains stable (RS) and/or for which the response of a closed loop system achieves the desired performance. The term ($I\text{-}N_{11}\Delta$) is only one source of instability of transfer function from w to z as presented in (6.14) [112]. For robust stability analysis, M-Δ structure in Figure 6.5(c) is analyzed where $M=N_{11}$. Two types of uncertainties (unstructured and structured uncertainties) use different methods to analyze robust stability.

For unstructured uncertainties, all perturbations are collected into a single matrix so that Δ includes the maximal normalized variation on uncertainties. The structure of Δ is ignored and it is considered as a full complex transfer function matrix or a full-box complex perturbation uncertainty satisfying $\|\Delta\|_\infty \leq 1$ [112]. Small gain theorem is used to define condition for stability [113]. The maximum uncertainty gain for which the system remains stable is defined according to the constraint: $\|\Delta\|_\infty \leq \delta \ \ if\ and\ only\ if\ \|M(s)\|_\infty < 1/\delta$ [120]. Any unstructured uncertainty can be presented as additive, output multiplicative, output inverse multiplicative, additive inverse, input multiplicative, and input inverse multiplicative as illustrated in Figure 6.5, where one known block of transfer function to present all concerned uncertainties (such as $W_A(s)$, $W_O(s)$, etc.) and one unknown block

denoted Δ with an index corresponding to the type of uncertainty [120]. The purpose is to find Δ which defines the maximal gain of concerned uncertainties ($W_A(s)$, $W_O(s)$, etc.).

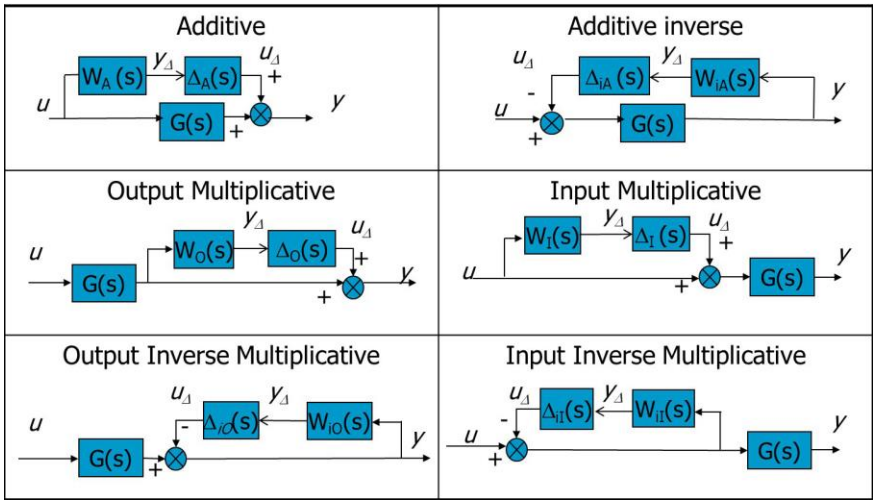

Figure 6.5 Uncertainties representation

On the other hand, structure of Δ is concerned for the structured uncertainty so that the unknown uncertainty Δ is in diagonal matrix and is defined as the maximal variation of each parameter with guarantee system stability and performance. The matrix Δ has thus more elements linked to system parameters than the previous case; a more complex tool is then needed to define the robustness in this case. Structure singular value (denoted μ) which is the function to define necessary and sufficient conditions for RS and RP [112] is introduced. Moreover, structured singular value (μ) can be defined as stability margin of the system (a margin which is not defined in the frequency domain) according to uncertainties [117].

In practice, due to numerical solution issues, only the maximum and minimum bounds of μ are computed. Using the Nyquist theorem, it can be seen that the stability limit is reached at det (I −M(s) Δ(s)) = 0. The MATLAB function "mussv" is used to calculated μ, which means a distance of the system to reach the instability. Conditions on value of μ for robust stability (RS) and robust performance (RP) are finally resumed [112]:

$$\text{Nominal stability (NS)} \leftrightarrow \text{N is internally stable}$$

$$\text{Robust stability (RS)} \leftrightarrow \forall\omega, \mu_{\Delta i}\left(N_{11}(j\omega)\right) < 1 \text{ and NS}$$

$$\text{Nominal performance (NP)} \leftrightarrow \forall\omega, \mu_{\Delta f}\left(N_{22}(j\omega)\right) < 1 \text{ and NS}$$

$$\text{Robust performance (RP)} \leftrightarrow \forall\omega, \mu_{\hat{\Delta}}\left(N(j\omega)\right) < 1 \text{ and NS}$$

The maximal and minimal value of μ is plotted through some frequency range to analyze the stability and performance of the closed loop system. If μ is less than 1 for RS and RP analysis, closed loop system is robust in stability and performance. For robust stability, system remains stable until 1/μ times the uncertainty level used to compute μ. However, this is not valid for robust performance. Uncertainty level has to be increased until μ moves near and then passes over 1 to signify the maximum acceptable uncertainties for robust performance.

6.3 Energy storage system modeling

The Energy Storage System is shown in Figure 4.2, with the energy storage device (ES), the DC/DC converter, the AC/DC inverter, and AC filter (RL) connected to power system composed with a diesel generator, a PV plant and an equivalent dynamic load as illustrated in Figure 6.7. The ESS is modeled as the initial plant G(s) as shown in Figure 6.8(a). Active and reactive powers are controlled by the switching function of DC/DC converter and the switching function in q-axis of the respectively. The DC bus voltage is regulated by the switching function in d-axis of the inverter. Therefore, the

outputs of performance (Δz) and measured outputs (Δy) in Figure 6.8(a) correspond to the frequency variation of the isolated grid (Δf_{res}) and the variation of the DC voltage (ΔV_{dc}). The control inputs (Δu) of Figure 6.8(a) correspond to the switching function of the DC/DC converter ($\Delta\alpha_h$), the switching function of the inverter in d-axis ($\Delta\beta_d$), and the switching function of in q-axis ($\Delta\beta_q$). The objective of the controller is to reject any small-signal output disturbance $d_y(t)$ in Figure 6.1. Therefore, the input disturbance (Δw) corresponds to the variation of load power and/or PV power variation (ΔP_{diff}) in equation (5.6). Although this system output can also include a reactive power variation when energy storage has to participate to voltage regulation, it will not be considered in this study. The different inputs, outputs and control variables of energy storage system G(s) are summarized in Figure 6.8(b).

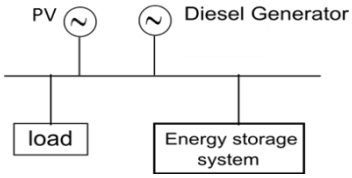

Figure 6.7 Studied power system

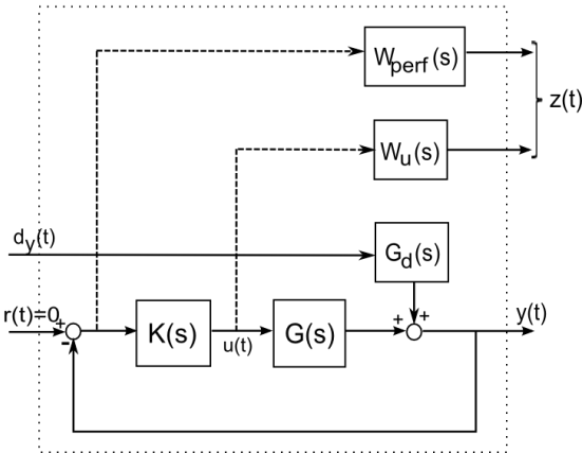

(a)

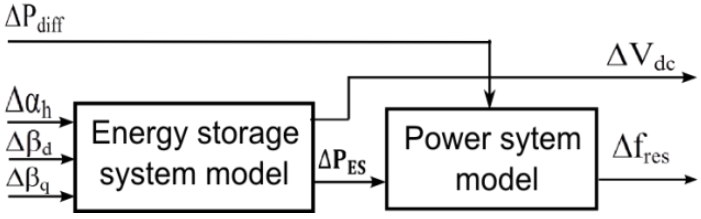

(b)

Figure 6.8 Summary of inputs and outputs of the model

Calculation of system frequency (i.e. the controlled output) and frequency regulation of diesel generator from Chapters 3 and 5 are firstly summarized. Then, the state space representation of frequency control with energy storage system is presented and validated with comparing to topological model in MATLAB-Simulink.

6.3.1 Power system model

Nonlinear equation of frequency shown in (3.8) is linearized around an operating point for small signal variation in (6.15). The symbol Δ is used to distinguish small variations of each variable. Furthermore, from equation (3.6) and (5.6), deviation of frequency variation ($\frac{d\Delta f_{res}^{pu}(t)}{dt}$) is then defined in (6.16). Frequency variation is induced by the unbalances of active powers between source and load. For the initial system without energy storage device, frequency regulation is assumed by diesel generator with droop control. Therefore, frequency regulation and dynamic response of diesel generator has to be considered. Power variation of diesel generator (ΔP_m^{pu}) in (6.16) depends on the

frequency variation. In Chapter 3, power deviation of diesel generator as a function of frequency variation has been defined in frequency domain (Laplace transform) as presented in (3.1) and (3.5). Consequently, the deviation of power variation of diesel generator in time domain ($\frac{d\Delta P_m^{pu}(t)}{dt}$) is defined in (6.17), which will take into account only primary frequency control because the transient of frequency response is focused on in this study, and dynamic model of diesel generator is included in the first order transfer function. All power values and frequencies in (6.15) to (6.17) are expressed in per unit.

$$\frac{d\Delta f_{res}^{pu}(t)}{dt} = \frac{1}{2.H}(\Delta P_m^{pu}(t) + \Delta P_{PV}^{pu}(t) - P_{load}^{pu}(t)) \quad (6.15)$$

$$\frac{d\Delta f_{res}^{pu}(t)}{dt} = \frac{1}{2.H}(\Delta P_m^{pu}(t) + \Delta P_{diff}^{pu}(t)) - \frac{D}{2.H}\Delta f_{res}^{pu}(t) \quad (6.16)$$

$$\frac{d\Delta P_m^{pu}(t)}{dt} = -\frac{1}{T_g}\Delta P_m^{pu}(t) - \frac{1}{s_d.T_g}\Delta f_{res}^{pu}(t) \quad (6.17)$$

6.3.2 Energy storage system modelling

The input voltage of the DC/DC converter is defined with the switching function (α_h) and the DC bus voltage (V_{dc}). And the output current of converter (I_{src}) is defined as a function of the switching function (α_h) and the current of energy storage. The output voltage of inverter (V_{sd}, V_{sq}) is then expressed with the switching function (β_d,β_q) and DC bus voltage (V_{dc}). The current of the DC bus (I_m) is a function of the switching function (β_d,β_q) and output current in AC bus (I_{sd},I_{sq}).

Storage device (denoted ESS) is connected to a DC/DC converter via a resistor and inductor (R_{fsj} and L_{fsj}) circuit as illustrated in Figure 6.9. Voltage input of converter DC/DC (denoted V_{hj}) is a function of the output voltage of energy storage (denoted V_{ES}), the current of energy storage (denoted I_{ES}), the resistor R_{fsj}, and the inductor L_{fsj} in (6.18). The DC/DC converter is connected to inverter AC/DC via a resistor (R_{dc}) and a capacitor (C_{dc}) filter. DC current of C_{dc} and R_{dc} bus (I_{dc}) has been defined in (6.19). The input current of the inverter AC/DC (I_m) is the difference between current output of converter DC/DC (I_{src}) and current of capacitor and resistor bus (I_{dc}) represented in (6.20).

The output of the inverter and the AC part is then modelled. The inverter is connected to the grid via a RL filter as shown in Figure 6.9. Output currents of AC/DC inverter (I_{s1}, I_{s2}, I_{s3} or I_{sd}, I_{sq}) are equal to output currents of the ESS (I_{r1}, I_{r2}, I_{r3} or I_{rd}, I_{rq}). Derivative of current output in d-axis and q-axis has been defined in (6.21) and (6.22) respectively; where R_{ac} and L_{ac} denote the resistance and the inductance of the filter respectively, V_{rd} and V_{rq} are voltage of power system in d-axis and q-axis, V_{dc} is the DC bus voltage.

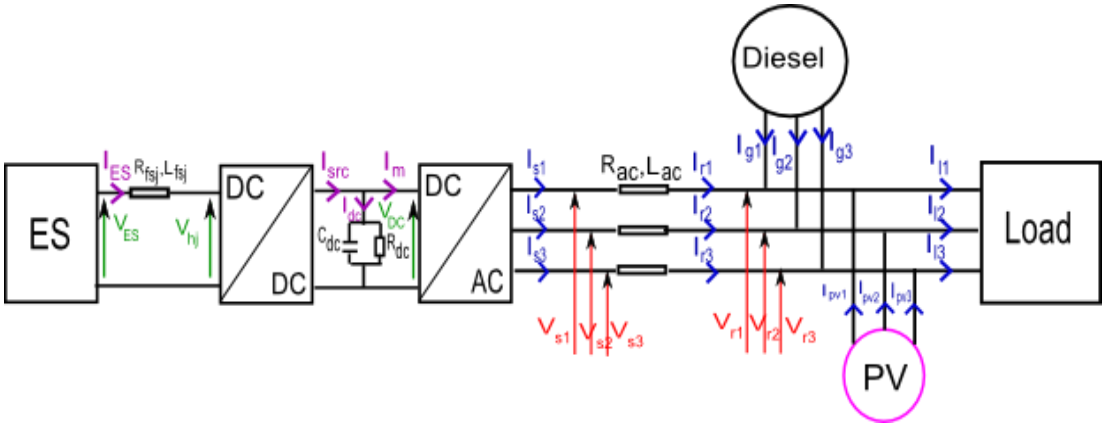

Figure 6.9 Energy storage system connects to power system

$$V_{hj}(t) + L_{fsj}\frac{dI_{ES}(t)}{dt} + R_{fsj}.I_{ES}(t) = V_{ES}(t) \quad (6.18)$$

$$\boldsymbol{I_{dc}(t) = C_{dc}\frac{dV_{dc}(t)}{dt} + \frac{V_{dc}(t)}{R_{dc}}} \quad (6.19)$$

$$\boldsymbol{I_m(t) = I_{src}(t) - I_{dc}(t)} \quad (6.20)$$

$$\frac{dI_{sd}(t)}{dt} = -\frac{R_{ac}}{L_{ac}}.I_{sd}(t) - \frac{1}{L_{ac}}.V_{rd}(t) + \frac{1}{L_{ac}}.V_{dc}(t).\beta_d(t) + \omega.I_{sq}(t) \quad (6.21)$$

$$\frac{dI_{sq}(t)}{dt} = -\frac{R_{ac}}{L_{ac}}.I_{sq}(t) - \frac{1}{L_{ac}}.V_{rq}(t) + \frac{1}{L_{ac}}.V_{dc}(t).\beta_q(t) - \omega.I_{sd}(t) \quad (6.22)$$

6.3.3 State space representation of studied system

The state variables (Δx) correspond to small variations of energy storage current (ΔI_{ES}), DC bus voltage (ΔV_{dc}), inverter current in d-axis (ΔI_{sd}), inverter current in q-axis (ΔI_{sq}), power of diesel generator (ΔP_m) and system frequency (Δf_{res}). Derivative of ESS current can be defined as a function of some state variations and selected control input in (6.23). Furthermore, the derivative of the DC bus voltage can also be expressed with these variables in (6.24).

$$\boldsymbol{\frac{dI_{ES}(t)}{dt} = \frac{1}{L_{fsj}}V_{ES}(t) - \frac{1}{L_{fsj}}\alpha_h(t).V_{dc}(t) - \frac{R_{fsj}}{L_{fsj}}.I_{ES}(t)} \quad (6.23)$$

$$\boldsymbol{\frac{dV_{dc}(t)}{dt} = \frac{1}{C_{dc}}.\alpha_h(t).I_{ES}(t) - \frac{1}{C_{dc}}\left[\beta_d(t).I_{sd}(t) + \beta_q(t).I_{sq}(t)\right] - \frac{V_{dc}(t)}{C_{dc}.R_{dc}}} \quad (6.24)$$

Participation of energy storage in frequency regulation is firstly controlled by switching function of DC/DC (α_h) via controlling current of energy storage. Therefore, power of energy storage (P_{ES}) is then calculated from voltage and current of the energy storage device (V_{ES} and I_{ES}) as shown in (6.25). For H infinity control synthesis, the equation is linearized around a steady-state operating point, i.e. when frequency variation is equal to zero (the frequency is equal to 50 Hz). Therefore, power variation of energy storage (ΔP_{ES}) is determined in (6.26) where V_{ES0} is the initial voltage of the ESS and I_{ES0} is its initial current. Furthermore, nonlinear equations (6.23), (6.24), (6.21) and (6.22) are also linearized around the initial point in (6.27), (6.28), (6.29) and (6.30) respectively where V_{dc0} represents the initial DC voltage, α_{h0} is the initial switching function of DC/DC, I_{ES0} is the initial current of energy storage, β_{d0} and β_{q0} are the initial switching function in d-axis and q-axis, I_{sd0} and I_{sq0} are the initial current output in d-axis and q-axis, and ω_0 is the initial frequency in rad/s.

$$\boldsymbol{P_{ES}(t) = V_{ES}(t).I_{ES}(t)} \quad (6.25)$$

$$\boldsymbol{\Delta P_{ES}(t) = V_{ES0}.\Delta I_{ES}(t) + \Delta V_{ES}(t).I_{ES0}} \quad (6.26)$$

$$\boldsymbol{\frac{d\Delta I_{ES}(t)}{dt} = \frac{1}{L_{fsj}}\Delta V_{ES}(t) - \frac{1}{L_{fsj}}\Delta\alpha_h(t).V_{dc0} - \frac{1}{L_{fsj}}\alpha_{h0}.\Delta V_{dc}(t) - \frac{R_{fsj}}{L_{fsj}}.\Delta I_{ES}(t)} \quad (6.27)$$

$$\boldsymbol{\frac{d\Delta V_{dc}(t)}{dt} = \frac{\alpha_{h0}.\Delta I_{ES}(t)}{C_{dc}} + \frac{I_{ES0}.\Delta\alpha_h(t)}{C_{dc}} - \frac{1}{C_{dc}}\left[\beta_{d0}.\Delta I_{sd}(t) + \Delta\beta_d(t).I_{sd0} + \beta_{q0}.\Delta I_{sq}(t) + \Delta\beta_q(t).I_{sq0}\right] - \frac{\Delta V_{dc}(t)}{C_{dc}.R_{dc}}} \quad (6.28)$$

$$\boldsymbol{\frac{d\Delta I_{sd}(t)}{dt} = -\frac{R_{ac}}{L_{ac}}.\Delta I_{sd}(t) - \frac{\Delta V_{rd}(t)}{L_{ac}} + \frac{\Delta V_{dc}(t).\beta_{d0}}{L_{ac}} + \frac{V_{dc0}.\Delta\beta_d(t)}{L_{ac}} + \omega_0.\Delta I_{sq}(t) + \Delta\omega(t).I_{sq0}} \quad (6.29)$$

$$\boldsymbol{\frac{d\Delta I_{sq}(t)}{dt} = -\frac{R_{ac}}{L_{ac}}.\Delta I_{sq}(t) - \frac{\Delta V_{rq}(t)}{L_{ac}} + \frac{\Delta V_{dc}(t).\beta_{q0}}{L_{ac}} + \frac{V_{dc0}.\Delta\beta_q(t)}{L_{ac}} - \omega_0.\Delta I_{sd}(t) - \Delta\omega(t).I_{sd0}} \quad (6.30)$$

Frequency variation in (6.16) is then modified to be (6.31) with participation of energy storage while assuming that voltage of the energy storage (V_{ES}) remains constant (i.e. $\Delta V_{ES}=0$) shown in

(6.26). Power of the energy storage in (6.26) has to be expressed in per unit for frequency calculation dividing it by the rated power of the grid (S_{rated}).

$$\frac{d\Delta f_{res}^{pu}(t)}{dt} = \frac{1}{2.H}(\Delta P_m^{pu}(t) + \Delta P_{diff}^{pu}(t) + \frac{V_{ES0}.\Delta I_{ES}(t)}{S_{rated}}) - \frac{D}{2.H}\Delta f_{res}^{pu}(t) \quad (6.31)$$

Equations (6.17), (6.27), (6.28), (6.29), (6.30), and (6.31) are arranged to form a linear state-space representation, as (6.7), (6.8), and (6.9) for the following H infinity design. State variables (x(t)), control inputs (u(t)), disturbance input (w(t)), measured outputs (y(t)), and performance outputs (z(t)) are summarized in (6.32). Matrix denoted A, B_1, B_2, C_1, C_2, D_{11}, D_{12}, and D_{21} are presented in (6.33) by assuming that voltage of power system in d-axis (V_{rd}) keeps constant at the initial value (V_{rd0}), voltage of power system in q-axis (V_{rq0}) is zero, and voltage of energy storage is constant at its initial value (V_{ES0}). So, $\Delta V_{rd}(t)$, $\Delta V_{rq}(t)$, and $\Delta V_{SST}(t)$ are all equal to zero.

$$x(t) = \begin{bmatrix} \Delta I_{ES} \\ \Delta V_{dc} \\ \Delta I_{sd} \\ \Delta I_{sq} \\ \Delta P_m^{pu} \\ \Delta f_{res}^{pu} \end{bmatrix}, u(t) = \begin{bmatrix} \Delta\alpha_h \\ \Delta\beta_d \\ \Delta\beta_q \end{bmatrix}, w(t) = \Delta P_{diff}^{pu}(t),\ z(t) = y(t) = \begin{bmatrix} \Delta f_{res}^{pu} \\ \Delta V_{dc} \end{bmatrix} \quad (6.32)$$

$$A = \begin{bmatrix} -\frac{R_{fsj}}{L_{fsj}} & -\frac{\alpha_{h0}}{L_{fsj}} & 0 & 0 & 0 & 0 \\ \frac{\alpha_{h0}}{C_{dc}} & -\frac{1}{C_{dc}.R_{dc}} & -\frac{\beta_{d0}}{C_{dc}} & -\frac{\beta_{q0}}{C_{dc}} & 0 & 0 \\ 0 & \frac{\beta_{d0}}{L_{ac}} & -\frac{R_{ac}}{L_{ac}} & \omega_0 & 0 & 2\pi.50.I_{sq0} \\ 0 & \frac{\beta_{q0}}{L_{ac}} & -\omega_0 & -\frac{R_{ac}}{L_{ac}} & 0 & -2\pi.50.I_{sd0} \\ 0 & 0 & 0 & 0 & -\frac{1}{T_g} & -\frac{1}{s_d.T_g} \\ \frac{V_{ES0}}{2.H.S_{rated}} & 0 & 0 & 0 & \frac{1}{2.H} & -\frac{D}{2.H} \end{bmatrix}, B_1 = \begin{bmatrix} 0 \\ 0 \\ 0 \\ 0 \\ 0 \\ \frac{1}{2.H} \end{bmatrix},$$

$$B_2 = \begin{bmatrix} -\frac{V_{dc0}}{L_{fsj}} & 0 & 0 \\ \frac{I_{ES0}}{C_{dc}} & -\frac{I_{sd0}}{C_{dc}} & -\frac{I_{sq0}}{C_{dc}} \\ 0 & \frac{V_{dc0}}{L_{ac}} & 0 \\ 0 & 0 & \frac{V_{dc0}}{L_{ac}} \\ 0 & 0 & 0 \\ 0 & 0 & 0 \end{bmatrix},\ C_1 = \begin{bmatrix} 0 & 0 & 0 & 0 & 1 \\ 0 & 1 & 0 & 0 & 0 \end{bmatrix}, D_{11}=D_{12}=D_{21}=0 \quad (6.33)$$

Furthermore, energy storage system can also be modeled using the control system #2 presented in Chapter 4 which controls the DC bus voltage by switching function of DC/DC and control power of energy storage (by controlling the output current in d-axis) by switching function in d-axis of AC/DC. Power of energy storage in (6.25) is then turned to be (6.34) and it is linearized in (6.35) by assuming that variation of voltage in d-axis is null. This modelling induces changet only in the frequency equation (6.31).

$$P_{ES}(t) = V_{rd}(t).I_{sd}(t) \quad (6.34)$$

$$\Delta P_{ES}(t) = V_{rd0}.\Delta I_{sd}(t) \quad (6.35)$$

6.3.4 Initial state calculation

Almost all parameters in (6.33) have been defined in Chapter 4 except the initial values. In order to simplify the equations, the resistance of the DC bus is firstly neglected. It will be considered afterward. Three initial known values are: the voltage of energy storage (V_{ES0}), the DC bus voltage (V_{dc}), and the voltage of power system in d-axis (V_{rd0}).

6.3.4.1 Case #1: R_{dc} is neglected

From (6.23), at t=0 (initial state), derivative of current of energy storage is equal to zero based on the assumption that voltage of energy storage and DC voltage are constant at its initial value (V_{ES0}, V_{dc0}), and current of energy storage is also zero (energy storage does not participate in frequency regulation at the initial state). The initial switching function of DC/DC is therefore defined in (6.36). For this case (without R_{dc}), equation in (6.24) is changed to be (6.37). Derivative of the DC voltage in (6.37) is equal to zero at t=0, then the equation (6.38) is obtained. Finally, (6.39) and (6.40) are derived from (6.21) and (6.22) where derivative of current in d-axis and q-axis are equal to zero at t=0. Equations (6.38) to (6.40) are used to define the initial switching function in d and q axis in (6.41).

$$\boldsymbol{\alpha_{h0} = \frac{V_{ES0}}{V_{dc0}}} \tag{6.36}$$

$$\boldsymbol{\frac{dV_{dc}(t)}{dt} = \frac{1}{C_{dc}}.\alpha_h(t).I_{ES}(t) - \frac{1}{C_{dc}}.\left[\beta_d(t).I_{sd}(t) + \beta_q(t).I_{sq}(t)\right]} \tag{6.37}$$

$$\boldsymbol{0 = -\frac{1}{C_{dc}}.\left[\beta_{d0}.I_{sd0} + \beta_{q0}.I_{sq0}\right]} \tag{6.38}$$

$$0 = -\frac{R_{ac}}{L_{ac}}.I_{sd0} - \frac{1}{L_{ac}}.V_{rd0} + \frac{1}{L_{ac}}.V_{dc0}.\beta_{d0} + \omega.I_{sq0} \tag{6.39}$$

$$0 = -\frac{R_{ac}}{L_{ac}}.I_{sq0} + \frac{1}{L_{ac}}.V_{dc0}.\beta_{q0} - \omega.I_{sd0} \tag{6.40}$$

$$\boldsymbol{\beta_{d0} = \frac{V_{rd0}}{V_{dc0}}, \beta_{q0} = 0} \tag{6.41}$$

6.3.4.2 Case #2: R_{dc} is taken into account

The initial switching functions in d and q axis are equivalent to previous case in (6.41). Nevertheless in this case, the initial current of energy storage (I_{ES0}) is not zero. Derivative of DC voltage in (6.24) is zero at t=0, then equation (6.42) is obtained and the initial switching function of DC/DC in function with DC voltage, the initial current of energy storage, and resistance at DC bus (R_{dc}) in (6.43); equation (6.23) becomes (6.44). From (6.43) and (6.44), the initial current of energy storage is derived as a function of known parameters in (6.45). Finally, the initial current of the ESS is defined in (6.46).

$$\boldsymbol{0 = \frac{1}{C_{dc}}.\alpha_{h0}.I_{ES0} - \frac{V_{dc0}}{C_{dc}.R_{dc}}} \tag{6.42}$$

$$\boldsymbol{\alpha_{h0} = \frac{V_{dc0}}{I_{ES0}.R_{dc}}} \tag{6.43}$$

$$\boldsymbol{0 = V_{ES0} - \alpha_{h0}.V_{dc0} - R_{fsj}.I_{ES0}} \tag{6.44}$$

$$\boldsymbol{0 = R_{dc}.R_{fsj}.(I_{ES0})^2 - R_{dc}.V_{ES0}.I_{ES0} + (V_{dc0})^2} \tag{6.45}$$

$$\boldsymbol{I_{ES0} = \frac{R_{dc}.V_{ES0} \pm \sqrt{(R_{dc}.V_{ES0})^2 - 4.R_{dc}.R_{fsj}.(V_{dc0})^2}}{2.R_{dc}.R_{fsj}}.R_{fsj}.(I_{ES0})^2 - R_{dc}.I_{ES0} + (V_{dc0})^2} \tag{6.46}$$

In the following sections, only the first case (where R_{dc} is neglected) will be studied.

6.3.5 Model validation

Nonlinear model and linear model of energy storage system and power system are compared to topological model described in MATLAB Simulink (see Chapter 4). The droop control is applied to ESS for primary frequency regulation. The time response of the DC bus voltage (V_{dc}), DC bus current of energy storage (I_{es}), AC current in d-axis (I_{sd}), and frequency (f_{res}) response of model in (6.33) according to variations of load power of ±100kW at 3 seconds (from initial load power 1MW) are separately illustrated in Figure 6.10 to Figure 6.13 respectively. All responses of non-linear and linear models are quite similar to responses of topological model. However, responses of topological model have some fast dynamics and oscillations which are not taken into account in state-space models.

Dynamics of DC bus voltage can be observed with non-linear and linear models; however, it is difficult to see them with the topological model because of oscillation as illustrated in Figure 6.10 (a) and (b). DC current of energy storage of non-linear and linear models shown in Figure 6.11 (a) and (b) are quite similar to average value of DC current of topological model and they well follow the reference signal. The AC current variations in d-axis of both non-linear and linear models are quite smaller than current in d-axis of topological model because the variation of AC voltage in d and q axis has been neglected. Finally, frequency responses of non-linear and linear models are quite identical to those estimated with the topological model except for dynamic transients. Fast dynamic frequency response of topological model is due to the PLL which is used to measure system frequency. But non-linear and linear models do not integrate any model of PLL.

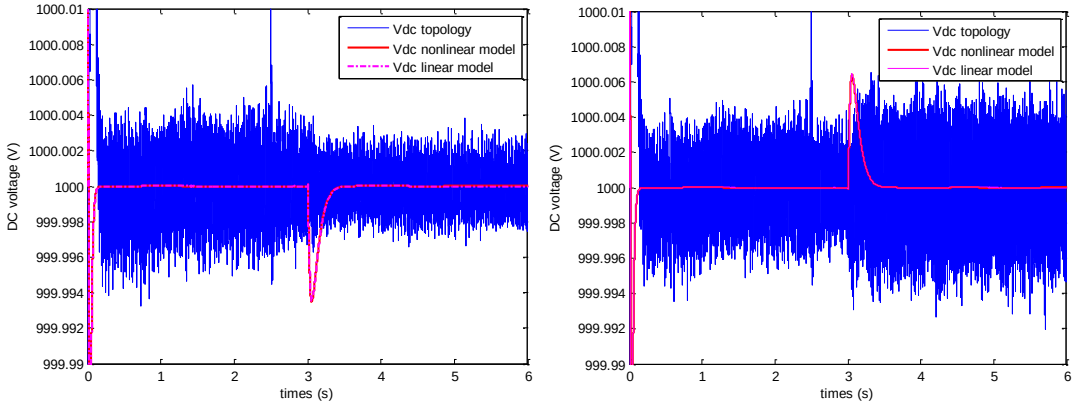

(a) (b)

Figure 6.10 DC voltage of energy storage system according to power variation (a) +100kW (b) -100kW

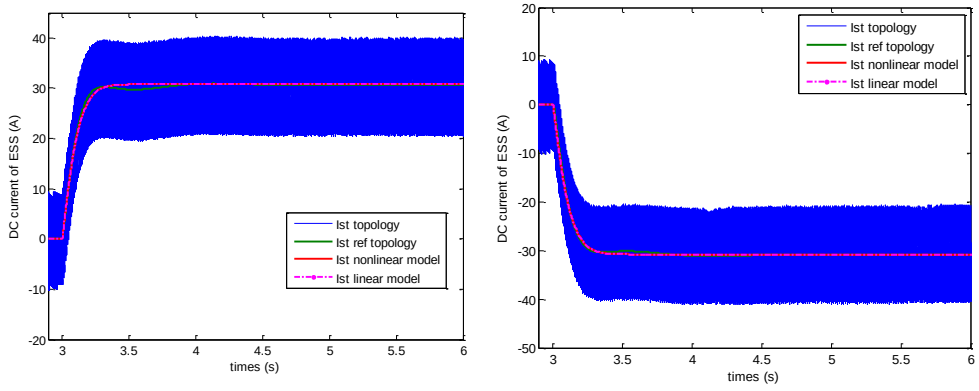

(a) (b)

Figure 6.11 DC current of energy storage according to power variation (a) +100kW (b) -100kW

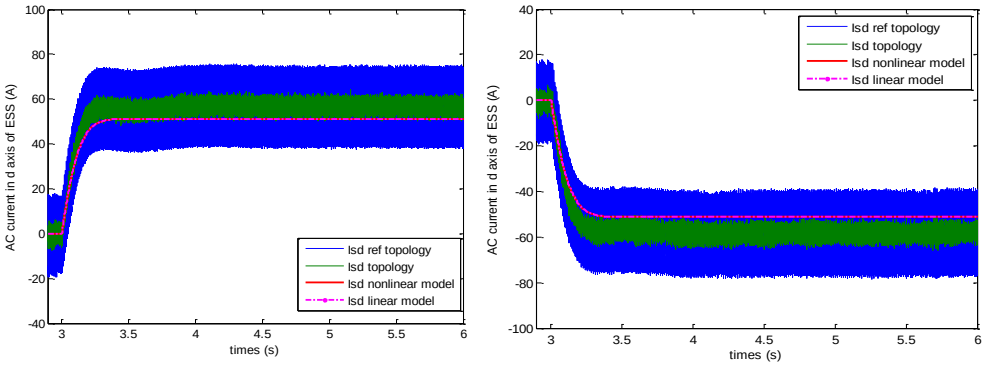

(a) (b)

Figure 6.12 AC current in d-axis of energy storage system according to power variation (a) +100kW (b) -100kW

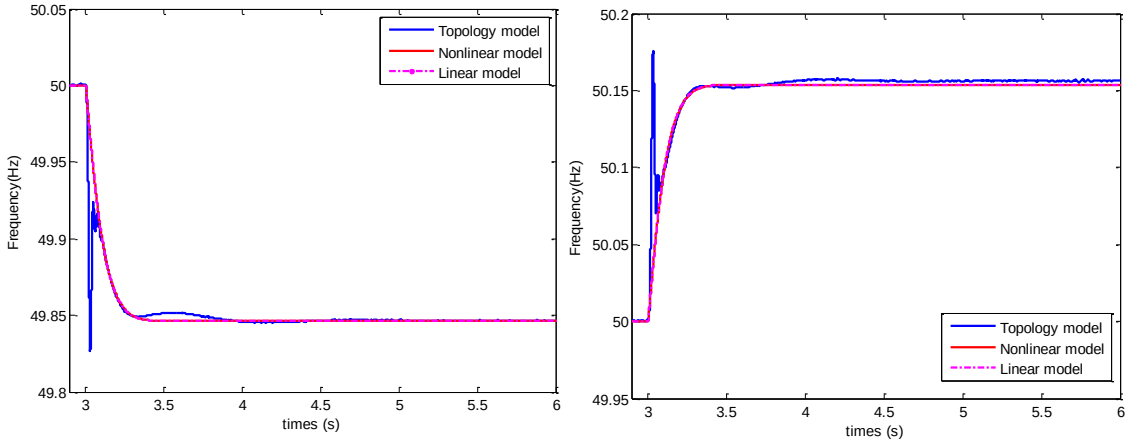

(a) (b)

Figure 6.13 Frequency of power system according to power variation (a) +100kW (b) -100kW

6.3.6 System analysis: stability, controllability and observability

From state space representation model presented in (6.32) and (6.33), Bode diagrams of transfer functions between frequency variation and all inputs (ΔP_{diff}, α_h, and β_d) are plotted in Figure 6.14 (a) to (c) while current and switching function in q-axis are assumed to be zero. Transfer function between DC bus voltage variation and inputs are also plotted in frequency domain in Figure 6.14 (d) to (f). Power variation has not effect on DC voltage variation in Figure 6.14(d).

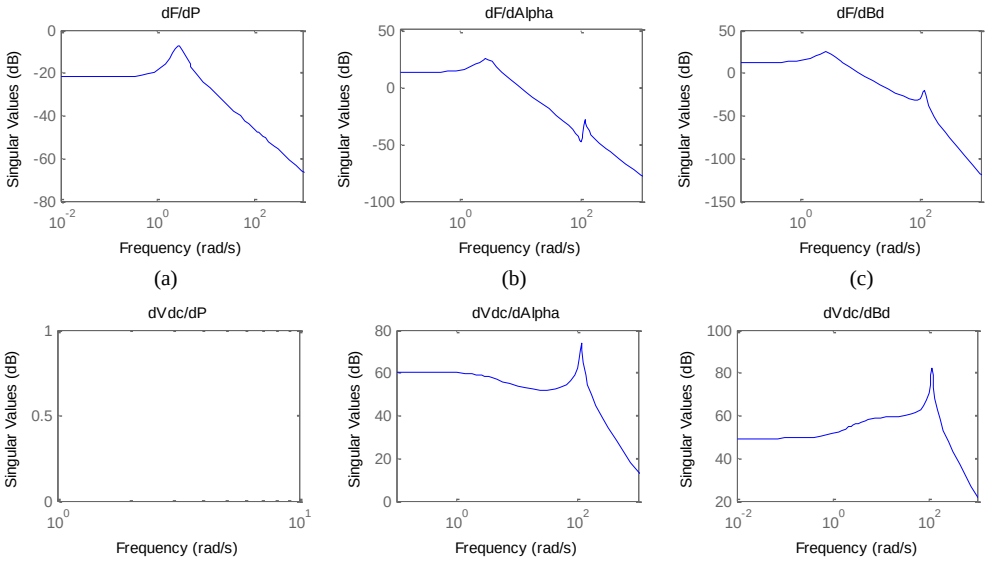

(a) (b) (c)

(d) (e) (f)

Figure 6.14 Singluar values (gain) of transfer functions: (a) $\Delta f_{res}/\Delta P_{diff}$ (b) $\Delta f_{res}/\Delta \alpha_h$ (c) $\Delta f_{res}/\Delta \beta_d$ (d) $\Delta V_{dc}/\Delta P_{diff}$ (e) $\Delta V_{dc}/\Delta \alpha_h$ (f) $\Delta V_{dc}/\Delta \beta_d$

Stability, controllability, and observability of modelled system in (6.32) and (6.33) are investigated. Eigenvalues of matrix A are equal to -3.68±99.7i, -4.43, -0.66±2.73i. All real parts of eigenvalue of matrix A are negative, so the system is stable for small variations around the steady-state operating point. Next, controllability is checked by MATLAB function "ctrb" for matrix A and B_1. Rank of ctrb(A,B_1) is equal to 6 so to the rank of A. Therefore, the system is controllable. Finally, MATLAB function "obsv" with matrix A and C is used to evaluate observability. Rank of obsv(A,C) is equivalent to the size of matrix A (6); the system is then well observable.

In our study, only the active power of energy storage will be studied. Therefore, the steady-state system presented in (6.33) is simplified under equation (6.47), with simplifications of the current and the switching function defined in q-axis (no control of reactive power is studied). The system in (6.47) remains stable, controllable and observable.

$$A=\begin{bmatrix} -\frac{R_{fsj}}{L_{fsj}} & -\frac{\alpha_{h0}}{L_{fsj}} & 0 & 0 & 0 \\ \frac{\alpha_{h0}}{C_{dc}} & -\frac{1}{C_{dc}.R_{dc}} & -\frac{\beta_{d0}}{C_{dc}} & 0 & 0 \\ 0 & \frac{\beta_{d0}}{L_{ac}} & -\frac{R_{ac}}{L_{ac}} & 0 & 2\pi.50.I_{sq0} \\ 0 & 0 & 0 & -\frac{1}{T_g} & -\frac{1}{s_d.T_g} \\ \frac{V_{ES0}}{2.H.S_{rated}} & 0 & 0 & \frac{1}{2.H} & -\frac{D}{2.H} \end{bmatrix}, B_1=\begin{bmatrix} 0 \\ 0 \\ 0 \\ 0 \\ \frac{1}{2.H} \end{bmatrix},$$

$$B_2=\begin{bmatrix} -\frac{V_{dc0}}{L_{fsj}} & 0 \\ \frac{I_{ES0}}{C_{dc}} & -\frac{I_{sd0}}{C_{dc}} \\ 0 & \frac{V_{dc0}}{L_{ac}} \\ 0 & 0 \\ 0 & 0 \end{bmatrix}, C_1=\begin{bmatrix} 0 & 0 & 0 & 1 \\ 0 & 1 & 0 & 0 \end{bmatrix}, D_{11}=D_{12}=D_{21}=0 \quad (6.47)$$

6.4 Controller design and validation

To design controller H infinity (K(s)), plant P(s) in (6.6) which consists of plant (G(s)), transfer function of output disturbance to output (G_d(s)), and weighting functions (W_u(s) and W_e(s)) is built. Plant G(s) or energy storage with converter DC/DC and inverter AC/DC has been modeled in small linear signal equation in the previous topic (6.3). Transfer function G_d(s) relates to frequency variation according to power variation of load and PV in (6.16). Prior to the calculation of controller H infinity, desired performance has to be defined by designing weighting functions. Performance outputs are DC voltage (ΔV_{dc}) and frequency (Δf_{res}). H infinity controller is desired to reject disturbance which is the variation of active power of load and/or PV. The H infinity controller has to keep the desired DC bus voltage level and to improve the transient response of the system frequency. In this analyze, the reactive power control is not taken into account. The switching function in q-axis is then assumed to be null. Therefore, the control inputs for studied system are defined as α_h and β_d. However, controlling current in q-axis or AC voltage regulation can be integrated to control objective by adding a switching function in q-axis (β_q) to another control input.

The weighting function is then defined for frequency and DC voltage to the desired responses. Furthermore, weighting functions are also applied to other two control inputs in order to signify their limit. Consequently, controller is designed and validated.

6.4.1 Weighting function design

The first weighting function (W_{e1}) is designed for system frequency having a time response around 0.1 second, with a corresponding frequency pulsation (ω_{B1}) of 25 rad/s. As mentioned in 6.2.1,

parameters A_ε and M can be expressed according to dynamic performance in time domain [116]. $A_{\varepsilon 1}$ which is related to the steady-state value of frequency response is defined as the ratio between frequency variation in steady-state and power variation of load and/or PV. Frequency variation in steady state of the power system without energy storage depends on droop value of primary frequency control of diesel generator in Figure 6.15. Equivalent inertia of the power system has effect on dynamic of frequency response as is has been described in Chapter 3. Steady-state frequency variation is 0.15Hz and 0.2Hz for a droop value of 6% and 8% respectively. Energy storage system has to be coordinated to reduce frequency variation of power system with droop value 8% (diesel generator less participates to frequency regulation). Desired steady-state frequency variation of system with energy storage is 49.9Hz (frequency variation 0.1Hz) for power variation of 100kW. Therefore, $A_{\varepsilon 1}$ is defined in per unit value as 0.04 ((0.1/50)/(100kW / 2MW)). The module margin of the sensitivity function is limited to 2 in order to increase the robustness of the control [121]. The maximum frequency variation in transient response of droop value 8% and inertia equivalent 1 second is 0.28Hz as shown in Figure 6.15. The maximum frequency variation (or overshoot) of desired frequency response is 0.2Hz or about 2 times of steady-state value. Therefore, M_{S1} is about 0.08 and the desired settling time of frequency response can be approximated as 2.3 seconds from $2.3/(\omega_{B1}.A_{\varepsilon 1})$.

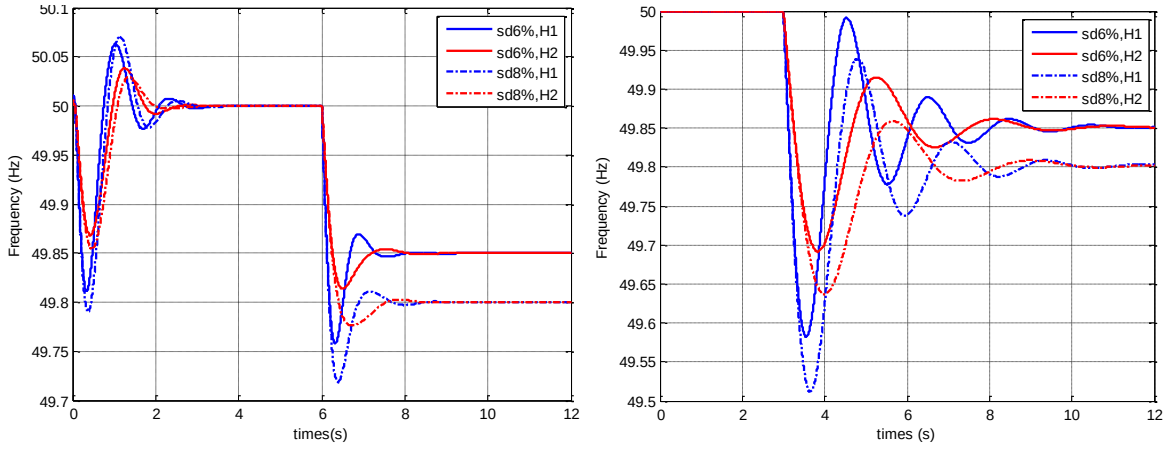

Figure 6.15 Frequency response of power system without energy storage with different droop value and equivalent inertia (H1=1s, H2=2s) according to rising of load active power of100 kW (T_g of diesel generator is equal to 0.22 seconds)

Energy storage by H infinity controller may not have deep effect on rise time of frequency response (from the choice of frequency pulsation (ω_{B1})). Rise time of frequency is fixed by the equivalent inertia of the power system (H) presented in figure 3.6(a) (Bode diagram of transfer function between frequency variation and power variation) and in Figure 6.15. Time response of frequency is slower (cut-off frequency of transfer function move to high frequency) when the equivalent inertia increases. Although the time response of the frequency variation cannot be reduced by the H infinity controller with measurement of only frequency variation, it can be decreased by adding derivative part of frequency to controller input and replace this part by H infinity controller for robustness to noise measurement [72].

The second weighting function (W_{e2}) is designed for DC bus voltage in order to have a time response around 50 millisecond (ω_B=50 rad/s). The objective of the DC bus voltage control is to retain its value at the reference value. From PI controller, DC voltage variation is maximal at 0.006 V for power variation of 100kW. So M_{S2} is fixed at 2 (0.1/(100kW/2MW)). Steady state value of DC voltage variation should be closed to zero so $A_{\varepsilon 2}$ will be equal to 0.2 (0.01/(100kW/2MW)). These two weighting functions are presented in (6.48) and (6.49).

Duty cycles of PWM of AC/DC inverter and DC/DC converter are both limited at 0.9 and cut off frequencies of W_{u1} and W_{u2} are both fixed at 7 kHz which is equivalent to Pulse Width Modulation

(PWM) frequency. Consequently, the weighting functions of switching functions α_h, β_d (W_{u1} and W_{u2}) are identical as defined in (6.50).

$$W_{e1}(s) = \frac{12.5s+25}{s+1} \tag{6.48}$$

$$W_{e2}(s) = \frac{0.5s+50}{s+10} \tag{6.49}$$

$$W_{u1}(s) = W_{u2}(s) = \frac{s+4.887e4}{0.01s+4.398e4} \tag{6.50}$$

6.4.2 Controller design and validation

Full-order Hinfinity controller is calculated according to the system modeling and the definition of weighting functions using MATLAB© software, and especially; the H infinity tool (function "hinfsyn"). In accordance with the objectives, S-over-KS design is used to find the optimal and robust controller K(s). A full-order H infinity controller of order 9 is founded with a global minimal value (γ_{min}) equal to 0.176. The output sensitivity function (S) which is defined as the ratio between output (y: Δf_{res} and ΔV_{dc}) and output disturbance (d_y; ΔP_{diff}) is plotted in comparison to their performance weighting functions (W_{e1} and W_{e2}) as illustrated in Figure 6.16. Moreover, the transfer function KS, which is the controller sensitivity function and is defined as the ratio between control input (u; α_h, β_d) and output disturbance (d_y; ΔP_{diff}), is also compared to weighting functions of control input (W_{u1} and W_{u2}) as illustrated in Figure 6.17 (a) and (b). Therefore, the sensitivity functions for studied system are:

$$S_1 = \frac{\Delta f_{res}^{pu}}{\Delta P_{diff}}, S_2 = \frac{\Delta V_{dc}}{\Delta P_{diff}}, S_1K_1 = \frac{\Delta \alpha_h}{\Delta P_{diff}}, S_2K_2 = \frac{\Delta \beta_d}{\Delta P_{diff}}$$

To validate performance of the obtained controller, sensitivity functions and complementary sensitivity functions should be lower all along the bandwidth of frequencues than γ_{min}/W_e or γ_{min}/W_u from (6.13). Although the sensitivity function and complementary sensitivity function of frequency (S1 and KS1) are below, they are quite near γ_{min}/W_{e1} or γ_{min}/W_{u1} in Figure 6.16(a) and Figure 6.17(a) respectively. It means that the steady-state value and the overshoot of the desired frequency variation (defined weighting function) is much smaller than the specification. According to γ_{min} = 0.176, the desired steady state and overshoot of frequency variation turns to be at 0.0176Hz and 0.035Hz respectively. Lower γ_{min} signifies that sensitivity function is quite further away from the initial weighting function.

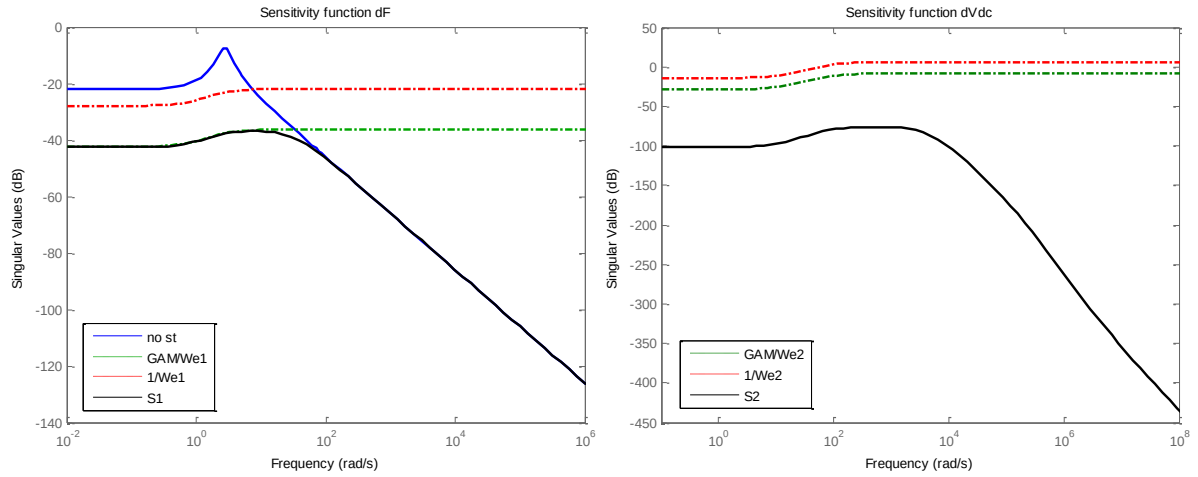

(a) (b)

Figure 6.16 Sensitivity function of (a) frequency variation (b) DC voltage variation

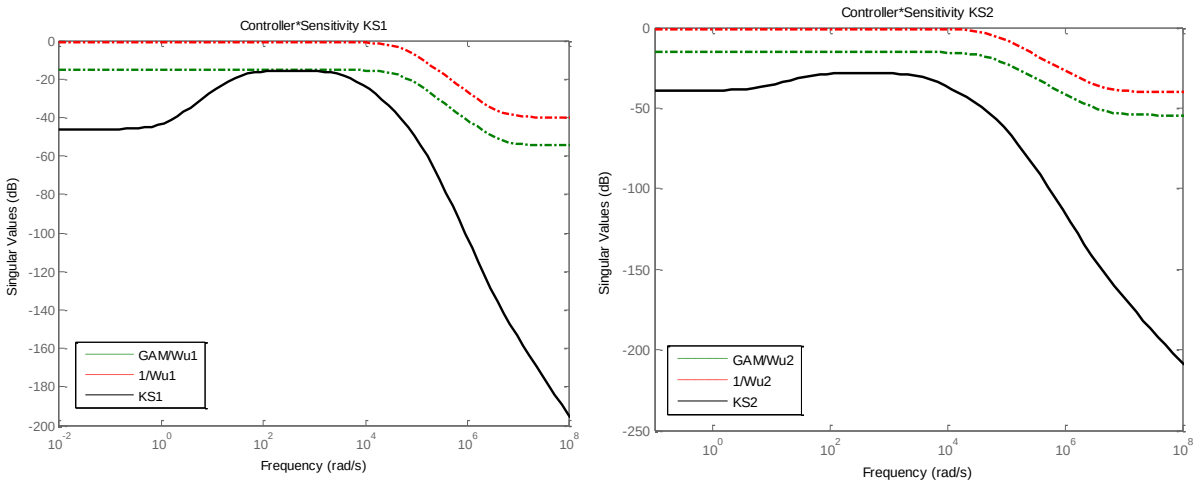

(a) (b)

Figure 6.17 Complementary sensitivity function of (a) frequency variation (b) DC voltage variation

The singular value of transfer function between frequency variation and power variation presented in Figure 6.16(a) also shows that energy storage can improve frequency response both for steady-state and dynamic behaviors. However, bandwidth in high frequency of system with and without energy storage is quite identical. As seen before, this is linked to the fact that the bandwidth in high frequency or rise time of frequency response is affected only by the equivalent inertia of the power system.

Furthermore, characteristics of transfer function between frequency variation and power deviation in frequency domain presents the critical frequency of power variation according to Figure 3.4 in Chapter 3. This critical frequency of power variation causes the largest frequency variation. Magnitude of transfer function between frequency variation and power deviation of system with energy storage (black line in Figure 6.16(a)) at a critical frequency is much below of system without energy storage in blue line. Therefore, impact of critical frequency is reduced by H-infinity controller.

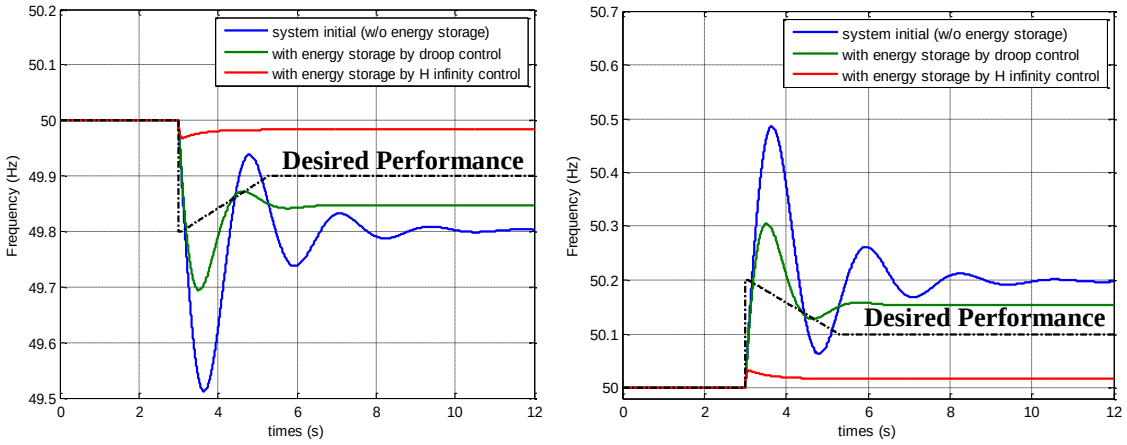

(a) (b)

Figure 6.18 Frequency response according to load power variation (a) +100kW (b) -100kW

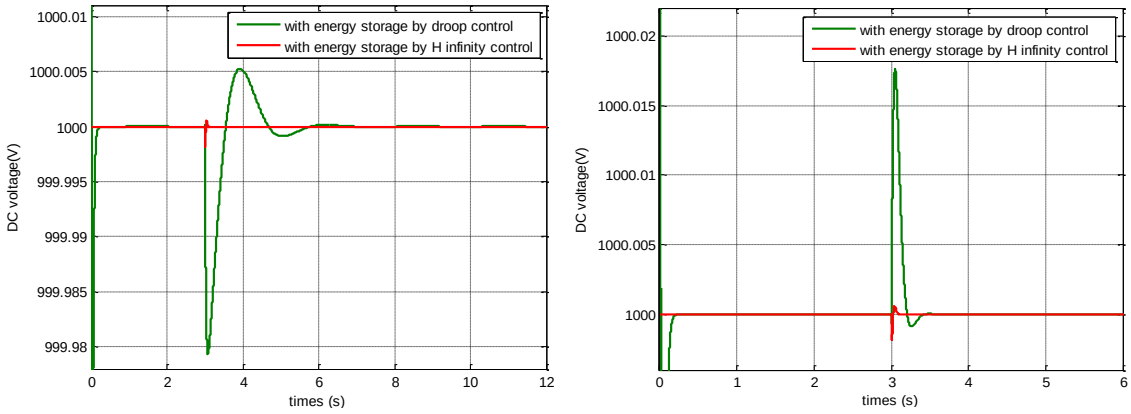

(a) (b)

Figure 6.19 DC voltage response according to load power variation (a) +100kW (b) -100kW

Previously, performance of system output has been validated in frequency domain. The system with its nominal parameters, controlled with K(s) in a closed loop system is then studied in time domain. A power variation of load is a disturbance of the studied system. The initial load power is equal to 1 MW, and variations of + 100kW are considered separately at 3 seconds. Frequency response of system with controller H infinity K(s) is illustrated in Figure 6.18, and compared to time response of the initial power system (without energy storage) and the system controlled with the droop control strategy (control #3). Indeed, the ESS controlled with the Hinfinity controller induces less frequency variations and DC voltage variation. As domain matter of fact, the frequency variation is within and far away from the desired response for robustness guarantee. Steady-state value of frequency variation of system with H infinity controller is about 0.018 Hz for both decreasing and increasing load power. Overshoot of frequency variation is reduced to 0.03 with the H infinity controller. Frequency response of system with energy storage is quite in respect to the desired performance (dash-dot black line in Figure 6.18). This coincides with results of frequency domain analysis. The DC voltage variations in Figure 6.19 (a) and (b) are quite small comparing to DC voltage response of ESS with control#3 (see Figure 6.10) and they are within the desired performance.

Moreover, energy storage by H infinity controller reduces power and slow down response of primary frequency control of diesel generator as shown in Figure 6.20 (a) and (b). Participated power of diesel generator for frequency regulation is reduced in low and medium frequencies up to 50 rad/s (8Hz) as presented in Figure 6.21. Energy storage system with small time response will participate to limit dynamic frequency response. However, such technologies require a maximal power larger than the others. Then, maximal power of energy storage by droop control and H infinity controller are equal to 45kW and 100kW respectively as illustrated in Figure 6.20 (c) and (d). After load power variation, energy storage by H infinity controller will participate in frequency regulation with the entire load power variation.

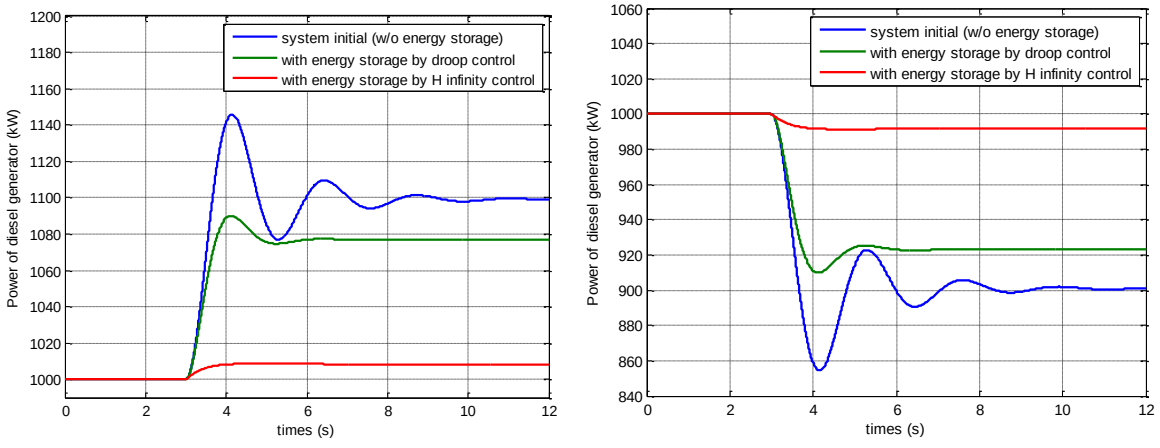

(a) (b)

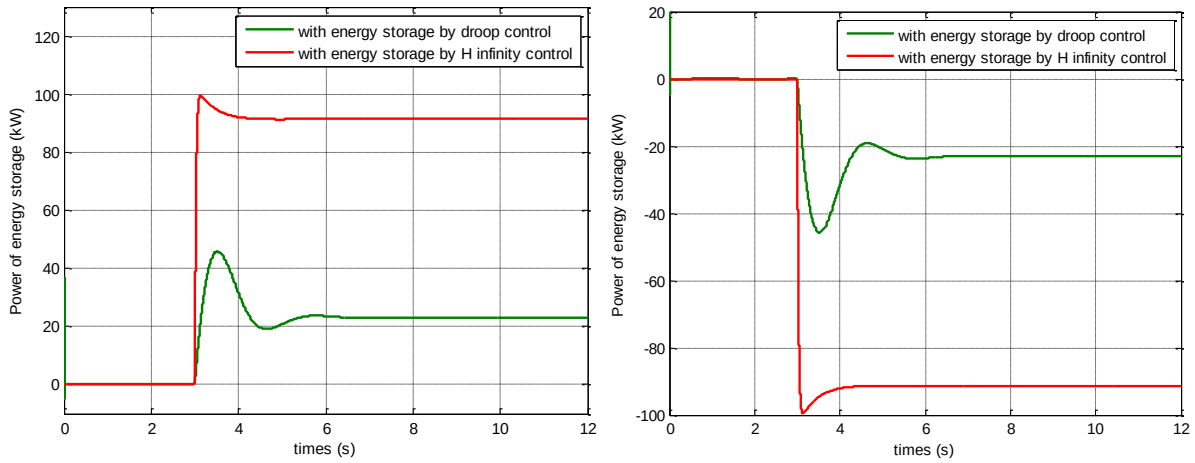

(c) (d)

Figure 6.20 (a) Power of diesel generator according to load power variation +100kW (b) -100kW (c) Power of energy storage according to load power variation +100kW (d) -100kW

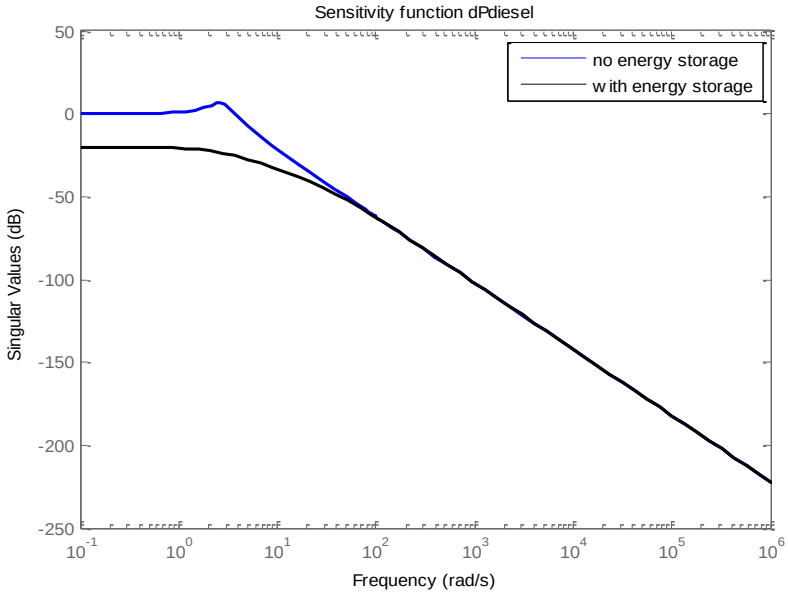

Figure 6.21 Sensitivity function of transfer function between power variation of diesel generator and power variation of load and PV (ΔP_{diff})

From power response of energy storage, the rated power of energy storage can be defined from the maximal power of load or PV variation. Then, an important peak of power provided by the ESS is needed if a small variation of transient frequency is required. A compromise between the frequency variation and the rated power of energy storage is necessary. As the frequency variation of the system with energy storage by H infinity controller is fixed by the definition of weighting function, the desired specification should be modified in order to increase some frequency variation for power reduction and energy used of energy storage which has impact on ESS cost. For example, the desired steady state value can be increased from 0.1Hz to 0.19Hz (nearer to response of system without energy storage) to reduce the participated power of energy storage.

The desired performance of frequency variation focuses only on primary frequency control. Therefore, energy storage does not participate to the secondary frequency control. Diesel generator will bring frequency back to 50 Hz after 15 seconds of disturbance. If energy storage is used to participate either to secondary frequency control, weighting function of frequency variation (W_{e1}) should be redesigned with small steady state value of frequency variation (small $A_{\varepsilon 1}$). However, in this case, a high rated energy of energy storage should be require and induces growth of investment costs.

Finally, sizing of energy storage according to robust control is studied. Frequency variation of system with energy storage by the classical primary frequency control depends on droop value of energy storage system and its rated power. To reduce frequency variation, droop value has to be decreased and/or power rated of energy storage should be increased. For robust controller, the participated power of energy storage for frequency regulation is quite equivalent to the power variation of load in dynamic region as illustrated in Figure 6.20(c). Therefore, energy storage can be designed according to the maximum power variation of load and PV.

6.5 Robustness analysis

Robust controller is designed according to desired performance in the previous section. Robustness of closed loop system is analyzed against parameter variation, uncertainties of operating point of diesel generator (that can be related to the time-varying PV power), and uncertainties on frequency measurement (through the Phase Lock Loop measurement of frequency). Controller K(s) is firstly designed to form a closed loop system while parameters of system are fixed to their nominal value (corresponding zero variation around the steady-state point). The sensitivity functions of frequency (S_1) and DC voltage (S_2) are analyzed against the desired weighting function W_{e1}, W_{e1n}, and W_{e2} in singular value plot. Afterward, μ-synthesis is applied to analyze robust stability (RS) and robust performance (RP) against parameter uncertainties. Uncertainties on system modelling are not studied in this thesis. Finally, an unstructured uncertainty is studied, modelling an error on frequency measurement.

6.5.1 Parametric uncertainties with sensitivity function analysis

Parameters of the system can be separated into three groups: parameters of the energy storage system (R_{fsj}, L_{fsj}, C_{dc}, L_{ac}, and R_{ac}), parameters of diesel generator (t_g, s_d), and parameters of the isolated grid (H, D). Maximal uncertainties on energy storage system parameters (R_{fsj}, L_{fsj}, C_{dc}, L_{ac}, and R_{ac}) have been calculated to ±66% and ±65% for robust stability and robust performance respectively [122].

The sensitivity of the grid equivalent inertia (H), the load damping constant (D), the droop associated to control of diesel generator (s_d), the time response of diesel engine (t_g), and the initial voltage of energy storage (V_{sst0}) is studied in this section with the help of the sensitivity functions. Then, Figure 6.22(a) shows that the equivalent inertia has a high impact on dynamic of frequency response but less important one on the DC voltage. The first sensitivity function (S_1) plot (relation between frequency and output disturbance (power variation)) in Figure 6.22(b) shows also that higher the equivalent inertia, smaller the overshoot of the frequency response is but with a longer rise time. The gain of frequency variation is always less than the desired specification. The DC bus voltage variation is always within the desired response for any value of equivalent inertia. Load damping constant, droop value and time response of diesel generator have also significant effects on frequency response but less effects on DC voltage. The droop value and time response of diesel generator have effects on steady-state value and some dynamic in medium frequency range respectively as shown in Figure 6.23.

On the other hand, the initial voltage of energy storage has an effect on the second sensitivity function (S2 – transfer function between DC voltage variation and power variation). It causes less effect on the first sensitivity function. Designed controller is robust in stability and performance according to the defined parameters uncertainties except that it does not have robust performance to uncertainty linked to initial voltage of energy storage as shown in Figure 6.24. Controller is designed according to critical parameters (small equivalent inertia, high time response of diesel generator, high droop linked to diesel generator and low load damping constant) to ensure the robustness against performance.

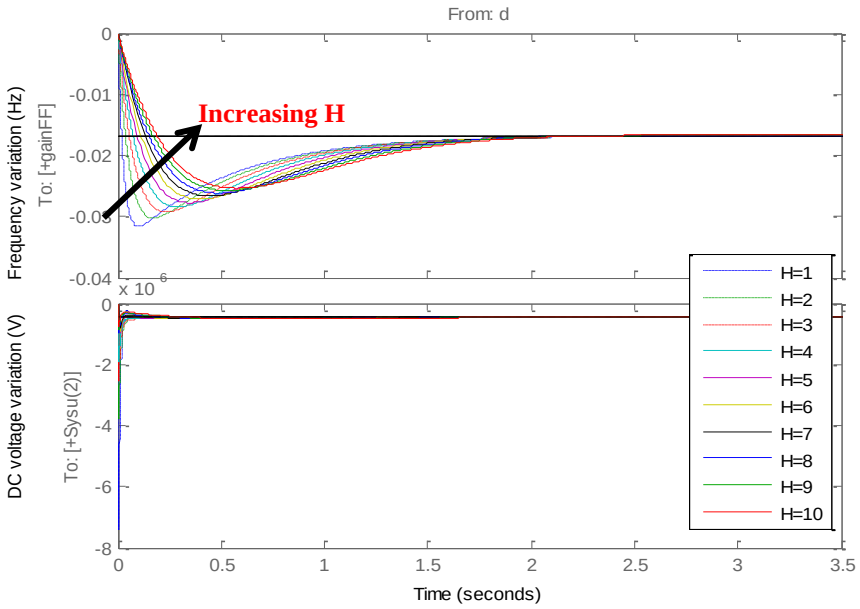

(a)

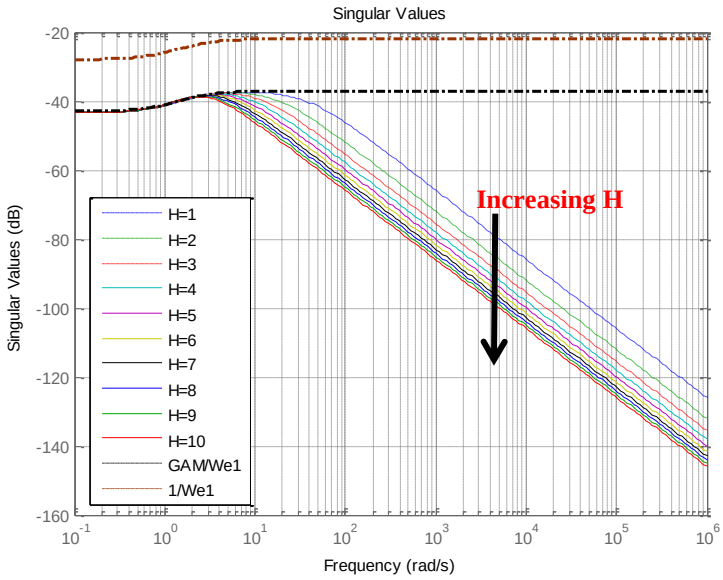

(b)

Figure 6.22 (a) Frequency and DC voltage response in time domain (b) S1 (sensitivity function of transfer function between frequency variation and power variation) for various inertia equivalents (H)

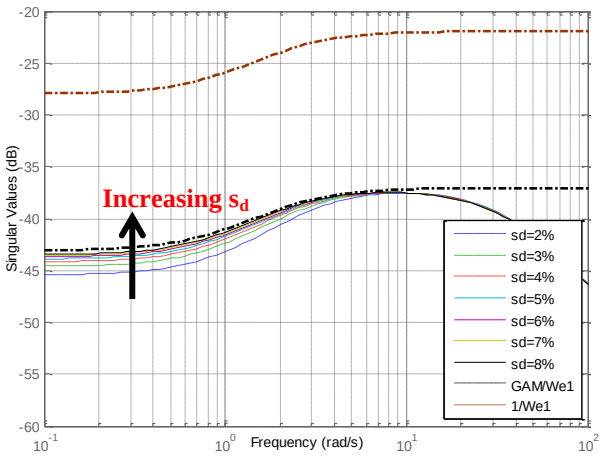

(a)

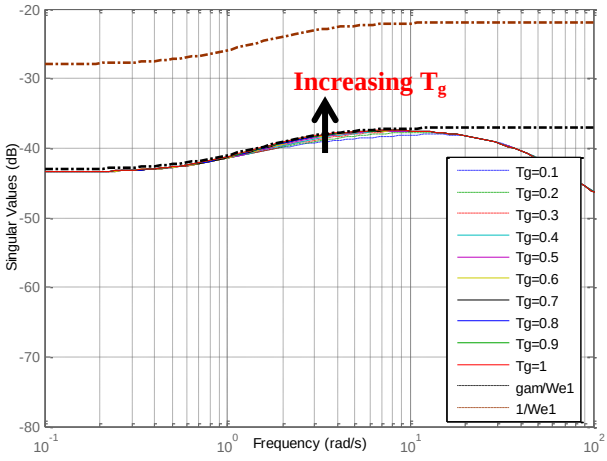

(b)

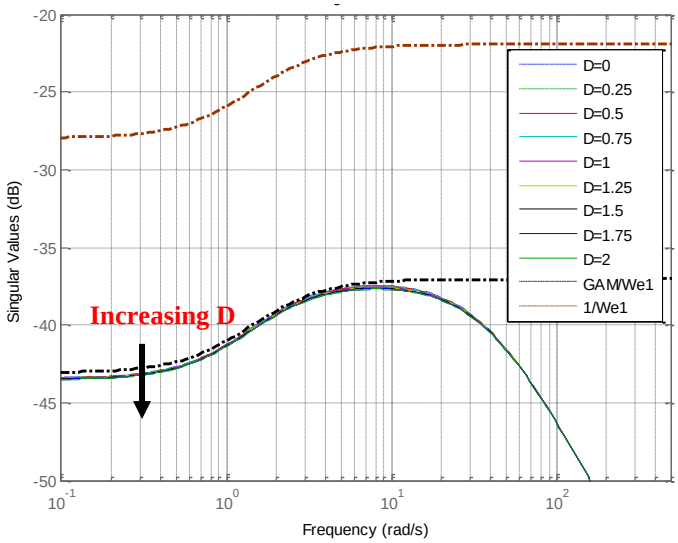

(c)

Figure 6.23 S1 (sensitivity function of transfer function between frequency variation and power variation) for (a) various droop value of diesel generator (s_d) (b) various time response of diesel generator (T_g) (c) various load damping constant (D)

Variation of the initial voltage of energy storage from its "rated" value (750V) which has been taken into account in the design of controller, cause larger DC voltage variation as illustrated in Figure 6.24(b). Response of DC voltage checks also the desired reference in dynamic response. Designed controller can ensure the desired performance up to 650V and 900V from sensitivity function analysis, which corresponds to variations of -13.33% and 20% from the reference value of 750V.

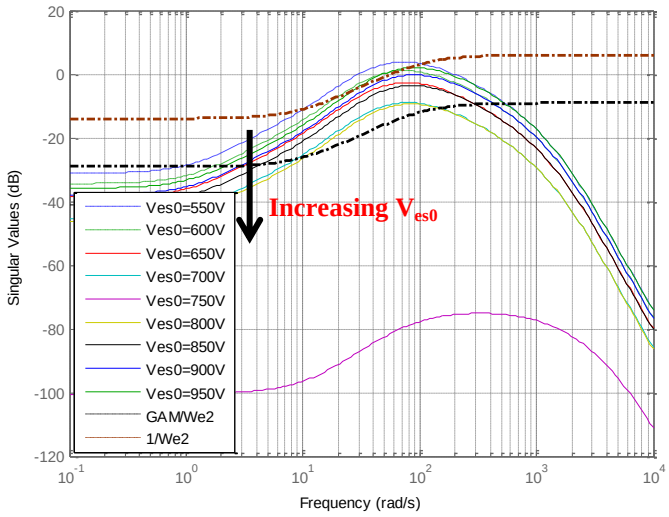

(a)

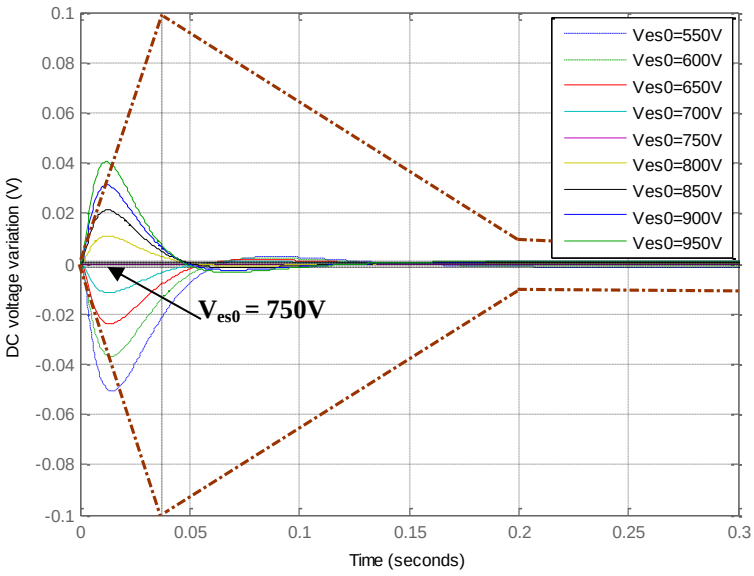

(b)

Figure 6.24 (a) S2 (sensitivity function of transfer function between DC voltage variation and power variation) (b) DC voltage response in time domain for various initial voltage of energy storage (V_{es0})

6.5.2 µ-analysis for robustness

In the previous section, robustness is analyzed in time and frequency domain. Then, robustness of system with H infinity controller is analyzed using the µ-analysis. It is analyzed according to the parametric uncertainties. Once a H infinity controller (K) has been designed, the matrix M which consists in P and K is determined. This matrix M is connected with matrix Delta using upper LFT. Matrix Delta contains unknown uncertainties. Robust stability and robust performance are then analyzed from M_{22} and M_{11} of matrix M. Uncertainty of each parameter is firstly defined by MATLAB function "ureal". Robust stability and robust performance are analyzed weather the controller is in respect to the estimated uncertainties by MATLAB function "robuststab" and "robustperf".

Maximal uncertainties of each parameter are then analyzed. The designed controller is then robust in stability up to 95-100% of uncertainties from the initial value for all parameters presented in Table 6.1. Moreover, the controller is robust in performance according to uncertainties of load damping constant, droop linked to diesel generator and time response of diesel generator for uncertainties up to 95100%. It is also robust in performance for uncertainties up to 82% of equivalent inertia as shown in Figure 6.25. The closed loop system is robust in stability according to uncertainties of the initial voltage of energy storage up to 100% as illustrated in Figure 6.26(a). However, it is robust in performance for uncertainties on voltage up to ±17% as shown in Figure 6.26(b).

Table 6.1 : Maximal uncertainties for robust stability and robust performance for different parameters

Parameters	Maximal uncertainties for Robust stability	Maximal uncertainties for Robust performance
H	99%	82%
D	>100%	>100%
S_d	99%	99%
T_g	95%	95%
V_{es0}	100%	17%

When energy storage is used to regulate grid frequency according to power variations of load and/or PV, the voltage of energy storage device will vary with time (quickly with supercapacitors, slower with lead-acid batteries). The designed controller can guarantee the desired performance only for variations of voltage up to 17%, i.e in the range of voltages between 622.5 and 877.5V, and in

practice between 622.5 and 750 V for security. It can be noticed that this range of evolution seems to be quite a small range, especially for supercapacitors for instance. The controller is then redesigned with equivalent desired performance for different voltage of energy storage: 650V and 550V. Time response of frequency and DC voltage according to the initial Hinfinity controller designed for 750V and adapted controllers for 650 and 550V are illustrated in Figure 6.27 and Figure 6.28, respectively. Voltage of energy storage is taken equal to 750V, 650V and 550V at 0, 60, and 120 seconds respectively. Load power is increased to 100kW at 3, 65, 125 seconds. Frequency variation of the adapted controller is larger than the fix controller at 750V but it is still within the desired performance. The adapted controller shows that it can improve DC voltage response of the fix controller at 750V and makes DC voltage response always in the acceptable limit for equivalent voltage at 550V.

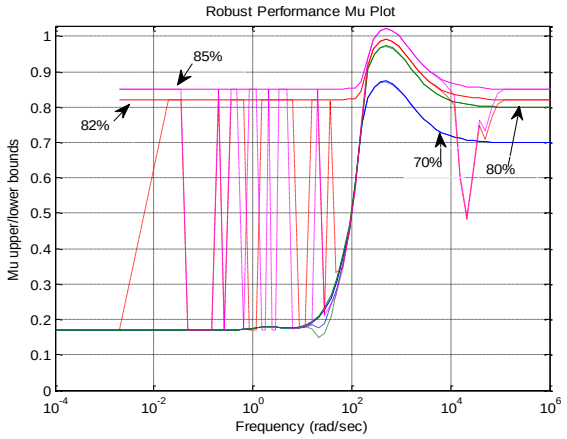

Figure 6.25 µ plot of robust performance according uncertainty of inertia equivalent

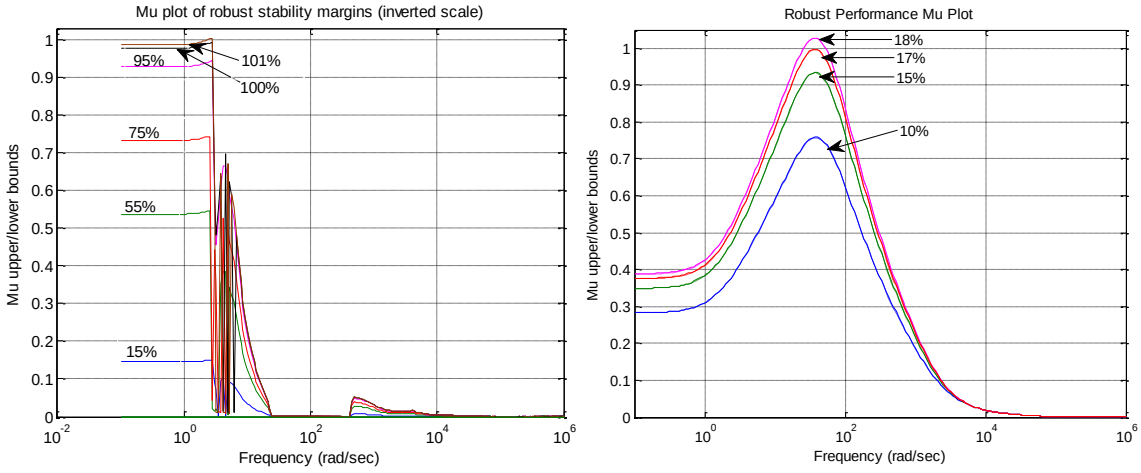

(a) (b)

Figure 6.26 µ plot of (a) robust stability (b) robust performance according to uncertainty of equivalent value of voltage of energy storage

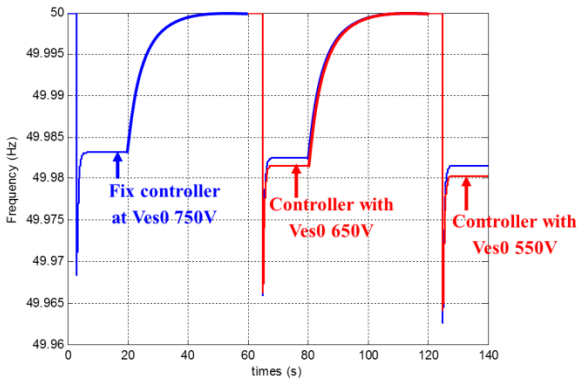

Figure 6.27 Frequency response with different equivalent point of voltage of energy storage at 0, 60, and 120 seconds and load power variation 100kW at 3, 65, and 125 seconds

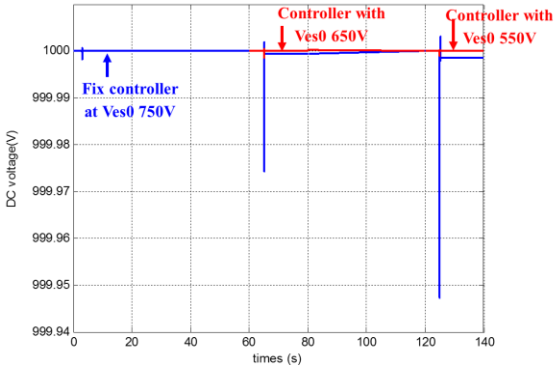

Figure 6.28 DC voltage response with different equivalent point of voltage of energy storage at 0, 60, and 120 seconds and load power variation 100kW at 3, 65, and 125 seconds

6.6 Conclusion

A Hinfinity controller retains the closed loop system stable and allows ensuring desired performance even with uncertainties. It also improves the frequency response in time domain and those of the DC bus voltage compared to the classical PI controller. Furthermore, it requires only grid frequency and DC voltage measurement. In case of PI controller, the measure of frequency, DC bus voltage, current and voltage of energy storage, AC current and AC voltage output of energy storage are needed. Therefore, the system with PI controller needs more sensors. Furthermore, the designed robust controller is quite robust in stability and performance according to parametric uncertainties except that equivalent voltage of energy storage has large effect on robust performance. The obtained H infinity controller is in high order. Reduction order of controller and PI H infinity controller should be studied.

In this study, limitation of energy storage such as variation of energy storage voltage, State of Charge (SoC) and maximal power have not been taken into account. For further study, these should be taken into account by adding equation of voltage of energy storage, measured and add weighting functions for control current of energy storage, etc. Moreover, R_{dc} (signify loss) which is neglected should be considered in the further study.

A Linear Parameter Variant (LPV) [112] approach should be also an interesting way of investigations to ensure stability and performances for any value of this voltage. Moreover, H infinity controller is quite promising for frequency regulation of diesel generator. Classical frequency regulation would then be replaced by a robust controller too. Weighting functions describing performances could be deduced from bandwidth filtering of the different sources.

Besides, the impact of the Phase Lock Loop (PLL) information that measure grid frequency would be also interesting because PLL induces some fast dynamics of frequency response (see Chapter 4). Unstructured uncertainties according to the measured frequency by PLL should be analyzed followed by the redesign of a new controller which may be robust to this uncertainty.

Chapter 7

Simulation and validation on experimental test bench (RTLAB)

7.1 Introduction

The different strategies presented in the preceding sections have been simulated with mathematical models in MATLAB©. More complex the model is; longer time of simulation is taken. To validate controller synthesis and control strategy with almost identical to real system, a real-time simulator (RTLAB in this study) has been used to simulate the hardware and the simulated system. Some parts of the studied system are replaced by hardware and others are modeled with mathematical model in computer which is called hardware-in-the-loop (HIL). Due to the merit of the real-time simulator, the simulated time has been lessened and time of simulation is identical to the real time. In this chapter, RTLAB is introduced firstly, followed by the presentation of the simulated system and hardware; as well as, the methodology of the real time simulation will also be elaborated. Finally, the simulated results with some significant issues will concluded this chapter. In this thesis, the different controls of energy storage system studied in Chapter 4 are validated with a real DC/DC converter, connected to a pack of supercapacitors. Because of the limitation of hardware development and the leak availability of the test bench (without any real PV connected to the system), the PV power variations, presented in Chapter 2, will be emulated in this experimental work. This is the first step which allows validating controller design, and then, the validation of the different strategies with the complete system, will be done in a further study (PhD thesis of Linh Lam Quinh).

7.2 RTLAB Presentation

RTLAB is a distributed real-time platform which facilitates the simulation of highly complex models. Simulink dynamic models are thus connected to hardware to build hardware-in-the-loop (HIL). This tool thus reduces simulation time and saves cost. Real time platform consists of Command station, Compilation node, Target nodes, and I/O boards [123] as illustrated in Figure 7.1. The Command station is a computer workstation whose functions are to modify the models, record simulated results, and distribute code, etc. by RT-LAB software (with MATLAB Simulink). This is the interface part for user. The Compilation node is used to compile generated C code. Simulations can be run on one or several target nodes (one of them is defined as the compilation node). The I/O board is a communication media which is used to link the command station to target node(s) and/or target nodes to hardware or external equipment.

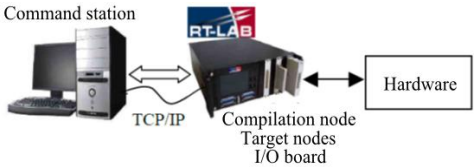

Figure 7.1 RTLAB platform

Fixed step time simulation should be used for power system simulation. Step time around 50 µs is enough to simulate power system in MATLAB, both in steady state and transients [66]. Sampling of time simulation should be small enough for reliable simulated results. Step time simulation should be smaller than inverse of 50-100 times of PWM frequency and 20 times of resonant frequency. Simulation inaccuracy could be caused if ratio between the simulated frequency and PWM frequency is small. High current distortion and jitter which does not exist in an actual system are detected because of the maximal time delay in one time step. This false current causes the difficulty to tune controller's parameters [66]. Besides, high PWM frequency is needed for good sine signal of AC voltage and current which causes small sampling time. Simulations in MATLAB Simulink take quite a long time to simulate power system as having presented in Chapter 4.

The real time simulation can increase the step time simulation (reduce simulation time) with guaranteed simulation accuracy. As one step time delay has been eliminated by RT-Event (RTE) in RTLAB platform simulation, ratio between the simulated frequency and PWM frequency is only 5-10. For a frequency of PWM equal to 5 kHz, the needed step time simulation are 4µs and 40 µs for off-line simulation in MATLAB and for real time simulation with RTLAB respectively.

For the real time simulation, mathematical model of system with designed controller is firstly validated. Then, hardware is determined and connected. Transmitting signal between hardware and RTLAB platform is tested. Finally, the real time simulation is evaluated in operation.

7.3 Simulated system and step of simulation

The studied power system consists of diesel generator, PV, ESS and load. As we have decided to analysis the behavior of the actual energy storage system, the others elements (diesel generator, PV, and load) are only modeled in MATLAB Simpowersystem Simulink as shown in Figure 7.2. The energy storage system consists of energy storage, DC/DC converter, AC/DC inverter and filter as illustrated in Figure 4.2. In this study, only the DC part is studied and has been modeled (energy storage device and DC/DC converter); of the DC/AC interface of the energy storage device has been also simulated, as illustrated in Figure 7.7(a).

Hardware of this simulation is then: a DC controllable source (Figure 7.3) which can be replaced by a pack of supercapacitor (Figure 7.5), a DC/DC reversible converter, a constant load resistance (Figure 7.4(a)), and a DC controllable load (Figure 7.4(b)). The HIL system is separated into two configurations. The energy storage device is firstly modeled as a DC source and a DC load for discharge and charge modes respectively. The discharge and charge modes of energy storage are simulated separately in order to simplify the simulation. Another HIL system is quite similar to the real energy storage system with a supercapacitor pack connected to controllable DC load and source via a DC/DC converter.

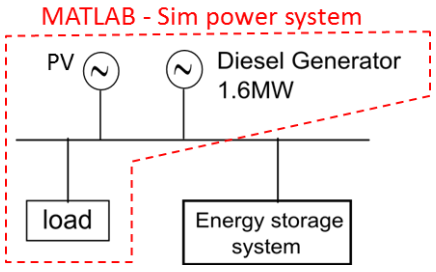

Figure 7.2 Real time studied system

7.3.1 Hardware specification

To emulate the DC side of the energy storage system, a pack of supercapacitor, a DC/DC reversible converter, a DC voltage source and a DC load are then needed and presented below.

7.3.1.1 Controllable DC source

This DC source, depicted in Figure 7.3, is in type Xantrex XDC 600-20, which maximal specifications are 600V and 20A. It is controlled by an analog input of 0-10V. One analog output of RTLAB platform transmits a signal of [0-10V] to control this source. Output signal can be either the information of voltage (to represent a DC voltage source) or current (to represent a DC current source). Specified voltage and current in RTLAB software should be multipled with a rate of 1/60 and 1/2 respectively before sending to this source. This DC source is used as to emulate the energy storage device in discharge mode (connected to input of DC/DC) and the AC part of energy storage in charge mode (connected to output of DC/DC).

Figure 7.3 Controllable DC source

7.3.1.2 DC loads

Two different DC loads are used in these tests: a constant resistor of 106Ω and a controllable DC load. The resistor is connected to input of DC/DC to represent the energy storage device in charging mode and the output of DC/DC converter to model the AC part in discharging mode.

Another DC load, illustrated in Figure 7.4, is a controllable DC load TDI RBL488 Series with a maximum power, voltage and current of 4kW, 400V, and 600A respectively. This DC load has three different ranges of operation: 0-20V, 0-200V, and 0-400V for voltage and 0-20A, 0-200A, and 0-600A for current. There are many modes of operation; for example, constant current mode, constant voltage mode, constant resistance mode, etc. In this simulation, [0-200V] and [0-20A] ranges have been selected with a constant current operation mode. The load current is calculated according to the AC part of energy storage system in RTLAB software with a multiplication rate of 1/2 for converting specified data to analog signal data in [0-10V] before being transmitted to the DC load.

Figure 7.4 Description of the DC controllable

7.3.1.3 Super capacitor pack with its reversible DC/DC converter

Supercapacitor system consists in one supercapacitor (type Maxwell BoostCap 165F), a Buck-Boost converter (350A, IGBTs SEMIKRON, SKM200GB123D with 1200V and 200A maximal) and their electrical and thermal protections, as illustrated in Figure 7.5 and Figure 7.6. Electrical circuit of super capacitor pack and converter is re-configurable. Then, the super capacitor can be disconnected from the DC/DC converter and replaced by a DC voltage source or DC load (following the simulation of discharging and charging modes). Protection system consists of switches for security (in series with supercapacitor and one placed in parallel to a series resistance dedicated to prevent overcurrent) and another resistance of 5Ω, dedicated to the discharge of supercapacitor at the end of the simulation (to make State of Charge reaching 0%).

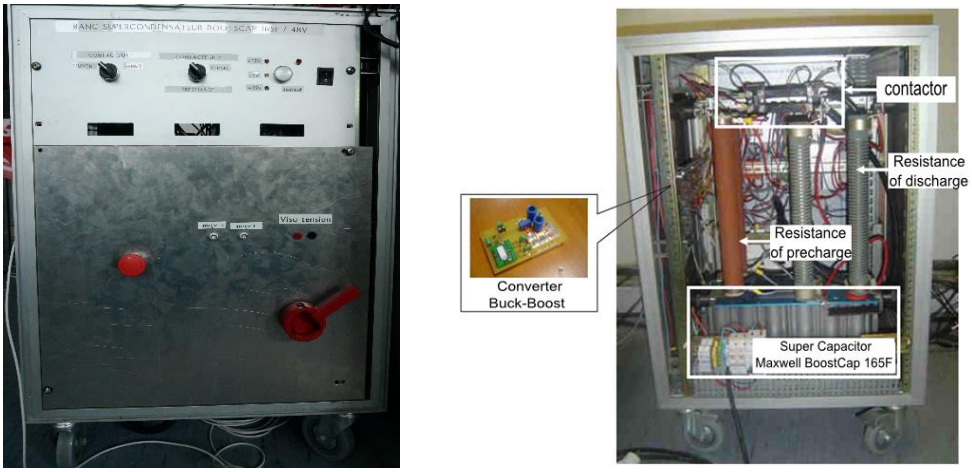

(a) (b)

Figure 7.5 Supercapacitor system (a) front view (b) back view

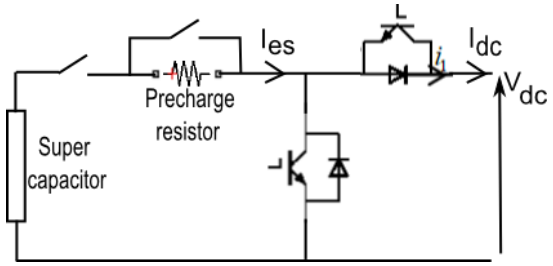

Figure 7.6 Protection circuit of supercapacitor with its converter

7.3.2 Hardware in a loop configuration

Hardware which is represented by the DC part of the ESS is connected to the AC part and power system via the RTLAB software (the grid is modelled with MATLAB-Simulink). This link is assumed with I/O board and target nodes as illustrated in Figure 7.7. The DC part of the ESS in RTLAB becomes controllable DC voltage source if the DC/DC converter controls the DC voltage (see section 4.4.3 of Chapter 4), or controllable DC current source for controlling the storage current (see section 4.4.4 of Chapter 4). And controllable DC voltage or current source is connected to AC power system via an AC/DC interface and filters in RTLAB as shown in Figure 7.7 (in pink dotted block).

Hardware of the DC part of ESS is more simplified than the simulated model in the previous chapter. According to hardware limitation, voltage of energy storage (SC) is reduced to 30-40V. This SC voltage has effect on the DC voltage output of DC/DC converter, as the switching function of DC/DC converter has been limited to 0.2-0.8. Therefore, the DC voltage reference equals to 150V for both separated simulations in discharge and charge modes, and to 70V for super capacitor simulation. Measured DC voltage will be multiplied with 1000/150 or 1000/70 to transform the DC voltage to be an appropriate value for connecting to AC system in RTLAB. Furthermore, power flow in hardware is also much smaller than the reference value because of limitation of the current.

To simulate complete ESS system, the supercapacitor with its associated chopper is connected to the AC system composed with a controllable AC source and load through the AC/DC inverter of Dspace as illustrated in Figure 7.8. The frequency regulation for the system via the AC/DC inverter is implemented in Dspace platform. Complete energy storage system is represented as an AC current source for connecting to AC grid in RTLAB simulator. All equipment, except the AC/DC inverter, are controlled by RTLAB. The output voltage of the chopper is controlled to 150V according Dspace specification [105]. Power variations of load and PV generate current signal to AC system as a disturbance. The Phase Lock Loop (PLL) is also implemented in Dspace in order to determine the frequency. Complete energy storage with DC and AC system is not simulated in this study because there was a problem of synchronization between the RTLAB and the Dspace platform. Moreover, the Phase Lock look has to be redesigned for robustness against noise of measured AC voltage.

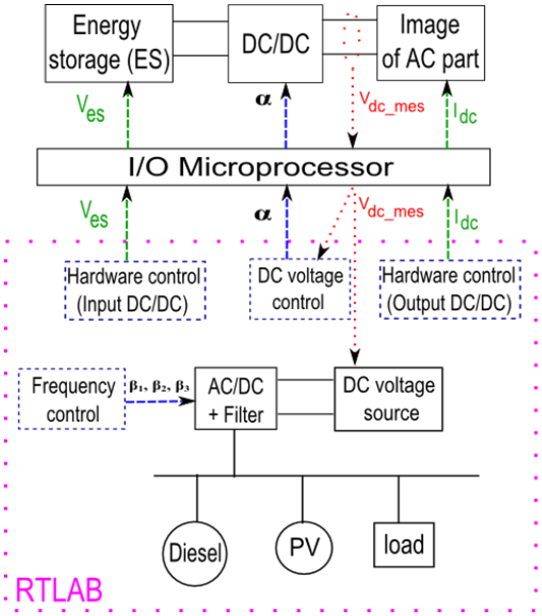

Figure 7.7 Hardware in a loop of DC part of energy storage system for DC voltage control

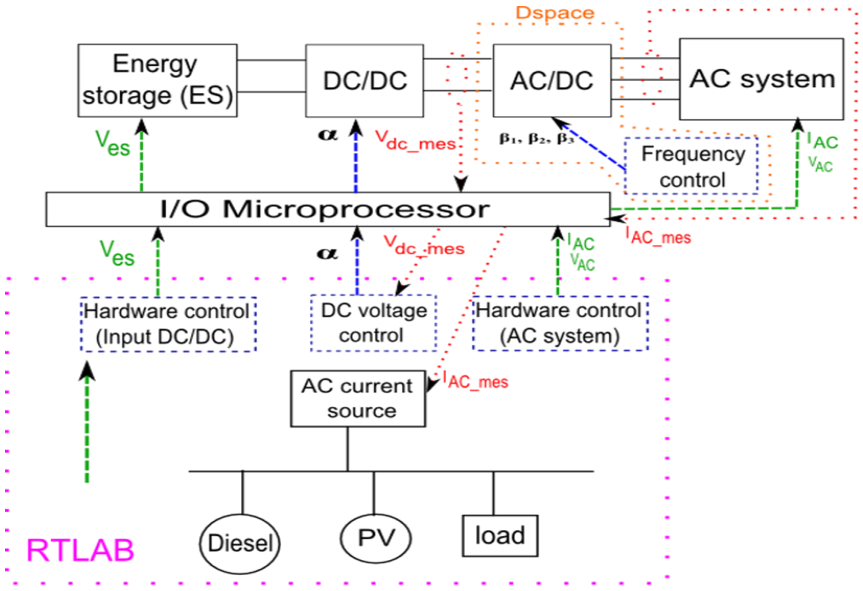

Figure 7.8 Hardware in a loop for complete energy storage system simulation

7.3.2.1 Separated charge and discharge mode simulation

The DC voltage source and load are firstly used to test the control system architecture because of their simplicity and robustness against the real pack of supercapacitor. Discharging and charging modes of the energy storage device are then separately operated. For the discharging mode, as

illustrated in Figure 7.9(b), the energy storage device (input of the DC/DC converter) is replaced by a controllable DC source and the AC part of energy storage system (output of DC/DC converter) is emulated by a DC load or a resistance. On the contrary, input of DC/DC converter is connected to resistance and output of DC/DC converter is considered as the controllable DC source to emulate the charging mode configuration, as shown in Figure 7.9(c). These two different configurations are simulated with two different control loops: one which allows controlling the DC bus voltage (V_{dc} – voltage output of DC/DC converter) and the other, which controls the current of energy storage device (I_{es} – current input of DC/DC converter). The mathematical model of the supercapacitor presented in Chapter 4 is introduced in RTLAB to calculate its voltage and its value is taken into account as a control signal to DC source or DC load.

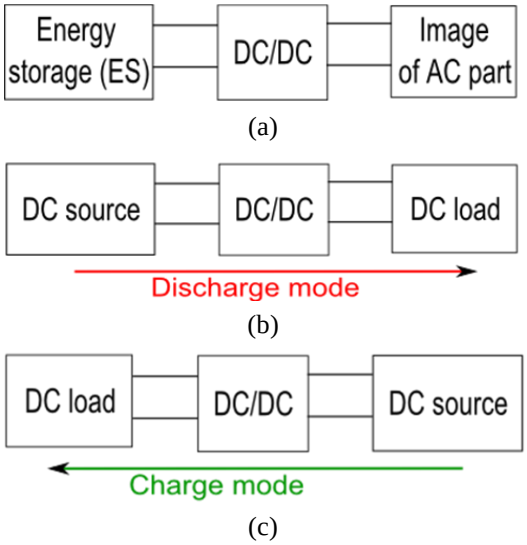

Figure 7.9 Configuration of HIL for separating charge and discharge mode (a) DC part of energy storage system (b) Discharge mode (c) Charge mode

a.) Current of energy storage control

To validate the current of energy storage controller, discharge and charge circuits shown in Figure 7.9 (b) and (c) are implemented as illustrated in Figure 7.10 (a) and (b). The current at input of DC/DC converter is measured by current sensor, and then sent back to the controller implemented in RTLAB software to compare with the reference value and generate switching function in order to control converter. In discharge mode simulation, the calculated voltage of supercapacitor is transmitted to DC voltage source. In charge mode, the DC voltage of circuit in RTLAB is measured and sent to control DC voltage source whose voltage is quite stable at 150V. For current control of energy storage system, a resistance is use in place of the controllable DC load because two DC current sources cannot be connected in series.

Active power of energy storage system (denoted P_{es_ref}), which has to be delivered to regulate frequency for different strategies as shown in Figure 7.11(a) is used to calculate the current reference of energy storage system ($I_{es\_ref\_r}$) (see Figure 7.10(b)) in (7.1) where *real_gain* is the ratio between maximal power of studied system and those of hardware and V_{ES0} is the initial voltage of energy storage. The voltage across the resistance is neglected. The DC bus voltage output of DC/DC converter in discharging mode is not controlled with hardware but by the AC/DC converter in RTLAB software.

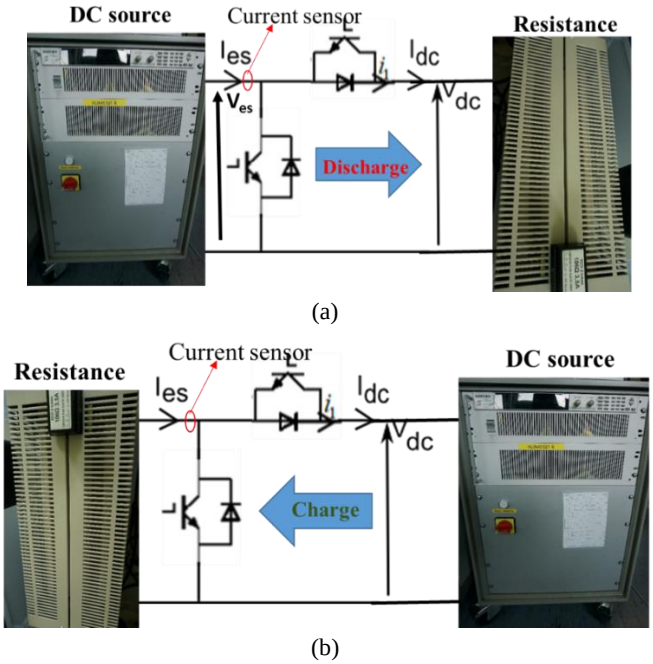

Figure 7.10 Hardware circuit of current of energy storage control (a) in discharge mode (b) in charge mode

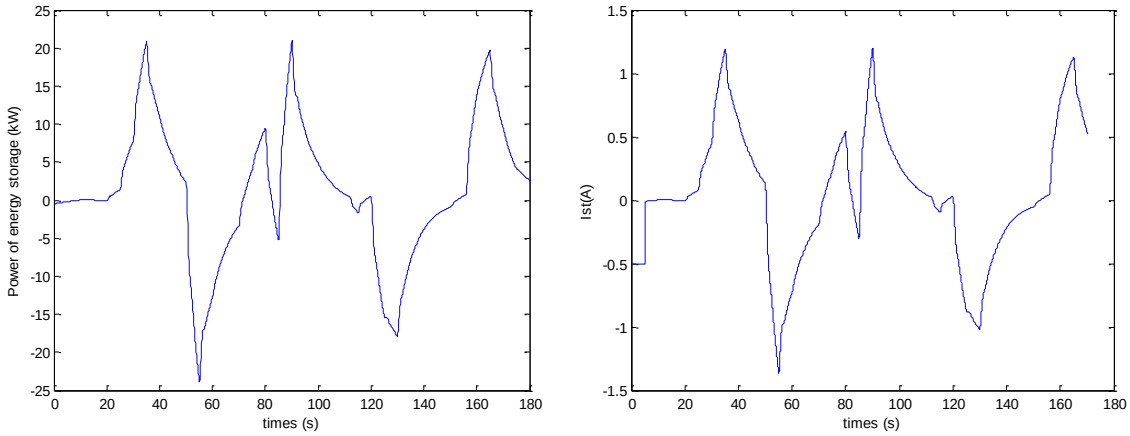

(a) (b)

Figure 7.11 (a) Power of energy storage according to droop control strategy (b) Current of energy storage signal

$$I_{es\_ref\_r} = \frac{P_{es\_ref}}{real\_gain.V_{ES0}} \tag{7.1}$$

b.) DC voltage control

The DC bus voltage control is assumed by the control of supercapacitor current, as it has been developed in chapter 4. Discharge and charge circuits shown in Figure 7.9 (b) and (c) are implemented as illustrated in Figure 7.12 (a) and (b) for validation of DC voltage control. The DC voltage (V_{dc_mes}) is measured at output of DC/DC and then transmitted to the I/O microprocessor for DC voltage controller. The DC voltage controller generates a switching function (α) to DC/DC converter. Furthermore, control signal for the equipment at input and output of DC/DC converter is also sent from RTLAB simulator. As it has been mentioned earlier, voltage of energy storage (V_{es}) is calculated from supercapacitor model in RTLAB and is transmitted to the equipment at input of the DC/DC converter for the simulation of discharge and charge modes. In discharge mode, the calculated voltage of supercapacitor is transmitted to the DC voltage source, and then calculated DC current is sent to the controllable DC load. In charge mode, the calculated DC current is sent to control DC source which is represented as the disturbance of control system.

The network power fluctuations are then only considered as disturbances for this control loop. The output voltage is controlled to a constant value of 150V (suitable for connecting to Dspace

platform) according to the variation of DC current. The output of DC/DC or image of AC part of energy storage is controlled by current signal. Active power of energy storage system (denoted P_{es_ref}), as shown in Figure 7.11(a), is used to calculate the DC bus current (I_{dc_r}) which corresponds to the disturbance of the system and modelled by equation (7.2) where V_{dc_ref} is the DC bus voltage reference.

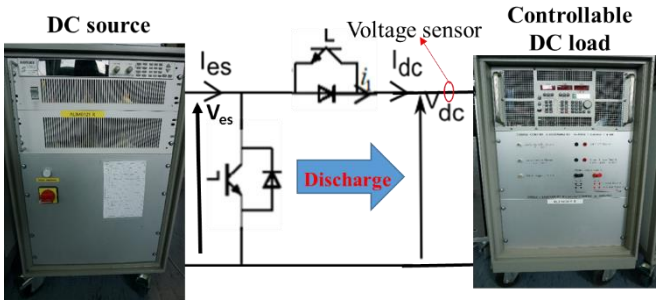

(a)

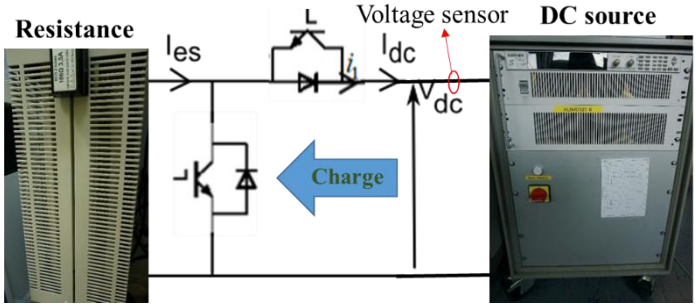

(b)

Figure 7.12 Hardware circuit of DC voltage control (a) in discharge mode (b) in charge mode

$$I_{dc\_r} = \frac{P_{es\_ref}}{real\_gain.V_{dc\_ref}} \tag{7.2}$$

Controlling DC voltage by switching function of DC/DC converter (α) defined in Chapter 4 (Energy storage system control 2) consists of DC voltage and current of energy storage via PI controllers. The output of these controllers corresponds to the switching function signal. This control system is not robust to measurement noise. In the real time simulation, two PI controllers are replaced by H infinity controller which has been analyzed in this thesis. The H infinity controller is redesigned from the DC model equation in (6.27) and (6.28) and weighting function for DC voltage and α in (6.49) and (6.50). H infinity controllers have to be designed for different DC voltage references (150V and 70V) to guarantee desired performance.

7.3.2.2 Supercapacitor simulation

Super capacitor of 165F is connected to input side of DC/DC to inject or absorb energy. Output of DC/DC converter consists in controllable DC load and controllable DC source which work in parallel as illustrated in Figure 7.13 [105]. DC current (I_{dc_r}) by equation (7.2) controls these two elements because only DC voltage control is simulated with this configuration. When DC current is positive, energy storage is in discharge mode and injects power to the DC load; the DC source is then disconnected in order to protect the equipment. On the contrary, DC source is connected when DC current is negative (charging mode). DC load is then disconnected to cease the absorption of energy from the DC source.

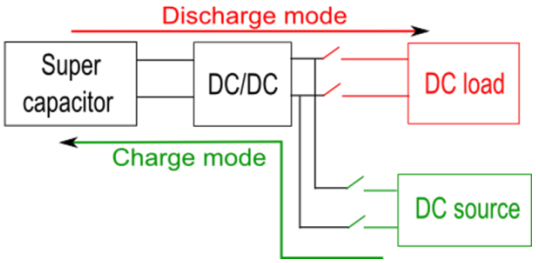

Figure 7.13 DC part of energy storage configuration for supercapacitor simulation

Super capacitor (SC) needs to be recharge because the initial State of Charge (SoC) is zero. Switching function of DC/DC and current of DC source is fixed for 15minutes. Simulation can be started when the voltage of supercapacitor (SC) is at least equal to 30V. However, voltage of supercapacitor has to be watched over. It is measured from real supercapacitor and is then sent to RTLAB for checking. As the maximum voltage of SC is equal to 48V, all simulations are ceased to prevent the breakdown of this source if the voltage of SC is over 45V.

7.4 Simulated results

Power of energy storage which is used to regulate frequency for different strategies (P_{es_ref}) has been defined from the PV power signal of 20/10/2011 which corresponds to the signal with the maximum of fluctuations (see Chapter 2), between $3.955x10^4$ to $3.975x10^4$ seconds (around 11 a.m. for duration of 200 seconds), as illustrated in Figure 7.14. Current of energy storage or DC current output of DC/DC is then calculated from this power.

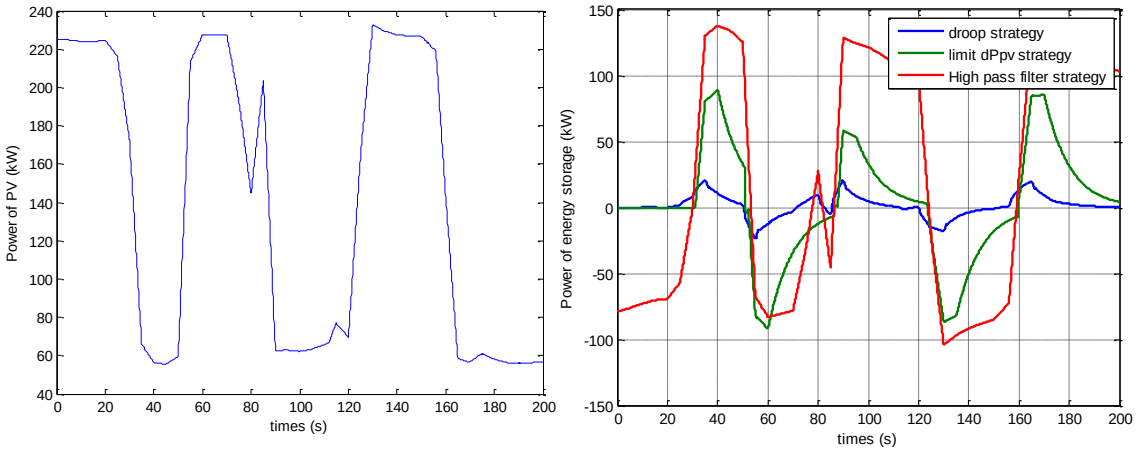

(a) (b)

Figure 7.14 (a) PV power profile (b) Power delivered by energy storage device for different strategies

7.4.1 Results of charging and discharging modes

Two different modes for charge and discharge are separated thanks to the sign of the power (Figure 7.12(a)). A positive or a negative current means that the storage device is either in a discharging or charging mode respectively. However, the discharge and charge currents cannot be at zero because of the limitation of switching function of DC/DC in the range [0.2-0.8] and limitation of resistance. The DC source (represented voltage of energy storage devices) always apply voltage to the converter; resulting in none zero voltage across the resistance. Therefore, the current can not be zero.

7.4.1.1 Current control of energy storage

From the power of ESS with a droop control strategy illustrated in Figure 7.14(b), reference of energy storage is calculated from (7.1) with *real_gain* of 50 and 250 in discharge and charge modes respectively. The gain *real_gain* of charge mode is much larger than the discharge mode because of the limitation of switching function. The acceptable range of switching function is 0.2-0.8 and DC voltage source is 150V. Therefore, the voltage across resistor is between 30-120V. Current passes

through resistor is limited between 0.28-1.13A for resistance 106Ω. The limitation current can be increased by reducing resistance but low current limit is more far away from the zero which causes small variation range of the reference current.

The measured current well follows its reference for both discharge and charge mode as illustrated in Figure 7.14 (a) and (b). The measured DC voltage at input of inverter AC/DC in RTLAB software is constant at 1000V (see Figure 7.14(c)).

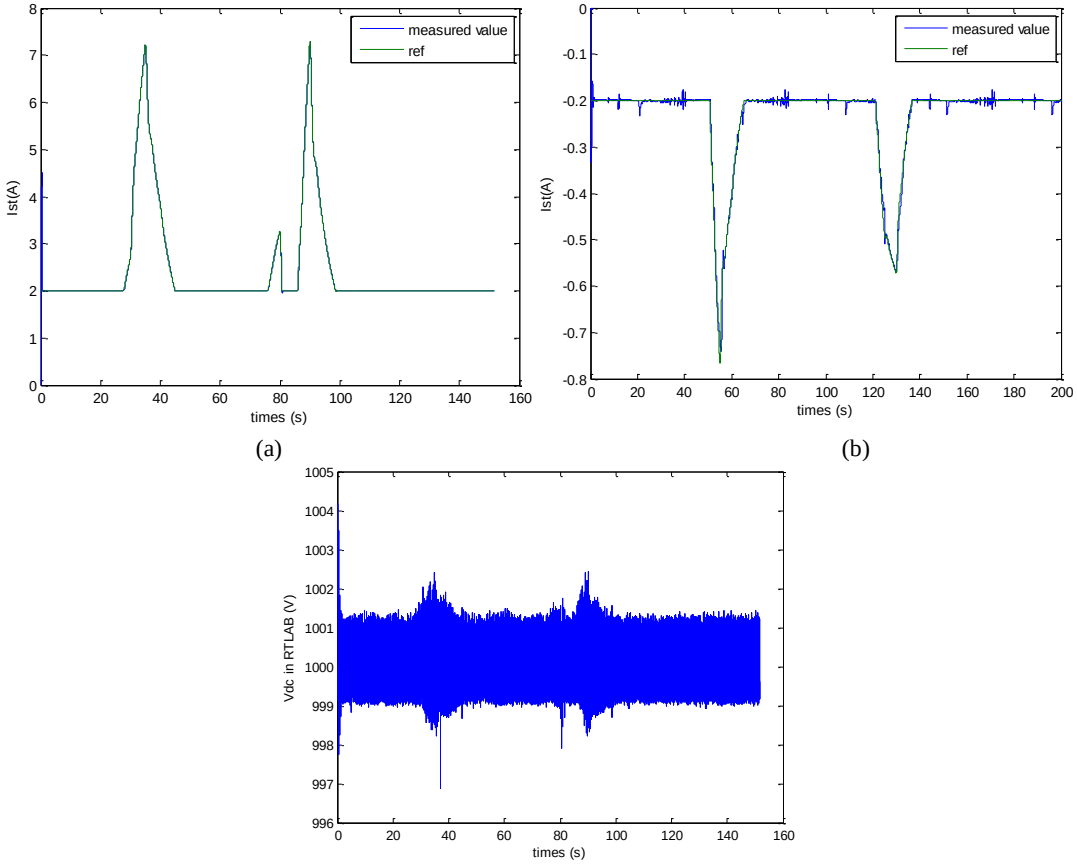

Figure 7.15 (a) Measured and reference current of energy storage in discharge mode (b) Measured and reference current of energy storage in charge mode (c) DC voltage (calculated in RTLAB software) for ESS with a droop control strategy

7.4.1.2 DC voltage control

In the previous simulation, input current of the DC/DC converter was controlled. In this section, its output voltage is controlled to a constant value of 150V (suitable for connecting to Dspace platform) according to the variation of DC current. The DC current is calculated from the power delivered by ESS with a droop control in Figure 7.14(b) and equation (7.1). In discharge mode, the calculated voltage of supercapacitor is transmitted to the DC voltage source, and then calculated DC current is sent to the controllable DC load. The output voltage of the DC/DC chopper is measured by a voltage sensor, and then transmitted to the DC voltage controller in RTLAB. Switching function is calculated from the error between measured DC voltage and its reference. In charge mode, the calculated DC current is sent to control DC source which is represented as the disturbance of control system. Finally, the DC voltage across this DC source is controlled.

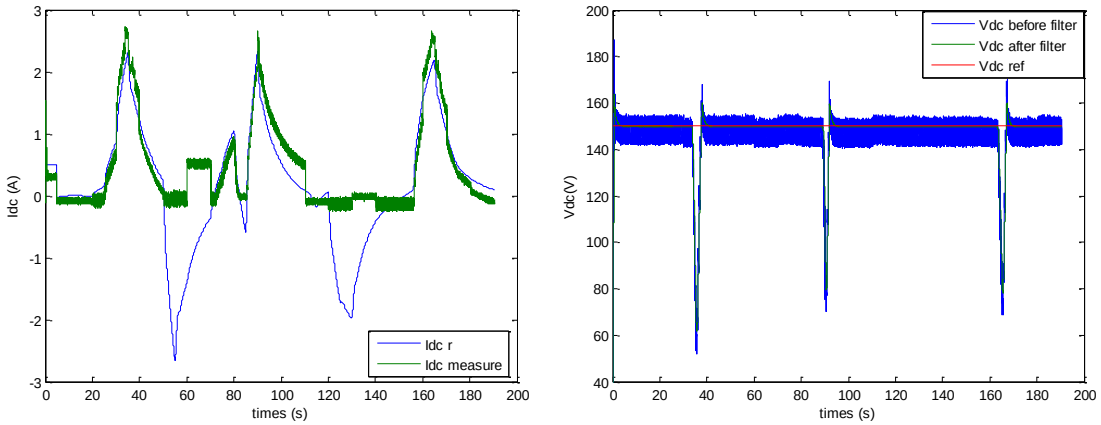

(a) (b)

Figure 7.16 (a) DC current for controlling controllable DC load (b) DC voltage reference and measured for discharging mode for ESS with a droop control strategy

The measured voltage is quite constant at 150V in both discharge and charge mode as illustrated in Figure 7.16(b) and Figure 7.17(b); in accordance to the current variation depicted in Figure 7.16(a) and Figure 7.17(a) respectively. As mentioned in 7.3.5, measurement noise is significant. Low pass filter is then added to filter the measured voltage signal before transmitting to the DC voltage controller.

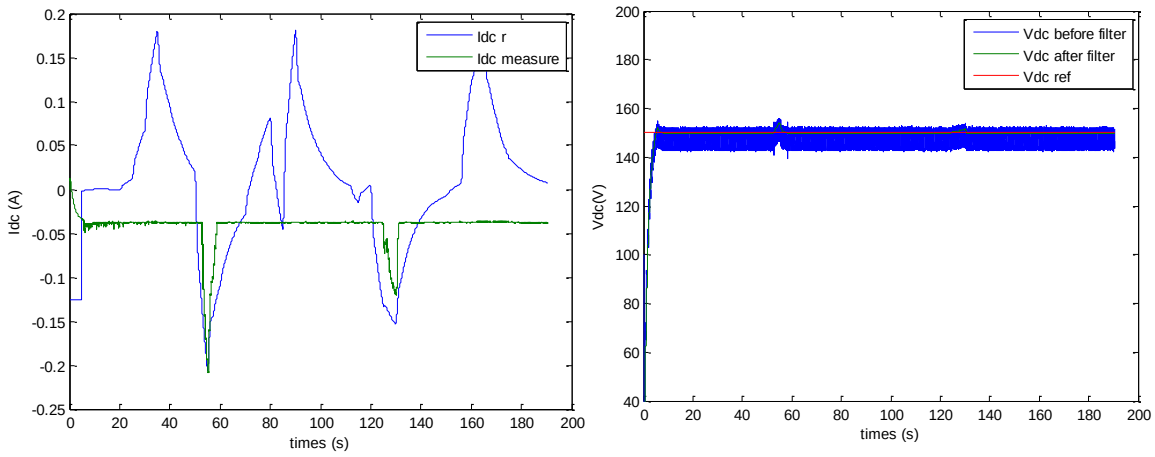

(a) (b)

Figure 7.17 (a) DC current for controlling controllable DC source (b) DC voltage reference and measured for charging mode for ESS with a droop control strategy

7.4.2 Supercapacitor behavior

From diagram shown in Figure 7.7, the DC part of energy storage system with supercapacitor is simulated with a DC voltage control. The power of energy storage illustrated in Figure 7.14(b) is converted to a DC current in Figure 7.18 with a gain equal to 1500. When current is over zero, the DC source will supply energy to charge super capacitor. On the contrary, the DC load will absorb energy from super capacitor when the current is negative. As having mentioned in 7.3.3, the DC load and DC source will not turn on simultaneously. Therefore, before starting this simulation, only the DC source is connected to the output of DC/DC in order to charged super capacitor with fixed switching function and charge current. Super capacitor has to be charged about 15 minutes in order to increase its voltage above 30V. During this charge, the contactor of pre-charge resister is closed for disconnecting it (charging current is not limited). Once the voltage of supercapacitor is above 30V, charging simulation will stop and the DC voltage controller is tested to fix the output voltage of DC/DC at 70V.

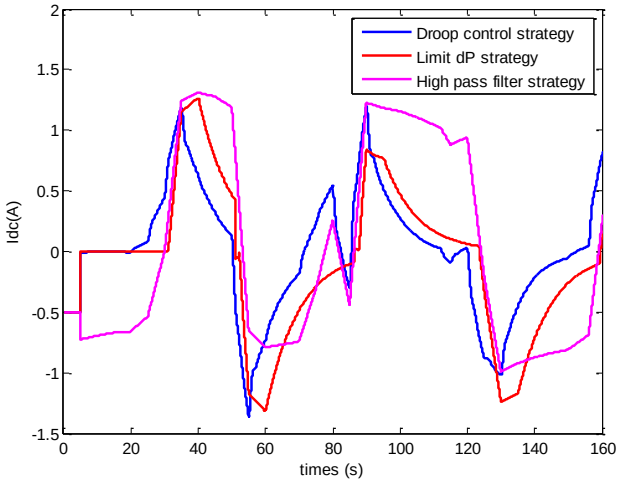

Figure 7.18 DC current of different control strategies

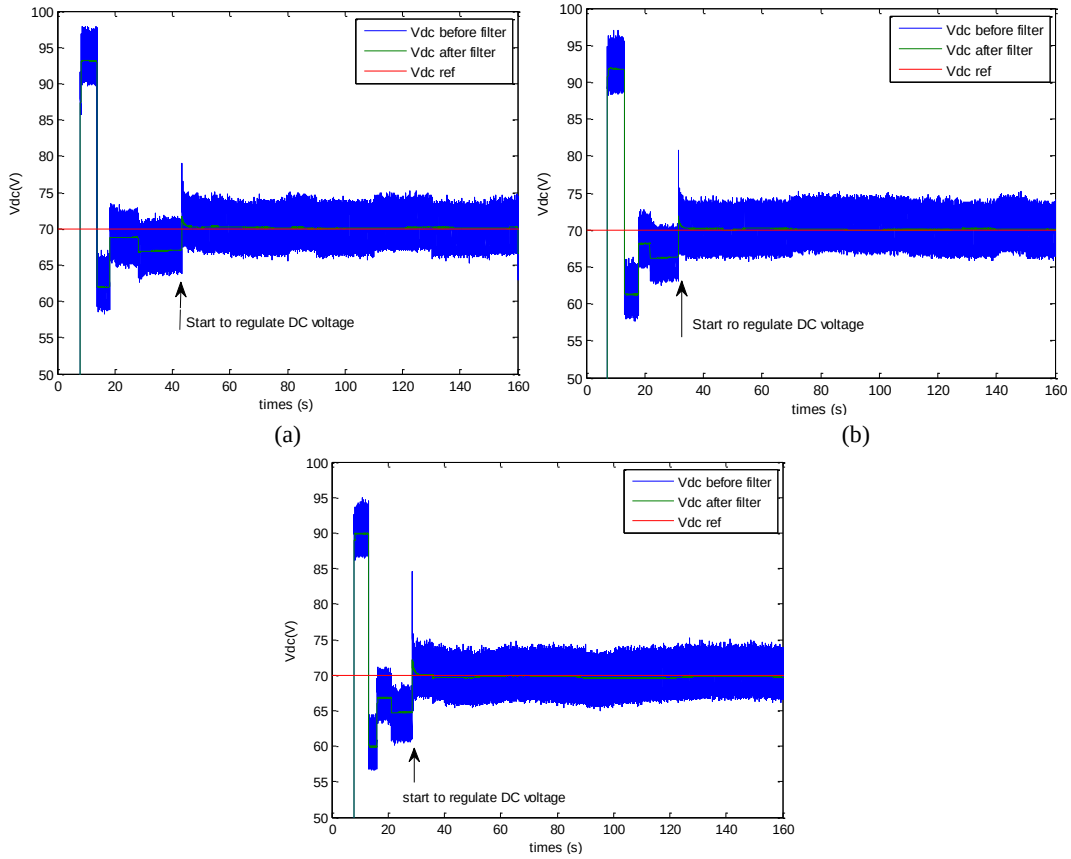

Figure 7.19 DC voltage output of converter according to current signal of (a) droop control strategy (b) limit dPpv strategy (c) high pass filter for energy storage strategy

During the first 20 seconds, the output DC voltage will not be controlled and the calculated DC current will not also be applied to the DC source and DC load. A current of 1A is fixed for the DC source and another zero for DC load. Switching function is fix at 0.5 and two contactors of super capacitor are opened (SC has not yet been connected to the DC/DC). Then, contactor in series with SC is closed but parallel contactor still opens to limit the current. Once the system is stable, the DC source and the DC load will be then controlled by the calculated current and the DC voltage output is also controlled.

The DC voltage output according to the different current signals is stable at 70V as shown in Figure 7.19. However, there is some steady-state error around 1-2V. The measured voltage signal has much noise indicates that robust controller is needed. The voltage of super capacitor is also measured and illustrated in Figure 7.20. The voltage of SC is quite constant during the DC voltage regulation.

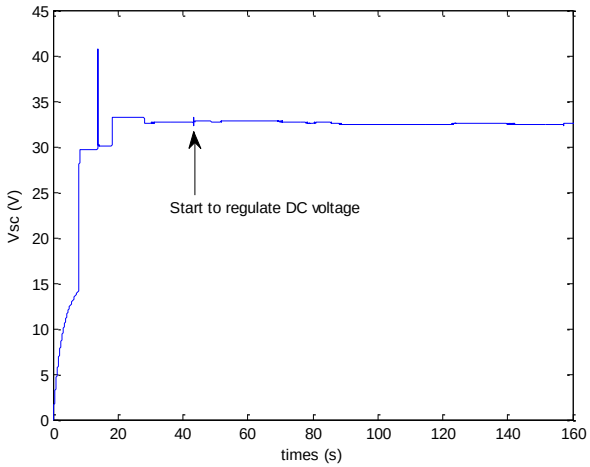

Figure 7.20 Voltage of super capacitor for droop control strategy simulation

7.5 Conclusion

The current of energy storage control with PI controller is validated with the real time simulation. However, the DC voltage control with PI controller cannot be applied to real system because of the measurement noise. Therefore, measurement noise becomes a significant problem which should be taken into account in controller design in order to minimize its influence on performances. The DC voltage controller is redesigned with H infinity controller and it is shown to be able to control the DC voltage with reliable robustness against measurement noise.

Above all, control of DC part of energy storage is validated. Complete energy storage control system (AC and DC) should be tested. Phase Lock Loop (PLL) which is used to calculate the frequency from the measured AC voltage of power system should be carefully analyzed because the control system in AC part is based on a precise measurement of the frequency and the phase angle used for Park transformation.

Conclusions

This study proposed a methodology to integrate energy storage technologies in isolated large microgrids with high penetration of photovoltaics. Energy storage is then a promising solution for primary frequency control in order to reduce the impact of power variation of photovoltaic on system frequency.

Frequency variation depends on parameters of power system and diesel generators (according to their equivalent inertia, the load damping constant and the droop value), and characteristics of the active power variation (amplitude and duration of change). To specify the frequency problem, the amplitude of any fluctuation is not sufficient; then, the duration of variation plays an important rule on frequency deviation. Therefore, statistic approach cannot be used to link power variation to frequency variation, against probabilistic or frequency domain analysis which give all the information.

Then, a limitation diagram defining the maximal PV power variation, for different durations of variation, is proposed to define the more appropriate participation of ESS for frequency regulation. Furthermore, energy storage is relevant to participate in medium frequency region. A strategy based on high-pass filtering of storage power has then been proposed and validated with simulations, according the characterization of PV fluctuations.

Frequency of system without ESS according to the most fluctuation signal of PV plant #1 (on 20/10/2011) is between 49.73-50.33Hz which is out of acceptable limit (49.8-50.2 Hz) 1480 times. The energy storage system with strategy limitation diagram reduces frequency to 50.18-49.79Hz which is almost within limit (out of limit 2 times). Moreover, frequency of system with ESS by filtering strategy is always within limit. Energy storage system with proposed strategies can decrease frequency variation and maintain frequency stability of isolated microgrids with a high penetration rate of PV.

Installed capacity of ESS depends on the design of PVs and the maximal percentage of predicted power variation. Selected strategy for primary frequency control of energy storage depends on the desired objectives. For example, if optimal use of energy storage is required while frequency performance is guaranteed, strategy elaborated from the limitation diagram is an appropriate solution. If the utilization of diesel generator or thermal generator should be optimal or if their capacity should be decreased, thanks to an environmental point of view, filter strategy with seems to be a better solution because ESS assumes the primary frequency control and diesel participates only in the secondary control. However, the installed capacity of energy storage will be larger. In other case, if the objective is to obtain a good frequency response, then other filter strategies presented in this document, with classical droop control for diesel and high pass or band pass of PV power are more appropriate.

Moreover, a complete architecture of control based on robustness issues has been proposed in this thesis, thanks to the design of a H infinity controller to optimize dynamic performances of the ESS, while ensuring robustness of stability and performances of the isolated microgrid. This study allows us to define a multivariable controller in an integrated design according to a methodology well-adapted for engineers. Then, the designed robust controller gives very interesting results for stability and performance issues.

The results show that it can retain the closed loop system stability in respect to the desired performance.

Perspectives

Various perspectives can then be proposed for further works:

Mid-term perspectives:

- Methodology of this thesis can be applied to design energy storage for isolated microgrids with photovoltaic of capacity around 250kW. For different capacity of photovoltaics, the defined strategies can be different. Therefore, characterizations of different photovoltaic sizes should be useful to validate the application of our strategies on any system, especially for PV plants with large capacity (>1 MW). Moreover, the combination of many photovoltaic plants connected in an isolated microgrid should also be characterized according to their impact on frequency variation.
- This thesis deals with only technical aspects. Of course, economic point of view may be analyzed to define the best strategy of control. This would be relevant to apply strategies to real power system. The important question is: whether the ESS is the principal solution for frequency regulation in order to replace diesel generator or if is just a way to coordinate diesel generator in frequency regulation in order to optimize the use of energy storage.
- Proposed ESS strategies should be coordinated with some solar forecasting systems [124]. Then, from forecasted variations of PV production, the best strategy should be defined and used to optimize performances of frequency regulation.
- Some improvements of modelling could be explored. Firstly, dynamic loads should be analyzed and taken into account in energy storage study. Besides, the Phase Lock Loop of inverter interface is an important element in frequency control because it measures and transmits frequency signal to control system. Moreover, it also measures rotating angle for Park transformation. Therefore, a robust PLL should be explored and adapted for frequency control system.
- In the study of robust control, the limitations of the energy storage device; such as, the variation of voltage, State of Charge (SoC), and the maximal power, have not yet been taken into account. For further study, these should be by adding equation of voltage of energy storage, measured and add weighting functions for control current of energy storage and taking into account of saturations in control strategies.
- From robust analysis, equivalent point which uses to transform non-linear system to linear system has large effect to robustness of system in chapter 6. Therefore, the Linear Parameter Varying (LPV) systems should be applied to ESS control. The LPV controller adapts its parameters for different equivalent point.

Long-term perspectives:

- Secondary frequency control needs large energy capacity of the source and PV integration induce the necessity to follow the production hours with a secondary control. Therefore, the rule of energy storage devices for secondary frequency control should be analyzed.
- The other advisable studies concern the possibility to apply the proposed methodology and the different strategies for isolated micro-grids with massive wind turbine energy and their ability to participate to frequency regulation.

Appendix I

Number of occurrences for each maximal power change of each plant

From number of occurrence in percentage is plotted versus the relative power fluctuation (ratio between the maximum power difference and the rated power ($\Delta P_{max}/P_{rated}$)) as shown in Figure 2.25, number of occurrences for each maximum power change of PV plant #2 with 10kW power rated (from 11/2010 to 09/2011), and PV plant #3 with 190kW power rated (from 11/2010 to 09/2011) are presented in Table A.1.

Table A.1: Summary results of number of occurrences for each maximal power change of each plant

	ΔP_{max}< -75%	-75%≤ΔP_{max}<-45%	-45%≤ΔP_{max}<-15%	-15%≤ΔP_{max}<-5%	-5%≤ΔP_{max}<5%
1min					
PV plant #2	0	299	2646	3299	43432
PV plant #3	0	52	1461	2697	35655
2 min					
PV plant #2	18	717	2495	3013	26907
PV plant #3	0	194	1636	2451	23468
5 min					
PV plant #2	44	820	2074	2413	13409
PV plant #3	0	261	1528	1909	12490
10 min					
PV plant #2	48	843	1841	2030	8417
PV plant #3	1	301	1363	1633	7944
15 min					
PV plant #2	60	818	1759	1736	6701
PV plant #3	1	320	1314	1463	6335

	5%≤ΔP_{max}<15%	15%≤ΔP_{max}<45%	45%≤ΔP_{max}<75%	ΔP_{max}>75%
1min				
PV plant #2	3430	2611	329	0
PV plant #3	2586	1490	61	0
2 min				
PV plant #2	3034	2416	749	18
PV plant #3	2386	1646	215	0
5 min				
PV plant #2	2449	2035	817	49
PV plant #3	1864	1454	285	0
10 min				
PV plant #2	2056	1871	797	52
PV plant #3	1554	1366	305	0
15 min				
PV plant #2	1851	1807	757	58
PV plant #3	1438	1293	315	0

Appendix II

Sensibility parameters (droop, inertia equivalent, and load damping constant) for step power variation signal

Frequency responses according step power variation of PV (from 200kW to 100kW) are analyzed while parameters of system such as a droop value, an inertia equivalent, and a damping load constant are varied. And the results are summarized in Table A.2, Table A.3, and Table A.4 for variation of droop value, an inertia equivalent, and a damping load constant, respectively. The power variation of source in negative value (-100kW), which means power of load is over power of generation; causes frequency reduces from 50Hz. Frequency response reaches its minimal value (f minimum) and returns back to its steady-state value (f_infinity). The minimum frequency can be explained as the maximum frequency deviation (Δf maximum) in absolute value which is the difference between nominal frequency (50Hz) and minimum frequency. And frequency deviation in steady stat (Δf steady state) can also be calculated from nominal frequency (50Hz) and steady-state frequency. Besides, rise time and settling time of frequency responses are also analyzed. The rise time is duration that the frequency response rises from 10% of steady-state value to 90% of frequency at steady state. The settling time is the time that frequency response is in the window +/-2% of frequency steady-state value.

Table A.2: The summary result of frequency response when a droop value is varied

Droop value; s_d (%)	f minimum (Hz)	Δf maximum (Hz)	f_infinity (Hz)	Δf steady state (Hz)	time at f minimum (seconds)	rise time (seconds)	settling time (seconds)
1	49.837	0.163	49.975	0.025	0.21	0.01	8.66
2	49.767	0.233	49.950	0.050	0.3	0.03	8.24
3	49.712	0.288	49.925	0.075	0.38	0.05	7.52
4	49.665	0.335	49.901	0.099	0.44	0.06	7.74
5	49.622	0.378	49.876	0.124	0.5	0.08	7.09
6	49.584	0.416	49.851	0.149	0.55	0.10	6.83
7	49.547	0.453	49.827	0.173	0.61	0.11	7.25
8	49.52	0.487	49.802	0.198	0.65	0.13	6.77
9	49.481	0.519	49.777	0.223	0.7	0.15	7.06
10	49.450	0.550	49.753	0.247	0.75	0.16	6.40

Table A.3: The summary result of frequency response when an inertia equivalent is varied

Inertia equivalent ; H (seconds)	f minimum (Hz)	Δf maximum (Hz)	time at f minimum (seconds)	rise time (seconds)	settling time (seconds)
1	49.52	0.487	0.65	0.13	6.77
2	49.637	0.363	1	0.28	6.55
3	49.691	0.309	1.32	0.42	6.27
4	49.722	0.278	1.62	0.58	5.35
5	49.743	0.257	1.92	0.75	5.97
6	49.758	0.242	2.24	0.93	6.32
7	49.769	0.231	2.57	1.13	4.71
8	49.777	0.223	2.93	1.33	5.17
9	49.784	0.217	3.32	1.55	5.59
10	49.789	0.211	3.75	1.78	5.94

When the droop value increases, the minimum frequency will fall down (the frequency deviation (Δf) from nominal frequency (50Hz) increases) but the frequency deviation (Δf) at steady state rises up. And frequency has fast time response (rise time) for small droop value. The frequency deviation in transient response decreases when the inertia equivalent (H) increases. This parameter does not cause any impacts on the frequency at steady-state value which equals to 49.802 Hz for all inertia equivalent values. Therefore, inertia equivalent does not cause any effects to frequency in steady state as mention earlier in Chapter 3. Small inertia equivalent depends on sizes and number of rotating machines in system and means small capability to insist an existing frequency value. Frequency has fast time response but large variation for small inertia equivalent.

Besides, the frequency response takes less time to recover to its steady state when the droop and inertia equivalent goes up. For studied system with time response of diesel generator 0.8 seconds, frequency response has some oscillations.

The frequency deviation decreases both in transient and steady state when the load damping constant goes up but the frequency response takes less time to be back to its steady state when a damping loads constant increases. In conclusion, frequency in steady state depends on droop value and load damping constant but is independent on inertia equivalent.

Table A.4: The summary result of frequency response when a damping load constant is varied

Load damping constant ; D	f minimum (Hz)	Δf maximum (Hz)	f_infinity (Hz)	Δf steady state (Hz)	time at f minimum (seconds)	rise time (seconds)	settling time (seconds)
0	49.504	0.496	49.800	0.200	0.66	0.13	6.84
0.25	49.523	0.477	49.804	0.196	0.65	0.13	6.68
0.5	49.541	0.459	49.808	0.192	0.64	0.13	5.64
0.75	49.558	0.442	49.811	0.189	0.63	0.13	5.53
1	49.573	0.427	49.815	0.185	0.62	0.13	5.38
1.25	49.588	0.412	49.818	0.182	0.61	0.13	5.47
1.5	49.602	0.398	49.821	0.179	0.6	0.12	4.40
1.75	49.614	0.386	49.825	0.175	0.59	0.12	4.31
2	49.627	0.374	49.828	0.172	0.58	0.12	4.21

Appendix III

Summary of parameters of energy storage system

III.1 DC bus design

Filter LCL is used in this design. The maximum DC voltage reference is defined by (A.1) where V_r is rms voltage phase to ground of power system (400/sqrt(3)), r_{max} is a maximal ratio between the maximum AC voltage output and DC voltage reference (1/2sqrt(2) for pure sinusoidal), and C_{LCL} is in function with the frequency of power system (ω_r; 2*pi*50rad/s), frequency of PWM (ω_p;2*pi*7e3 rad/s) and resonant frequency of filter LCL (ω_{f0}) in (A.2). Parameter k_n is selected at 0.5% (French standard) to eliminate harmonic pair n>4 of AC bus [19].

$$V_{dc\_ref\_\max} = \frac{V_r}{r_{\max} - C_{LCL}} \tag{A.1}$$

$$C_{LCL} = \frac{\omega_r}{2k_n\left|1-\frac{\omega_p^2}{\omega_{f0}^2}\right|\omega_p} \tag{A.2}$$

Frequency resonant of filter LCL can be defined by (A.3) where k_{LCL} is ratio of L_{ac1} and L_{ac2} and k_{conv} is fraction of apparent current of nominal installation (usually 15-20%).

$$f_{f0} \geq f_p\sqrt{\frac{\pi.k_n.(1+k_{LCL})}{\pi.k_n.(1+k_{LCL})+2.k_{conv}}} \tag{A.3}$$

From (A.3), resonant frequency of filter is selected at 2.8 kHz, resulting in the maximum DC voltage of 1.06kV from (A.1) is obtained. Therefore, the selected DC voltage reference (V_{dc_ref}) is 1000V.

Capacitor and resistor at DC bus are defined. Capacitor at DC bus (C_{dc}) should limit the variation of DC voltage and it is defined by (A.4) where S_{n_ES} is apparent power of energy storage (300kVA), t_r is time response of current controller (7ms), k_{dc} is percentage of acceptable maximal DC voltage variation from reference value (1%), and V_{dc_ref} is DC voltage reference (1000V). From the selected values, capacitor at DC bus (C_{dc}) should be more than 0.21F. Consequently, capacitor at DC bus is selected at 0.5F.

$$C_{dc} \geq \frac{S_{n\_ES}t_r}{k_{dc}V_{dc\_ref}^2} \tag{A.4}$$

Furthermore, resistor at DC bus (R_{dc}) is designed. This resistor signifies loss that is proportional to apparent power of energy storage (μ_{dc}). From (A.5), resistor at DC bus is 333Ω for μ_{dc} 1%.

$$R_{dc} = \frac{V_{dc\_ref}^2}{\mu_{dc} S_{n\_ES}} \quad \text{(A.5)}$$

Parameters of DC bus depend on selected DC voltage and rated power of energy storage. Frequency of PWM which has impact on the maximum DC voltage as having described earlier will be varied later but the selected DC voltage is still fixed (this selected value always in acceptable limit). Therefore, all parameters of DC bus are constant while frequency of PWM and resonant frequency of filter change.

III.2 AC bus design – Filter LCL

Filter LCL in Figure A.1 is designed in case that filter has to eliminate harmonic of output current. Current output of filter (I_r) at frequency of PWM (ω_p) should be less than current at harmonic n (I_{hn}^{max}) which is eliminated in (A.6) [19]. In this study, current at harmonic n>4 is eliminated as having mentioned earlier and this current I_{hn}^{max} is proportional to the maximum current of energy storage with parameter k_n.

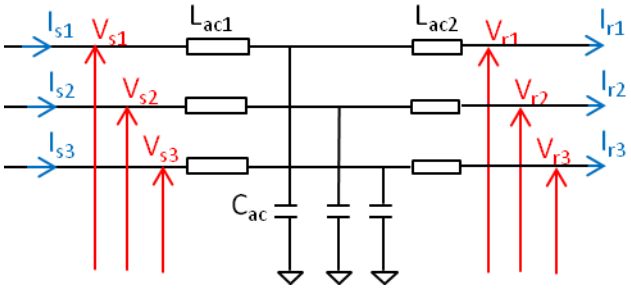

Figure A.1 Filter LCL

$$I_r(j\omega_p) \le I_{hn}^{max}; \quad I_{hn}^{max} = k_n \frac{S_{n\_ES}}{3V_r} \quad \text{(A.6)}$$

Amplitude of transfer function between current output of filter (I_r) and voltage output of inverter (voltage before filter) (V_s) is defined in (A.7) and its value at frequency of PWM is half of DC voltage reference in (A.8). Therefore, from equation (A.6)-(A.8), inductance of filter LCL (L_{ac1}) can be defined in (A.9) which two inductance of filter (L_{ac1} and L_{ac2}) are equivalent (k_{LCL}=1) at the value 0.5mH.

$$\left|\frac{I_r(j\omega_p)}{V_s(j\omega_p)}\right| = \frac{1}{\omega_p(L_{ac1}+L_{ac2})\left|1-\frac{\omega_p^2}{\omega_{f0}^2}\right|} \quad \text{(A.7)}$$

$$V_s(j\omega_p) = \frac{V_{dc\_ref}}{2} \quad \text{(A.8)}$$

$$L_{ac1} = \frac{3V_r V_{dc\_ref}}{2\omega_p(1+k_{LCL})k_n S_{n\_ES}\left|1-\frac{\omega_p^2}{\omega_{f0}^2}\right|} \quad \text{(A.9)}$$

From resonant frequency (f_{f0}) in (A.10) and selected values of L_{ac1} and L_{ac2}, capacitor of LCL filter (C_{ac}) can be defined by (A.11). Capacitor of filter LCL calculated is 15 µF for resonant frequency 2.8 kHz.

$$f_{f0} = \frac{\omega_{f0}}{2\pi} = \frac{1}{2\pi}\sqrt{\frac{L_{ac1} + L_{ac2}}{L_{ac1}.L_{ac2}.C_{ac}}} \quad \text{(A.10)}$$

$$C_{ac} = \frac{1 + k_{LCL}}{k_{LCL} L_{ac1} \omega_{f0}^{\ 2}} \quad \text{(A.11)}$$

III.3 AC bus design – Filter RL

Filter RL in Figure A.2 is designed. Inductance (L_{ac}) is approximated as the summation of two inductances of LCL filter (L_{ac1} + L_{ac2}). Resistance of filter RL (R_{ac}) that signifies loss of filter is designed from imperfection of inductance (L_{ac}). It therefore is proportional to inductance in (A.12) where σ is factor of material quality that depends on apparent power of energy storage (σ=25 for 300kVA) [19].

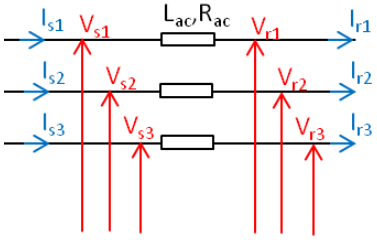

Figure A.2 Filter RL

$$R_{ac} = \frac{X_f}{\sigma} \quad \text{(A.12)}$$

III.4 AC bus design – Filter LC (Thesis of Valero)

Filter LC in Figure A.3 is analyzed. This filter can be analyzed as current source if capacitor of filter (C_{ac}) is very small. This capacitor assists in the elimination of harmonic in voltage output. Inductance of filter (L_{ac}) reduces the variation in current output [109]. Its minimum value can be calculated by (A.13) where T_{PWM} is period of PWM ($1/f_P$; 1/7e3), ΔI_{s_max} is maximum variation of current output (15% of I_{s_max}=$S_{n\_ES}/3V_r$) (15% of 307.7A). Therefore, minimum inductance is 0.39 mH. The maximum inductance of filter can be defined by limitation of DC voltage in (A.14). If sin (φ) is zero and cos (φ) is 1, inductance maximal is 1.5H. If this inductance (L_{ac}) equals to two times of inductance of LCL filter (L_{ac1}), inductance designed before 1mH (2x0.5mH) is in acceptable limit. Therefore, inductance of LC filter (L_{ac}) is 1mH.

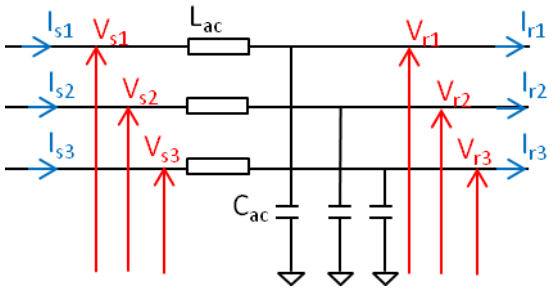

Figure A.3 Filter LC

$$L_{ac\_min} = \frac{T_{PWM}.V_{dc}}{8.\Delta I_{s\_max}} \quad \text{A.13)}$$

$$\frac{2.V_{dc}}{3} \geq \sqrt{\left(V_{r\_max} + L_{ac}\omega I_{s\_max}.\sin(\varphi)\right)^2 + \left(L_{ac}\omega I_{s\_max}.\cos(\varphi)\right)^2} \quad \text{(A.14)}$$

The capacitor (C_{ac}) is designed. From resonant frequency in (A.15) and f_{f0_LC} 2.8 kHz, capacitor of LC filter is 3.2 µF.

$$f_{f0\_LC} = \frac{1}{2.\pi.\sqrt{L_{ac}C_{ac}}} \quad \text{(A.15)}$$

Table A.5: Summary of parameters of energy storage system 7kHz

Parameter	Description	Value	Unity
Sn_ES	Apparent power of energy storage	300	kVA
Vr	RMS voltage phase to ground of power system	400/sqrt(3)	V
Vdc_ref	DC voltage reference	1000	V
wr	Frequency of power system	2*pi*50	rad/s
fr	Frequency of power system	50	Hz
wp	Frequency of PWM	2*pi*7e3	rad/s
fp	Frequency of PWM	7	kHz
ωf0	Resonant frequency of filter	2*pi*2.8e3	rad/s
ff0	Resonant frequency of filter	2.8	kHz
kn	Parameter eliminate harmonic pair n>4	0.50%	
klcl	ration of Lac1 and Lac2	1	
kconv	percentage of nominal apparent current of installation (15%-20% in general)	15%	
rmax	ratio maximal between AC voltage output maximal and DC voltage reference	1/2sqrt(2)	
tr	time response of current controller	7	ms
kdc	percentage of DC voltage variation maximal	1%	
ΔIs_max	variation maximal of current output	15%	
DC bus			
Cdc	Capacitor at DC bus	0.5	F
Rdc	Resistor at DC bus	333	Ω
Filter LCL			
Lac1	First inductance of LCL filter	0.5	mH
Lac2	Second inductance of LCL filter	0.5	mH
Cac	Capacitor of LCL filter	15	µF
Filter LC			
Lac	Inductance of LC filter	1	mH
Cac	Capacitor of LC filter	3.2	µF

Table A.6: Summary of parameters of energy storage system with different frequency of PWM

Parameter	Description	Value (Different fp)			Unity
wp	Frequency of PWM	2*pi*5e3	2*pi*7e3	2*pi*10e5	rad/s
fp	Frequency of PWM	5	7	10	kHz
ωf0	Resonant frequency of filter	2*pi*1.8e3	2*pi*2.8e3	2*pi*4.5e5	rad/s
ff0	Resonant frequency of filter	1.8	2.8	4.5	kHz
Filter LCL					
Lac1	First inductance of LCL filter	0.55	0.5	0.47	mH
Lac2	Second inductance of LCL filter	0.55	0.5	0.47	mH
Cac	Capacitor of LCL filter	30	15	5.38	µF
Filter LC					
Lac	Inductance of LC filter	1.1	1	0.98	mH
Cac	Capacitor of LC filter	7.2	3.2	1.35	µF

Appendix IV

Parameters of energy storage control systems

Table A.7: Parameters of different energy storage control systems

Parameter	Description	Value
Droop control of energy storage		
Pes		300kW
Res	Droop value of energy storage	4%
K	Reserved energy	30MW/Hz
Energy storage control system 1		
t_r	time response of three phase current controller	7ms
Kpi	Proportional gain of three phase current controller	1
Kii	Integral gain of three phase current controller	510.2
Energy storage control system 2		
BP_ES	Bandwidth of energy storage current controller (P type)	1000rad/s
Kp_es	Proportional gain of energy storage current controller (P type)	1.5
tr_ies	Time response of energy storage current controller (PI type)	7ms
Kp_ies	Proportional gain of energy storage current controller (PI type)	1.5
Ki_ies	Integral gain of energy storage current controller (PI type)	765.3
trv	Time response of DC voltage controller	70ms
Kpv	Proportional gain of DC voltage controller	0.048
Kiv	Integral gain of DC voltage controller	1.70
t_r	Time response of three phase current controller	7ms
Kpi	Proportional gain of three phase current controller	1
Kii	Integral gain of three phase current controller	510.2
Energy storage control system 3		
tr_ies	Time response of energy storage current controller (PI type)	7ms
Kp_ies	Proportional gain of energy storage current controller (PI type)	1.5
Ki_ies	Integral gain of energy storage current controller (PI type)	765.3
tr_vdc	Time response of DC voltage controller	70ms
K_{p_vdc}	Proportional gain of DC voltage controller	71.43
K_{i_vdc}	Integral gain of DC voltage controller	2.55
t_r	Time response of three phase current controller	7ms
K_{pi}	Proportional gain of three phase current controller	1
K_{ii}	Integral gain of three phase current controller	510.2
Phase Lock Loop (PLL)		
ξ_{PLL}	Damping factor of PLL	1
ω_{n_PLL}	Bandwidth of PLL	50rad/s
K_{P_PLL}	Proportional gain of Phase Lock Loop	-81.65
K_{I_PLL}	Integral gain of Phase Lock Loop	-2.04

Appendix V

Simulation of strategy limitation diagram with simulated signal (fast fluctuation)

The continuous power fluctuation in Figure A.4 is then simulated. The power of PV is fluctuated around the initial point of 0.1 per unit. The acceptable maximal frequency variation is 0.2 Hz so that the range of acceptable frequency is 49.8Hz to 50.2Hz. From Figure A.4, the system with energy storage is compared to the initial system (without energy storage) and they are separated into 3 situations.

Situation a: From t=0 to t=2 seconds, the power of PV increases from 0.1 per unit. The power difference (ΔP) is less than the limited power (ΔP limit) so that the power reference of energy storage should be at 85% of the former power reference ($85\%*P_{es\_ref}(t-t_s)$) (condition 2a). The initial power reference of energy storage is zero. Therefore, the power reference of energy storage during this time is also zero. The frequency rises from 50 Hz and reaches 50.2 Hz at t=2 seconds.

Situation b: This is the case that the power difference is out of limit. From t=2 to t=7 seconds, the power of PV rises continuously and reaches the optimal power 0.15 per unit at t=5 seconds and then decreases. During this period, the power variation (ΔP) is larger than the limited power difference (ΔP limit) as shown in Figure A.4 (d). Therefore, the power of energy storage is calculated by equation (5.1) (condition 3a) and it is negative which signify that the energy storage is in the charge mode. Figure A.4 (c) also shows that during this period the frequency in blue line (without energy storage) is more than 50.2Hz (means out of limit) but the frequency in green line is still in acceptable value because of the participation of energy storage. The periods 12-16 seconds and 22-27 seconds are in the same situation; with as exception that during 12 to 16 seconds the battery is in the discharge mode (the power of energy storage is positive) because the power of PV is less than the initial power (0.1 per unit).

Situation c: In this case, the power of PV decreases or increases continuously and passes 0.1 per unit and the power difference is always in acceptable zone. From t=7 seconds, the power of PV falls down and reaches 0.1 per unit at t=10 seconds. The power variation (ΔP) during this situation is always less than the limit (ΔP limit) so the power of energy storage is reduced continuously in negative value (in charge mode). The power reference of the actual energy storage is at 85% of the former power reference ($85\%*P_{es\_ref}(t-t_s)$) (condition 2a). The frequency is also in acceptable range during this period. The period 17-22 seconds and 27-44 seconds are also in this situation; except that during 17 to 22 seconds the battery is in the discharge mode (the power of energy storage is positive) because the former power of energy storage is also positive.

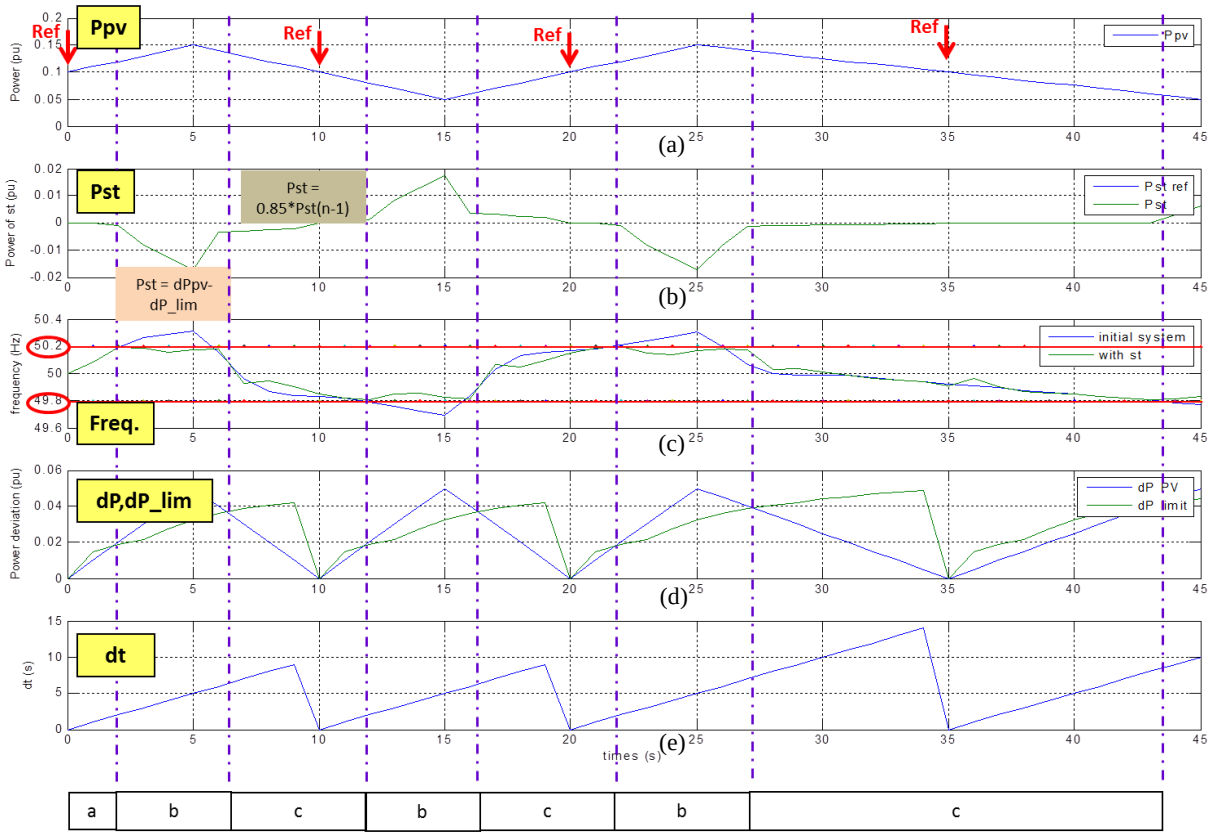

Figure A.4 (a) Simulated power of PV (fast and continuous fluctuation) (b) Power of ESS (c) Frequency response of system without and with ESS (d) Calculated power variation of PV and limitation (e) Calculated duration of change

Bibliography

[1] P. Kundur, N. J. Balu, and M. G. Lauby, *Power system stability and control*. New York: McGraw-Hill, 1994.

[2] A. Davigny, "Participation aux services système de fermes d'éoliennes à vitesse variable intégrant du stockage inertiel d'énergie," Thèse de doctorat, Université Lille 1 - Sciences et technologies, France, 2007.

[3] A. Teninge, "Paticipation Aux Services système de Parcs Éoliens Mixtes : Application En Milieu Insulaire," Institut National Polytechnique de Grenoble - INPG, 2009.

[4] Y. G. Rebours, D. S. Kirschen, M. Trotignon, and S. Rossignol, "A Survey of Frequency and Voltage Control Ancillary Services—Part II: Economic Features," *IEEE Trans. Power Syst.*, vol. 22, no. 1, pp. 358–366, Feb. 2007.

[5] Y. G. Rebours, D. S. Kirschen, M. Trotignon, and S. Rossignol, "A Survey of Frequency and Voltage Control Ancillary Services mdash;Part I: Technical Features," *IEEE Trans. Power Syst.*, vol. 22, no. 1, pp. 350–357, Feb. 2007.

[6] V. Courtecuisse, "Supervision d'une centrale multisources à base d'éoliennes et de stockage d'énergie connectée au réseau électrique," Arts et Métiers ParisTech, 2008.

[7] G. S. Stavrakakis and G. N. Kariniotakis, "A general simulation algorithm for the accurate assessment of isolated diesel-wind turbines systems interaction. I. A general multimachine power system model," *IEEE Trans. Energy Convers.*, vol. 10, no. 3, pp. 577–583, Sep. 1995.

[8] H. Omara, "A Methodology for Determining the Load Frequency Sensitivity," The University of Manchester, Manchester, UK, 2012.

[9] S. W. Blume, *Electric Power System Basics for the Nonelectrical Professional*, 1 edition. Wiley-IEEE Press, 2007.

[10] R. H. Lasseter, "MicroGrids," in *IEEE Power Engineering Society Winter Meeting, 2002*, 2002, vol. 1, pp. 305–308 vol.1.

[11] *Microgrids for disaster preparedness and recovery*. International Electrotechnical Commission, 2014.

[12] M. A. Pedrasa, "A Survey of Techniques Used to Control Microgrid Generation and Storage during Island Operation."

[13] Microgrid Institute, "About Microgrids," *Microgrid Institute*. .

[14] J. A. Peas Lopes, C. L. Moreira, and A. G. Madureira, "Defining control strategies for MicroGrids islanded operation," *IEEE Trans. Power Syst.*, vol. 21, no. 2, pp. 916–924, May 2006.

[15] A. Etxeberria, I. Vechiu, H. Camblong, and J. M. Vinassa, "Hybrid Energy Storage Systems for renewable Energy Sources Integration in microgrids: A review," in *IPEC, 2010 Conference Proceedings*, 2010, pp. 532–537.

[16] F. Katiraei, M. R. Iravani, and P. W. Lehn, "Micro-grid autonomous operation during and subsequent to islanding process," *IEEE Trans. Power Deliv.*, vol. 20, no. 1, pp. 248–257, Jan. 2005.

[17] D. H. Marin, "Intégration des éoliennes dans les réseaux électriques insulaires," Ecole Centrale de Lille, 2009.

[18] O. I. Elgerd, *Electric energy systems theory: an introduction*. New York: McGraw-Hill, 1982.

[19] G. M. A. Delille, "Contribution du Stockage à la Gestion Avancée des Systèmes Électriques : approches Organisationnelles et Technico-économiques dans les Réseaux de Distribution," Ecole Centrale de Lille, 2010.

[20] N. Jayawarna, X. Wu, Y. Zhang, N. Jenkins, and M. Barnes, "Stability of a MicroGrid," in *The 3rd IET International Conference on Power Electronics, Machines and Drives, 2006*, 2006, pp. 316–320.

[21] "EDF Corse et Outre-mer," *EDF*. .

[22] "PLAN ENERGETIQUE REGIONAL PLURIANNUEL DE PROSPECTION ET D'EXPLOITATION DESENERGIES RENOUVELABLES ET D'UTILISATION RATIONNELLE DE L'ENERGIE DE LA GUADELOUPE." Region Guadeloupe, Sep-2012.

[23] “Réactualisation du PRERURE Guyane: Plan Energétique Régional Pluriannuel de Prospection et d’Exploitation des Energies Renouvelables et d’Utilisation Rationnelle de l’Energie,” Explicit and Alter, Sep. 2012.
[24] “Power,” *Energy Policy and Planning Office, Ministry of Energy, Thailand*. [Online]. Available: http://www.eppo.go.th/index-E.html.
[25] Issarachai Ngamroo, “Status of Microgrid R&D in Thailand,” presented at the Vancouver Microgrid Symposium, Vancouver, 21-Jul-2010.
[26] R. Nidhiritdhikrai, B. Eua-Arporn, and R. Diewvilai, “Impact of renewable energy on Thailand power Development Plan,” in *2012 9th International Conference on Electrical Engineering/Electronics, Computer, Telecommunications and Information Technology (ECTI-CON)*, 2012, pp. 1–4.
[27] Wilaiporn Ittiwiroon and Ernst and Young, “Renewable Year-end Focus: Thailand,” *Renewable energy world*, Dec-2013. [Online]. Available: http://www.renewableenergyworld.com/rea/news/article/2013/12/renewable-year-end-focus-thailand.
[28] C. Thammasorn, “Generation unit commitment in microgrid with renewable generators and CHP,” in *2013 10th International Conference on Electrical Engineering/Electronics, Computer, Telecommunications and Information Technology (ECTI-CON)*, 2013, pp. 1–6.
[29] “Renewable energy Development Plan (REDP)2008-2022,” *International Energy Agency*, 16-Apr-2013. [Online]. Available: http://www.iea.org/policiesandmeasures/pams/thailand/.
[30] Meena Agrawal and Arvind Mittal, “An Appraisal of Microgrid Project Implementations in the East & South-East Asia,” *Int. J. Emerg. Trends Eng. Dev.*, vol. 3, no. Issue 4, May 2014.
[31] *Grid integration of large-capacity Renewable Energy sources and use of large-capacity Electrical Energy Storage*. International Electrotechnical Commission, 2012.
[32] S. Vazquez, S. M. Lukic, E. Galvan, L. G. Franquelo, and J. M. Carrasco, “Energy Storage Systems for Transport and Grid Applications,” *IEEE Trans. Ind. Electron.*, vol. 57, no. 12, pp. 3881–3895, Dec. 2010.
[33] E. Alegria, T. Brown, E. Minear, and R. H. Lasseter, “CERTS Microgrid Demonstration With Large-Scale Energy Storage and Renewable Generation,” *IEEE Trans. Smart Grid*, vol. 5, no. 2, pp. 937–943, Mar. 2014.
[34] N. Saito, T. Niimura, K. Koyanagi, and R. Yokoyama, “Trade-off analysis of autonomous microgrid sizing with PV, diesel, and battery storage,” in *IEEE Power Energy Society General Meeting, 2009. PES ’09*, 2009, pp. 1–6.
[35] I. Serban, R. Teodorescu, J. M. Guerrero, and C. Marinescu, “Modeling of an autonomous microgrid for renewable energy sources integration,” in *35th Annual Conference of IEEE Industrial Electronics, 2009. IECON ’09*, 2009, pp. 4311–4316.
[36] “Les systèmes énergétiques intelligents.” Ministère de l’écologie, du développement durable et de l’énergie, 05-Aug-2014.
[37] Yiping Dai, Ting Zhao, Yunfeng Tian, and Lin Gao, “Research on the Primary Frequency Control Characteristics of Generators in Power System,” presented at the 2nd IEEE Conference on Industrial Electronics and Applications, 2007. ICIEA 2007, 2007, pp. 569–574.
[38] J. Mongkoltanatas, D. Riu, and X. Lepivert, “Energy Storage design for Primary Frequency Control for Islanding Micro grid,” in *IECON 2012*, Montréal, Canada, 2012, p. .
[39] G. Delille, B. François, and G. Malarange, “Dynamic frequency control support: A virtual inertia provided by distributed energy storage to isolated power systems,” presented at the Innovative Smart Grid Technologies Conference Europe (ISGT Europe), 2010 IEEE PES, 2010, pp. 1 –8.
[40] Wei Li, G. Joos, and C. Abbey, “Wind Power Impact on System Frequency Deviation and an ESS based Power Filtering Algorithm Solution,” presented at the Power Systems Conference and Exposition, 2006. PSCE ’06. 2006 IEEE PES, 2006, pp. 2077–2084.
[41] Changling Luo and Boon-Teck Ooi, “Frequency deviation of thermal power plants due to wind farms,” *IEEE Trans. Energy Convers.*, vol. 21, no. 3, pp. 708–716, Sep. 2006.
[42] J. N. Baker and A. Collinson, “Electrical energy storage at the turn of the Millennium,” *Power Eng. J.*, vol. 13, no. 3, pp. 107–112, Jun. 1999.

[43] H. Chen, T. N. Cong, W. Yang, C. Tan, Y. Li, and Y. Ding, “Progress in electrical energy storage system: A critical review,” *Prog. Nat. Sci.*, vol. 19, no. 3, pp. 291–312, Mar. 2009.
[44] Electrical Energy storage project team, “Electrical Energy Storage.” International Electrotechnical Commission, Dec-2011.
[45] “Battery Energy Storage for Smart Grid Applications.” EUROBAT, 2013.
[46] “Important of Battery Energy Storage for Renewable Energy Supply: An analysis of battery systems and their application in Off-grid, Mini-grid and On-grid Configurations.” EUROBAT, Nov-2011.
[47] Edgar Maza, “Grid-Connected Storage Market Set to Explode,” *Energy Storage Association*, Jan-2014. .
[48] “Energy Storage for Microgrids,” *Navigant Research*, 26-Aug-2014. .
[49] H. Ibrahim, A. Ilinca, and J. Perron, “Energy storage systems—Characteristics and comparisons,” *Renew. Sustain. Energy Rev.*, vol. 12, no. 5, pp. 1221–1250, Jun. 2008.
[50] Susan M. Schoenung, “Characteristics and Technologies for Long-vs. Short-Term Energy Storage: A study by the DOE Energy Storage Systems Program,” Sandia National Laboratories, SAND2001-0765, Mar. 2001.
[51] Imre Gyuk, Mark Johnson, John Vetrano, Kevin Lynn, William Parks, Rachna Handa, Landis Kannberg, Sean Hearne, Karen Waldrip, and Ralph Braccio, “Grid Energy storage,” U.S Department of Energy, Dec. 2013.
[52] R. Chandrasekaran, “Modeling of electrochemical energy storage and energy conversion devices,” Dissertation, Georgia Institute of Technology, 2010.
[53] *Electrochemical Supercapacitors - Scientific Fundamentals and Technological Applications*. .
[54] HARRICHE Farah and SOULETIS Romain, “Étude technico-économique du stockage de l’électricité,” Supélec, Mar. 2013.
[55] J. D. Maclay, J. Brouwer, and G. S. Samuelsen, “Dynamic modeling of hybrid energy storage systems coupled to photovoltaic generation in residential applications,” *J. Power Sources*, vol. 163, no. 2, pp. 916–925, Jan. 2007.
[56] Carlos Moreira and Manolis Voumvoulakis, “Microgrids On-Line Security Assessment,” DB2. Forecasting Functions and on-line Security Assessment (Seamless Transition) Part 2: On-Line Security Assessment, Nov. 2007.
[57] Bieshoy Awad and J.B. Ekanayake, “Intelligent Load Control for Frequency Regulation in MicroGrids,” Feb. 2008.
[58] R. B. Schainker, “Executive overview: energy storage options for a sustainable energy future,” in *IEEE Power Engineering Society General Meeting, 2004*, 2004, pp. 2309–2314 Vol.2.
[59] J. P. Barton and D. G. Infield, “Energy storage and its use with intermittent renewable energy,” *IEEE Trans. Energy Convers.*, vol. 19, no. 2, pp. 441–448, Jun. 2004.
[60] D. Thirault, “Architectures des Réseaux de Distribution pour l’Electrification rurale des Pays en Développement,” Institut National Polytechnique de Grenoble - INPG, 2004.
[61] Nikos Hatziargyriou, Xavier Le Pivert, Hicham Bousmaha, João Peças Lopes, Carlos Moreira, José Oyarzabal1, André Madureira, Floriane Fesquet, and Patrick Geraldo, “Report on Steady State and Dynamic Analysis of MicroGrids,” Deliverable DI2, Dec. 2005.
[62] Nikos Hatziargyriou, Hiroshi Asano, Reza Iravan, and Chris Marnay, “Microgrids: An Overview of Ongoing Research, Development, and Demonstration Projects,” *IEEE Power and Energy Magazine*, vol. july/august 2007, 2007.
[63] T. Zhou, “Commande et supervision énergétique d’un générateur hybride actif éolien incluant du stockage sous forme d’hydrogène et des super-condensateurs pour l’intégration dans le système électrique d’un micro réseau,” Ecole Centrale de Lille, 2009.
[64] Basem Idlbi, “Dynamic Simulation of a Pv-diesel-battery Hybrid Plant for Off Grid Electricity Supply,” Cairo University, A Thesis For The Degree Of MASTER OF SCIENCE In RENEWABLE ENERGY AND ENERGY EFFICIENCY, Mar. 2012.
[65] M. R. Aghamohammadi and H. Abdolahinia, “A new approach for optimal sizing of battery energy storage system for primary frequency control of islanded Microgrid,” *Int. J. Electr. Power Energy Syst.*, vol. 54, pp. 325–333, Jan. 2014.

[66] W. Li, “An embedded energy storage system for attenuation of wind power fluctuations,” McGill University, Montreal, Canada, 2010.
[67] P. Degobert, S. Kreuawan, and X. Guillaud, “Use of super capacitors to reduce the fast fluctuations of power of a hybrid system composed of photovoltaic and micro turbine,” in *International Symposium on Power Electronics, Electrical Drives, Automation and Motion, 2006. SPEEDAM 2006*, 2006, pp. 1223–1227.
[68] A. Masahisa and S. Sueo, “A Hybrid Photovoltaic-Diesel Power Generation System for Miyako Island,” *A Quarterly Survey of New Products, Systems, and Technology*, vol. 80, p. 9, Sep-1997.
[69] T. Tadokoro, K. Taira, and M. Asaoka, “A photovoltaic-diesel hybrid generation system for small islands,” in *IEEE Photovoltaic Specialists Conference - 1994, 1994 IEEE First World Conference on Photovoltaic Energy Conversion, 1994., Conference Record of the Twenty Fourth*, 1994, vol. 1, pp. 708–715 vol.1.
[70] P. Mercier, R. Cherkaoui, and A. Oudalov, “Optimizing a Battery Energy Storage System for Frequency Control Application in an Isolated Power System,” *IEEE Trans. Power Syst.*, vol. 24, no. 3, pp. 1469–1477, Aug. 2009.
[71] E. Omine, T. Senjyu, E. B. Muhando, A. Yona, H. Sekine, T. Funabashi, and A. Y. Saber, “Coordinated control of battery energy storage system and diesel generator for isolated power system stabilization,” in *Power and Energy Conference, 2008. PECon 2008. IEEE 2nd International*, 2008, pp. 925–930.
[72] T. Goya, E. Omine, Y. Kinjyo, T. Senjyu, A. Yona, N. Urasaki, and T. Funabashi, “Frequency control in isolated island by using parallel operated battery systems applying H∞ control theory based on droop characteristics,” *IET Renew. Power Gener.*, vol. 5, no. 2, pp. 160–166, Mar. 2011.
[73] O. Perpinan and E. Lorenzo, “Analysis and synthesis of the variability of irradiance and PV power time series with the wavelet transform,” pp. 188–197, May 2012.
[74] J. Marcos, L. Marroyo, E. Lorenzo, D. Alvira, and E. Izco, “From irradiance to output power fluctuations: the PV plant as a low pass filter,” *Prog. Photovolt. Res. Appl.*, vol. 19, no. 5, pp. 505–510, 2011.
[75] E. Wiemken, H. G. Beyer, W. Heydenreich, and K. Kiefer, “Power characteristics of PV ensembles : Experiences from the combined power production of 100 grid connected PV systems distributed over the area of Germany,” pp. 513–518, May 2012.
[76] J. Marcos, L. Marroyo, E. Lorenzo, D. Alvira, and E. Izco, “Power output fluctuations in large scale PV plants: one year observations with one second resolution and a derived analytic model,” pp. 218–227, 2011.
[77] T. E. Hoff and R. Perez, “Quantifying PV power Output Variability,” pp. 1782–1793, May 2012.
[78] T. Tomson and G. Tamm, “Short-term variability of solar radiation,” pp. 600–606, May 2006.
[79] J. Marcos, L. Marroyo, E. Lorenzo, and M. Garcia, “Smoothing of PV power fluctuations by geographical dispersion,” pp. 226–237, May 2012.
[80] Yih-Huei Wan, “Wind Power Plant Behaviors: Analyses of Long-Term Wind Power Data,” Technical report NREL/TP-500-36551, Sep. 2004.
[81] R. Peck, C. Olsen, and J. L. Devore, *Introduction to statistics and data analysis*. Boston, MA: Brooks/Cole Cengage Learning, 2012.
[82] Clifford W. Hansen, Joshua S. Stein, and Abraham Ellis, “Statistical Criteria for Characterizing Irradiance Time Series,” SANDIA REPORT SAND2010-7314, Oct. 2010.
[83] J. Jay, S. Benjamin, E. Abraham, Q. Jimmy, and L. Carl, “Initial Operating Experience of the La Ola 1.2-MW Photovoltaic System,” SANDIA REPORT SAND2011-8848, Oct. 2011.
[84] J. Johnson, B. Schenkman, A. Ellis, J. Quiroz, and C. Lenox, “Initial operating experience of the 1.2-MW La Ola photovoltaic system,” in *Photovoltaic Specialists Conference (PVSC), Volume 2, 2012 IEEE 38th*, 2013, pp. 1–6.
[85] A. Murata, H. Yamaguchi, and K. Otani, “A method of estimating the output fluctuation of many photovoltaic power generation systems dispersed in a wide area,” *Electr. Eng. Jpn.*, vol. 166, no. 4, pp. 9–19, 2009.

[86] N. Kawasaki, T. Oozeki, K. Otani, and K. Kurokawa, “An evaluation method of the fluctuation characteristics of photovoltaic systems by using frequency analysis,” *Sol. Energy Mater. Sol. Cells*, vol. 90, no. 18–19, pp. 3356–3363, Nov. 2006.
[87] A. Woyte, V. V. Thong, K. Purchala, R. Belmans, and J. Nijs, “Quantifying the occurrence and duration of power fluctuations introduced by photovoltaic systems,” 2003, vol. 3, p. 7 pp. Vol.3.
[88] J. Apt, “The spectrum of power from wind turbines,” *J. Power Sources*, vol. 169, no. 2, pp. 369–374, Jun. 2007.
[89] A. E. Curtright and J. Apt, “The character of power output from utility-scale photovoltaic systems,” *Prog. Photovolt. Res. Appl.*, vol. 16, no. 3, pp. 241–247, 2008.
[90] T. Kato, T. Inoue, and Y. Suzuoki, “Estimation of total power output fluctuation of high penetration photovoltaic power generation system,” in *2011 IEEE Power and Energy Society General Meeting*, 2011, pp. 1–7.
[91] T. C. Urdan, *Statistics in plain English*. New York: Routledge, 2010.
[92] D. C. Montgomery and G. C. Runger, *Applied statistics and probability for engineers*. Hoboken, NJ: Wiley, 2011.
[93] Migrant & Seasonal Head Start, “Introduction to Data Analysis Handbook.” AED/TAC-12, Spring-2006.
[94] D. Howitt and D. Cramer, *Introduction to statistics in psychology*. Harlow, England; New York: Pearson, 2011.
[95] R. A. Witte, *Spectrum and network measurements*. Englewood Cliffs, N.J.: Prentice Hall, 1993.
[96] National Semiconductor Corporation, “Power Spectra Estimation.” Application Note 255, Nov-1980.
[97] N. Kawasaki, T. Oozeki, K. Otani, and K. Kurokawa, “An evaluation method of the fluctuation characteristics of photovoltaic systems by using frequency analysis,” *Sol. Energy Mater. Sol. Cells*, vol. 90, no. 18–19, pp. 3356–3363, Nov. 2006.
[98] M. Torres and L. A. C. Lopes, “Inverter-Based Diesel Generator Emulator for the Study of Frequency Variations in a Laboratory-Scale Autonomous Power System,” *Energy Power Eng.*, vol. 05, no. 03, pp. 274–283, 2013.
[99] S. Roy, O. P. Malik, and G. S. Hope, “An adaptive control scheme for speed control of diesel driven power-plants,” *IEEE Trans. Energy Convers.*, vol. 6, no. 4, pp. 605–611, Dec. 1991.
[100] P. B. Malatestas, M. P. Papadopoulos, and G. S. Stavrakakis, “Modeling and identification of diesel-wind turbines systems for wind penetration assessment,” *IEEE Trans. Power Syst.*, vol. 8, no. 3, pp. 1091–1097, Aug. 1993.
[101] C. Concordia and S. Ihara, “Load Representation in Power System Stability Studies,” *IEEE Trans. Power Appar. Syst.*, vol. PAS-101, no. 4, pp. 969–977, 1982.
[102] H. Huang and F. Li, “Sensitivity Analysis of Load-Damping Characteristic in Power System Frequency Regulation,” *IEEE Trans. Power Syst.*, vol. 28, no. 2, pp. 1324–1335, May 2013.
[103] F. Katiraei, M. R. Iravani, and P. W. Lehn, “Small-signal dynamic model of a micro-grid including conventional and electronically interfaced distributed resources,” *IET Gener. Transm. Distrib.*, vol. 1, no. 3, pp. 369–378, May 2007.
[104] D. Lu, “Conception et contrôle d’un générateur PV actif à stockage intégré : application à l’agrégation de producteurs-consommateurs dans le cadre d’un micro réseau intelligent urbain,” Ecole Centrale de Lille, 2010.
[105] A. Florescu, “Gestion optimisée des flux énergétiques dans le véhicule électrique,” Université de Grenoble, 2012.
[106] Z. Chen, M. Ding, and J. Su, “Modeling and control for large capacity battery energy storage system,” in *2011 4th International Conference on Electric Utility Deregulation and Restructuring and Power Technologies (DRPT)*, 2011, pp. 1429–1436.
[107] C.-F. Lu, C.-C. Liu, and C. J. Wu, “Dynamic modelling of battery energy storage system and application to power system stability,” *Gener. Transm. Distrib. IEE Proc.-*, vol. 142, no. 4, pp. 429–435, Jul. 1995.

[108] F. Salha, F. Colas, and X. Guillaud, “Dynamic behavior analysis of a voltage source inverter for microgrid applications,” in *2010 IEEE Power and Energy Society General Meeting*, 2010, pp. 1–7.
[109] I. V. Exposito, “INTERFAÇAGE ET CONTROLE COMMANDE DE PILES A COMBUSTIBLE POUR APPLICATIONS STATIONNAIRES ET TRANSPORT,” Université Joseph-Fourier - Grenoble I, 2004.
[110] C. GOMBERT, “Simulation temps-réel des dispositifs d’Electronique de Puissance dédiés aux Réseaux d’Energie Electrique,” INSTITUT NATIONAL POLYTECHNIQUE DE GRENOBLE, Grenoble, France, 2005.
[111] A. Timbus, M. Liserre, R. Teodorescu, and F. Blaabjerg, “Synchronization methods for three phase distributed power generation systems - An overview and evaluation,” in *Power Electronics Specialists Conference, 2005. PESC ’05. IEEE 36th*, 2005, pp. 2474–2481.
[112] S. Skogestad and I. Postlethwaite, *Multivariable feedback control : analysis and design*. Chichester: John Wiley & Sons, 2005.
[113] Da-Wei Gu, Petko Hristov Petkov, and Mihail Mihaylov Konstantinov, *Robust Control Design with MATLAB®*. .
[114] K. Zhou, J. C. Doyle, and K. Glover, *Robust and Optimal Control*, 1 edition. Prentice Hall, 1995.
[115] Yong He and Qing-Guo Wang, “An Improved ILMI Method for Static Output Feedback Control With Application to Multivariable PID Control,” *IEEE Trans. Autom. Control*, vol. 51, no. 10, pp. 1678–1683, Oct. 2006.
[116] M. SAUTREUIL, “La robustesse : Une nouvelle approche pour l’intégration des systèmes de génération aéronautique,” Joseph Fourier, Grenoble, France, 2009.
[117] D. HERNANDEZ-TORRES, “Command Robuste de Générateurs Electrochimiques Hybrides,” Université de Grenoble, Grenoble, France, 2011.
[118] J. Lofberg, “YALMIP : a toolbox for modeling and optimization in MATLAB,” in *2004 IEEE International Symposium on Computer Aided Control Systems Design*, 2004, pp. 284–289.
[119] D. Hernández-Torres, D. Riu, O. Sename, and F. Druart, “Robust optimal control strategies for a hybrid fuel cell power management system,” in *IECON 2010 - 36th Annual Conference on IEEE Industrial Electronics Society*, 2010, pp. 698 –703.
[120] S. Olivier, “Robust control of MIMO systems,” presented at the Robust control class of Grenoble INP, Grenoble, France, Sep-2013.
[121] H.-T. David, “On the Robust Control of DC-DC Converters: Application to a Hybrid Power Generation System,” 2010, pp. 123–130.
[122] LAM Quang Linh, “Gestion énergétique de systèmes multi sources multiconvertisseurs – Application aux micro-réseaux avec forte intégration d’énergies renouvelables,” Laboratoire de Génie Electrique de Grenoble (G2Elab), Rapport de stage, Jun. 2014.
[123] “RTLAB manual.” .
[124] “Steady Sun.” .